

https://dspace.org/

Interaction between reaction and phase equilibria in the Fischer-Tropsch reaction.

Masuku, Cornelius Mduduzi

2012-09-11
http://hdl.handle.net/10539/11926

Downloaded from a DSpace repository. https://dspace.org/

Interaction between Reaction and Phase Equilibria in the Fischer–Tropsch Reaction

Cornelius Mduduzi Masuku

A thesis submitted to the Faculty of Engineering and the Built Environment, University of the Witwatersrand, in fulfilment of the requirements for the degree of Doctor of Philosophy.

Johannesburg, 2011

DECLARATION

I declare that this thesis is my own, unaided work, unless otherwise stated. It is being submitted for the Degree of Doctor of Philosophy to the University of the Witwatersrand, Johannesburg. It has not been submitted before for any degree or examination to any other University.

……

Cornelius Masuku

…… day of ……, 2011

ABSTRACT

The aim of the thesis is to describe the behaviour and performance of the Fischer–Tropsch (FT) reactor by considering the dynamic interaction between reaction equilibrium and vapour–liquid equilibrium (VLE) inside the reactor. There may be an equilibrium set up between species of either an olefin precursor or the olefins themselves which leads to the Flory-type distribution found in the FT reaction. Experimental results obtained show that VLE is attained inside an FT reactor. The measured vapour and liquid compositions (K-values) can be sufficiently described by Raoult's law. Hydrocarbons with carbon number greater than 18 deviates from Raoult's law. The deviations from Raoult's law are due to diffusion limitations. Elaborate thermodynamic models could be used given the pure component parameters with relevant mixing rules for a higher degree of accuracy.

VLE can explain the observed two-alpha product distribution in FT reactors. This further predicts a relationship between the two values of alpha that is consistent with the measured experimental results. Experimental results show that the average residence time increase with carbon number and the higher carbon number products have a longer residence time in the reactor. Products with a chain length of 22 and higher have the same residence time as the liquid. This suggests that VLE is the predominant cause for chain length dependencies of secondary olefin reactions in FT synthesis and diffusion limited removal of products is only significant for products with carbon number greater than 17.

A mathematical model to describe the behaviour and performance of an FT reactor by considering the dynamic interaction between reaction and VLE was developed. The model results show that the rate of formation of component hydrocarbons is dependent on either the reaction rate or stripping rate, depending on which one is rate-limiting. Furthermore, that at steady state, the rate of formation of hydrocarbons is given by the stripping rate. Modelling an

FT reactor as a reactive distillation column can explain a rate increment when the reactor is switched from Batch to CSTR mode and is also consistent with the observed two-alpha positive deviation product distribution observed experimentally and industrially.

ACKNOWLEDGEMENTS

I would like to express my gratitude to my supervisors, Professor Diane Hildebrandt and Professor David Glasser for their guidance, advice and insight which have been invaluable.

My gratitude also goes to Professor Mike Scurrel and the whole Catalysis Group for the fruitful discussions at research meeting, and everyone at COMPS for contributing in various ways.

It's an honour to have worked with Dr. Burtron Davis at the Center for Applied Energy Research at the University of Kentucky, USA. I would also like to thank the whole Clean Fuels and Chemicals Group at Kentucky for their help and making my stay in the U.S. a productive and memorable one.

Big thanks to my friends and family for your support and belief in me which kept me going.

I would like to acknowledge the financial support from the National Research Foundation (NRF), South African Research Chairs Initiative (SARChI), Technology and Human Resources for Industry Programme (THRIP), South African National Energy Research Institute (SANERI), the University of the Witwatersrand, Johannesburg and the Commonwealth of Kentucky.

PUBLICATIONS

Chapter 2: C.M. Masuku, D. Hildebrandt, D. Glasser, Olefin pseudo-equilibrium in the Fischer–Tropsch reaction, *Chem. Eng. J. 181–182* (2012) 667–676.

Chapter 3: C.M. Masuku, W. Ma, D. Hildebrandt, D. Glasser, B.H. Davis, A vapor–liquid equilibrium thermodynamic model for a Fischer–Tropsch reactor, *Fluid Phase Equilib. 314* (2012) 38–45.

Chapter 4: C.M. Masuku, D. Hildebrandt, D. Glasser, The role of vapour–liquid equilibrium in Fischer–Tropsch product distribution, *Chem. Eng. Sci. 66* (2011) 6254–6263.

Chapter 5: C.M. Masuku, W.D. Shafer, W. Ma, M.K. Gnanamani, G. Jacobs, D. Hildebrandt, D. Glasser, B.H. Davis, Variation of residence time with chain length for products in a slurry phase Fischer–Tropsch reactor, *J. Catal. 287* (2012) 93–101.

Chapter 6: C.M. Masuku, X. Lu, D. Hildebrandt, D. Glasser, Reactive distillation in conventional Fischer–Tropsch reactors, *Fuel Process. Technol.*, submitted for publication.

CONTENTS

DECLARATION i
ABSTRACT ii
ACKNOWLEDGEMENTS iv
PUBLICATIONS v
LIST OF FIGURES xi
LIST OF TABLES xiv

Chapter 1 : INTRODUCTION 1
ABSTRACT 1
1.1 INTRODUCTION 1
1.2 ENERGY DEMAND 2
1.3 EFFICIENT AND ECONOMIC INTEGRATION OF ENERGY SOURCES 4
1.4 PETROCHEMICALS 5
1.5 A BRIEF ACCOUNT OF FISCHER–TROPSCH SYNTHESIS 6
1.5.1 Syngas Production 7
1.5.2 Syngas Cleaning and Conditioning 8
1.5.3 FT Reactors 9
1.5.4 Product Distribution 12
1.5.5 Fuels versus Chemicals 13
1.5.6 Economics 14
1.5.7 Capital Cost 14
1.6 THESIS OVERVIEW 15
REFERENCES 17

Chapter 2 : OLEFIN PSEUDO-EQUILIBRIUM IN THE FISCHER–TROPSCH REACTION. 20
ABSTRACT 20
2.1 INTRODUCTION 21
2.2 EQUILIBRIUM CONSIDERATIONS 24

2.3 THERMODYNAMIC BASIS FOR A FLORY-TYPE PRODUCT DISTRIBUTION 25
2.4 MINIMISING GIBBS FREE ENERGY FOR PARAFFINS AND/OR ALCOHOLS 28
2.5 MINIMISING GIBBS FREE ENERGY FOR OLEFINS 35
2.6 DISCUSSION 41
2.7 CONCLUSIONS 42
APPENDIX A: FULL SERIES DERIVATION 44
APPENDIX B: DERIVATIONS FOR MINIMISING GIBBS FREE ENERGY FOR PARAFFINS AND/OR ALCOHOLS 46
APPENDIX C: DERIVATIONS FOR MINIMISING GIBBS FREE ENERGY FOR OLEFINS 50
NOMENCLATURE 53
REFERENCES 54

Chapter 3 : A VAPOUR–LIQUID EQUILIBRIUM THERMODYNAMIC MODEL FOR A FISCHER–TROPSCH REACTOR 59
ABSTRACT 59
3.1 INTRODUCTION 60
3.2 A REVIEW OF RELEVANT VLE THERMODYNAMIC MODELS 62
3.3 EXPERIMENTAL SECTION 63
3.4 FISCHER–TROPSCH RESULTS AND DISCUSSION 65
3.5 POLYWAX MASS FRACTION INSIDE THE REACTOR 68
3.6 VAPOUR–LIQUID EQUILIBRIUM RESULTS AND DISCUSSION 73
3.7 VERIFICATION OF EXPERIMENTAL RESULTS 79
3.8 CONCLUSIONS 82
REFERENCES 82

Chapter 4 : THE ROLE OF VAPOUR–LIQUID EQUILIBRIUM IN FISCHER–TROPSCH PRODUCT DISTRIBUTION 87
ABSTRACT 87
4.1 INTRODUCTION 87
4.2 THE EFFECT OF VLE IN THE FISCHER–TROPSCH REACTION 91
4.3 PRODUCT DIFFUSION LIMITATION 93

4.4 REACTION MODELLING 93
4.5 MODEL DEVELOPMENT AND CALCULATIONS 95
Case 1: The total product distribution follows a single α 96
Case 2: A single α distribution is set up in the vapour phase. 104
Case 3: A single α distribution is set up in the liquid phase, and the vapour is in equilibrium with the liquid. 108
4.6 DISCUSSION 113
4.7 EXPERIMENTAL RESULTS 114
4.8 CONCLUSIONS 118
NOMENCLATURE 120
REFERENCES 121

Chapter 5 : VARIATION OF RESIDENCE TIME WITH CHAIN LENGTH FOR PRODUCTS IN A SLURRY PHASE FISCHER–TROPSCH REACTOR 125
ABSTRACT 125
5.1 INTRODUCTION 126
5.2 DEUTERIUM TRACER EXPERIMENTS 128
5.3 EXPERIMENTAL SECTION 129
5.3.1 FT Reactor and Analysis of Products 129
5.3.2 Analysis of Accumulated Products 131
5.3.3 CO Conversion 131
5.4 ESTIMATION OF THE RESIDENCE TIME OF THE GAS PHASE 132
5.5 MEASUREMENT OF RESIDENCE TIME OF POLYWAX IN THE REACTOR 135
5.6 ANALYSIS OF THE LIQUID PHASE PRODUCT DISTRIBUTION 139
5.7 ANALYSIS OF THE VAPOUR PHASE PRODUCT DISTRIBUTION 140
5.8 THE INTERACTION OF PRODUCT ACCUMULATION WITH VAPOUR–LIQUID EQUILIBRIUM 141
5.9 OVERALL PRODUCT DISTRIBUTION OF DEUTERATED PRODUCTS 144
5.10 UNSTEADY STATE MASS BALANCE ON THE DEUTERATED PRODUCTS INSIDE THE REACTOR 146
5.11 TIME REQUIRED FOR PRODUCTS TO REACH STEADY STATE 154
CONCLUSIONS 157

NOMENCLATURE 158
REFERENCES 159

Chapter 6 : REACTIVE DISTILLATION IN CONVENTIONAL FISCHER–TROPSCH REACTORS 165
ABSTRACT 165
6.1 INTRODUCTION 166
6.2 REACTIVE DISTILLATION CONSIDERATIONS 166
6.3 REACTOR MODELLING 168
6.4 STRIPPING AS A RATE LIMITING PHENOMENA 171
6.5 CSTR TO BATCH REACTOR EXPERIMENT 173
6.6 CSTR TO BATCH REACTOR RESULTS 175
6.7 PRODUCT DISTRIBUTION 178
6.8 CONSTANT ALPHA PRODUCT DISTRIBUTION IN THE LIQUID PHASE 180
6.9 VAPOUR FRACTION INSIDE THE REACTOR 183
6.10 PRODUCT DISTRIBUTION EXPERIMENTAL RESULTS 185
6.11 TWO-ALPHA LITERATURE RESULTS 188
6.12 CONCLUSIONS 189
NOMENCLATURE 190
ACKNOWLEDGEMENTS 191
REFERENCES 191

Chapter 7 : CONCLUDING REMARKS 195
7.1 INTRODUCTION 195
7.2 REACTION EQUILIBRIUM 195
7.3 VAPOUR–LIQUID EQUILIBRIUM THERMODYNAMIC MODEL 196
7.4 VAPOUR–LIQUID EQUILIBRIUM IN FISCHER–TROPSCH PRODUCT DISTRIBUTION 197
7.5 PRODUCT RESIDENCE TIME 197
7.6 REACTIVE DISTILLATION 198
7.7 FUTURE WORK AND RECOMMENDATIONS 199

LIST OF FIGURES

Figure 1.1: Estimates of the world population (Data from U.S. Census Bureau [5]) 3

Figure 2.1: Typical product distribution for a Flory-type distribution reproduced from Reference [15]. The Flory distribution with a single alpha (α) is fitted to the data, where log(α) is the slope of the line. The data shows significantly higher methane and lower ethane selectivities than the Flory predictions. 22
Figure 2.2: Two-alpha Fischer–Tropsch product distribution reproduced from Reference [16]. 23
Figure 2.3: The change of enthalpies of formation with carbon number for paraffins. 26
Figure 2.4: The change of Gibbs free energies of formation with carbon number for paraffins.. 27
Figure 2.5: Gibbs free energies of formation/reaction with carbon number for paraffins at different temperatures. 32
Figure 2.6: Change of enthalpies of formation/reaction for alcohols with carbon number. 33
Figure 2.7: Gibbs free energies of formation/reaction with carbon number for alcohols at different temperatures. 34
Figure 2.8: Change of enthalpies of formation/reaction for olefins with carbon number. 39
Figure 2.9: Gibbs free energies of formation/reaction with carbon number for olefins at different temperatures. 40

Figure 3.1: A schematic diagram of the Fischer–Tropsch reactor system. 64
Figure 3.2: Percentage CO conversion at various space velocities for the FT experiment (220 °C, 2.0 MPa, H_2:CO = 2:1). 66
Figure 3.3: FT product distribution at a space velocity of 4 slph/g_cat (α ≈ 0.91, 220 °C, 2.0 MPa, H_2:CO = 2:1) 67
Figure 3.4: Polywax mass fraction inside the reactor for the duration of the experiment calculated by considering constant volume inside the reactor. The TOS in this Figure corresponds to the TOS presented in Figure 3.2. 72
Figure 3.5: Variation of the reactor liquid mass and the reactor liquid density with time on stream calculated by considering constant liquid volume inside the reactor. 73
Figure 3.6: Vapour–liquid equilibrium distributions for samples collected at a space velocity of 5 and 4 slph/g_cat. The solid line gives the predicted change of K_i versus carbon number using Raoult's law. 75
Figure 3.7: Change of liquid phase product distribution with time on stream. The TOS in this Figure corresponds to the TOS presented in Figure 2. 77
Figure 3.8: Vapour phase product distribution at a space velocity of 5 and 4 slph/g_cat (220 °C, 2.0 MPa, H_2:CO = 2:1). 78

Figure 3.9: Vapour–liquid equilibrium distributions for an iron catalyst at 270 °C, 1.3 MPa, 10 slph/g_cat. The solid line gives the predicted change of K_i versus carbon number using Raoult's law. 80
Figure 3.10: Average relative deviations with carbon number for all data points at 220 °C, 2.0 MPa using cobalt catalyst and relative deviations with carbon number at 270 °C, 1.3 MPa using iron catalyst. 81

Figure 4.1: Classical Anderson–Schulz–Flory distribution, single-alpha distribution. 89
Figure 4.2: Two-alpha positive-deviation product distribution. 90
Figure 4.3: Schematic diagram of the conceptual FT reactor. 94
Figure 4.4: The expected product distribution if the overall product distribution is described by a single alpha (α=0.85). The vapour and liquid are assumed to be in VLE. 101
Figure 4.5: Predicted vapour phase product distribution for Case 1 at different overall chain-propagation probability. 103
Figure 4.6: The expected liquid and total product distribution if the vapour phase has a single alpha (α=0.85) product distribution. 107
Figure 4.7: The expected product distribution for a single-alpha liquid product distribution. Alpha in liquid is 0.85 and beta is 0.63, corresponding to a temperature of 200 °C 111
Figure 4.8: Setup of experimental Fischer-Tropsch system. 116
Figure 4.9: Total product distribution from the experimental results obtained using an iron catalyst at 270 °C and 8 bar. 117

Figure 5.1: A schematic diagram of the Fischer–Tropsch reactor system. 130
Figure 5.2: Percentage CO conversion for the duration of the experiment. Time = 0 corresponds to the reactor start up. (T = 493 K, P = 2.0 MPa, H_2/CO = 2) 132
Figure 5.3: Measurement of hydrogen–deuterium replacement in the gas phase as indicated by the TCD response as a function of time. (T = 493 K, P = 2.0 MPa, H_2/CO = 2) 133
Figure 5.4: Logarithm of the mole fraction of hydrogen after switching from CO/H_2 to CO/D_2. Time = 0 is when H_2 is replaced by D_2 in the feed. 135
Figure 5.5: Calculated Polywax mass fraction inside the reactor as a function of time. Time = 0 corresponds to start up of the reactor. (T = 493 K, P = 2.0 MPa, H_2/CO = 2) 136
Figure 5.6: Logarithm of the polywax mass fraction inside the reactor as a function of time on stream. 138
Figure 5.7: Liquid phase product distribution of deuterated products as a function of carbon number on different days on stream. Day 0 represents the end of D_2 tracing. (T = 493 K, P = 2.0 MPa, H_2/CO = 2) 139
Figure 5.8: The log of the mole fraction of deuterated products in the vapour phase plotted against length of hydrocarbon n distribution for different days. Day 0 represents the end of D_2 tracing. (T = 493 K, P = 2.0 MPa, H_2/CO = 2) 140

Figure 5.9: The ratio of the mole fraction in the vapour phase to the mole fraction in the liquid phase ($K_n \equiv y_n/x_n$) with carbon number. Solid line is calculated from Raoult's law and is given by $P_{vap,n}/P$. (T = 493 K, P = 2.0 MPa, H_2/CO = 2) 143
Figure 5.10: Calculated mole fractions of total (vapour + liquid) deuterated products after introducing D_2 into the reactor. The D_2 is switched off and replace with H_2 at the end of Day 0. (T = 493 K, P = 2.0 MPa, H_2/CO = 2) 145
Figure 5.11: Schematic diagram of the reactor as a stripping vessel for deuterated products. (F is the total molar feed flow rate, Q_G is the vapour molar flow, Q_L is the liquid molar flow, y_n is the mole fraction of component n in the vapour phase, and x_n is the mole fraction of component n in the liquid phase.) 147
Figure 5.12: The log of mole fraction of deuterated products in the liquid phase with time on stream. The slope of each line represents the inverse of the residence time of that product in the reactor. (T = 493 K, P = 2.0 MPa, H_2/CO = 2) 149
Figure 5.13: The log of mole fraction of deuterated products in the vapour phase with time on stream. The slope of each line represents the inverse of the residence time of that product in the reactor. (T = 493 K, P = 2.0 MPa, H_2/CO = 2) 150
Figure 5.14: The average residence time with carbon number for products inside a reactor calculated from the slopes of the curves in Figures 12 and 13. (T = 493 K, P = 2.0 MPa, H_2/CO = 2) 151
Figure 5.15: Olefin to paraffin ratio of deuterated products with carbon number. Day 0 represents the end of D_2 tracing. (T = 493 K, P = 2.0 MPa, H_2/CO = 2) 153
Figure 5.16: Overall mole fractions of products with different carbon numbers with time on stream as an indication for time required for each carbon number to reach steady state. (Only a few carbon numbers are show in this Figure for ease of visualization. Time = 0 corresponds to reactor start up.) (T = 493 K, P = 2.0 MPa, H_2/CO = 2) 156

Figure 6.1: Schematic diagram of a Fischer–Tropsch reactor with vapour and liquid removal. 168
Figure 6.2: Schematic illustration of reaction rate limitation and stripping rate limitation for a particular reactor parameter, e.g. pressure in this case. The temperature dependence of the stripping rate limitation might have a different form but the discussion still holds. 172
Figure 6.3: Reaction rates in the CSTR and Batch operation modes as a function of time on stream. (T = 483 K, P = 2.0 MPa, H_2/CO = 2) 176
Figure 6.4: Observed product distribution for modelling reaction and stripping in an FT reactor reproduced from Ref. [9]. 182
Figure 6.5: Schematic diagram for a reactive flash drum 183
Figure 6.6: Mole fractions of hydrocarbons at different vapour fractions. 185
Figure 6.7: Total product distribution from the experimental results obtained using a cobalt catalyst at 493 K and 0.8 MPa. 187

LIST OF TABLES

Table 2.1: The predicted chain growth probability factor (α) at various temperatures for paraffins 32
Table 2.2: The predicted chain growth probability factor (α) at various temperatures for alcohols 34
Table 2.3: The predicted chain growth probability factor (α) at various temperatures for olefins40

Chapter 1 : INTRODUCTION

ABSTRACT

Economic activity along with population growth are fundamental drivers of energy demand. The challenge engineers face is to meet the world's growing energy needs while also reducing the impact of energy use on the environment. Improvements in efficiency must be at the forefront of the effort to conserve resources and reduce the damage energy consumption inflicts on the natural environment. This chapter comprises a brief background section on the Fischer–Tropsch (FT) process and motivation for its use; a discussion of the practical, chemical, engineering and economic aspects of FT reactors; and an outline of the thesis.

1.1 INTRODUCTION

Energy stands highest on the list of priorities and prerequisites for human development. Access to energy is essential to the reduction of poverty and the achievement of the Millennium Development Goals in developing countries [1]. Advances in technology have led to an enormous expansion of energy resources and means of utilization, both of which have improved the quality of life of ordinary people. As the conversion of natural sources of energy into useful forms, and in the quantities needed for industrial, transportation and domestic use has progressed, the benefits have been demonstrated in improved standards of living and higher birth rates.

Conversion technologies have largely kept pace with demand [2]. However, because some of the traditional sources of energy, such as fossil fuels, are becoming depleted, new technologies are required to harness other, less traditional sources, such as renewable energy. These have not kept

pace with the rising demand for energy of developed and (more significantly) developing countries. This is a cause for concern, not only on the energy-demand front. The carbon dioxide emitted by the use of fossil fuels, and the role it plays in global warming, is a matter of international debate, and at present poses the most vexing problem scientists face.

Given the current infrastructure and end-product utilization patterns, it is unlikely that the dependence on fossil fuels as the major raw source for transportation, fuel production and industrial use will change significantly in the coming decades. Therefore, improving energy efficiency must be at the forefront of the effort to conserve resources and reduce the impact of energy consumption on the environment.

1.2 ENERGY DEMAND

Developing nations, including the population giants China and India, are entering their most energy-intensive phase of economic growth as they industrialise, build infrastructure, and increase their use of transportation [3]. Despite the efforts made by scientists to come up with alternatives, gasoline and diesel will continue to power the engines of the overwhelming majority of our cars and trucks for many decades to come. Around the world people rely on petrochemicals to supply their energy needs because the former have a proven record of versatility, affordability and reliability.

Furthermore, products based on petrochemicals are essential to modern life in a variety of ways, because they are used to manufacture just about everything that is not made of wood or metal, or based on plants or other living things. These products include medicines and medical devices, cosmetics, furniture, appliances, TVs and radios, computers, parts used in every type of transportation, solar power panels and wind turbines, and all items made of plastic.

As the global population soars (see Figure 1.1), food, energy, and fresh water are becoming increasingly scarce because of the competing needs of so many people. Water is a basic requirement for survival, while energy is the gateway to development beyond subsistence level. To further complicate matters, these two critical needs, clean water and on-demand energy, are intimately intertwined. Each is necessary for a productive and healthy society [4].

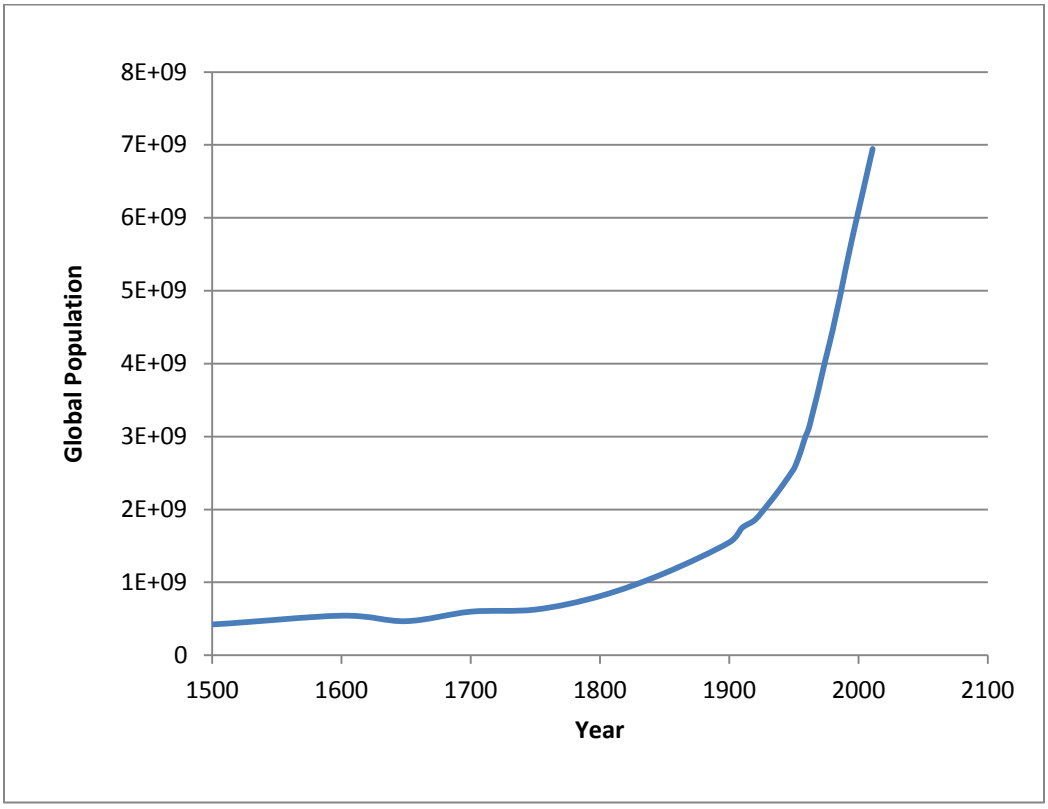


Figure 1.1: Estimates of the world population (Data from U.S. Census Bureau [5])

Those who plan to meet the needs of the population of today as well as those of the future require an understanding of the driving forces and feedback relationships in the water and energy cycles before they can devise efficient and sustainable ways to use both of these essential commodities. Engineers need to consider how they can maximize the supply of one while minimizing the use of the other. Advances in chemical engineering can facilitate reductions in energy consumption for water processing and vice versa.

1.3 EFFICIENT AND ECONOMIC INTEGRATION OF ENERGY SOURCES

Electricity-generating utilities and chemical manufacturers face two major challenges. The cost of their fuels and feedstocks is rising to unprecedented levels, and they are under increasing pressure, both regulatory and moral, to reduce carbon dioxide emissions. A potential solution to both of these issues is to gasify low-cost coal, petroleum coke, or biomass (which are widely available), and use the resulting effluent gas stream to produce electricity and chemicals [6]. If capital costs and certain operating costs are split between electricity and chemicals production by using a portion of this gas as a fuel to produce electricity and the remaining gas to produce higher value chemicals, there may be substantial economic advantages.

If we are to reach a new energy equilibrium, that is, a situation in which energy and environmental needs are met simultaneously, it will be critical to integrate biomass energy sources into existing infrastructure for the chemical conversion of fossil fuels. The co-gasification of coal and biomass, coupled with Fischer–Tropsch (FT) processing [7], is capable of bringing about this synergy. Using biomass in this fashion makes it possible for the economies of scale inherent in coal conversion to be exploited for biomass, taking advantage of lower average feedstock costs than would be the case for a facility processing only biomass. Synthesis gas that is not converted into liquid fuels in one pass through the synthesis reactor can be used to generate electricity in a gas turbine combined cycle [8]. In this way new energy sources can be integrated into existing chemical-conversion infrastructure, ensuring that energy sources can be integrated both efficiently and economically with chemical manufacturing and processing.

Systems that produce synthetic liquid fuels and electricity from coal and biomass with carbon capture and storage offer an attractive cost-competitive approach for decarbonising liquid fuels and electricity simultaneously [9]. The reason is the synergistic effects of co-producing liquid

hydrocarbons and electricity from coal, which make the facilities that produce them more efficient than facilities manufacturing one or the other separately [10].

1.4 PETROCHEMICALS

Since the FT end products, chemicals and fuels, have to compete directly with those produced from crude oil, the price of crude oil is one of the key factors in the demand for alternative feedstocks [11]. The oil crisis of 1973 initiated a number of new attempts to convert unconventional feedstocks to automotive fuels, one of them the Shell Middle Distillate Synthesis process [12]. World oil prices reached unprecedentedly high levels in 2008, in part because of a strong increase in demand for transportation fuels, particularly in emerging economies [13]. This need can be met by the conversion of certain natural resources into energy. Natural gas is a particularly attractive fuel for regions that are urbanising and seeking to satisfy an expanding demand for energy while keeping greenhouse gas emissions to a minimum. The global natural gas resource base is vast, and widely dispersed geographically [14]. Coal and natural gas can be converted to liquid transportation fuels through the Fischer–Tropsch synthesis (FTS) process [15].

The recent escalation of interest in FTS is a consequence of three factors: renewed concern about environmental degradation, technological developments, and changes in fossil-based energy reserves. More specifically, the world's reserves of natural gas, whether or not associated with petroleum, have increased. A significant proportion of this has been assigned 'stranded', that is, unusable because it is situated in an inaccessible place, or cannot be exploited for other reasons. For example, in a world where CO_2 emissions are believed to be a major cause of global warming, there are stringent regulations governing the control of natural gas, and heavy taxes imposed on flaring. In such circumstances, natural gas might even be considered of negative value in the places where it is found [16]. However, such gas in remote locations can be converted into shippable hydrocarbon liquids by means of FTS.

1.5 A BRIEF ACCOUNT OF FISCHER–TROPSCH SYNTHESIS

In the last few decades, the conversion of syngas (CO and H_2) through gas-to-liquids (GTL) technology has proved to be an excellent alternative to conventional sources of liquid transportation fuel [17]. This fact, allied to a growing demand world-wide for clean-burning fuels, has prompted a renewed interest in the study of FTS [18].

Industrial FT facilities are currently used for coal-to-liquid (CTL) and GTL conversion [19]. The purpose of such facilities is to convert solid or gaseous carbon-based energy sources into products that may be used as fuels or chemicals. The types of feed material that can be converted to synthesis gas (syngas) are not restricted to coal and natural gas: it is possible to employ almost any other carbon source as feed material. The conversion of biomass in a biomass-to-liquids (BTL) process and waste in a waste-to-liquids (WTL) process are good examples of sustainable technology, since biomass represents a renewable source of energy and waste conversion is connected with the beneficial recycling of discarded material. Another instance is the use of FTS to produce clean diesel via syngas from residual heavy oils. In general feed-to-liquid conversions can be referred to as XTL.

Analysts estimate that world coal consumption will increase from 127 quadrillion Btu in 2006 to 190 quadrillion Btu in 2030 [20]. If these amounts are to be produced without serious ecological harm, much more efficient and clean coal-to-liquids (CTL) technologies will be required. This explains why FT CTL technologies have received particular attention in oil-poor countries as a way of exploiting abundant coal reserves to produce high-grade fuels. The world's reserves of coal are about six times the sum of other proven carbon reserves [15]. Therefore, over the long term, even if alternative sources of energy are evolved, coal will become the main source of liquid fuels and chemicals. At present, natural gas is the preferred raw material for syngas production, for reasons both economic and environmental.

Steam/O_2 reforming of CH_4 is more efficient than steam/O_2 gasification of coal. In CH_4 reforming about 20% of the carbon ends up as CO_2, while in coal gasification the figure is about 50% [15]. Thus the use of CH_4 results in lower CO_2 emissions than in the case of coal. This indicates that to convert coal to liquid fuels and chemicals via the FT process requires that the price of coal is cheap relative to that of CH_4 or oil. This will become the case as the reserves of CH_4 and oil approach depletion.

FTS is a catalytic process that converts syngas into a multi-component mixture of hydrocarbons. FT-derived products are excellent high-performance, clean diesel fuels, because of their high cetane number and lack of sulphur and aromatic compounds. Although FTS lies at the heart of the conversion, it is actually only a small part of the whole. The process can be divided into three steps: syngas production, syngas conversion, and product refining. Generically, this is called indirect liquefaction, because the feed is first transformed into syngas, which is then transformed into products.

1.5.1 Syngas Production

Syngas production is an energy-intensive operation, and also the most expensive step in indirect liquefaction. The latter has the inherent ability to process and separate carbon matter from mineral matter in mineral-containing carbon sources like oil shales, peat, coal, and oil sands. Such solid feed materials are typically converted in gasifiers to produce syngas. Once the carbon in these carbon sources has been oxidized to carbon monoxide, separation of the gaseous products from the mineral matter is easily achieved. The physical state of the rejected mineral matter may be a dry ash or a slag, depending on the gasification technology employed.

Carbon-containing feed material usually contains elements other than carbon and hydrogen. When the feed is converted into a raw synthesis gas, heteroatoms in the feed are also changed

into gaseous compounds, such as hydrogen sulphide (H_2S), carbonyl sulphide (COS), and ammonia (NH_3). When the raw synthesis gas is purified, these heteroatom-containing compounds are removed to produce a synthesis gas consisting of unadulterated carbon monoxide and hydrogen. With the exception of oxygen, all other heteroatoms are therefore removed during syngas purification [19].

All syngas production technologies involve some form of partial oxidation. Regardless of the feed used, it must be selected for its compatibility with the requirements of FT syngas production technology. The H_2:CO ratio is contingent on the general FT technology and the design of the FT gas loop.

The two reforming technologies most commonly used for syngas production are steam and adiabatic oxidative reforming. Steam reforming, the dominant process for hydrogen production in refineries, is able to convert hydrocarbon feed materials ranging from natural gas to heavy naphtha. Solid feed materials have to be gasified in order to produce syngas.

The syngas production step requires accommodation in the refinery design because the co-production of pyrolysis liquids in some gasification technologies increases the volume and complexity of the feed material that has to be refined. This is not necessarily detrimental, and the co-refining of pyrolysis liquids may be synergetic.

1.5.2 Syngas Cleaning and Conditioning

Syngas cleaning is required to remove compounds that are FT catalyst poisons from the syngas. The most important and universal poison for FT catalysts is sulphur, but other species such as nitrogen-containing compounds, oxygen, chlorides, and bromides may also lead to catalyst deactivation. Depending on the feed material, the raw syngas also contains NH_3, which dissolves

readily in the aqueous product obtained from cooling the raw syngas, and can be removed almost completely by water washing [19].

Syngas conditioning is necessary to adjust the H_2:CO ratio of the synthesis gas to meet the requirements of FT conversion. This is performed by a combination of one or more of the following: water gas shift (WGS) conversion, methane reforming, and gas recycle after FTS.

Once the syngas has been cleaned and conditioned by whatever combination of FT technology is used in the individual operation, the syngas can be converted into synthetic crude (syncrude) oil that is comparable to, but different from, conventional crude oil. It is only by upgrading or refining that syncrude can be transformed into useful products. All industrial FT facilities carry out at least partial refining for the syncrude-to-product conversion.

1.5.3 FT Reactors

The need to remove the heat released by the FT reaction is a major consideration in the design of reactors suitable for syngas conversion. Radial differences in temperature between the tube centre and wall of 2–4 °C and axial differences between the peak in the upper section and the exit of 15–20 °C have been measured in 5 cm ID tubes during FT synthesis [15]. As in most exothermic processes, heat is removed by heat exchangers, which are fed with water and produce useful steam. The objective is to minimise the temperature rise within the catalyst bed, which requires rapid heat removal in a direction perpendicular to the flow of reactants. Consequently, when FT reactors are discussed, engineers have to bear practical chemical, engineering and economic factors in mind as well as the need to find the best means of controlling conversion and selectivity.

SASOL uses Arge tubular fixed bed reactors for low-temperature FT (LTFT) synthesis [21]. The advantages of multi-tubular fixed bed reactors are as follows. They are simple to operate. They can be used over wide temperature ranges irrespective of whether the FT products are gaseous or liquid, or both, under reaction conditions. Separating liquid products from the catalyst is unproblematic, as any liquid product simply trickles down through the bed and is readily removed from the exit gas in a downstream knock-out vessel. For all of these reasons, Arge reactors are well suited to FT wax production.

Even when it has been purified, syngas commonly contains traces of H_2S, which poisons Fe or Co FT catalysts. Temporary upsets in the gas purification plant, even if only brief, can result in 'slugs' of H_2S entering the FT reactors. In fixed bed reactors, the bulk of the H_2S is absorbed by the top layers of the catalyst while the remainder of the bed remains unaffected. In such cases the loss of activity is not serious [22].

There are, however, many economic disadvantages to using multi-tubular reactors. Not only are they expensive to construct, but all FT catalysts lose activity with time on stream (TOS) and so have to be replaced periodically. This is a major labour-intensive operation for large multi-tubular reactors, and the narrower the tubes, the more difficult and time-consuming the process. The longer the period of operational downtime lasts, the bigger the production loss.

An alternative way of transferring heat rapidly is to 'move the particles to the heat exchanger', which is what actually occurs in two-phase fluidised beds. The frequent direct physical contact between hot catalyst particles and the heat exchanger tube walls also contributes significantly to heat exchange. The combination of all these factors results in a much more efficient heat exchange in fluidized beds than in fixed catalyst beds. This in turn means that a smaller heat exchange area is required for fluidized bed reactors, another cost-reducing factor. At the gas linear velocity used in commercial reactors, the fluidized beds are very turbulent. Rapid

circulation/back-mixing occurs throughout the bed, creating a near isothermal reaction zone in which the differential temperatures across the bed are 2°C or less [15].

An important feature of fluidized solids is that they flow like a low-viscosity liquid. This makes it possible to add fresh catalyst and take away old catalyst from fluidized bed reactors without interrupting the process. Because of the easy removal and addition of catalysts, the 'turnaround' time (from shut down to start-up) is much shorter for fluidized than for fixed bed reactors.

Despite their many and important advantages, fluidized beds do have several shortcomings. In general, these reactors are more difficult to operate, particularly the circulating fluidized types. Because the catalyst particles are necessarily small (< 100 μm), effective separation of catalyst fines from the exhaust gas is not simple. The two-phase SASOL fluidized FT reactors use cyclones to achieve this separation. But even though cyclone efficiencies are well above 99%, a 0.1% loss amounts to a significant amount of catalyst in view of the high mass flows through the cyclones [15]. To ameliorate this problem, the reactors have oil scrubber units placed immediately down- stream to remove entrained fines. These units add significantly to capital costs, and reduce the thermal efficiency of the process. A development programme undertaken by SASOL led to the successful commissioning of a commercial-scale conventional fixed fluidised bed (FFB) reactor as an alternative to the circulating fluidised bed (CFB) reactor [23].

The slurry reactor is another version of the fluidized bed reactor. The small catalyst particles are suspended in a liquid through which the feed gas is bubbled, that is, it is a three-phase system. In its FT application, it is used for the production of high molecular waxes, which are liquids under synthesis conditions. The natural choice of the liquid phase is, therefore, the FT wax product itself.

For FT wax production, the slurry reactor has many advantages over the multi-tubular fixed bed type. In May 1993 SASOL commissioned a commercial slurry bed reactor [24].The construction cost of equivalent capacity reactors is about 40% less for a slurry type. Also, the pressure drop over the slurry is significantly lower than in fixed bed reactor, and this translates into lower compression costs. A slurry bed is also more isothermal than a fixed bed. On the other hand, an obvious disadvantage of a slurry system operating in the wax-producing mode is that a special additional operation/device is required to separate the nett wax production from the suspended catalyst.

1.5.4 Product Distribution

Over the years, many apparently different mechanisms have been proposed for product distribution. Common to them all has been the concept that it involves a stepwise chain growth process. This assumption is strongly supported by the fact that the carbon number product distributions calculated solely on probabilities of chain growth were matched by the experimentally observed results obtained in different reactor types and sizes over widely varying process conditions and with different catalysts.

The two major improvements researchers are attempting to make in catalytic processes are higher activity and better selectivity of the required products. Regardless of the catalyst type or feed gas composition, the researchers always find that as the temperature is increased, the CH_4 selectivity rises, or, put in another way, the probability of chain growth drops.

Since the probability of chain growth determines the overall carbon number distribution there are theoretical limits to the yields of specific cuts that can be achieved in the FT process. To further increase the yield of gasoline and of diesel fuel requires the application of additional downstream operations. Thus, oligomerization of the lighter olefins (such as propene and butenes) over acidic zeolites can produce high-quality gasoline and diesel fuel, while selective hydrocracking of FT

waxes produces a high-quality diesel fuel (cetane number 65), which could increase the overall diesel fuel yield to as much as 73% [15].

1.5.5 Fuels versus Chemicals

The nature of FT syncrudes is such that it lends itself to the recovery and refining of certain chemicals. The abundance of alkenes (olefins), oxygenates, and n-alkanes from iron based FTS presents the refinery designer with an extensive array of options for both extractive and synthetic approaches to the refining of chemicals. The chemicals that can be produced in an XTL facility are not limited to those obtained from FTS.

Because chemicals generally command a higher price than fuels, it makes sense from an economic point of view to produce as large a proportion of chemicals as possible. On the other hand, some of the high-value chemicals that are commercially produced from FT syncrude have rather small markets. In the case of linear α-olefins (1-hexene and 1-octene) and some oxygenates (1-propanol), 20–30% of global demand is being satisfied by a single Fe-HTFT facility [19].

Historically, investment in FT facilities was motivated more by the wish for energy security than by economic considerations. As a result, most FT facilities were primarily designed to produce transportation fuels. Over time, the original motivation may dissipate, and be replaced by financial prudence, which will favour the use of these facilities to produce chemicals rather than fuels. A flexible FT refinery design that accommodates the manufacturing of both fuels and chemicals has some advantages over those that produces only one of them.

On a molecular level, fuel and chemical co-production makes sense. Some molecules can easily be converted into either chemicals or fuels, whereas other molecules have efficient refining

pathways to only one of the two products. Forcing the conversion of a molecule into a product that requires a less efficient refining pathway is inherently wasteful. It also violates a number of 'green' chemistry principles (such as preventing waste, maximizing atom economy, and increasing energy efficiency).

1.5.6 Economics

The economics of indirect liquefaction are strongly affected by three factors: the cost of the carbon-containing feed material; product pricing; and the capital cost of the facility. What can be controlled is the design of the facility, which can contribute significantly to the efficiency of feed conversion. The feed cost can be trimmed through feed selection based on conversion efficiency, the carbon efficiency of the design, and the energy efficiency of the design. Carbon efficiency refers to the percentage of carbon in the feed that is incorporated into the product. It is also a means of measuring the success of the plant in converting one type of carbon-based energy carrier to another.

An FT refinery ultimately determines the extent of value addition. Product pricing is never constant, and more important, relative product pricing also changes over time. These variations, which are caused by global and local factors, cannot be anticipated or managed. What *can* be controlled is the design of the facility, which can provide the flexibility to respond to changes in product pricing. Philosophically speaking, the main aim of XTL is not power generation, although power generation may be a valuable (and inevitable) by-product.

1.5.7 Capital Cost

There is a large capital cost associated with indirect coal liquefaction based on FTS. The break-even crude oil price for a 50 000 bbl/day crude-oil-equivalent FT-based CTL facility in 2007 was reportedly around US$50–70 [20]. The capital cost associated with GTL facilities is lower, since

the conversion of natural gas into synthesis gas is less complex. Coal preparation and gasification contribute 30% or more of the capital cost, even before the price of utilities, gas cleaning, and air separation are taken into account, which brings the total for syngas preparation to more than 70% of the capital cost for CTL [19].

The production of the required synthesis gas can account for over 60% of the total spent on an FT complex [11]. There are interesting developments in the field of smaller scale FT-based designs for BTL. Of necessity their designers have to make compromises to reduce their complexity and size. In doing so, they can exploit some options for process integration and intensification that are not seen in the larger-scale designs. The decision to build an FT plant is still fraught with risk, because it has to be based on what the future price is perceived to be, the availability of petroleum crude oil, and local politics [25].

A great deal of the inertia in the modern energy system is attributable to its vast complexity and scale. Timescales that cover extended periods are required for planning and constructing new energy infrastructure, and these mean that strains within the system cannot be resolved easily or quickly. In the effort to conserve resources and reduce the impact of energy consumption on the environment researchers can contribute to improving the efficiency of the system by investigating the interaction between reaction and phase equilibrium in the FT reaction.

1.6 THESIS OVERVIEW

The aim of this thesis is to describe the behaviour and performance of an FT reactor in terms of the dynamic interaction between reaction equilibrium and vapour–liquid equilibrium (VLE). The chapters in the thesis have been written in the style of journal articles. Each of them has been published or submitted for publication in a reputable international science/engineering journal. The current status of each paper is given in the list of publications. The chapters were written independently of each other and can be read independently, as every one has its own abstract,

introduction and conclusion. The chapters have been arranged in a suggested order for reading, as each builds on the work and ideas described in the prior chapter.

Chapter 2 focuses on thermodynamic reaction equilibrium, because limited work has been done previously on the relationship between FT product distribution and thermodynamics. It starts with a review of the published research into FT thermodynamics, and explores the implications of thermodynamic equilibrium in the FT process. A stepwise chain-growth thermodynamic model is developed that predicts results and demonstrates that one-parameter Flory distribution can be developed from a thermodynamic basis, and uses thermodynamics to determine which the primary products of the FT reaction are. Finally, the thermodynamically-predicted product distribution under a constrained approach to equilibrium is determined.

Chapter 3 concerns the design of a VLE thermodynamic model for an FT reactor. Having studied a variety of the VLE models used by different researchers, the author considered it appropriate to conduct an experiment to measure actual vapour and liquid compositions under FT reaction conditions to ascertain whether Raoult's law is sufficient or whether other, more elaborate VLE models are required.

Chapter 4 uses VLE to explain the observed two-alpha product distribution in FT reactors. The writer discusses three possible scenarios of the Flory product distribution and VLE. The three cases assume that the reaction sets up a single alpha Flory distribution in the total (vapour + liquid) products; the vapour phase follows a single alpha distribution; and a single alpha distribution is set up in the liquid phase. Thereafter the consequences of these assumptions in conjunction with a simple Raoult's law VLE model on the exit product distributions are examined. A model is developed that further predicts a relationship between the two values of alpha.

Chapter 5 explores the connection between variation of residence time and chain length for products in a slurry phase FT reactor, applying an experimental method using deuterium tracer. This is followed by a discussion of the implications of these results for the modelling of the product distribution. The chain-length dependencies of secondary olefin reactions in FTS are also investigated.

Chapter 6 outlines a mathematical model that describes the behaviour and performance of an FT reactor as a reactive distillation column. This model is consistent with the two-alpha positive deviation product distribution observed earlier. It can explain the reaction rate behaviour observed when a switch was made from a continuously stirred tank reactor to a batch reactor.

Chapter 7 contains the writer's concluding remarks.

REFERENCES

[1] T. Nakata, D. Silva, M. Rodionov, Application of energy system models for designing a low-carbon society, *Prog. Energy Combust. Sci. 37* (2011) 462–502.

[2] A.F. Ghoniem, Needs, resources and climate change: Clean and efficient conversion technologies, *Prog. Energy Combust. Sci. 37* (2011) 15–51.

[3] Shell International BV, *Shell energy scenarios to 2050*, pp 7–8, http://www-static.shell.com/static/public/downloads/brochures/corporate_pkg/scenarios/shell_energy_scenarios_2050.pdf, Accessed 07 Nov. 2011.

[4] S. Desai, D.A. Klanecky, Meeting the needs of the water–energy nexus, *Chem. Eng. Prog. 107* (2011) 22–27.

[5] U.S. Census Bureau, Historical estimates of world population, International Data Base, http://www.census.gov/population/international/data/idb/worldpopinfo.php, Accessed 07 Nov. 2011.

[6] H.W. Cooper, Producing electricity and chemicals simultaneously, *Chem. Eng. Progress 106(2)* (2010) 24–32.

[7] V.W. Weekman, Gazing into an energy crystal ball, *Chem. Eng. Progress 106(6)* (2010) 23–27.

[8] E.D. Larson, G. Fiorese, G. Liu, R.H. Williams, T.G. Kreutz, S. Consonni, Co-production of synfuels and electricity from coal + biomass with zero net carbon emissions: an Illinois case study, *Energy Procedia 1* (2009) 4371–4378.

[9] R.H. Williams, E.D. Larson, G. Liu, T.G. Kreutz, Fischer–Tropsch fuels from coal and biomass: Strategic advantages of once-through ("polygeneration") configurations, *Energy Procedia 1* (2009) 4379–4386.

[10] A.P. Steynberg, H.G. Nel, Clean coal conversion options using Fischer–Tropsch technology, *Fuel 83* (2004) 765–770.

[11] M.E. Dry, Present and future applications of the Fischer–Tropsch process, *Appl. Catal. A: Gen. 276* (2004) 1–3.

[12] S.T. Sie, M.M.G. Senden, H.M.H. van Wechem, Conversion of natural gas to transportation fuels via the shell middle distillate synthesis process (SMDS), *Catal. Today 8* (1991) 371–394.

[13] U.S. Energy Information Administration, *International Energy Outlook 2011*, pp 6, http://www.eia.gov/forecasts/ieo/pdf/0484(2011).pdf, Accessed 07 Nov. 2011.

[14] International Energy Agency, Are we entering a golden age of gas?, *World Energy Outlook 2011 Special Report*, pp 7, http://www.worldenergyoutlook.org/docs/weo2011/WEO2011_GoldenAgeofGasReport.pdf, Accessed 07 Nov. 2011.

[15] M.E. Dry, Practical and theoretical aspects of the catalytic Fischer–Tropsch process, *Appl. Catal. A: Gen. 138* (1996) 319–344.

[16] H. Schulz, Short history and present trends of Fischer–Tropsch synthesis, *Appl. Catal. A: Gen. 186* (1999) 3–12.

[17] A.C. Vosloo, Fischer–Tropsch: a futuristic view, *Fuel Process. Technol. 71* (2001) 149–155.

[18] V.R. Ahon, E.F. Costa, J.E.P. Monteagudo, C.E. Fontes, E.C. Biscaia, P.L.C. Lage, A comprehensive mathematical model for the Fischer–Tropsch synthesis in well-mixed slurry reactors *Chem. Eng. Sci. 60* (2005) 677–694.

[19] A. de Klerk, *Fischer–Tropsch Refining*, 1st Ed., Wiley-VCH Verlag GmbH & Co. KGaA, 2011, pp 1–20.

[20] U.S. Energy Information Administration, *International Energy Outlook 2009*, pp 3, http://www.eia.gov/FTPROOT/forecasting/0484(2009).pdf, Accessed 29 May 2009.

[21] R.L. Espinoza, A.P. Steynberg, B. Jager, A.C. Vosloo, Low temperature Fischer–Tropsch synthesis from a Sasol perspective, *Appl. Catal. A: Gen. 186* (1999) 13–26.

[22] M.E. Dry, Fischer–Tropsch synthesis over iron catalysts, *Catal. Lett. 7* (1990) 241–252.

[23] B. Jager, M.E. Dry, T. Shingles, A.P. Steynberg, Experience with a new type of reactor for Fischer–Tropsch synthesis, *Catal. Lett. 7* (1990) 293–302.

[24] B. Jager, R. Espinoza, Advances in low temperature Fischer–Tropsch synthesis, *Catal. Today 23* (1995) 17–28.

[25] M.E. Dry, The Fischer–Tropsch process: 1950–2000, *Catal. Today 71* (2002) 227–241.

Chapter 2 : OLEFIN PSEUDO-EQUILIBRIUM IN THE FISCHER–TROPSCH REACTION

ABSTRACT

Overall or global thermodynamic equilibrium predicts a predominately methane product for the Fischer–Tropsch (FT) reaction. Even though the FT product distribution may not be described by overall thermodynamic equilibrium, there may be aspects of it that can be described by equilibrium. We postulate that an equilibrium is set up in the FT reaction between species, i.e. between hydrocarbon or a surface precursor of chain length n and that of chain length n+1, and thus although we do not have global equilibrium, we have an approach to equilibrium between the product species. As olefins are reactive under FT reaction conditions we initially postulate that an equilibrium distribution is set up between the α-olefins or a species that leads to α-olefins.

The calculated results predict that equilibrium between the species of any homologous series would results in a Flory-type distribution, where the ratio of the moles of species n to that of the moles of species n+1 would be constant. When the value of this ratio α is calculated for olefins, it is found that the experimentally measured values match those calculated and thus the measured and predicted distribution of the olefins agree. However, assuming that the alcohols or paraffin distribution approaches equilibrium, leads to calculated values of α that are not consistent with the experimental results. Therefore, there may be an equilibrium set up between species of either an olefin precursor or the olefins themselves which leads to the Flory-type distribution found in the FT reaction.

Keywords: *Fischer–Tropsch Thermodynamics; Product Distribution; Reaction Equilibrium; Olefin Reactivity.*

2.1 INTRODUCTION

The future of energy is directly linked to the future well-being and prosperity of the people of the world. One of the biggest challenges is to reduce poverty and raise living standards around the world. An important factor in achieving this goal is to meet the world energy needs safely, reliably and affordably, even as population and economic growth particularly in developing countries pushes global demand higher. At the same time we need to ensure that the progress of today does not come at the expense of future generations. We need to manage the risks to our climate and environment which includes taking meaningful steps to curb carbon dioxide emissions, while at the same time utilizing local resources to help maintain secure supplies. To meet these interlocking challenges we need an integrated set of solutions that includes expanding all economic energy sources, improving efficiency and mitigating emissions through the use of cleaner-burning fuels.

The Fischer–Tropsch (FT) process is an area that is receiving revived interest worldwide as a technology alternative to produce both clean transportation fuels and chemicals from synthesis gas. Fischer–Tropsch synthesis (FTS) is a process in which synthesis gas, a mixture of predominantly CO and H_2, obtained from gasification of coal, peat, biomass or natural gas is converted to a multi-component mixture of hydrocarbons [1, 2]. Products from the FTS form a complex multi-component mixture with substantial variation in carbon number and product type [3–8]. The main products are linear paraffins and α-olefins [9, 10]. FTS products can be described by a Flory-type [11] carbon number distribution when chain growth and termination rates are independent of chain size as shown in Equation (1):

$$m_n = (1-\alpha)\alpha^{n-1} \quad (1)$$

where m_n is the mole fraction of a hydrocarbon with chain length n and α is the chain growth probability factor independent of n. The chain growth probability factor α determines the total carbon number distribution of the FT products. Thus a simple polymerization mechanism should describe the FTS product distribution [12–14]. It can be seen from Equation (1) that a plot of the logarithm of the molar concentration versus the carbon number would produce a straight line plot whose slope is related to alpha (α) as shown in Figure 2.1.

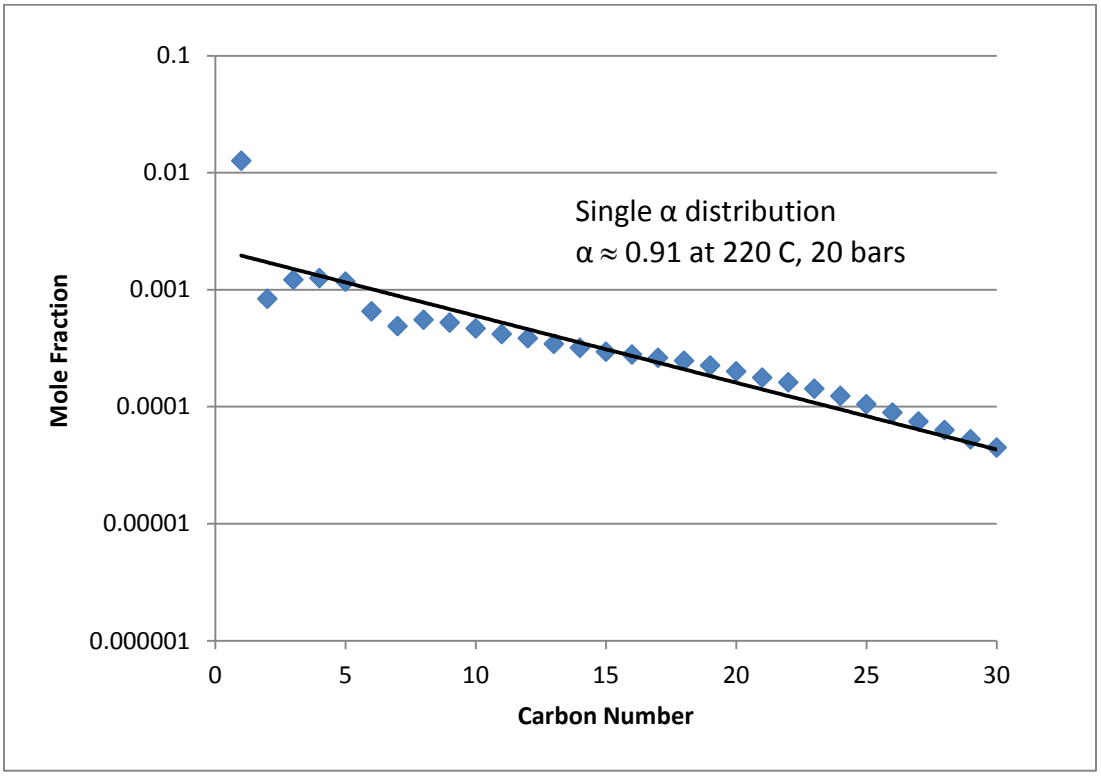


Figure 2.1: Typical product distribution for a Flory-type distribution reproduced from Reference [15]. The Flory distribution with a single alpha (α) is fitted to the data, where log(α) is the slope of the line. The data shows significantly higher methane and lower ethane selectivities than the Flory predictions.

Observed deviations from Flory distribution are abnormally high methane selectivity, low C_2 selectivity, and sometimes a two-alpha distribution with a positive deviation (this is discussed in Reference [16] and Chapter 4) as shown in Figure 2.2.

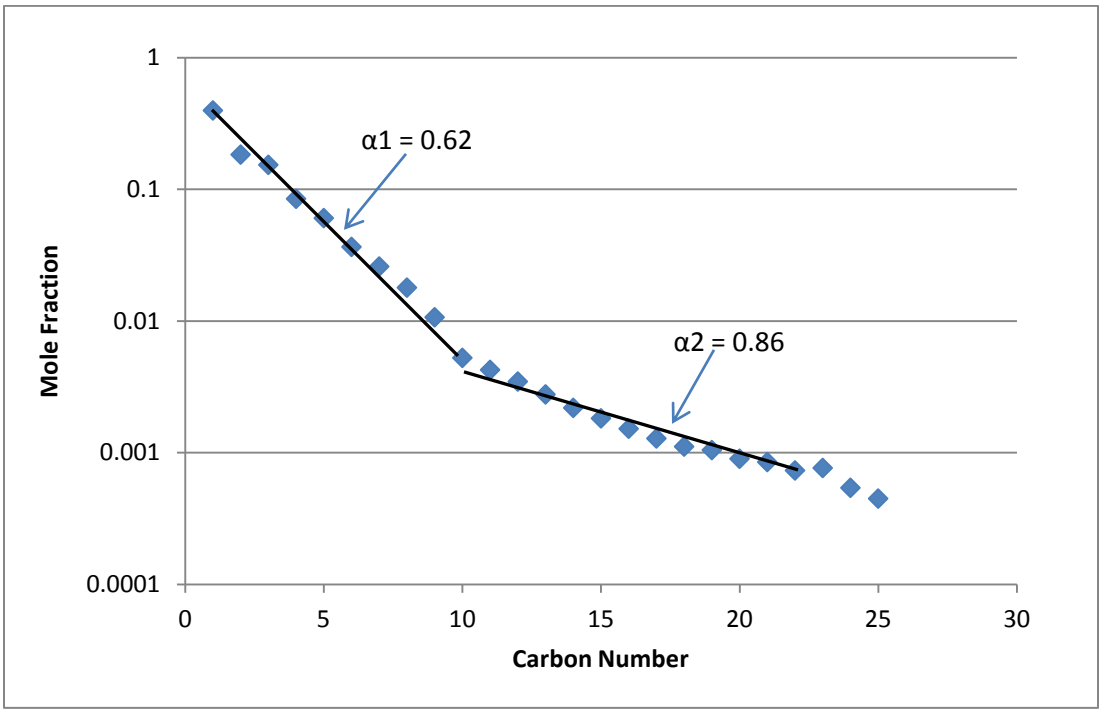


Figure 2.2: Two-alpha Fischer–Tropsch product distribution reproduced from Reference [16].

Most attempts to explain FTS have considered the reactions to be kinetically controlled and centre on mechanistic chain growth models or Flory product distribution models [17–20]. None of these mechanistic models can adequately handle the abnormally high methane and low ethane anomalies or explain the large effects of temperature on the product distribution [21].

Only limited work has been done on the relationship between the FT product distribution and thermodynamics [22–32]. There continues to be much work on the FTS with a key goal being to investigate the impact of changes in feed composition on the reaction rate and product distributions [33–37]. This continued search for a kinetic explanation ignores the issue that the FT process has many features of an equilibrium controlled system [38].

Therefore the aim of this article is to expand on the implications of thermodynamic equilibrium in the FT process, to develop a thermodynamic model that would predict similar results to a stepwise chain-growth model, to demonstrate that the one-parameter Flory distribution can be developed from a thermodynamic basis, to use thermodynamics to determine which are the primary products of the FT reaction, and finally to determine the thermodynamically predicted product distribution under constrained approach to equilibrium situations.

2.2 EQUILIBRIUM CONSIDERATIONS

Thermodynamic equilibrium analysis is an important tool in the study of reacting systems. It is an aid in reactor modelling, in examining kinetic schemes or reaction mechanisms, and in identifying rate-controlling processes [38].

Thermodynamic treatments of FTS given by a number of authors [22, 23] have tabulated the Gibbs free energies of reactions to form individual hydrocarbons. They showed that if global thermodynamic equilibrium was assumed, inevitably methane was the only stable hydrocarbon reaction product. This leaves us with a long-standing dilemma that, thermodynamically, long chain hydrocarbons should be present only in small concentrations. Yet large scale plants are operating using FTS. The thermodynamic driving force to form methane is so high that in practise the selective catalysis of longer chain hydrocarbons appears to be kinetically limited.

Bell [27] showed that this dilemma occurs because the thermodynamic properties of the catalyst were not correctly integrated with the thermodynamic equilibrium of hydrocarbon synthesis. He showed that it is thermodynamically possible to form hydrocarbons other than methane in the presence of a catalyst. This suggests that thermodynamic equilibrium is of much greater importance to the FT system than previously thought, and the decision to use a complex kinetics-based model rather than a simpler equilibrium based model should be taken with care.

Conventional equilibrium analysis, considers equilibrium with respect to the set of all specified reacting species of a system and all possible chemical reactions (that is, global equilibrium). However, in some situations arising in reactor or reaction modelling, partial equilibria may exist in which a subset of species attains equilibrium within the larger set of reacting species. Furthermore, equilibrium (whether full or partial) may be stoichiometrically restricted in that all possible chemical reactions are not involved. The usefulness of identifying partial equilibria stems from at least two considerations: reduction in the number of rate equations required in reactor modelling, for example, in calculating concentration profiles; and establishing and examining kinetic schemes and reaction mechanisms [26].

2.3 THERMODYNAMIC BASIS FOR A FLORY-TYPE PRODUCT DISTRIBUTION

Norval and Phillips [39] demonstrated that the Flory distribution can be derived from an equilibrium basis. In their development, they considered an FT product to be a partial equilibrium system; both the n-alkene and n-alkane homologous series achieve equilibrium among themselves, not with each other. Complete equilibrium among all the species does not occur. These results indicate that equilibrium may have a greater role in determining the product distribution of the FT process than has been thought previously.

Anderson [29] performed global equilibrium analyses for the FT synthesis and demonstrated that global equilibrium is not achieved. FT products could be a system at partial equilibrium; where some but not all species equilibrate. Such equilibrium would occur if reaction kinetics controlled the yield of hydrocarbons, and equilibrium controlled the hydrocarbon distribution. Thus, the chain growth/equilibration step must be fast relative to the rate of formation of the initial hydrocarbon species. This work assumes that the Fischer–Tropsch reaction can be described by a stepwise chain-growth reaction as shown below:

$$CO + 2H_2 + [-CH_2-]_{n-1} \leftrightarrow [-CH2-]_n + H_2O$$

This implies that the equilibrium constant for a hydrocarbon of chain length n is given by

$$K_n = \frac{[-CH_2-]_n}{[-CH_2-]_{n-1}} \frac{[H_2O]}{[CO][H_2]^2} \quad (2)$$

which results in

$$K_n = \alpha \frac{[H_2O]}{[CO][H_2]^2} \quad (3)$$

because the chain growth probability, α, is given by the ratio of the mole fraction of successive hydrocarbons. The values of the enthalpies of formation and the Gibbs free energies of formation of hydrocarbons [40] are plotted in Figure 2.3 and Figure 2.4 respectively.

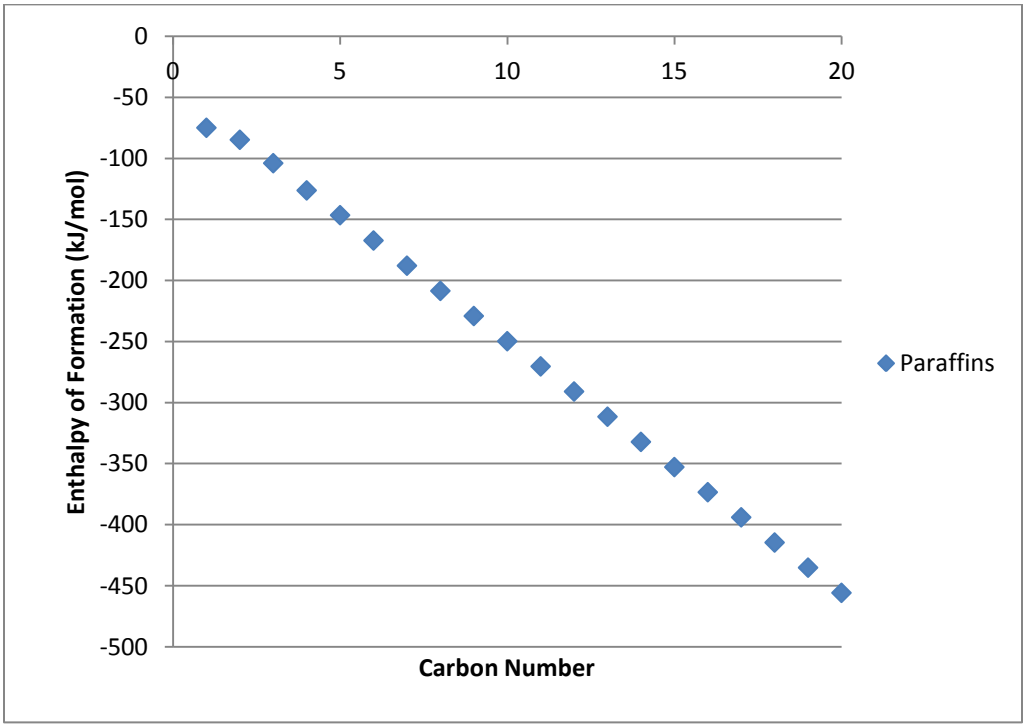


Figure 2.3: The change of enthalpies of formation with carbon number for paraffins.

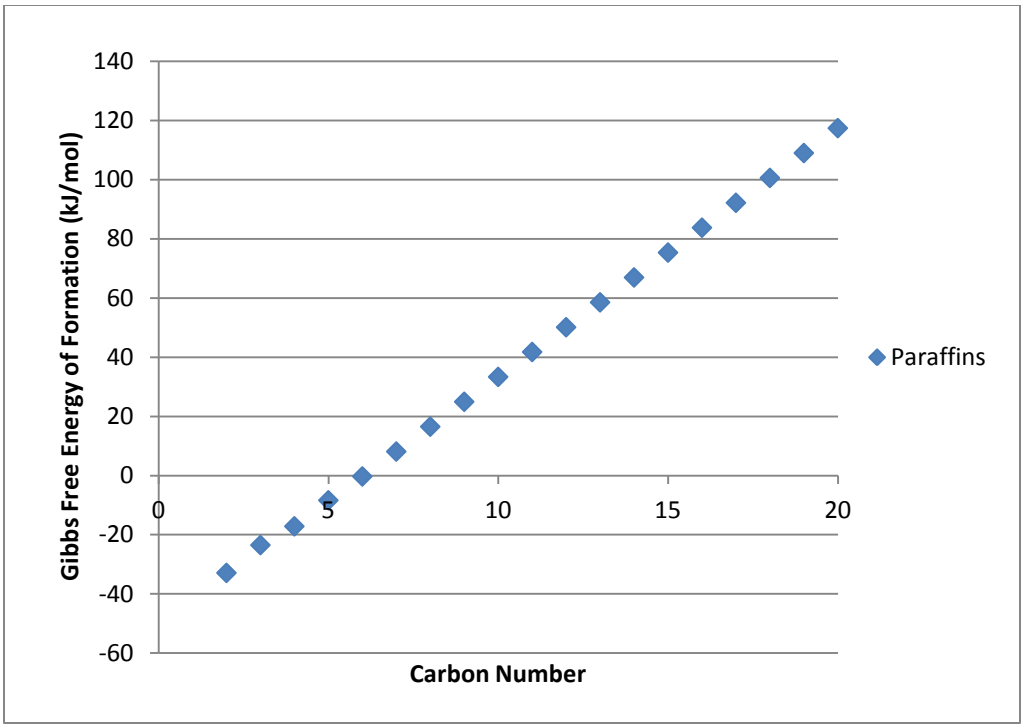


Figure 2.4: The change of Gibbs free energies of formation with carbon number for paraffins.

It can be seen from Figure 2.3 and 2.4 that the enthalpies and Gibbs free energies of formation vary linearly with carbon number for n > 2. Therefore the equilibrium constant is not a function of n for n > 2. Hence, $K_n \approx K$ for n>2.

For a gas phase reaction, assuming ideal gas behaviour, the equilibrium constant becomes:

$$K = \alpha \frac{y_{H2O}}{y_{CO} y_{H_2}^2 P^2} \qquad (4)$$

Thus for given conditions in a reactor at steady state; all compositions, pressure and temperature are not a function of n. Hence α is constant. This is consistent with the Flory product distribution which is consistent with a lot of experimental data [15].

Thus the result that the ratio of mole fractions of species (n+1) to that of species n being a constant ratio of α, is consistent both with the Flory distribution as well as the predictions of simple constrained thermodynamic equilibrium. The equilibrium model provides an equally acceptable mathematical fit of observed product distributions as do kinetics/mass transfer based models.

Even though overall system may not be at global equilibrium (as per Anderson) the relative amounts of the different species may be in pseudo constrained equilibrium. The focus of this constrained equilibrium is on the product thermodynamics and not the thermodynamics of the overall system including the catalyst. Therefore instead of minimising the Gibbs free energy for the whole system, we minimise it only for the specified products.

2.4 MINIMISING GIBBS FREE ENERGY FOR PARAFFINS AND/OR ALCOHOLS

If we consider that the products are formed from the elements inside the reactor then the Gibbs free energy of reaction to produce each product would be same as the Gibbs free energy of formation of that product. As shown in Figure 2.4 the Gibbs free energy of paraffins varies linearly with carbon number. This is also true for other homologous series. Therefore we can write

$$G_n = n\hat{G} + G_0 \qquad (5)$$

where G_n is the Gibbs free energy of formation/reaction for product with carbon number n, $\hat{G}$ is the average Gibbs free energy of formation/reaction per mole for the homologous series (hydrocarbons), and G_0 is the intercept for the plot of Gibbs free energy of formation versus carbon number.

If we convert a fixed N_C moles of carbon to hydrocarbons, and given that

$$\alpha = \frac{N_{i+1}}{N_i} \quad (6)$$

where α is the chain growth probability, and N_i is the amount (mole) of component i, it therefore follows that:

$$N_i = \alpha^{i-1} N_1 \quad (7)$$

This assumes that the graph of Gibbs free energy of formation versus carbon number is a straight line. Typically species n = 1 and 2, do not fit the straight line, and this could be taken into account if required by making the model slightly more complicated. This however does not change the overall conclusions from this approach. Under these simple assumptions, the amount of CO converted, N_C, is given by:

$$N_C = N_1 + 2N_2 + 3N_3 + \cdots \quad (8)$$

Which simplifies to

$$N_C = \frac{N_1}{(1-\alpha)^2} \quad (9)$$

For full derivation refer to Appendix A. Therefore

$$N_1 = (1-\alpha)^2 N_C \quad (10)$$

The total number of moles of hydrocarbons N_T is given by

$$N_T = \sum_{i=1}^{\infty} N_i = \frac{N_1}{1-\alpha} \quad (11)$$

Hence

$$N_T = (1-\alpha) N_C \quad (12)$$

The total Gibbs free energy of hydrocarbons is given by the Gibbs free energy of reaction plus the Gibbs free energy of mixing i.e.

$$G = \left(\hat{G}N_1 + 2\hat{G}N_2 + 3\hat{G}N_3 + \cdots\right) + (N_1 + N_2 + N_3 + \cdots)G_0 + RT(N_1 ln x_1 + N_2 ln x_2 + N_3 ln x_3 + \cdots) \quad (13)$$

where R is the universal gas constant, T is the temperature, and x_i is the mole fraction of component i, where $x_i = N_i/N_T$. Equation (13) simplifies to:

$$G = \hat{G}N_C + \frac{N_1}{1-\alpha}G_0 + RT\left(\frac{N_1 lnN_1}{1-\alpha} + \frac{N_1 \alpha ln\alpha}{(1-\alpha)^2} - N_T lnN_T\right) \quad (14)$$

Full derivations are shown in Appendix B. Substituting N_1 and N_T in terms of N_C gives

$$G = \hat{G}N_C + (1-\alpha)N_C G_0 + RT\{(1-\alpha)N_C ln[(1-\alpha)^2 N_C] + \alpha N_C ln\alpha - (1-\alpha)N_C ln[(1-\alpha)N_C]\} \quad (15)$$

Which is the same as

$$G = \hat{G}N_C + (1-\alpha)N_C G_0 + RTN_C\left\{(1-\alpha)ln\left[\frac{(1-\alpha)^2 N_C}{(1-\alpha)N_C}\right] + \alpha ln\alpha\right\} \quad (16)$$

Therefore

$$\frac{G}{N_C} - \hat{G} = (1-\alpha)G_0 + RT[(1-\alpha)ln(1-\alpha) + \alpha ln\alpha] \quad (17)$$

We have thus derived an expression for the Gibbs free energy of the mixture of hydrocarbons G given that a fixed number of moles of carbon or CO (N_C) are converted, which depends on α. Thus the value of α which minimizes G, would be the value equivalent to the product distribution that satisfies thermodynamic equilibrium. Taking the derivative of the Gibbs free energy with respect to alpha results in:

$$\frac{\partial G}{\partial \alpha} = -G_0 + RT[ln\alpha - ln(1-\alpha)] \quad (18)$$

At minimum

$$\frac{\partial G}{\partial \alpha} = 0 \quad (19)$$

Therefore

$$ln\alpha - ln(1-\alpha) = \frac{G_0}{RT} \quad (20)$$

which is the same as

$$ln\left(\frac{\alpha}{1-\alpha}\right) = \frac{G_0}{RT} \quad (21)$$

Equation (21) shows that the value of α at thermodynamic equilibrium depends on the intercept of the Gibbs free energy of reaction versus carbon number curve G_o and temperature T. Under the ideal assumption for the Gibbs free energy modelling, the resultant α is independent of pressure.

Alberty [41] observed that the Gibbs free energies of formation of alkene isomer groups are significantly less positive than for corresponding n-alkenes thus the alkene isomer groups would be expected to have significantly higher equilibrium mole fractions than would be expected if the increments per carbon atom for the n-alkenes applied. These observations are related to the slope of the Gibbs free energy versus carbon number curve. One fascinating finding of this constrained equilibrium approach is that the chain growth probability is dependent on the intercept of the Gibbs free energy of reaction/formation (G_0) versus carbon number. This has not previously been shown.

If we assume that the enthalpy of reaction does not change much with temperature then we can use the Gibbs–Helmholtz equation to determine the change of the Gibbs free energy of reaction with temperature. The integrated form of the Gibbs–Helmholtz equation is given by:

$$\frac{G_B}{T_B} = H\left(\frac{1}{T_B} - \frac{1}{T_A}\right) + \frac{G_A}{T_A} \quad (22)$$

Where G_B is the Gibbs free energy of reaction at temperature T_B, H is the enthalpy of reaction, and G_A is the Gibbs free energy of reaction at temperature T_A. Therefore the Gibbs free energies of reactions [40] at various temperatures were calculated for paraffins and are presented in Figure 2.5.

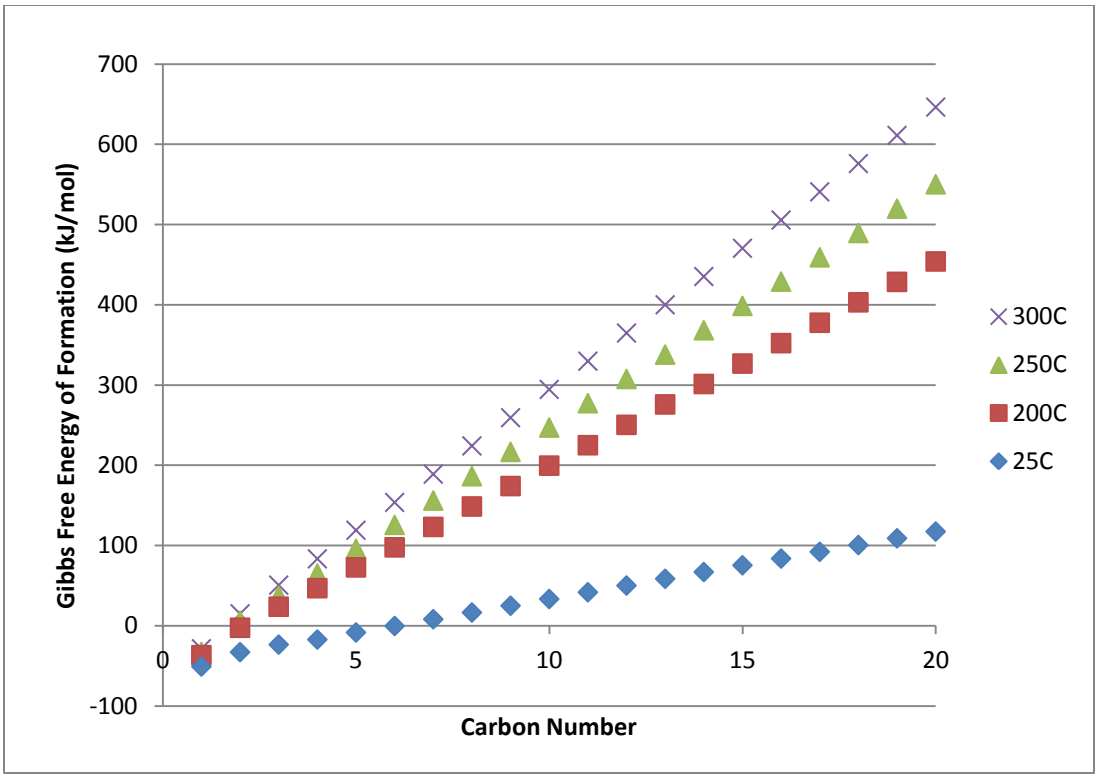


Figure 2.5: Gibbs free energies of formation/reaction with carbon number for paraffins at different temperatures.

The value of α in Equation (21) for paraffins was calculated using the intercepts in Figure 2.5 at various temperatures. The results are shown in Table 2.1.

Table 2.1: The predicted chain growth probability factor (α) at various temperatures for paraffins

Intercept/G_0 (kJ/mol)	Temperature (°C)	Alpha (α)
-54.037	200	1.08×10^{-6}
-55.181	250	3.09×10^{-6}
-56.326	300	7.34×10^{-6}

The value of α is very low which means that almost exclusively methane would be formed according to this analysis. This is consistent with literature results which showed that almost exclusively methane would be formed if global equilibrium was reached inside an FT reactor. However, this is not observed under normal FT operation. This suggests that the production of methane or paraffins is not at thermodynamic equilibrium and must therefore be kinetically determined.

A similar analysis could be done for other homologous series, such as alcohols. To calculate the Gibbs free energies of reaction for alcohols at different temperatures using Equation (22) the enthalpies of reaction are required. The values of the enthalpies of reactions with carbon number for alcohols [40] are presented Figure 2.6.

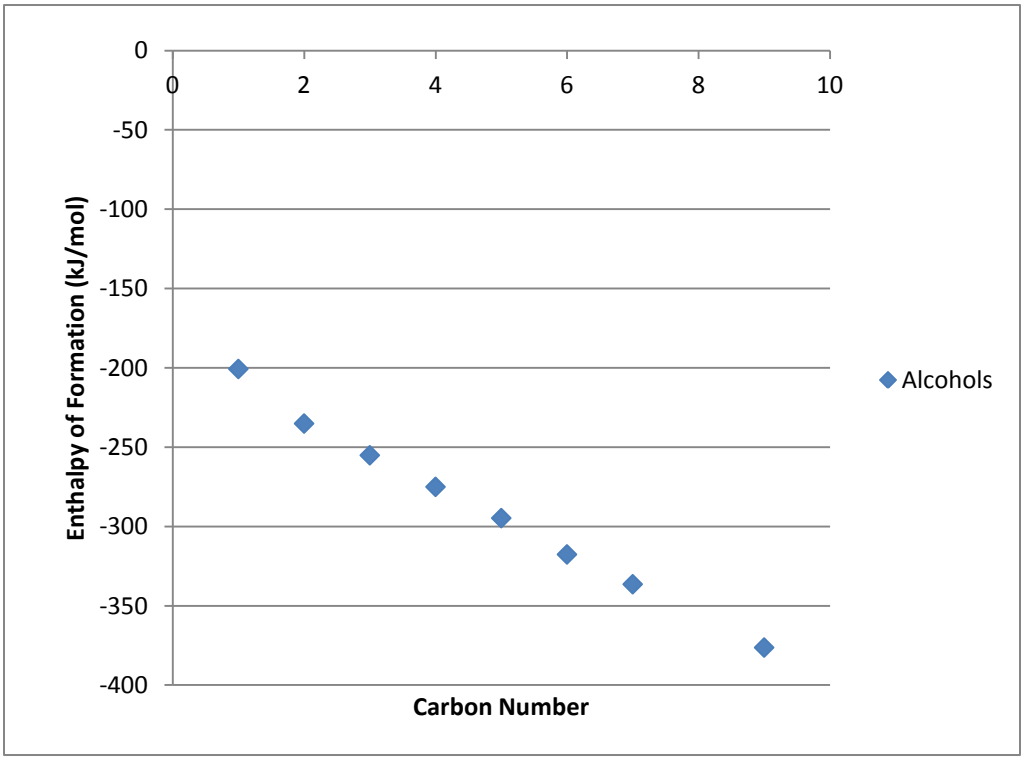


Figure 2.6: Change of enthalpies of formation/reaction for alcohols with carbon number.

The Gibbs–Helmholtz equation (Equation (22)) was used to work out the change of the Gibbs free energy of reaction [40] for alcohols with temperature and the results are shown in Figure 2.7.

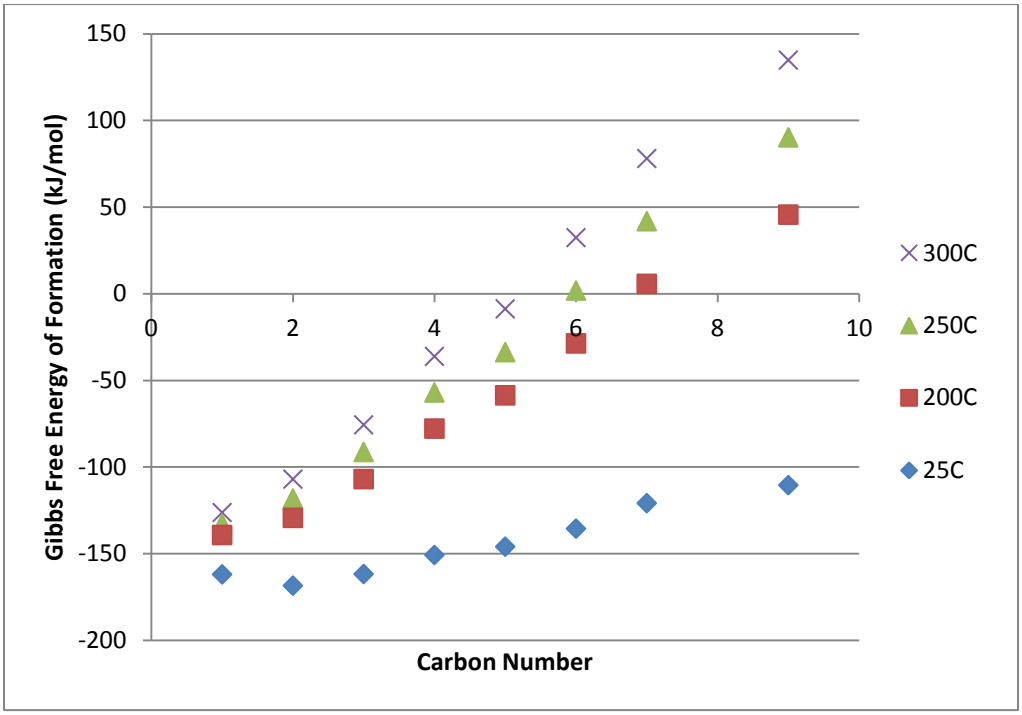


Figure 2.7: Gibbs free energies of formation/reaction with carbon number for alcohols at different temperatures.

The value of α in Equation (21) for alcohols was calculated using the intercepts in Figure 2.7 at various temperatures. The results are shown in Table 2.2.

Table 2.2: The predicted chain growth probability factor (α) at various temperatures for alcohols

Intercept/G_0 (kJ/mol)	Temperature (°C)	Alpha (α)
-182.12	200	0

-180.82	250	0
-179.53	300	0

The values of α are very small (approximately zero) at the temperatures explored. This implies that only methanol would be formed if equilibrium was set up as described here. This is not observed under normal FT operation.

Olefin readsorption has been experimentally verified [38, 42, 43]. A number of researchers have incorporated olefin readsorption on product distribution models [4, 44, 45]. As olefins are reactive under FT reaction conditions we suggest that it might be possible that an equilibrium distribution is set up between the α-olefins or a species that leads to α-olefins.

Furthermore, olefins had been extensively proposed to be the primary products for the FT reaction and were therefore considered as primary products. Paraffins and alcohols start with carbon number one. However, olefins start with carbon number two. Therefore, to work out the minimum Gibbs free energy for olefins the derivation has to begin with carbon-number two and we next look at the impact of this on the thermodynamic model.

2.5 MINIMISING GIBBS FREE ENERGY FOR OLEFINS

Similarly, if we consider that the olefin products are formed from elements inside the reactor then the Gibbs free energy of reaction to produce each product would be same as the Gibbs free energy of formation of that product. As before we can write

$$G_n = n\hat{G} + G_0 \tag{5}$$

We define α as before as:

$$\alpha = \frac{N_{i+1}}{N_i} \tag{6}$$

Therefore, from C_2 onwards ($i \geq 2$) then

$$N_i = \alpha^{i-2} N_2 \tag{23}$$

Then the amount of CO converted N_C is given by

$$N_C = 2N_2 + 3N_3 + 4N_4 + \cdots \tag{24}$$

which simplifies to

$$N_C = N_2 \left(\frac{2-\alpha}{(1-\alpha)^2}\right) \tag{25}$$

For full derivation refer to Appendix C. Therefore

$$N_2 = \frac{(1-\alpha)^2}{2-\alpha} N_C \tag{26}$$

The total number of moles of hydrocarbons N_T is given by

$$N_T = \sum_{i=2}^{\infty} N_i = \frac{N_2}{1-\alpha} \tag{27}$$

hence

$$N_T = \frac{1-\alpha}{2-\alpha} N_C \tag{28}$$

The total Gibbs free energy of hydrocarbons is given by the Gibbs free energy of reaction plus the Gibbs free energy of mixing i.e.

$$G = \left(2\hat{G}N_2 + 3\hat{G}N_3 + 4\hat{G}N_4 + \cdots\right) + (N_2 + N_3 + N_4 + \cdots)G_0 + RT[N_2 \ln(x_2) + N_3 \ln(x_3) + N_4 \ln(x_4) + \cdots] \tag{29}$$

which becomes

$$G = \hat{G}N_C + \frac{N_2}{1-\alpha} G_0 + RT\{[N_2 \ln(N_2) + N_3 \ln(N_3) + N_4 \ln(N_4) + \cdots] - N_T \ln(N_T)\} \tag{30}$$

Relating the moles of species i, N_i, to N_2 results in

$$G = \hat{G}N_C + \frac{N_2}{1-\alpha}G_0 + RT\{[N_2\ln(N_2) + \alpha N_2\ln(\alpha) + \alpha^2 N_2\ln(\alpha^2) + \cdots] + [\alpha N_2\ln(N_2) + \alpha^2 N_2\ln(N_2) + \alpha^3 N_2\ln(N_2) + \cdots] - N_T\ln(N_T)\} \quad (31)$$

which simplifies to

$$G = \hat{G}N_C + \frac{N_2}{1-\alpha}G_0 + RT\left\{\frac{N_2\ln(N_2)}{1-\alpha} + \frac{\alpha}{(1-\alpha)^2}N_2\ln(\alpha) - N_T\ln(N_T)\right\} \quad (32)$$

Substituting N_2 and N_T in terms of N_C gives

$$G = \hat{G}N_C + \frac{1-\alpha}{2-\alpha}N_C G_0 + RT\left\{\frac{1-\alpha}{2-\alpha}N_C ln\left[\frac{(1-\alpha)^2}{2-\alpha}N_C\right] + \frac{\alpha}{2-\alpha}N_C\ln(\alpha) - \frac{1-\alpha}{2-\alpha}N_C ln\left[\frac{1-\alpha}{2-\alpha}N_C\right]\right\} \quad (33)$$

which simplifies to

$$\frac{G}{N_C} - \hat{G} = \frac{1-\alpha}{2-\alpha}G_0 + RT\frac{1}{2-\alpha}\left[\alpha ln\left(\frac{\alpha}{1-\alpha}\right) + ln(1-\alpha)\right] \quad (34)$$

We thus have related the Gibbs free energy of the system to product distribution (α) and thus the equilibrium value of α would be that value which minimised the Gibbs free energy of the system G. Thus taking the derivative of the Gibbs free energy with respect to alpha results in

$$\frac{\partial G}{\partial \alpha} = \frac{-1(2-\alpha)-(1-\alpha)(-1)}{(2-\alpha)^2}G_0 + RT\left\{\frac{\alpha}{2-\alpha}\left[\frac{1-\alpha}{\alpha}\left(\frac{1(1-\alpha)-\alpha(-1)}{(1-\alpha)^2}\right)\right] + ln\left(\frac{\alpha}{1-\alpha}\right) * \left[\frac{1(2-\alpha)-\alpha(-1)}{(2-\alpha)^2}\right] + \frac{1}{2-\alpha}\left(\frac{-1}{1-\alpha}\right) + ln(1-\alpha) * \frac{1}{(2-\alpha)^2}\right\} \quad (35)$$

which simplifies to

$$\frac{\partial G}{\partial \alpha} = \frac{-1}{(2-\alpha)^2}G_0 + RT\frac{1}{(2-\alpha)^2}ln\left(\frac{\alpha^2}{1-\alpha}\right) \quad (36)$$

At the minimum value of G

$$\frac{\partial G}{\partial \alpha} = 0 \quad (19)$$

Therefore

$$RT\frac{1}{(2-\alpha)^2}ln\left(\frac{\alpha^2}{1-\alpha}\right) = \frac{1}{(2-\alpha)^2}G_0 \quad (37)$$

hence

$$ln\left(\frac{\alpha^2}{1-\alpha}\right) = \frac{G_0}{RT} \quad (38)$$

Full derivations are shown in Appendix C.

Equation (38) shows that the value of α again depends on the intercept of the Gibbs free energy of reaction versus carbon number curve and temperature, but the functional form of the dependence is somewhat different, in that the value of α is squared in the numerator of the natural logarithm term on the left hand side of Equation (38).

If we assume that the enthalpy of reaction does not change much with temperature then we can use the Gibbs–Helmholtz equation (Equation (22)) to work out the change of the Gibbs free energy of reaction with temperature as before. The enthalpies of reactions with carbon number for olefins [40] are presented Figure 2.8.

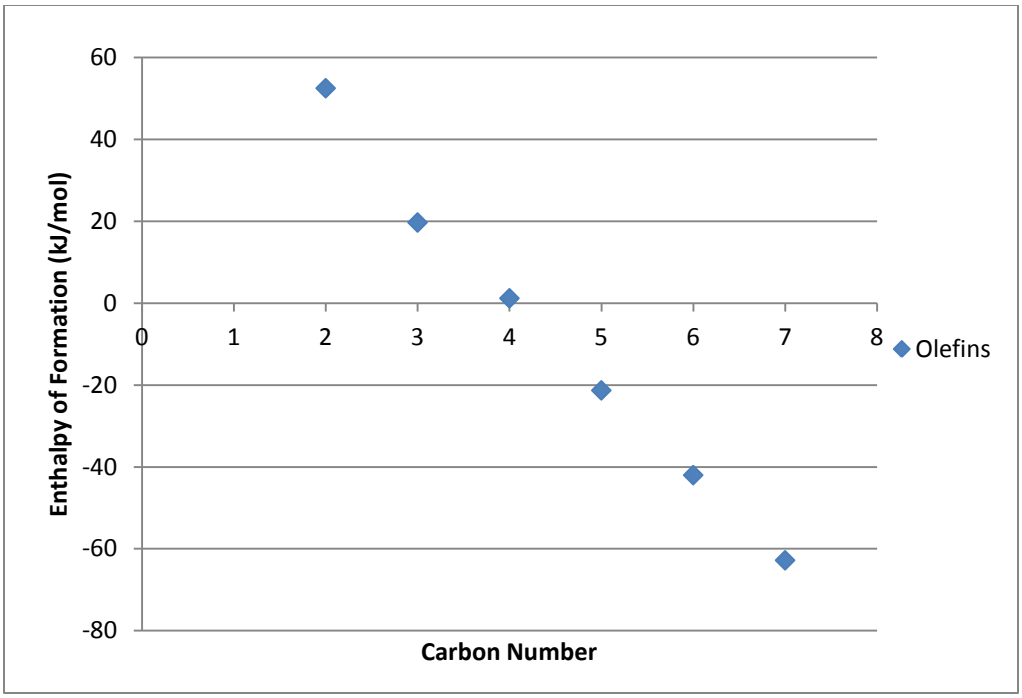


Figure 2.8: Change of enthalpies of formation/reaction for olefins with carbon number.

The enthalpies of reaction in Figure 2.8 were used in Equation (23) to calculate the Gibbs free energies of reaction at different temperatures. The Gibbs free energies of reactions [40] calculated for olefins are presented in Figure 2.9.

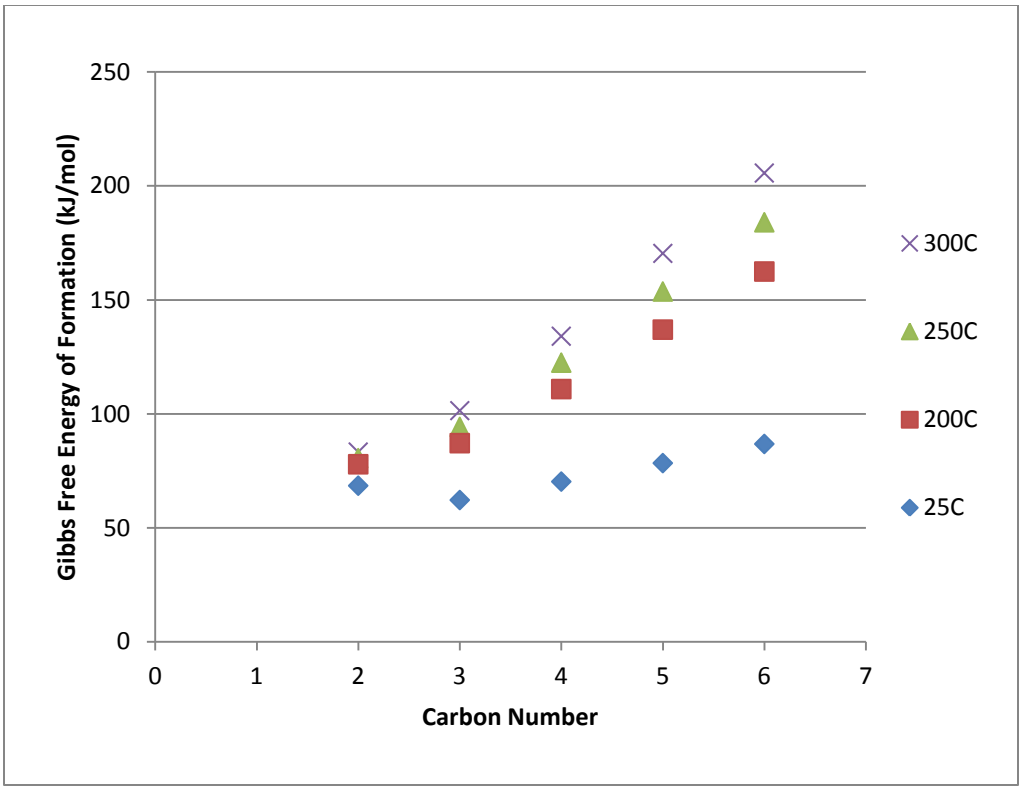


Figure 2.9: Gibbs free energies of formation/reaction with carbon number for olefins at different temperatures.

The value of α in Equation (38) for olefins was calculated using the intercepts in Figure 2.9 at various temperatures. The results are shown in Table 2.3.

Table 2.3: The predicted chain growth probability factor (α) at various temperatures for olefins

Intercept/G_0 (kJ/mol)	Temperature (°C)	Alpha (α)
10.997	200	0.945
3.4047	250	0.746
-4.1876	300	0.469

The results in Table 2.3 show that alpha decreases with increasing temperature. Dry [46] noted that the probability of chain growth (α) decreases as the temperature is increased irrespective of the catalyst type or of the feed gas composition. The predicted alpha values are in the range of the experimentally and industrially observed FT product distributions. Satterfield and Huff [47] found that the chain growth probability factor was 0.71 at 234 °C, 0.68 at 249 °C, and 0.67 at 269 °C. Jager and Espinoza [48] reported that the Sasol Tubular Fixed Bed Reactors operated at a shell-side temperature of about 220 °C with an alpha of 0.95. This suggests that even though we do not have global equilibrium, we might have an approach to equilibrium between the product species.

2.6 DISCUSSION

In kinetic models, the constant probability to react with a monomer of a growing chain results in a Flory-type product distribution. The equilibrium model provides an equally acceptable mathematical fit of the observed product distributions. The constant addition of CH_2-group to the free energy of formation of aliphatic chains causes the linear logarithmic molar distribution over carbon number. However, the value of the chain growth probability factor is set by the intercept of the Gibbs free energy of formation of the aliphatic group. These results imply that FT products could be a system at partial equilibrium in which some but not all species equilibrate. Such equilibrium would occur if the chain growth/equilibration step is fast relative to the rate of formation of the initial species.

The application of molecular modelling in heterogeneous catalysis research as a complement to experimental studies has grown rapidly in recent years [49, 50]. Density functional theory has been used to investigate the chain growth mechanisms of the FTS [51]. These approaches contribute to the understanding of the FT mechanism. However, the product distributions derived in this work are independent of mechanism and catalyst and therefore represent generic distributions. This presents an opportunity to compare catalysts on a generic basis.

These results illustrate that a pseudo-equilibrium may be set up between species of either an olefin precursor or the olefins themselves which leads to the Flory distribution found in the FT reaction. These results substantiate the fact that olefins are primary FT products and paraffins are formed from them since the product distribution is determined by the olefins. S. Soled *et al.* [52] presented results of a catalyst structure-function that supports a CO hydrogenation model with α-olefins formed as the primary products and n-paraffins formed during secondary reactions.

2.7 CONCLUSIONS

Literature results indicate that some equilibrium exists under Fischer–Tropsch conditions as indicated by the readsorption of olefins under FT conditions. The results obtained, consistent with literature results, show that overall thermodynamic equilibrium does not exist. If it did, exclusively methane would be the FT product.

A stepwise chain-growth thermodynamic model supports a single alpha Flory product distribution. The reaction model described in this work provides a method for calculating alpha from thermodynamic formulation. The model results show that the olefin product distribution is equilibrium determined. This also shows that α-olefins follow a single alpha product distribution at Fischer–Tropsch reaction conditions consistent with experimentally observed alphas. This substantiates the fact that olefins are primary FT products and paraffins are formed from them since the whole product distribution is determined by the olefins.

The results suggest that paraffins are formed by secondary reactions which are kinetically determined. Some paraffins might be primary products which would explain the abnormally high methane yields in the FT reactor. Therefore, equilibrium is of much greater importance to the FT system than previously thought.

One fascinating finding of this constrained equilibrium approach is that the chain growth probability is dependent on the intercept of the Gibbs free energy of reaction/formation (G_0) versus carbon number. This has not been exemplified before.

APPENDIX A: FULL SERIES DERIVATION

It is well known that the series

$$1 + \alpha + \alpha^2 + \cdots = \frac{1}{1-\alpha} \tag{A1}$$

For α < 1. Therefore the series

$$1 + 2\alpha + 3\alpha^2 + \cdots \tag{A2}$$

Can be written as

$$(1 + \alpha + \alpha^2 + \cdots) + (\alpha + 2\alpha^2 + 3\alpha^3 + \cdots) \tag{A3}$$

Which is the same as

$$\frac{1}{1-\alpha} + \alpha(1 + 2\alpha + 3\alpha^2 + \cdots) \tag{A4}$$

Therefore

$$\frac{1}{1-\alpha} + \alpha[(1 + \alpha + \alpha^2 + \cdots) + (\alpha + 2\alpha^2 + 3\alpha^3 + \cdots)] \tag{A5}$$

Thus

$$\frac{1}{1-\alpha} + \alpha\left[\frac{1}{1-\alpha} + \alpha(1 + 2\alpha + 3\alpha^2 + \cdots)\right] \tag{A6}$$

Hence

$$\frac{1}{1-\alpha} + \frac{\alpha}{1-\alpha} + \alpha^2[(1 + \alpha + \alpha^2 + \cdots) + (\alpha + 2\alpha^2 + 3\alpha^3 + \cdots)] \tag{A7}$$

Which is the same as

$$\frac{1}{1-\alpha} + \frac{\alpha}{1-\alpha} + \alpha^2\left[\frac{1}{1-\alpha} + \alpha(1 + 2\alpha + 3\alpha^2 + \cdots)\right] \tag{A8}$$

This results in

$$\frac{1}{1-\alpha} + \frac{\alpha}{1-\alpha} + \frac{\alpha^2}{1-\alpha} + \alpha^3[(1 + \alpha + \alpha^2 + \cdots) + (\alpha + 2\alpha^2 + 3\alpha^3 + \cdots)] \tag{A9}$$

Which reduces to

$$\frac{1}{1-\alpha} + \frac{\alpha}{1-\alpha} + \frac{\alpha^2}{1-\alpha} + \frac{\alpha^3}{1-\alpha} + \cdots \quad \text{(A10)}$$

Which can be written as

$$\frac{1}{1-\alpha}(1 + \alpha + \alpha^2 + \cdots) \quad \text{(A11)}$$

This is the same as

$$\frac{1}{1-\alpha}\left(\frac{1}{1-\alpha}\right) \quad \text{(A12)}$$

Which results in

$$\frac{1}{(1-\alpha)^2} \quad \text{(A13)}$$

APPENDIX B: DERIVATIONS FOR MINIMISING GIBBS FREE ENERGY FOR PARAFFINS AND/OR ALCOHOLS

Given that the Gibbs free energy of a homologous series varies linearly with carbon number. Then we can write

$$G_n = n\hat{G} + G_0 \tag{B1}$$

Where G_n is the Gibbs free energy of formation/reaction for product with carbon number n, $\hat{G}$ is the average Gibbs free energy of formation/reaction per mole for the homologous series (hydrocarbons), and G_0 is the intercept for the plot of Gibbs free energy of formation versus carbon number.

If we convert a fixed N_C moles of carbon to hydrocarbons, and given that

$$\alpha = \frac{N_{i+1}}{N_i} \tag{B2}$$

Where α is the chain growth probability, and N_i is the amount (mole) of component i, it therefore follows that:

$$N_i = \alpha^{i-1} N_1 \tag{B3}$$

The amount of CO converted, N_C, is given by:

$$N_C = N_1 + 2N_2 + 3N_3 + \cdots \tag{B4}$$

Or

$$N_C = N_1 + 2\alpha N_1 + 3\alpha^2 N_1 + \cdots \tag{B5}$$

Which is the same as

$$N_C = N_1(1 + 2\alpha + 3\alpha^2 + \cdots) \tag{B6}$$

Which becomes

$$N_C = \frac{N_1}{(1-\alpha)^2} \tag{B7}$$

For full series derivation refer to Appendix A. Therefore

$$N_1 = (1-\alpha)^2 N_C \tag{B8}$$

The total number of moles of hydrocarbons N_T is given by

$$N_T = \sum_{i=1}^{\infty} N_i = \frac{N_1}{1-\alpha} \tag{B9}$$

Hence

$$N_T = (1-\alpha) N_C \tag{B10}$$

The total Gibbs free energy of hydrocarbons is given by the Gibbs free energy of reaction plus the Gibbs free energy of mixing i.e.

$$G = \left(\hat{G}N_1 + 2\hat{G}N_2 + 3\hat{G}N_3 + \cdots\right) + (N_1 + N_2 + N_3 + \cdots)G_0 + RT(N_1 lnx_1 + N_2 lnx_2 + N_3 lnx_3 + \cdots) \tag{B11}$$

Where R is the universal gas constant, T is the temperature, and x_i is the mole fraction of component i, where $x_i = N_i/N_T$. But

$$N_i lnx_i = N_i ln\left(\frac{N_i}{N_T}\right) = N_i lnN_i - N_i lnN_T \tag{B12}$$

Therefore Equation (B11) can be written as

$$G = \hat{G}N_C + \frac{N_1}{1-\alpha}G_0 + RT[(N_1 lnN_1 + N_2 lnN_2 + N_3 lnN_3 + \cdots) - (N_1 lnN_T + N_2 lnN_T + N_3 lnN_T + \cdots)] \tag{B13}$$

Or

$$G = \hat{G}N_C + \frac{N_1}{1-\alpha}G_0 + RT[(N_1 lnN_1 + \alpha N_1 ln\alpha + \alpha^2 N_1 ln\alpha^2 + \cdots) + (\alpha N_1 lnN_1 + \alpha^2 N_1 lnN_1 + \alpha^3 N_1 lnN_1 + \cdots) - (N_1 + N_2 + N_3 + \cdots) lnN_T] \tag{B14}$$

Which simplifies to

$$G = \hat{G}N_C + \frac{N_1}{1-\alpha}G_0 + RT[N_1 lnN_1(1 + \alpha + \alpha^2 + \cdots) + N_1(\alpha ln\alpha + 2\alpha^2 ln\alpha + 3\alpha^3 ln\alpha + \cdots) - N_T lnN_T] \quad \text{(B15)}$$

Hence

$$G = \hat{G}N_C + \frac{N_1}{1-\alpha}G_0 + RT\left(\frac{N_1 lnN_1}{1-\alpha} + \frac{N_1 \alpha ln\alpha}{(1-\alpha)^2} - N_T lnN_T\right) \quad \text{(B16)}$$

Substituting N_1 and N_T in terms of N_C gives

$$G = \hat{G}N_C + (1-\alpha)N_C G_0 + RT\{(1-\alpha)N_C ln[(1-\alpha)^2 N_C] + \alpha N_C ln\alpha - (1-\alpha)N_C ln[(1-\alpha)N_C]\} \quad \text{(B17)}$$

Which is the same as

$$G = \hat{G}N_C + (1-\alpha)N_C G_0 + RTN_C\left\{(1-\alpha)ln\left[\frac{(1-\alpha)^2 N_C}{(1-\alpha)N_C}\right] + \alpha ln\alpha\right\} \quad \text{(B18)}$$

Therefore

$$\frac{G}{N_C} - \hat{G} = (1-\alpha)G_0 + RT[(1-\alpha)ln(1-\alpha) + \alpha ln\alpha] \quad \text{(B19)}$$

Taking the derivative of the Gibbs free energy with respect to alpha gives:

$$\frac{\partial G}{\partial \alpha} = -G_0 + RT\left[-1ln(1-\alpha) + (1-\alpha)\left(\frac{-1}{1-\alpha}\right) + 1ln\alpha + \alpha\left(\frac{1}{\alpha}\right)\right] \quad \text{(B20)}$$

Which is the same as

$$\frac{\partial G}{\partial \alpha} = -G_0 + RT[-ln(1-\alpha) - 1 + ln\alpha + 1] \quad \text{(B21)}$$

Or

$$\frac{\partial G}{\partial \alpha} = -G_0 + RT[ln\alpha - ln(1-\alpha)] \quad \text{(B22)}$$

At minimum

$$\frac{\partial G}{\partial \alpha} = 0 \quad \text{(B23)}$$

Therefore

$$ln\alpha - ln(1-\alpha) = \frac{G_0}{RT} \quad \text{(B24)}$$

Which is the same as

$$ln\left(\frac{\alpha}{1-\alpha}\right) = \frac{G_0}{RT} \quad \text{(B25)}$$

APPENDIX C: DERIVATIONS FOR MINIMISING GIBBS FREE ENERGY FOR OLEFINS

As in Appendix B we can write

$$G_n = n\hat{G} + G_0 \tag{C1}$$

We define α as before as:

$$\alpha = \frac{N_{i+1}}{N_i} \tag{C2}$$

Therefore, from C_2 onwards (i≥2) then

$$N_i = \alpha^{i-2} N_2 \tag{C3}$$

Then the amount of CO converted N_C is given by

$$N_C = 2N_2 + 3N_3 + 4N_4 + \cdots \tag{C4}$$

Or

$$N_C = 2N_2 + 3\alpha N_2 + 4\alpha^2 N_2 + \cdots \tag{C5}$$

Thus

$$N_C = 2N_2 + (2+1)\alpha N_2 + (2+2)\alpha^2 N_2 + \cdots \tag{C6}$$

Or

$$N_C = 2N_2(1 + \alpha + \alpha^2 + \cdots) + N_2(\alpha + 2\alpha^2 + 3\alpha^3 + \cdots) \tag{C7}$$

Which becomes

$$N_C = \frac{2N_2}{1-\alpha} + \frac{\alpha N_2}{(1-\alpha)^2} \tag{C8}$$

Or

$$N_C = N_2\left(\frac{2-\alpha}{(1-\alpha)^2}\right) \tag{C9}$$

Therefore

$$N_2 = \frac{(1-\alpha)^2}{2-\alpha} N_C \quad \text{(C10)}$$

The total number of moles of hydrocarbons N_T is given by

$$N_T = \sum_{i=2}^{\infty} N_i = \frac{N_2}{1-\alpha} \quad \text{(C11)}$$

Hence

$$N_T = \frac{1-\alpha}{2-\alpha} N_C \quad \text{(C12)}$$

The total Gibbs free energy of hydrocarbons is given by the Gibbs free energy of reaction plus the Gibbs free energy of mixing i.e.

$$G = \left(2\hat{G}N_2 + 3\hat{G}N_3 + 4\hat{G}N_4 + \cdots\right) + (N_2 + N_3 + N_4 + \cdots)G_0 + RT[N_2 \ln(x_2) + N_3 \ln(x_3) + N_4 \ln(x_4) + \cdots] \quad \text{(C13)}$$

Which becomes

$$G = \hat{G}N_C + \frac{N_2}{1-\alpha} G_0 + RT\{[N_2 \ln(N_2) + N_3 \ln(N_3) + N_4 \ln(N_4) + \cdots] - [N_2 \ln(N_T) + N_3 \ln(N_T) + N_4 \ln(N_T) + \cdots]\} \quad \text{(C14)}$$

Or

$$G = \hat{G}N_C + \frac{N_2}{1-\alpha} G_0 + RT\{[N_2 \ln(N_2) + N_3 \ln(N_3) + N_4 \ln(N_4) + \cdots] - N_T \ln(N_T)\} \quad \text{(C15)}$$

Relating the moles of species i, N_i to N_2 results in

$$G = \hat{G}N_C + \frac{N_2}{1-\alpha} G_0 + RT\{[N_2 \ln(N_2) + \alpha N_2 \ln(\alpha) + \alpha^2 N_2 \ln(\alpha^2) + \cdots] + [\alpha N_2 \ln(N_2) + \alpha^2 N_2 \ln(N_2) + \alpha^3 N_2 \ln(N_2) + \cdots] - N_T \ln(N_T)\} \quad \text{(C16)}$$

Or rearranging

$$G = \hat{G}N_C + \frac{N_2}{1-\alpha}G_0 + RT\{N_2\ln(N_2)\,[1+\alpha+\alpha^2+\cdots] + N_2[\alpha\ln(\alpha) + 2\alpha^2\ln(\alpha) + 3\alpha^3\ln(\alpha)+\cdots] - N_T\ln\,(N_T)\} \quad \text{(C17)}$$

Which simplifies to

$$G = \hat{G}N_C + \frac{N_2}{1-\alpha}G_0 + RT\left\{\frac{N_2\ln(N_2)}{1-\alpha} + \frac{\alpha}{(1-\alpha)^2}N_2\ln\,(\alpha) - N_T\ln\,(N_T)\right\} \quad \text{(C18)}$$

Substituting N_2 and N_T in terms of N_C gives

$$G = \hat{G}N_C + \frac{1-\alpha}{2-\alpha}N_C G_0 + RT\left\{\frac{1-\alpha}{2-\alpha}N_C ln\left[\frac{(1-\alpha)^2}{2-\alpha}N_C\right] + \frac{\alpha}{2-\alpha}N_C\ln(\alpha) - \frac{1-\alpha}{2-\alpha}N_C ln\left[\frac{1-\alpha}{2-\alpha}N_C\right]\right\} \quad \text{(C19)}$$

Which simplifies to

$$G = \hat{G}N_C + \frac{1-\alpha}{2-\alpha}N_C G_0 + RTN_C\frac{1}{2-\alpha}\left\{\alpha\ln\left(\frac{\alpha}{1-\alpha}\right) + ln(1-\alpha)\right\} \quad \text{(C20)}$$

Therefore

$$\frac{G}{N_C} - \hat{G} = \frac{1-\alpha}{2-\alpha}G_0 + RT\frac{1}{2-\alpha}\left[\alpha ln\left(\frac{\alpha}{1-\alpha}\right) + ln(1-\alpha)\right] \quad \text{(C21)}$$

Thus taking the derivative of the Gibbs free energy with respect to alpha results in

$$\frac{\partial G}{\partial\alpha} = \frac{-1(2-\alpha)-(1-\alpha)(-1)}{(2-\alpha)^2}G_0 + RT\left\{\frac{\alpha}{2-\alpha}\left[\frac{1-\alpha}{\alpha}\left(\frac{1(1-\alpha)-\alpha(-1)}{(1-\alpha)^2}\right)\right] + ln\left(\frac{\alpha}{1-\alpha}\right) * \left[\frac{1(2-\alpha)-\alpha(-1)}{(2-\alpha)^2}\right] + \frac{1}{2-\alpha}\left(\frac{-1}{1-\alpha}\right) + ln(1-\alpha) * \frac{1}{(2-\alpha)^2}\right\} \quad \text{(C22)}$$

Which simplifies to

$$\frac{\partial G}{\partial\alpha} = \frac{-1}{(2-\alpha)^2}G_0 + RT\left[\frac{2}{(2-\alpha)^2}ln\left(\frac{\alpha}{1-\alpha}\right) + \frac{1}{(2-\alpha)^2}ln(1-\alpha)\right] \quad \text{(C23)}$$

Same as

$$\frac{\partial G}{\partial\alpha} = \frac{-1}{(2-\alpha)^2}G_0 + RT\frac{1}{(2-\alpha)^2}\left[ln\left(\frac{\alpha}{1-\alpha}\right)^2 + ln(1-\alpha)\right] \quad \text{(C24)}$$

Therefore

$$\frac{\partial G}{\partial \alpha} = \frac{-1}{(2-\alpha)^2} G_0 + RT \frac{1}{(2-\alpha)^2} ln\left(\frac{\alpha^2}{1-\alpha}\right) \quad \text{(C25)}$$

At the minimum value of G

$$\frac{\partial G}{\partial \alpha} = 0 \quad \text{(C26)}$$

Therefore

$$RT \frac{1}{(2-\alpha)^2} ln\left(\frac{\alpha^2}{1-\alpha}\right) = \frac{1}{(2-\alpha)^2} G_0 \quad \text{(C27)}$$

Hence

$$ln\left(\frac{\alpha^2}{1-\alpha}\right) = \frac{G_0}{RT} \quad \text{(C28)}$$

NOMENCLATURE

m_n	mole fraction of hydrocarbon with chain length n
α	chain growth probability factor
K	equilibrium constant
y_i	mole fraction of component i in the vapour phase
P	total operating pressure
T	operating temperature
R	universal gas constant
G_n	Gibbs free energy of formation/reaction for product with carbon number n
$\hat{G}$	average Gibbs free energy of formation/reaction per mole for the homologous series
G_0	the intercept for the plot of Gibbs free energy of formation versus carbon number
G	total Gibbs free energy of hydrocarbons

G_A Gibbs free energy of reaction at temperature T_A

G_B Gibbs free energy of reaction at temperature T_B

H enthalpy of reaction

N_C moles of carbon converted to hydrocarbons

x_i mole fraction of component i ($x_i = N_i/N_T$)

N_i amount/mole of component i

N_T total number of moles of hydrocarbons

REFERENCES

[1] C.G. Visconti, E. Tronconi, G. Groppi, L. Lietti, M. Iovane, S. Rossini, R. Zennaro, Monolithic catalysts with high thermal conductivity for the Fischer–Tropsch synthesis in tubular reactors, *Chem. Eng. J. 171* (2011) 1294–1307.

[2] G.P. van der Laan, A.A.C.M. Beenackers, Kinetics and Selectivity of the Fischer–Tropsch synthesis: A literature review, *Catal. Rev. –Sci. Eng. 41* (1999**)** 255–318.

[3] A. Behkish, R. Lemoine, L. Sehabiague, R. Oukaci, B.I. Morsi, Gas holdup and bubble size behavior in a large-scale slurry bubble column reactor operating with an organic liquid under elevated pressures and temperatures, *Chem. Eng. J. 128* (2007) 69–84.

[4] E.W. Kuipers, I.H. Vinkenburg, H. Oosterbeek, Chain length dependence of α-olefin readsorption in Fischer–Tropsch synthesis, *J. Catal. 152* (1995) 137–146.

[5] X. Lu, D. Hildebrandt, X. Liu, D. Glasser, Making sense of the Fischer–Tropsch synthesis reaction: start-up, *Ind. Eng. Chem. Res. 49* (2010) 9753–9758.

[6] X. Zhu, X. Lu, X. Liu, D. Hildebrandt, D. Glasser, Study of radial heat transfer in a tubular Fischer–Tropsch synthesis reactor, *Ind. Eng. Chem. Res. 49* (2010) 10682–10688.

[7] Y. Yao, D. Hildebrandt, D. Glasser, X. Liu, Fischer–Tropsch synthesis using $H_2/CO/CO_2$ syngas mixtures over a cobalt catalyst, *Ind. Eng. Chem. Res. 49* (2010) 11061–11066.

[8] M.E. Dry, Catalytic aspects of industrial Fischer–Tropsch synthesis, *J. Mol. Catal. 17* (1982) 133–144.

[9] X. Lu, X. Zhu, D. Hildebrandt, X. Liu, D. Glasser, A new way to look at Fischer–Tropsch synthesis using flushing experiments, *Ind. Eng. Chem. Res. 50* (2011) 4359–4365.

[10] W. Zimmerman, D. Bukur, S. Ledakowicz, Kinetic model of Fischer–Tropsch synthesis selectivity in the slurry phase, *Chem. Eng. Sci. 47* (1992) 2707–2712.

[11] P.J. Flory, Molecular size distribution in linear condensation polymers, *J. Am. Chem. Soc. 58* (1936) 1877–1885.

[12] R.B. Anderson, H. Friedel, H.H. Scorch, Fischer–Tropsch reaction mechanism involving stepwise growth of carbon chain, *J. Chem. Phys. 19* (1951) 313–319.

[13] T.J. Donnelly, I.C. Yates, C.N. Satterfield, Analysis and prediction of product distributions of the Fischer–Tropsch Synthesis, *Energy Fuels 2* (1988) 734–739.

[14] A. Tavakoli, M. Sohrabi, A. Kargari, Application of Anderson–Schulz–Flory (ASF) equation in the product distribution of slurry phase FT synthesis with nanosized iron catalysts, *Chem. Eng. J. 136* (2008) 358–363.

[15] C.M. Masuku, W. Ma, D. Hildebrandt, D. Glasser, B.H. Davis, A vapor–liquid equilibrium thermodynamic model for a Fischer–Tropsch reactor, *Fluid Phase Equilib. 314* (2012) 38–45.

[16] C.M. Masuku, D. Hildebrandt, D. Glasser, The role of vapour–liquid equilibrium in Fischer–Tropsch product distribution, *Chem. Eng. Sci. 66* (2011) 6254–6263.

[17] N.E. Tsakoumis, M. Rønning, Ø. Borg, E. Rytter, A. Holmen, Deactivation of cobalt based Fischer–Tropsch catalysts: A review, *Catal. Today 154* (2010) 162–182.

[18] E. Iglesia, S.C. Reyes, R.J. Madon, Transport-enhanced α-olefin readsorption pathways in Ru-catalyzed hydrocarbon synthesis, *J. Catal. 129* (1991) 238–256.

[19] T. Komaya, A.T. Bell, Estimates of rate coefficients for elementary processes occurring during Fischer–Tropsch synthesis over Ru/TiO_2, *J. Catal. 146* (1994) 237–248.

[20] X. Zhan, B.H. Davis, Assessment of internal diffusion limitation on Fischer–Tropsch product distribution, *Appl. Catal. A: Gen 236* (2002) 149–161.

[21] Y.H. Kim, K.–W. Jun, H. Joo, C. Han, I.K. Song, A simulation study on gas-to-liquid (natural gas to Fischer–Tropsch synthetic fuel) process optimization, *Chem. Eng. J. 155* (2009) 427–432.

[22] D.F. Smith, Equilibrium conditions in the formation of hydrocarbons and alcohols from water gas, *Ind. Eng. Chem. 19* (1927) 801–803.

[23] A.W. Weitkamp, C.G. Frye, Relation of product composition to reaction mechanism, *Ind. Eng. Chem. 45* (1953) 363–367

[24] R.B. Anderson, Thermodynamics of the hydrogenation of oxides of carbon, *J. Phys. Chem. 90* (1986) 4806–4810.

[25] H.G. Stenger, C.F. Askonas, Thermodynamic product distributions for the Fischer–Tropsch synthesis, *Ind. Eng. Chem. Fundam. 25* (1986) 410–413.

[26] G.W. Norval, M.J. Phillips, R.W. Missen, W.R. Smith, Identification and application of partial chemical equilibria in reactor modeling, *AIChE J. 38* (1992) 1288–1293.

[27] M.C. Bell, Thermodynamically controlled catalysis: equilibria in Fischer–Tropsch synthesis, *Can. Metall. Q. 34* (1995) 331–341.

[28] R.J. Madon, E. Iglesia, Catalytic reaction rates in thermodynamically non-ideal systems, *J. Mol. Catal. A: Chem. 163* (2000) 189–204.

[29] B.W. Wojciechowski, Mechanistic consideration of paraffin, olefins and alcohol distributions in FT synthesis, *Can. J. Chem. Eng. 64* (1986) 149–153.

[30] E.W. Kuipers, C. Scheper, J.H. Wilson, I.H. Vinkenburg, H. Oosterbeek, Non-ASF product distributions due to secondary reactions during Fischer–Tropsch synthesis, *J. Catal. 158* (1996) 288–300.

[31] H. Schulz, M. Claeys, Kinetic modeling of Fischer–Tropsch product distribution, *Appl. Catal. A: Gen. 186* (1999) 91–107.

[32] E. Iglesia, Design, synthesis, and use of cobalt–based Fischer–Tropsch synthesis catalysts, *Appl. Catal. A: Gen. 161* (1997) 59–78.

[33] G.W. Norval, Notes on the issues of equilibrium in the Fischer–Tropsch synthesis, *Can. J. Chem. Eng. 86* (2008) 1062–1069.

[34] R.B. Anderson, The thermodynamics of the hydrogenation of carbon monoxide and related reactions, in: P.H. Emmett (Ed.), *Catalysis*, Vol. IV, Reinhold, New York, 1956, pp 1–27.

[35] H.H. Storch, N. Golumbic, R.B. Anderson, *The Fischer–Tropsch and related syntheses*, John Wiley & Sons Inc., New York, 1951, pp 9–35.

[36] R.B. Anderson, C.B. Lee, J.C. Machiels, The thermodynamics of the hydrogenation of oxides of carbon, *Can. J. Chem. Eng. 54* (1976) 590–594.

[37] R.B. Anderson, *The Fischer–Tropsch synthesis*, Academic Press Inc., 1984, pp 9–25.

[38] B. Shi, R.J. O'Brien, S. Bao, B.H. Davis, Mechanism of the isomerization of 1-alkene during iron-catalyzed Fischer–Tropsch synthesis, *J. Catal. 199* (2001) 202–208.

[39] G.W. Norval, M.J. Phillips, Application of equilibrium analysis to a Fischer–Tropsch product, *J. Catal. 126* (1990) 87–91.

[40] S.I. Sandler, *Chemical and Engineering Thermodynamics*, 3rd Ed., John Wiley & Sons Inc., 1999, pp 758–760.

[41] R.A. Alberty, Extrapolation of standard chemical thermodynamic properties of alkene isomer groups to higher carbon numbers, *J. Phys. Chem. 87* (1983) 4999–5002.

[42] C.A. Mims, J.J. Krajewski, K.D. Rose, M.T. Melchior, Residence times and coverage by surface intermediates during the Fischer–Tropsch synthesis, *Catal. Lett. 7* (1990) 119–126.

[43] L.–M. Tau, H.A. Dabbagh, B.H. Davis, Fischer–Tropsch synthesis: ^{14}C tracer study of alkene incorporation, *Energy Fuels 4* (1990) 94–99.

[44] R.J. Madon, S.C. Reyes, E. Iglesia, Primary and secondary reaction pathways in ruthenium-catalyzed hydrocarbon synthesis, *J. Phys. Chem. 95* (1991) 7795–7804.

[45] R.J. Madon, E. Iglesia, The importance of olefin readsorption and H_2/CO reactant ratio for hydrocarbon chain growth on ruthenium catalysts, *J. Catal. 139* (1993) 576–590.

[46] M.E. Dry, Practical and theoretical aspects of the catalytic Fischer–Tropsch process, *Appl. Catal. A: Gen. 138* (1996) 319–344.

[47] C.N. Satterfield, G.A. Huff, Carbon number distribution of Fischer–Tropsch products formed on an iron catalyst in a slurry reactor, *J. Catal. 73* (1982) 187–197.

[48] B. Jager, R. Espinoza, Advances in low temperature Fischer–Tropsch synthesis, *Catal. Today 23* (1995) 17–28.

[49] L.J. Broadbelt, R.Q. Snurr, Applications of molecular modeling in heterogeneous catalysis research, *Appl. Catal. A: Gen. 200* (2000) 23–46.

[50] I.M. Ciobîcă, G.J. Kramer, Q. Ge, M. Neurock, R.A. van Santen, Mechanisms for chain growth in Fischer–Tropsch Synthesis over Ru(0001), *J. Catal. 212* (2002) 136–144.

[51] D.–B. Cao, Y.–W. Li, J. Wang, H. Jiao, Chain growth mechanism of Fischer–Tropsch synthesis on Fe_5C_2(001), *J. Mol. Catal. A: Chem. 346* (2011) 55–69.

[52] S. Soled, E. Iglesia, R.A. Fiato, Activity and selectivity control in iron catalyzed Fischer–Tropsch synthesis, *Catal. Lett. 7* (1990) 271–280.

Chapter 3 : A VAPOUR–LIQUID EQUILIBRIUM THERMODYNAMIC MODEL FOR A FISCHER–TROPSCH REACTOR

ABSTRACT

Caldwell and van Vuuren (1986) were the first to realize the importance of vapour–liquid equilibrium (VLE) considerations in the Fischer–Tropsch (FT) synthesis modelling. They used Raoult's law to describe VLE. Recently, a variety of VLE thermodynamic models have been used to model FT products. Thus the aim of this study was to conduct an experiment to measure actual vapour and liquid compositions of long chains hydrocarbons under FT reaction conditions to ascertain whether Raoult's law is sufficient or other elaborate VLE models are required.

The results obtained show that VLE is attained inside an FT reactor. The measured vapour and liquid compositions (K-values) can be sufficiently described by Raoult's law. Hydrocarbons with carbon number greater than 18 deviates from Raoult's law. The deviations from Raoult's law are due to diffusion limitations. Elaborate thermodynamic models could be used given the pure component parameters with relevant mixing rules for a higher degree of accuracy.

Keywords: *Fischer–Tropsch Reactor Modeling, Vapour–Liquid Equilibrium, Thermodynamic Model, Raoult's Law*

3.1 INTRODUCTION

The case for investing in alternative fuel-production technology to reduce dependence on crude oil has become increasingly compelling due to the uncertainty in oil prices combined with diminishing oil reserves. The Fischer–Tropsch synthesis (FTS) is an area that is receiving revived interest worldwide as an alternative technology to produce transportation fuels as well as chemicals from synthesis gas. Earlier FTS models ignored the existence of vapour–liquid equilibrium (VLE) in the Fischer–Tropsch (FT) reactor.

Caldwell and van Vuuren [1] were the first to realize the importance of VLE considerations in the FTS modeling. They developed a criterion for predicting liquid phase formation and a method for calculating what fraction of the products will condense, and what the liquid and vapour compositions will be in FT reactors. The criterion is readily derived by determining the conditions under which the dew-point is reached for the mixture of reactants and products as formed by the catalyst in the reactor. They showed that for all practical purposes a liquid phase will form or persist if the Schulz–Flory plot intersects the vapour-pressure plot; i.e., at 220 °C the slope of the vapour-pressure versus carbon number curve is log(0.653) hence the dew-point will not be reached if $\alpha < 0.653$. They used Raoult's law to describe vapour–liquid equilibrium (VLE) because, the FT liquid product consists of mainly a mixture of n-alkanes which is certainly a good approximation to an ideal liquid mixture, and although the pressure in the FT synthesis usually exceeds that for which ideal gas behavior may be assumed, the partial pressures of the individual product components are very small.

Marano and Holder [2] argued against the simplifying assumption of using Raoult's law to describe all phase equilibria. They contended that while the heavier hydrocarbon components of the wax phase may well exhibit ideal-solution behavior, the non-hydrocarbons and lighter hydrocarbons do not. They also pointed out that neither can ideal-gas behavior be assumed for the vapour phase at typical reaction conditions (200–330 °C, 10–25 bar). Thus they developed K-value formulations for use in performing VLE calculations on FT systems. They showed that their model gives superior predictions of the dew point temperature relative to the formulation of

Caldwell and van Vuuren [1]. However their results also show that the vapour phase is nearly ideal and the vapour-phase fugacity coefficients are all near unity.

Recently, a number of researchers have considered VLE in the development of FT product distribution models. Fox and Tam [3] used the Peng–Robinson (PR) equation modified for the presence of water to simulate VLE on Aspen for a FT slurry reactor. Raje and Davis [4] used Raoult's law to investigate the effect of VLE on FT hydrocarbon selectivity for a deactivating catalyst in a slurry reactor. Zhan and Davis [5, 6] used Raoult's law to work out the role of VLE on two-alpha FT product distribution and to assess internal diffusion limitation on FT product distribution. Derevich *et al.* [7] used a modified PR equation of state (EOS) to develop methods for calculating the vapour–liquid thermodynamic equilibrium in FTS products. Srinivas *et al.* [8] used the ASPEN built in PR–EOS with modified Huron–Vidal mixing rules which has the same EOS and mixing rules as those in the model of Marano and Holder [2] to simulate the Fischer–Tropsch reactor as a reactive distillation system.

However, Ahon *et al.* [9] made rigorous calculation of the VLE through cubic EOS to describe the phase behavior for a well-mixed FT slurry reactor. Their rigorous VLE method uses parameters and mixture properties for C_{4+} estimated through the correlations of Marano and Holder [2], which are based on the asymptotic behavior of normal paraffins and 1-olefins. It shows that the ideal gas assumption does not affect appreciably the gas product distribution. On the other hand, it shows that the assumption of an almost ideal liquid solution affects the gas and liquid product distributions. However, the effect of this approximation on the overall product distribution was surprisingly small. This resulted from the fact that the largest relative deviations in the liquid and gas product distributions occur for the species with the smallest concentrations in these phases, i.e. the heavy hydrocarbons, which do not contribute substantially to the overall production of these species.

Considering a variety of VLE models used by different researcher to model FT products it was befitting to conduct an experiment to measure actual vapour and liquid compositions under FT reaction conditions to ascertain whether Raoult's law is sufficient or other elaborate VLE models are required.

3.2 A REVIEW OF RELEVANT VLE THERMODYNAMIC MODELS

In common practice, a chemical engineer is concerned with models for predicting VLE from a minimum amount of data, with a minimum set of parameters. For this purpose Raoult's law assumes that, the vapour phase is an ideal gas which is valid for low to moderate pressures, and it also assumes that the liquid phase is an ideal solution which is valid for systems comprised of chemically similar species.

However, non-idealities are always encountered. Thus, Redlich and Kwong [10] proposed an EOS containing two individual coefficients. While the equation can be used to calculate, with a good degree of accuracy, volumetric and thermal properties of pure components and of mixtures, its application to multi-component VLE calculations often gives poor results.

Soave [11] modified the Redlich–Kwong equation with the introduction of the acentric factor as a third parameter to propose an equation that could be extended successfully to multi-component VLE calculations. The Soave–Redlich–Kwong (SRK) equation rapidly gained acceptance by the hydrocarbon processing industry because of the relative simplicity of the equation and because of its capability for generating reasonably accurate equilibrium ratios in VLE calculations.

Although a two-constant EOS cannot be expected to give reliable predictions for all of the thermodynamic properties, Peng and Robinson [12] proposed an equation which gives improved liquid density values as well as accurate vapour pressures and equilibrium ratios.

Good correlations of VLE can be achieved by applying the same two-parameter cubic EOS to both phases. The results primarily depend on the method used for calculating parameters and, for mixtures, on the mixing rule. Using classical quadratic mixing rules to obtain parameters of the cubic EOS restricts its use to non-polar mixtures [13]. Huron and Vidal [14] proposed mixing rules in simple EOS for representing VLE of strongly non-ideal mixtures.

Many other thermodynamic models are not considered here because they have not been used to describe VLE in the FTS even though a few others have been considered in measuring the solubility of synthesis gas in the FT products [15–17].

Modeling VLE requires a choice of the EOS, the choice of pure component parameters, and the choice of mixing rules. The more constants the EOS has, the more mixing rules are required, and the more data is required for evaluating pure-component parameters. The Fischer–Tropsch reaction mechanism has been researched for over 80 years because of its complexity. Hence including VLE in modeling an FT reactor only compounds the intricacy. Thus simplicity and accuracy in VLE modeling is preferred. Consequently Raoult's law is tested to determine if it can model VLE in an FT reactor. If it is not sufficient other elaborate models would be investigated to find a simpler model that sufficiently describes VLE in an FT reactor.

3.3 EXPERIMENTAL SECTION

The FT reaction is carried out in a 1 L slurry phase CSTR autoclave reactor as shown in Figure 3.1. CO and H_2 are metered separately and premixed in a 0.5 L vessel before being fed to the reactor. The vapour phase products exit the reactor at the top and pass through a fritted filter and then through two traps in series. The warm trap is maintained at 100 °C, while the cold trap is maintained at 0 °C. The uncondensed gases from these two traps pass through a back-pressure regulator to a flow meter to measure the exit gas flow rate. The uncondensed gases are

periodically sampled and analysed by on-line gas chromatographs (GCs). The condensed products from the warm and cold traps are collected as required and analysed through off-line GCs. The liquid phase product is collected as required through the internal filter into the hot trap maintained at 200 °C.

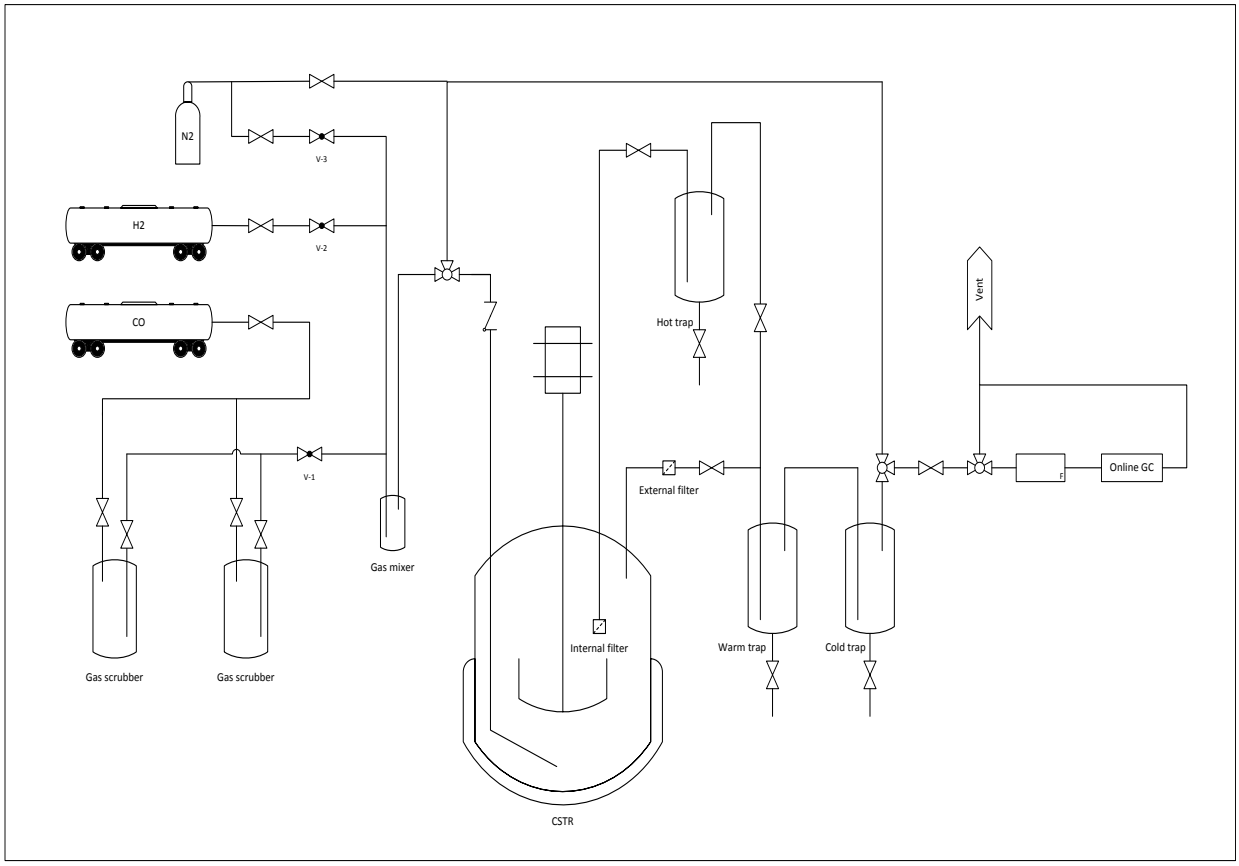


Figure 3.1: A schematic diagram of the Fischer–Tropsch reactor system.

A cobalt catalyst on alumina (25 % Co/Al_2O_3) with 0.5 % Pt was used. 8.6 grams of calcined catalyst were reduced ex situ in a plug flow reactor using 25 % H_2/He mixture at 350 °C for 10 h. The reduced catalyst was transferred to the 1 L CSTR which already contained 310 g of melted Polywax 3000 (polyethylene with average MW of 200) as a start-up solvent under flowing nitrogen. The catalyst was further reduced in situ using pure H_2 (15 slph) for 24 h at 230 °C. The

FT synthesis reaction was conducted at 220 °C, 2.0 MPa with space velocities ranging from 6.0 to 4.0 slph/g_cat) and at a constant H_2/CO ratio of 2.0.

The composition of the uncondensed product gases is obtained from a Hewlett–Packard Quad Series Micro GC, specifically used as a refinery gas analyser (RGA). The micro GC has four columns that run in parallel. This is used to obtain the mole fractions of CO, H_2, N_2, CO_2, and C_1 to C_6 hydrocarbons in the uncondensed product gases.

The condensed liquid products are separated into an aqueous and a hydrocarbon (oil + wax) phase. The aqueous phase is analysed in a Hewlett–Packard 5790A gas chromatograph with a Porapak Q packed column using a thermal conductivity detector. The oil (vapour) phase is analysed using a 6890 Agilent GC with a DB-5 capillary column and a flame ionization detector (FID). The wax (liquid) phase is analysed using 6890 Agilent GC FID with a high temperature DB-1 capillary column.

3.4 FISCHER–TROPSCH RESULTS AND DISCUSSION

Current commercial FT reactors operate at two different temperature ranges [18]. The high temperature FT operates with iron catalysts at about 340 °C and is geared mainly at the production of olefins and gasoline. The low temperature FT, using either iron or cobalt based catalysts at about 230 °C, is geared at the production of diesel and linear waxes. Raoult's law is valid for low pressures and high temperatures. Therefore if it is possible to describe VLE for low temperature FT then it should be sufficient for high temperature FT as well. VLE modeling is catalyst insensitive. Either cobalt or iron can be used to investigate VLE in an FT reactor. Therefore a cobalt catalyst was used at 220 °C, 2.0 MPa for the investigation. One can of course use more complicated models but if the results show that it is satisfactory to use Raoult's law which requires no extra parameters would be a huge advantage.

A number of FT catalysts have a high initial activity and then decline to a lower stable reaction rate [19, 20]. It is well known that the CO conversion increases with decreasing space velocity [21–24]. Therefore the synthesis experiment was started at a high space velocity to get a lower initial activity. As the activity dropped the space velocity was gradually decreased to have a reasonable synthesis rate and conversion. Therefore the FT reaction was started at a space velocity of 6 standard litres per hour per gram of catalyst (slph/g_cat). The space velocity was changed from 6 to 5 and then to 4 over the course of the experiment as shown in Figure 3.2.

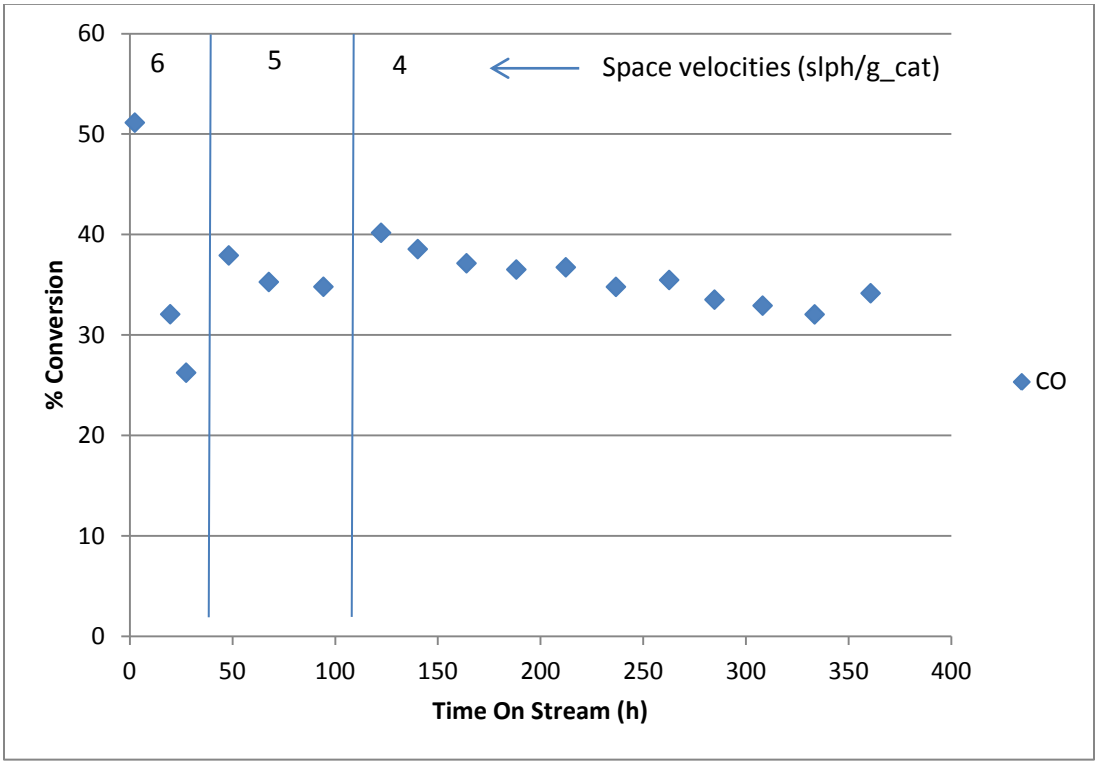


Figure 3.2: Percentage CO conversion at various space velocities for the FT experiment (220 °C, 2.0 MPa, H_2:CO = 2:1).

The results show that at 6 slph/g_cat the system was not yet at steady state. Thus the results for 6 slph/g_cat are not considered as part of the model evaluation. It has been shown that alpha increases as the space velocity decreases [21–24]. VLE is not a function of space velocity. Once VLE is reached inside a reactor, changing the space velocity should not change the ratio of the

mole fraction in the vapour phase to the mole fraction in the liquid phase (i.e. y_i/x_i). Therefore VLE results are expected to be insensitive to the changes in space velocity.

Most studies assume that the Anderson–Schulz–Flory (ASF) distribution is a model of the product selectivity [25–27]. It describes the entire product range by means of a single parameter, α, which represents the probability of the addition of a carbon intermediate to a chain. However, significant deviations have been reported in literature [28–30], and the results of some of these researchers show a two-alpha negative deviation [23, 31]. However, the most prevalent deviation is the two-alpha positive deviation [21, 23, 24, 32–35]. Other reported deviations are relatively high yield of methane and low yield of ethane [36]. An FT product distribution as presented in Figure 3.3 with an alpha of around 0.91 was obtained at a space velocity of 4 slph/g_cat.

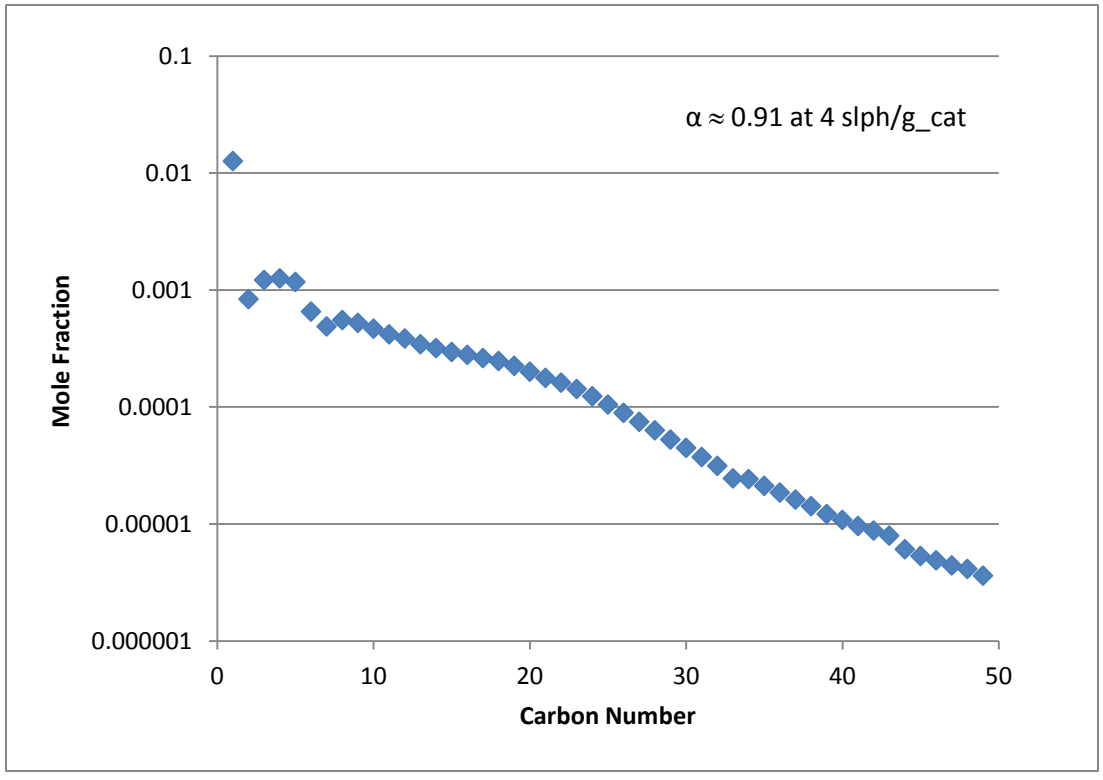


Figure 3.3: FT product distribution at a space velocity of 4 slph/g_cat (α ≈ 0.91, 220 °C, 2.0 MPa, H_2:CO = 2:1)

The observed product distribution is a single alpha ASF distribution with a relatively high yield of methane and low yield of ethane. On average alpha was 0.88 at a space velocity of 6, 0.9 at a space velocity of 5 and 0.91 at a space velocity of 4 slph/g_cat.

3.5 POLYWAX MASS FRACTION INSIDE THE REACTOR

The CSTR initially contained 310 g of polywax 3000 start-up solvent. To be able to determine the liquid composition, the amount of solvent inside the reactor has to be quantified. The liquid phase product is collected as required through the internal filter into the hot trap maintained at 200 °C. This product contains FT products and the polywax solvent.

The polywax mass fraction inside the reactor is estimated by considering that the volume of liquid is constant inside the reactor. This describes the way the reactor operates because the tube through which the liquid sample is collected is at a fixed level/height inside the reactor. Once the liquid volume inside the reactor reaches the liquid sampling tube, the liquid in contact with the tube is collected at the subsequent sampling time. Thus, maintaining an almost constant liquid level inside the reactor.

According to the material safety data sheet the density of polywax 3000 at 25 °C is 980 kg/m^3. For an ASF product distribution, Caldwell and van Vuuren [1] showed that the average carbon number is given by

$$\bar{n} = \frac{1}{1-\alpha} \qquad (1)$$

Therefore, for an average alpha of 0.9 the average carbon number is 10. If we assume that the properties of the FT products can be approximated by the properties of the average carbon number then according to ASPEN PLUS 13.2 the average density decane at 25 °C is 726 kg/m^3 and at 220 °C it is 556 kg/m^3. If we assume that the density of the polywax changes in a similar

manner as the density of decane then the density of the polywax 3000 at 220 °C using ratio and proportion is 750 kg/m^3.

The initial liquid volume inside the reactor is given by

$$V_i = \frac{310g}{0.75g/ml} \tag{2}$$

If B_1 grams of FT products are formed inside the reactor before sampling, then the mass fraction of polywax inside the reactor would be

$$m_{polywax1} = \frac{310}{310+B_1} \tag{3}$$

The mass fraction of FT products would be

$$m_{FT1} = \frac{B_1}{310+B_1} \tag{4}$$

Therefore, the density of the reactor content would be given by

$$\rho_{R1} = \frac{\rho_{polywax}\rho_{FT}}{m_{polywax1}\rho_{FT}+m_{FT1}\rho_{polywax}} \tag{5}$$

Hence, the volume inside the reactor before sampling

$$V_1 = \frac{310+B_1}{\rho_{R1}} \tag{6}$$

To maintain a constant volume inside the reactor, during sampling the volume of the material collected would be

$$V_{s1} = V_1 - V_i \tag{7}$$

Therefore, the mass of the material collected would be

$$A_1 = \rho_{R1}V_{s1} \tag{8}$$

This mass should match the mass of the liquid sample collected which is achieved by varying the mass of FT products formed inside the reactor (B_1) until A_1 is the same as the mass of sample collected. Therefore, the mass of polywax removed would be

$$M_{polywax,removed1} = m_{polywax1} \times A_1 \quad (9)$$

Thus, the mass of polywax remaining in the reactor would be

$$M_{polywax1} = 310 - M_{polywax,removed1} \quad (10)$$

The FT product removed would be

$$M_{FT,removed1} = m_{FT1} \times A_1 \quad (11)$$

Therefore, the FT products remaining inside the reactor would be

$$M_{FTR1} = B_1 - M_{FT,removed1} \quad (12)$$

Hence, the total liquid mass remaining in the reactor is

$$M_{R1} = M_{polywax1} + M_{FTR1} \quad (13)$$

For the next liquid sample; if B_2 grams of FT products are formed inside the reactor before sampling, then the mass fraction of polywax inside the reactor would be

$$m_{polywax2} = \frac{M_{polywax1}}{M_{R1}+B_2} \quad (14)$$

Therefore, the mass fraction of FT products would be

$$m_{FT2} = \frac{M_{FTR1}+B_2}{M_{R1}+B_2} \quad (15)$$

Thus, the density of the reactor content would be given by

$$\rho_{R2} = \frac{\rho_{polywax}\rho_{FT}}{m_{polywax2}\rho_{FT}+m_{FT2}\rho_{polywax}} \quad (16)$$

Hence, the volume inside the reactor before sampling would be

$$V_2 = \frac{M_{FTR1}+B_2}{\rho_{R2}} \quad (17)$$

To maintain a constant volume inside the reactor, during sampling the volume of the material collected would be

$$V_{s2} = V_2 - V_i \tag{18}$$

Therefore, the mass of the material collected would be

$$A_2 = \rho_{R2} V_{s2} \tag{19}$$

This mass should match the mass of the liquid sample collected which is achieved by varying the mass of FT products formed inside the reactor (B_2) until A_2 is the same as the mass of sample collected. Therefore, the mass of polywax removed would be

$$M_{polywax,removed2} = m_{polywax2} \times A_2 \tag{20}$$

Thus, the mass of polywax remaining in the reactor would be

$$M_{polywax2} = M_{polywax1} - M_{polywax,removed2} \tag{21}$$

The FT product removed would be

$$M_{FT,removed2} = m_{FT2} \times A_2 \tag{22}$$

Therefore, the FT products remaining inside the reactor would be

$$M_{FTR2} = M_{FTR1} + B_2 - M_{FT,removed2} \tag{23}$$

Hence, the total liquid mass remaining in the reactor is

$$M_{R2} = M_{polywax2} + M_{FTR2} \tag{24}$$

This calculation is done for each liquid sample taken at different times. The polywax mass fractions obtained are presented in Figure 3.4.

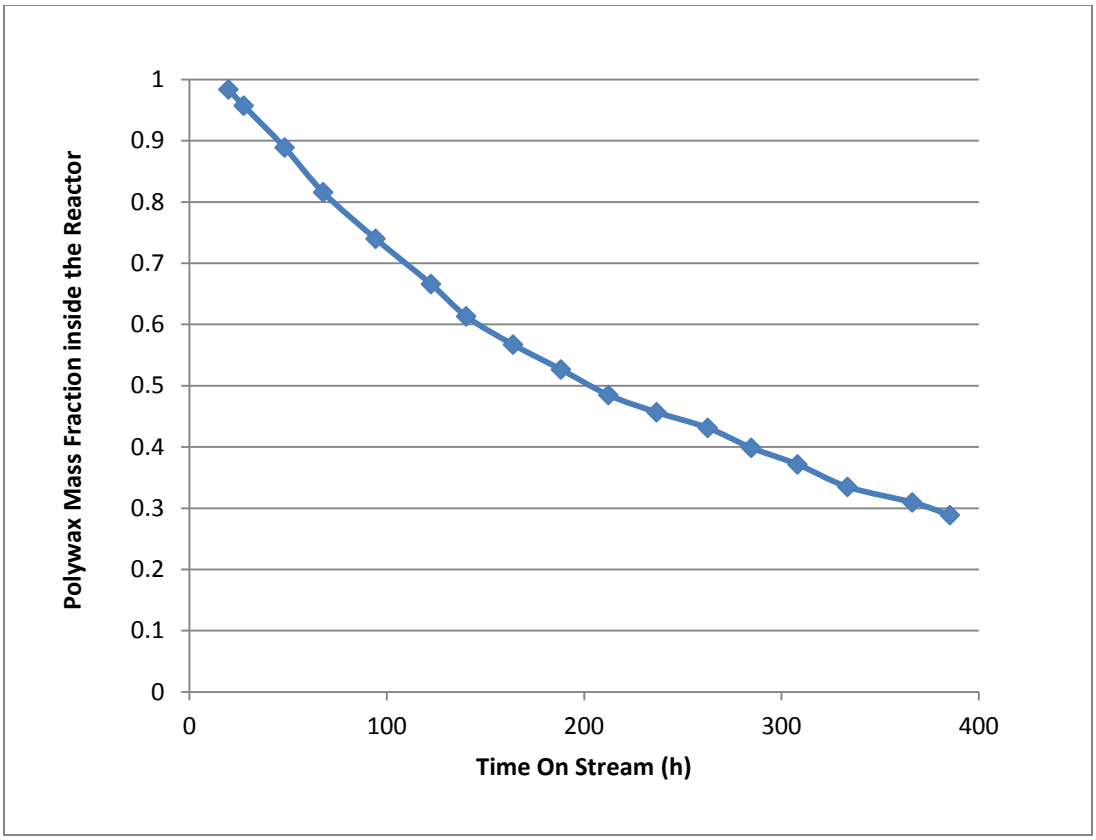


Figure 3.4: Polywax mass fraction inside the reactor for the duration of the experiment calculated by considering constant volume inside the reactor. The TOS in this Figure corresponds to the TOS presented in Figure 3.2.

The result in Figure 3.4 show that the polywax mass fraction changes with time on stream which would result in a liquid density change inside the reactor. Considering the constant liquid volume permits the variation of the liquid mass and the liquid density. The results for the variation of the liquid mass and the liquid density with time on stream are presented in Figure 3.5.

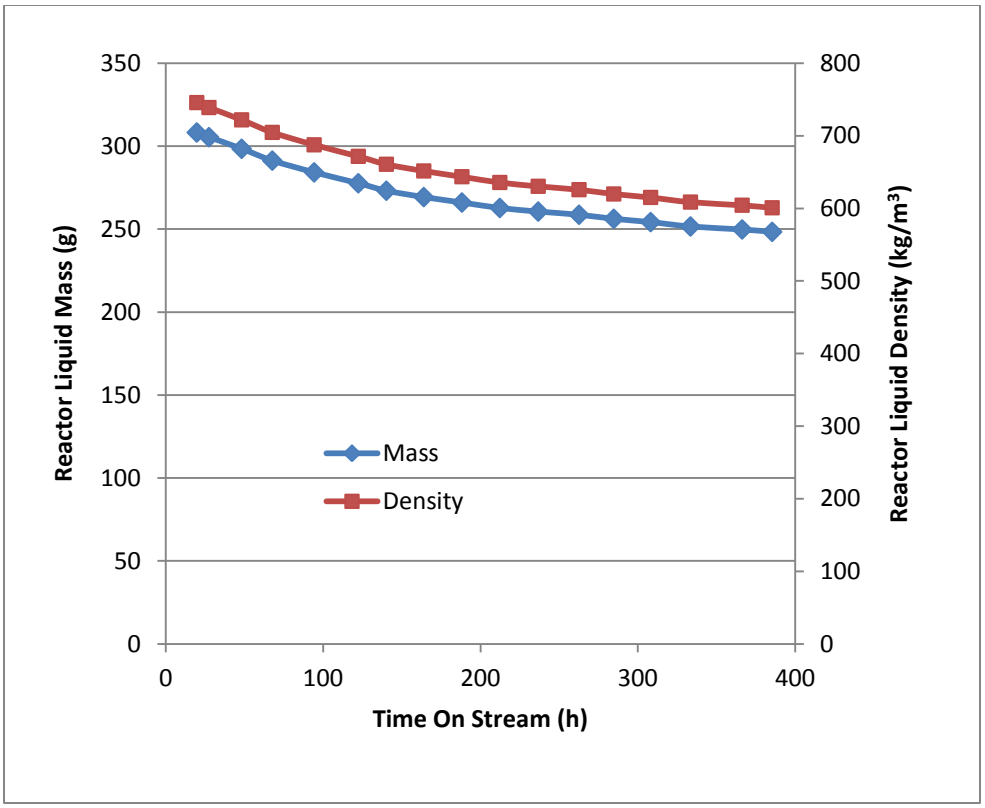


Figure 3.5: Variation of the reactor liquid mass and the reactor liquid density with time on stream calculated by considering constant liquid volume inside the reactor.

These results quantify the reactor content which is used to determine the liquid phase composition. The experimental setup is designed such that the vapour phase products from the reactor can be collected and analysed separately from the liquid phase products as explained in the Experimental Section. The liquid phase products were also collected and analysed separately. The vapour and the liquid phases are assumed to be in equilibrium inside the reactor.

3.6 VAPOUR–LIQUID EQUILIBRIUM RESULTS AND DISCUSSION

At vapour–liquid equilibrium, K-value is defined as:

$$K_n \equiv \frac{y_n}{x_n} \tag{25}$$

where y_n is the mole fraction of species n in the vapour phase, while x_n is the mole fraction of species n in the liquid phase. According to Raoult's law:

$$y_n P = x_n P_{vap,n} \tag{26}$$

where $P_{vap,\,n}$ is the vapour pressure of component n and P is the operating pressure. This results in:

$$K_n = \frac{P_{vap,n}}{P} \tag{27}$$

Subsequently, the K-values calculated from the vapour pressure can be plotted and compared with the experimental results to determine if Raoult's law is sufficient to describe VLE in a FT reactor. The vapour pressure data was obtained from *Yaws' Handbook of Antoine Coefficients for Vapor Pressure (2nd Electronic Edition)* [37]. Caldwell and van Vuuren [1] noted that the vapour pressures of the pure n-alkane components at any temperature decrease with carbon number in a geometrical progression of the form of the ASF distribution. They used the slope of the vapour pressure curve to determine when a liquid phase will form in a Fischer–Tropsch reactor. This presents an opportunity to represent the results in a familiar ASF type plots.

An optimal design of an FT reactor with respect to product yield and selectivity requires a deep understanding of hydrodynamics, reaction kinetics, FT chemistry and VLE. Raoult's law helps with predicting VLE in an FT reactor from a minimum amount of data with a minimum set of parameters. Such calculations are important for slurry reactors, where the hydrodynamics are strongly dependent on liquid composition, and for experimental fixed-bed reactors for the purpose of obtaining a mass balance. ASF type plots are familiar in the FT field. Raoult's law on a homologous series predicts $\ln(K_i)$ versus carbon number to be a reasonably good straight line as shown in Figure 3.6. This is presented along with experimental results.

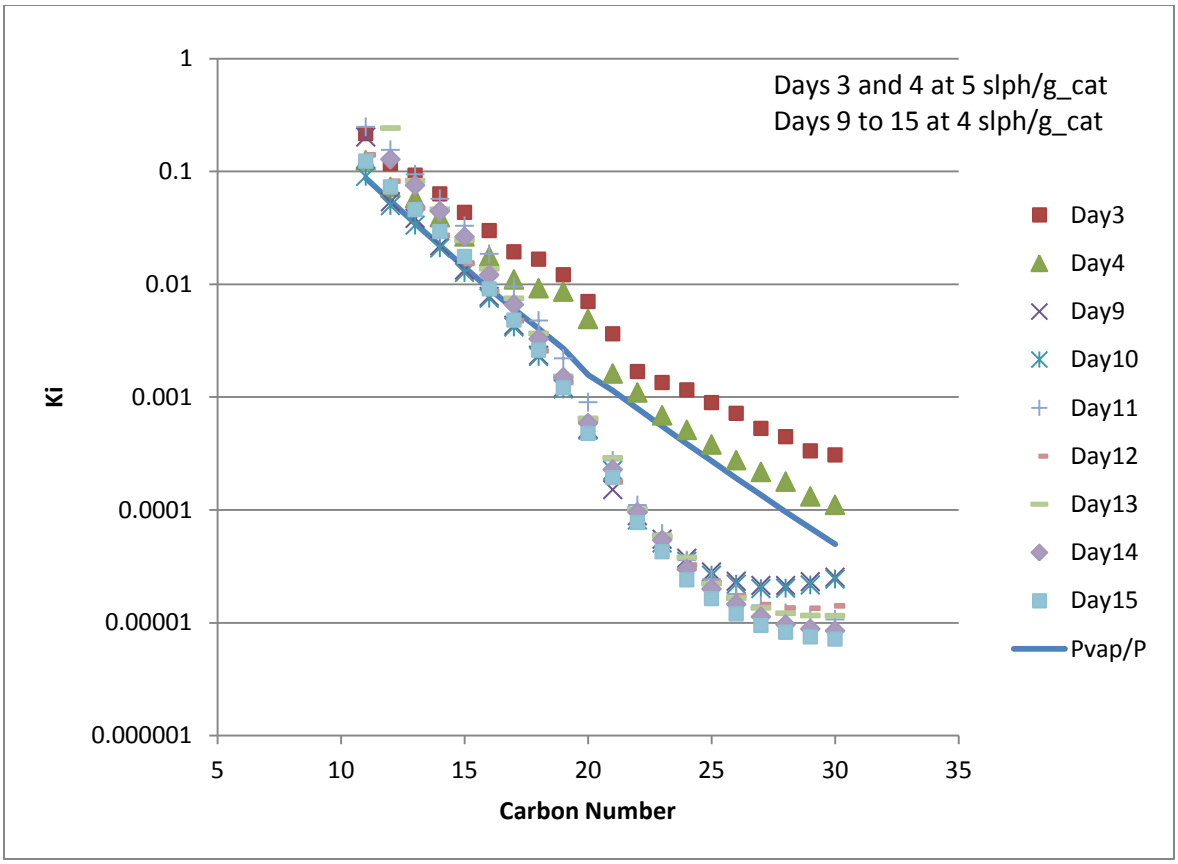


Figure 3.6: Vapour–liquid equilibrium distributions for samples collected at a space velocity of 5 and 4 slph/g_cat. The solid line gives the predicted change of K_i versus carbon number using Raoult's law.

Samples obtained at 6 slph/g_cat are not considered as part of the model evaluation because the system was not at steady state. Consequently, they are not included in the results. The results in Figure 3.6 show that VLE is attained in an FT reactor since most of the measured results can be sufficiently described by Raoult's law, while a few show some deviations. Heavier hydrocarbons which would mainly be in the liquid phase tend to show more deviation from Raoult's law. This might be because heavier hydrocarbons are preferentially retained inside the reactor which causes a change in the liquid phase composition; or because of diffusion limitation of heavier products.

The phrases ‘‘product accumulation’’ or ‘‘accumulated products’’ or ‘‘product hold-up’’ have appeared in the literature during the past several decades to qualitatively explain the experimental results for the FTS [25, 31, 38, 39]. However, since the amount of accumulated products was not determined experimentally, the seriousness of accumulated products in FTS was underestimated by many researchers.

Satterfield and Huff [25] found that at the end of their experiment the analysis of the liquid indicated that an additional 1 to 2 % of the products had accumulated in the reactor. Dictor and Bell [40] noted that accumulation of heavy products in the molten wax prevented their system from ever fully reaching steady-state operation. Therefore slow accumulation of high-molecular-weight products should be quantified to fully describe FT products. Modeling accumulated products in an FT reactor requires a VLE model. If Raoult’s law is sufficient in describing VLE in an FT reactor then Raoult’s law can be used in a model to estimate the accumulated products. As a result the change in the liquid composition inside the reactor with time on stream was measured and is presented in Figure 3.7.

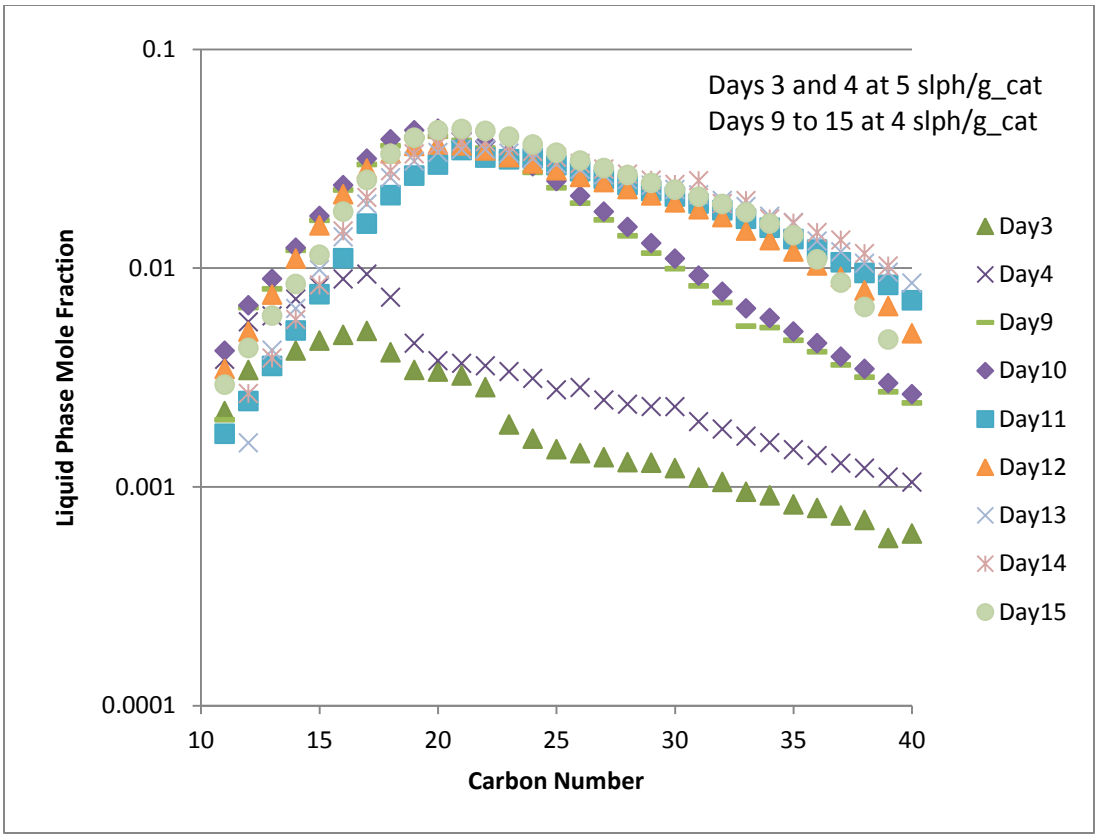


Figure 3.7: Change of liquid phase product distribution with time on stream. The TOS in this Figure corresponds to the TOS presented in Figure 3.2.

The results presented in Figure 3.7 indicate that there is a change in the liquid phase composition with time on stream up to Day 11. After that the liquid phase composition is relatively constant. If accumulation of heavier products was causing the deviation from Raoult's law's prediction then the deviations would be for the samples while the liquid phase composition was changing. Due to the fact that, the instantaneous liquid composition measured from the sample, and the average liquid composition assumed to be constant for the mass balance period, would be different. However, the results in Figure 3.6 show that the deviation of heavier products from Raoult's law is for all the samples at a space velocity of 4 slph/g_cat. Hence product hold-up cannot account for the observed deviation.

Diffusion coefficients decreases with carbon number [21, 27, 41, 42]. Zhan and Davis [27] investigated the conditions under which product diffusion limitation might exist in catalyst pores and how reaction conditions affect this diffusion limitation. Their model results show that in the presence of VLE internal diffusion limitation of products for carbon numbers lower than 20 does not exist. They postulated that for carbon numbers higher than 30, there might be diffusion limitation starting with some hydrocarbon component. The results in Figure 3.6 suggest that products with carbon numbers higher than 20 are diffusion limited. Since the experimental setup was designed such that the vapour phase products can be collected separately from the liquid phase. The vapour phase product distribution was measured for each sample and is presented in Figure 3.8.

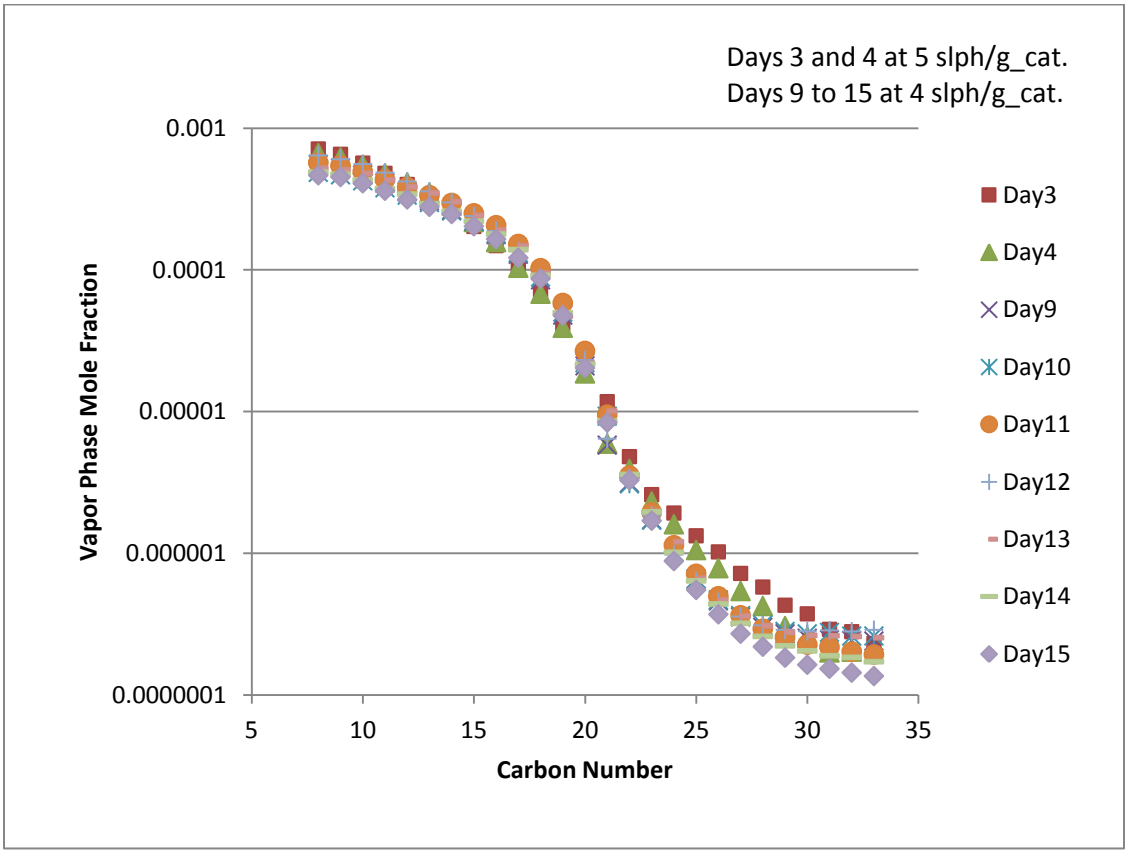


Figure 3.8: Vapour phase product distribution at a space velocity of 5 and 4 slph/g_cat (220 °C, 2.0 MPa, H_2:CO = 2:1).

The results in Figure 3.8 show that the vapour phase mole fraction decreases with carbon number as expected from an ASF type distribution. However there's a sudden drop in the mole fraction around C_{20}. This implies that diffusion limitation is significant for products with carbon number higher than 18 for the experimental conditions (1 L slurry phase CSTR at 220 °C, 2.0 MPa, H_2:CO = 2:1). This can explain the observed deviation from Raoult's law.

The solubility of CO, H_2, H_2O and C_{1-9} are not discussed here because the focus was on the heavier hydrocarbons. Most of the lighter components come out in the gas phase. Therefore, they are only accounted for in the overall mass balance but not in the VLE modeling because their quantity in the liquid phase is very low. The experimental setup is limited in analysing components with very high vapour pressures in the liquid phase because the liquid phase can be collected at reaction pressure (2.0 MPa) but is analysed at atmospheric pressure. Hence the lighter components in the liquid phase vaporize before they can be quantified. Breman and Beenackers [16] investigated various thermodynamic models to predict gas–liquid solubilities in the FTS via gas–slurry processes. Their results are instructive in this regard. Non-idealities in the FT reactor are expected however we are looking for a balance between simplicity and accuracy in modeling VLE in an FT reactor. From the results obtained Raoult's law is sufficient at the experimental conditions used.

3.7 VERIFICATION OF EXPERIMENTAL RESULTS

To verify the applicability of Raoult's law under general FT conditions another experiment was conducted using an iron catalyst at 270 °C, 1.3 MPa at a space velocity of 10 slph/g_cat on the same experimental setup. VLE results are catalyst insensitive. Since Raoult's law was sufficient in a reactor with a cobalt catalyst using an iron catalyst should not affect VLE modeling. The start-up solvent used was C_{30} oil. The vapour phase and the liquid phase data was collected and analysed as explained before. The ratio of the mole fraction of component n in the vapour phase to the mole fraction of the same component in the liquid phase (K-values) is presented in Figure 3.9 together with Raoult's law's predictions.

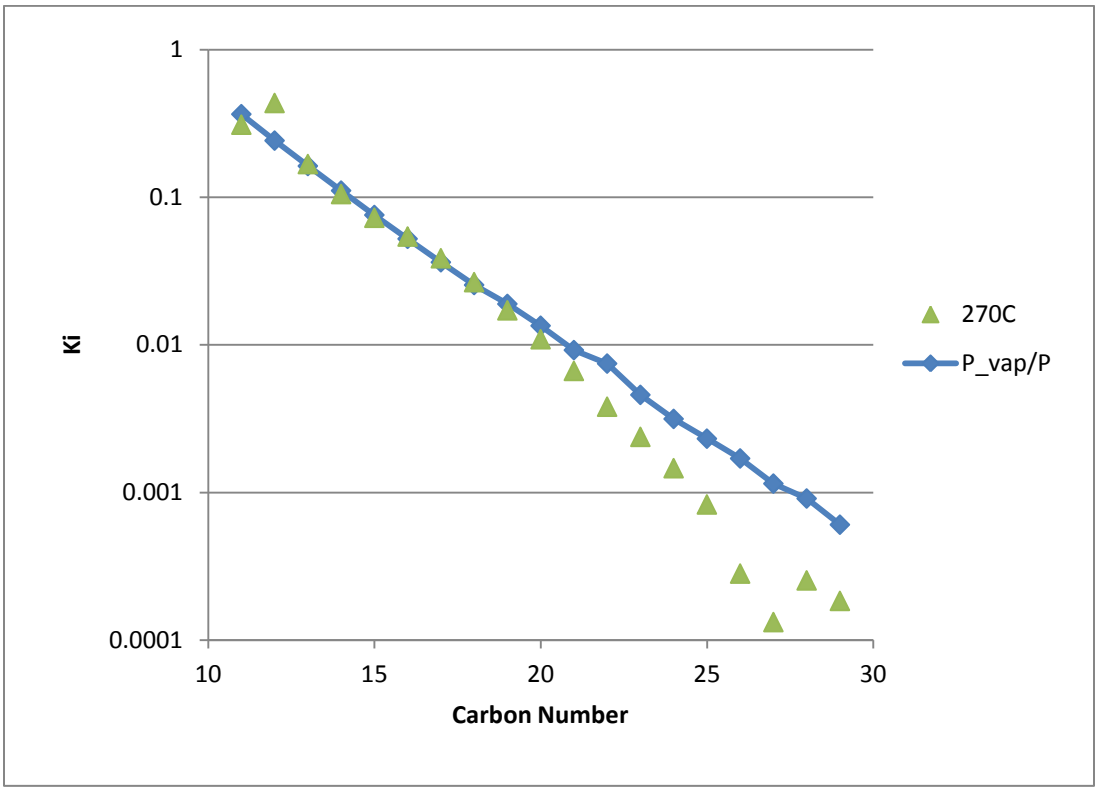


Figure 3.9: Vapour–liquid equilibrium distributions for an iron catalyst at 270 °C, 1.3 MPa, 10 slph/g_cat. The solid line gives the predicted change of K_i versus carbon number using Raoult's law.

The results in Figure 3.9 show that Raoult's law adequately describes VLE for products with chain length less than 20. Heavier products exhibit a similar deviation observed using cobalt catalyst at 220 °C, 2.0 MPa. This deviation is also ascribed to product diffusion limitation of heavier products. This confirms the assertion by Zhan and Davis [27] that product diffusion limitation might occur for heavier products starting with some hydrocarbon component. In this case product diffusion limitation starts with C_{20}.

To obtain a statistical analysis of the prediction of Raoult's law on the partition coefficients (K-values) percentage relative deviations were calculated for each data point. The data at different

TOS were combined for each carbon number to work out the percentage relative deviations. The average relative deviations with carbon number are presented in Figure 3.10.

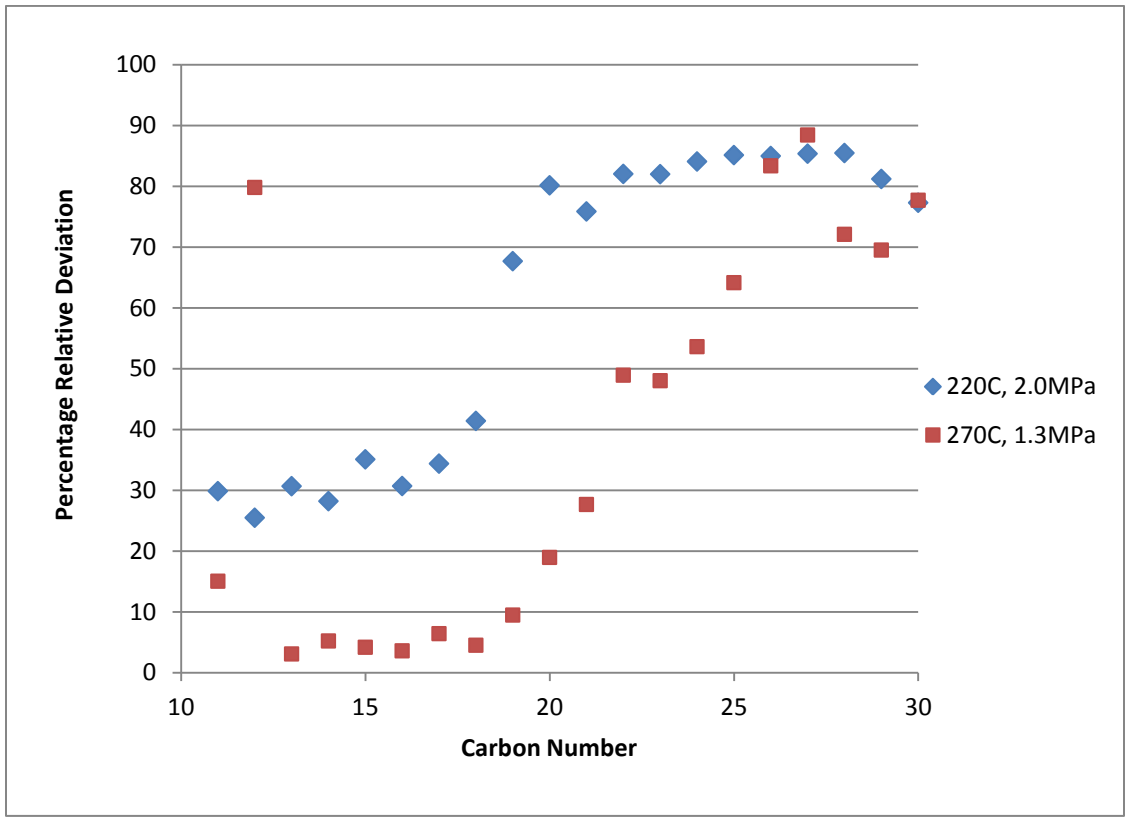


Figure 3.10: Average relative deviations with carbon number for all data points at 220 °C, 2.0 MPa using cobalt catalyst and relative deviations with carbon number at 270 °C, 1.3 MPa using iron catalyst.

The results in Figure 3.10 show a relative deviation less than 40% for C_{18} and lighter products. This is sufficient for a thermodynamic model that does not require acentric factors, activity coefficients, binary interaction parameters or mixing rules. Elaborate thermodynamic models can be used given the pure component parameters with relevant mixing rules for a higher degree of accuracy. An increase in temperature and a reduction in pressure typically makes vapour phase more ideal. It is also evident in these results that the relative deviation at 270 °C, 1.3 MPa is less than 10% for products with carbon number less than 20. The higher deviation for higher hydrocarbon is due to product diffusion limitation as explained before.

The results at 220 °C, 2.0 MPa using a cobalt catalyst and at 270 °C, 1.3 MPa using an iron catalyst show the reactor content tends towards vapour–liquid equilibrium and furthermore that Raoult's law sufficiently describes VLE in an FT reactor.

3.8 CONCLUSIONS

Vapour–liquid equilibrium plays an important role in modeling an FT reactor. An FT experiment was conducted such that both the vapour and the liquid phase were collected and analysed separately. The results show that VLE is attained inside an FT reactor. Raoult's law sufficiently describes the VLE in an FT reactor. Hydrocarbons with carbon number greater than 18 deviates from Raoult's law. Accumulation of heavier products in the reactor does not account for the observed deviation. The deviations from Raoult's law are due to diffusion limitations. Elaborate thermodynamic models could be used given the pure component parameters with relevant mixing rules for a higher degree of accuracy. However, elaborate thermodynamic models would not solve the diffusion limitation of heavier products.

REFERENCES

[1] L. Caldwell, D.S. van Vuuren, On the formation and composition of the liquid phase in Fischer–Tropsch reactor, *Chem. Eng. Sci. 41* (1986) 89–96.

[2] J.J. Marano, G.D. Holder, Characterization of Fischer–Tropsch liquids for vapor–liquid equilibria calculations, *Fluid Phase Equilib. 138* (1997) 1–21.

[3] J.M. Fox, S.S. Tam, Correlation of slurry reactor Fischer–Tropsch yield data, *Top. Catal. 2* (1995) 285–300.

[4] A.P. Raje, B.H. Davis, Effect of Vapor–Liquid Equilibrium on Fischer–Tropsch Hydrocarbon Selectivity for a Deactivating Catalyst in a Slurry Reactor, *Energy Fuels 10* (1996) 552–560.

[5] X. Zhan, B.H. Davis, Two alpha Fischer–Tropsch product distribution. A role for vapor–liquid equilibrium?, *Petrol. Sci. Technol. 18* (2000) 1037–1053.

[6] X. Zhan, B.H. Davis, Assessment of internal diffusion limitation on Fischer–Tropsch product distribution, *Appl. Catal. A: Gen. 236* (2002) 149–161.

[7] I.V. Derevich, V.S. Ermolaev, V.Z. Mordkovich, Liquid–Vapor thermodynamic equilibrium in Fischer–Tropsch synthesis products, *Theor. Found. Chem. Eng. 42* (2008) 216–219.

[8] S. Srinivas, R.K. Malik, S.M. Mahajani, Feasibility of reactive distillation for Fischer–Tropsch synthesis, *Ind. Eng. Chem. Res. 47* (2008) 889–899.

[9] V.R. Ahon, E.F. Costa, J.E.P. Monteagudo, C.E. Fontes, E.C. Biscaia, P.L.C. Lage, A comprehensive mathematical model for the Fischer–Tropsch synthesis in well-mixed slurry reactors, *Chem. Eng. Sci. 60* (2005) 677–694.

[10] O. Redlich, J.N.S. Kwong, On the thermodynamics of solutions. V. An equation of state. Fugacities of gaseous solutions, *Chem. Rev. 44* (1949) 233–244.

[11] G. Soave, Equilibrium constants from a modified Redlich–Kwong equation of state, *Chem. Eng. Sci. 27* (1972) 1197–1203.

[12] D.–Y. Peng, D.B. Robinson, A new two-constant equation of state, *Ind. Eng. Chem. Fundam. 15* (1976) 59–64.

[13] J. Vidal, Mixing rules and excess properties in cubic equations of state, *Chem. Eng. Sci. 33* (1978) 787–791.

[14] M.–J. Huron, J.Vidal, New mixing rules in simple equations of state for representing vapour–liquid equilibria of strongly non-ideal mixtures, *Fluid Phase Equilib. 3* (1979) 255–271.

[15] S.H. Huang, H.–M. Lin, F.–N. Tsai, K.–C. Chao, Solubility of synthesis gases in heavy n-paraffins and Fischer–Tropsch wax, *Ind. Eng. Chem. Res. 27* (1988) 162–169.

[16] B.B. Breman, A.A. Beenackers, Thermodynamic models to predict gas–liquid solubilities in the methanol synthesis, the methanol–higher alcohol synthesis, and the Fischer–Tropsch synthesis via gas–slurry processes, *Ind. Eng. Chem. Res. 35* (1996) 3763–3775.

[17] Y.–N. Wang, Y.–W Li, L. Bai, Y.–L. Zhao, B.–J. Zhang, Correlation for gas–liquid equilibrium prediction in Fischer–Tropsch synthesis, *Fuel 78* (1999) 911–917.

[18] M.E. Dry, Present and future applications of the Fischer–Tropsch process, *Appl. Catal. A: Gen. 276* (2004) 1–3.

[19] X. Lu, D. Hildebrandt, X. Liu, D. Glasser, Making sense of the Fischer–Tropsch synthesis reaction: start-up, *Ind. Eng. Chem. Res. 49* (2010) 9753–9758.

[20] N.E. Tsakoumis, M. Rønning, Ø. Borg, E. Rytter, A. Holmen, Deactivation of cobalt based Fischer–Tropsch catalysts: A review, *Catal. Today 154* (2010) 162–182.

[21] E. Iglesia, S.C. Reyes, R.J. Madon, Transport-enhanced α-olefin readsorption pathways in Ru-catalyzed hydrocarbon synthesis, *J. Catal. 129* (1991) 238–256.

[22] T. Komaya, A.T. Bell, Estimates of rate coefficients for elementary processes occurring during Fischer–Tropsch synthesis over Ru/TiO_2, *J. Catal. 146* (1994) 237–248.

[23] A.P. Raje, B.H. Davis, Effect of vapor–liquid equilibrium on Fischer–Tropsch hydrocarbon selectivity for a deactivating catalyst in a slurry reactor, *Energy Fuels 10* (1996) 552–560.

[24] B. Shi, B.H. Davis, Fischer–Tropsch synthesis: accounting for chain-length related phenomena, *Appl. Catal. A: Gen. 277* (2004) 61–69.

[25] C.N. Satterfield, G.A. Huff, Carbon number distribution of Fischer–Tropsch products formed on an iron catalyst in a slurry reactor, *J. Catal. 73* (1982) 187–197.

[26] C.N. Satterfield, G.A. Huff, Product distribution from iron catalysts in Fischer–Tropsch slurry reactors, *Ind. Eng. Chem. Process Des. Dev. 21* (1982) 465–470.

[27] X. Zhan, B.H. Davis, Assessment of internal diffusion limitation on Fischer–Tropsch product distribution, *Appl. Catal. A: Gen 236* (2002) 149–161.

[28] B.H. Davis, The two-alpha value for iron Fischer–Tropsch catalyst: fact or fiction?, *ACS Div. Fuel Chem. Preprints 37* (1992) 172–183.

[29] T.J. Donnelly, I.C. Yates, C.N. Satterfield, Analysis and prediction of product distributions of the Fischer–Tropsch synthesis, *Energy Fuels 2* (1988) 734–739.

[30] G.A. Huff, C.N. Satterfield, Evidence for two chain growth probabilities on iron catalysts in the Fischer–Tropsch synthesis, *J. Catal. 85* (1984) 370–379.

[31] R.A. Dictor, A.T. Bell, An explanation for deviations of Fischer–Tropsch products from a Schulz–Flory distribution, *Ind. Eng. Chem. Process Des. Dev. 22* (1983) 678–681.

[32] B.W. Wojciechowski, Mechanistic consideration of paraffin, olefins and alcohol distributions in FT synthesis, *Can. J. Chem. Eng. 64* (1986) 149–153.

[33] E.W. Kuipers, C. Scheper, J.H. Wilson, I.H. Vinkenburg, H. Oosterbeek, Non-ASF product distributions due to secondary reactions during Fischer–Tropsch synthesis, *J. Catal. 158* (1996) 288–300.

[34] H. Schulz, M. Claeys, Kinetic modeling of Fischer–Tropsch product distribution, *Appl. Catal. A: Gen. 186* (1999) 91–107.

[35] G.P. van der Laan, A.A.C.M. Beenackers, Kinetics and selectivity of the Fischer–Tropsch synthesis: A literature review, *Catal. Rev. –Sci. Eng. 41* (1999) 255–318.

[36] E. Iglesia, Design, synthesis, and use of cobalt-based Fischer–Tropsch synthesis catalysts, *Appl. Catal. A: Gen. 161* (1997) 59–78.

[37] C.L. Yaws, P.K. Narasimhan, C. Gabbula, Yaws' Handbook of Antoine Coefficients for Vapor Pressure, *2nd Electronic Ed.*, Knovel, 2009 (Accessed 30/08/2010).

[38] L.–M. Tau, H.A. Dabbagh, B. Chawla, B.H. Davis, Fischer–Tropsch synthesis with an iron catalyst: Incorporation of ethene into higher carbon number alkanes, *Catal. Lett. 7* (1990) 141–149.

[39] L.–M. Tau, H.A. Dabbagh, B.H. Davis, Fischer–Tropsch synthesis: comparison of carbon-14 distributions when labeled alcohol is added to the synthesis gas, *Energy Fuels 5* (1991) 174–179.

[40] R.A. Dictor, A.T. Bell, Fischer–Tropsch synthesis over reduced and unreduced iron oxide catalysts, *J. Catal. 97* (1986) 121–136.

[41] E.W. Kuipers, I.H. Vinkenburg, H. Oosterbeek, Chain length dependence of α-olefin readsorption in Fischer–Tropsch synthesis, *J. Catal. 152* (1995) 137–146.

[42] R.J. Madon, E. Iglesia, Catalytic reaction rates in thermodynamically non-ideal systems, *J. Mol. Catal. A: Chem. 163* (2000) 189–204.

Chapter 4 : THE ROLE OF VAPOUR–LIQUID EQUILIBRIUM IN FISCHER–TROPSCH PRODUCT DISTRIBUTION

ABSTRACT

This work uses vapour–liquid equilibrium (VLE) to explain the observed two-alpha product distribution in Fischer–Tropsch (FT) reactors. We discuss three possible scenarios or cases of Anderson–Schulz–Flory (ASF) product distribution and VLE. The three cases assume that: (1) the reaction sets up a single alpha ASF distribution in the total (vapour + liquid) products, (2) the vapour phase follows a single alpha distribution, and (3) a single alpha distribution is set up in the liquid phase. We then look at the consequences of these assumptions in conjunction with a simple Raoult's law VLE model on the exit product distributions. We find that only Case 3 gives rise to a two-alpha model in accordance with experimental results that is frequently observed in FT reactors. This model further predicts a relationship between the two values of alpha that are consistent with the measured experimental results.

Keywords: *Fischer–Tropsch Reaction, Vapour–Liquid Equilibrium (VLE), Phase Equilibria, Product Distribution Model, Chain propagation probability (α), ASF.*

4.1 INTRODUCTION

In April 1926, Fischer and Tropsch announced that higher homologs of methane are formed when mixtures of hydrogen and carbon monoxide are passed at atmospheric pressure over

catalysts of iron or cobalt mixed with various supporting materials, at temperatures from 250–300°C [1]. Fischer–Tropsch synthesis (FTS) designates a process through which synthesis gas (a mixture of predominantly CO and H_2) that is obtained from coal, natural gas or biomass, is converted to a multi-component mixture of hydrocarbons. The FT process is used mainly for the production of fuels, although other valuable products can be tailor-made from FTS when it is combined with upgrade or downstream processes that result, for example, in high yields of gasoline, excellent quality diesel fuel and linear α-olefins [2, 3].

The FT is a surface polymerization reaction [4, 5]. The accepted model is that reactants, CO and H_2, adsorb and dissociate at the surface of the catalyst and react to form a chain initiator (CH_3), a methylene (CH_2) monomer, and water. The hydrocarbons are formed by CH_2 insertion into metal-alkyl bonds, and subsequent dehydrogenation or hydrogenation to an α-olefin or paraffin respectively [6].

According to Anderson [7], the product distribution of hydrocarbons can be described by the Anderson–Schulz–Flory (ASF) equation (1):

$$m_n = (1-\alpha)\alpha^{n-1} \quad (1)$$

where

m_n is the mole fraction of a hydrocarbon with chain length n = (moles of hydrocarbon of chain length n) / (total moles) and

α is the chain growth probability factor and is independent of n. α determines the total carbon number distribution of the FT products.

The logarithm of the above equation gives:

$$\log(m_n) = \log(\tfrac{1-\alpha}{\alpha}) + n\log(\alpha) \quad (2)$$

Hence, a plot of the logarithm of the molar concentration of hydrocarbon of chain length n, m_n versus the carbon number n would produce a straight-line plot the slope of which is log (α), and the intercept log((1-α)/α), as shown in Figure 4.1. The mole fractions used in the product distribution plots are the overall mole fractions which is similar to z_n used in later figures.

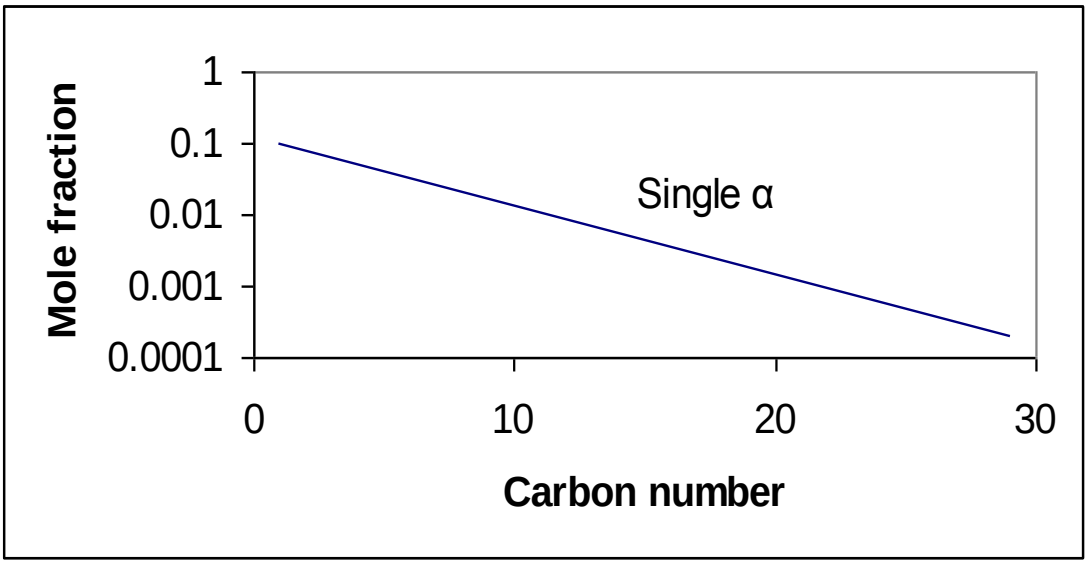


Figure 4.1: Classical Anderson–Schulz–Flory distribution, single-alpha distribution.

Most studies assume that the ASF distribution is a model of the product selectivity [8–10]. It describes the entire product range by means of a single parameter, α, which represents the probability of the addition of a carbon intermediate to a chain. However, significant deviations have been reported in the literature [11–14], and the results of some of these researchers show a two-alpha negative deviation [15, 16]. However, the most prevalent deviation is the two-alpha positive deviation product distribution model [11, 17], which is shown in Figure 4.2.

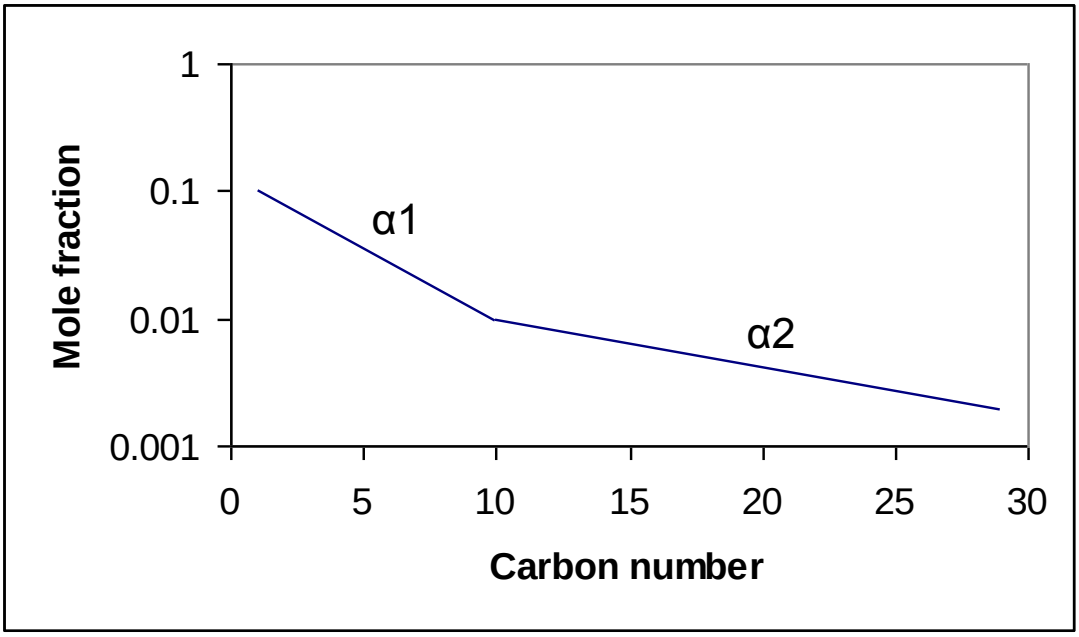


Figure 4.2: Two-alpha positive-deviation product distribution.

Previous attempts to explain the deviations from ASF distribution in FTS have led to a two-active-site model [18], or other models related to olefin readsorption [19–21] or VLE-based explanations [14, 16]. Several of these postulates suggest that the reversible olefin termination path is responsible for the two-alpha product distribution [22, 23]. However, none of the theories suggested has been able to explain all of these chain-length-related observations.

Although according to Caldwell and van Vuuren [24], liquid forms inside the FT reactor for high values of α, many researchers have ignored the presence of VLE in their reactor models. This study takes VLE into account in the development of a model that explains the deviations from the classical ASF model that have been observed.

4.2 THE EFFECT OF VLE IN THE FISCHER–TROPSCH REACTION

Caldwell and van Vuuren [24] provided a criterion for predicting liquid phase formation as well as a method for calculating what fraction of the products will condense, and what the liquid and vapour compositions will be. The criterion is readily derived by determining the conditions under which the dew-point is reached for the mixture of reactants and products formed by the catalyst in the reactor. These scientists showed that for all practical purposes a liquid phase will form or persist if the Schulz–Flory plot intersects that of the vapour-pressure. In other words, at 220 °C the slope of the vapour-pressure versus carbon number curve is 0.653, hence the dew-point will not be reached if $\alpha < 0.653$. Their VLE calculations are the same as those used in the Case 1 described in this paper.

While Caldwell and van Vuuren [24] used Raoult's law to describe VLE, Fox and Tam [25] applied the Peng–Robinson (PR) equation modified to take the presence of water into account, to simulate VLE on Aspen. Marano and Holder [26] argued against the simplifying effect of using Raoult's law to describe all phase equilibria in FTS. They contended that while the heavier hydrocarbon components of the wax phase may well exhibit ideal-solution behaviour, the non-hydrocarbons and lighter hydrocarbons do not. They also pointed out that ideal-gas behaviour cannot be assumed for the vapour phase under typical reaction conditions (200–330 °C, 10–25 bar). They therefore developed K-value formulations for use in performing VLE calculations on FT systems, and claimed that their model gives predictions superior to those yielded by the Caldwell and van Vuuren [24] formulation. However, the results of Marano and Holder [26] also show that the vapour phase is nearly ideal, and the fugacity coefficients are all near unity.

Derevich *et al*. [27] developed methods for calculating the vapour–liquid thermodynamic equilibrium in FTS products based on a modified PR equation of state (EOS). Srinivas *et al*. [28] used the ASPEN built-in PR-EOS with modified Huron–Vidal mixing rules, which has the same EOS and mixing rules as those of Marano and Holder [26], to simulate the FT reactor as a reactive distillation system.

However, Ahon *et al*. [29] made rigorous VLE calculations through cubic EOS to describe the phase behaviour for a well-mixed FT slurry reactor. Their model results were similar to those obtained by Zhan and Davis [30], which find that the composition profiles of the total product show a negative deviation from the ASF distribution before the steady state is reached. (This is the same as our own findings in Case 1.)

The VLE method propounded by Ahon *et al.* [29] uses parameters and mixture properties for C_{4+} estimated through the correlations of Marano and Holder [26], which are based on the asymptotic behaviour of normal paraffins and 1-olefins. It shows that the ideal gas assumption does not alter the results appreciably. On the other hand, it also demonstrates that the assumption of an almost ideal liquid solution affects the gas and liquid product distributions. However, the effect of this approximation on the overall product distribution is surprisingly small, because the largest relative deviations in the liquid and gas product distributions occur for the species with the lowest concentrations in these phases, which do not contribute appreciably to the total production.

Actual measurements of the vapour and the liquid phase composition have been done (Chapter 3, [31]) under FT conditions to ascertain whether Raoult's law is sufficient or other elaborate thermodynamic models have to be used to model VLE in FT reactors. The results show that Raoult's law is sufficient. Therefore ideal VLE correlation (Raoult's law) is the theoretical model used in this study. The temperatures in FT reactors are well above the critical temperatures of the lighter paraffins such as C_1 and C_2. Hence the vapour pressures for these components have no physical meaning. It is, however, common practice [24] to use hypothetical vapour pressures in VLE calculations.

4.3 PRODUCT DIFFUSION LIMITATION

Diffusional restrictions which prevent the attainment of VLE can give rise to liquid phase effects on FTS selectivity by introducing chemical potential gradients between the gas and liquid phases [32]. Slurry bubble column reactors (SBCRs) are becoming more popular and gradually replacing fixed bed reactors in several important industrial applications such as the FTS [33–35]. The design and scale-up of SBCRs require, among others, precise knowledge of the kinetics, thermodynamics, hydrodynamics, and heat as well as mass transfer characteristics [36]. In SBCRs, the gas-phase is conventionally sparged through the slurry at the bottom of the reactor through a specially designed distributor, leading to different flow regimes and complex hydrodynamic as well as mass transfer behaviours. Sehabiague *et al.* [37] developed correlations and a calculation algorithm to predict the hydrodynamics and mass transfer parameters in bubble column reactors (BCRs) and SBCRs based on a large experimental database covering typical FT conditions.

For FT synthesis products, it is true that the heavier the hydrocarbon, the more difficult its diffusion in catalyst pores because diffusivity decreases significantly with increasing carbon number [19, 22]. Zhan and Davis [10] investigated the conditions under which product diffusion limitation might exist in catalyst pores and how reaction conditions affect this diffusion limitation. Their model results show that in the presence of VLE internal diffusion limitation of products for carbon numbers lower than 20 does not exist. They postulated that for carbon numbers higher than 30, there might be diffusion limitation starting with some hydrocarbon component. Experimental results in Chapter 3 and [31] show that VLE is attained inside an FT reactor. Therefore all the products are assumed to be in VLE in this study.

4.4 REACTION MODELLING

To develop a model to explain two-alpha positive-deviation product distribution we conceptualised a reactor into which CO and H_2 flow continuously at constant rates in a ratio of 1:2. Vapour phase products, that is unconverted CO and H_2, water, and volatile hydrocarbons of

mole fraction y_n, stream out at a constant flow rate of V mol/s. Liquid phase hydrocarbon products, of mole fraction x_n, are either continually removed or allowed to accumulate in the reactor for some designated interval and removed periodically as necessary. In either instance the reactor is modelled assuming the liquid level that is approximately uniform. The drained liquid L is added to the vapour phase product to obtain the total reaction product of molar flow rate Z mol/s and composition z_n for the sampling period, as shown in Figure 4.3,

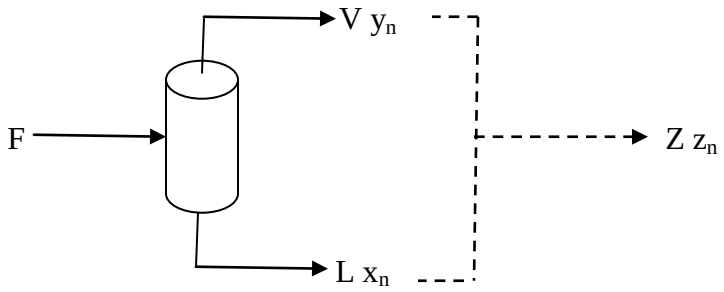


Figure 4.3: Schematic diagram of the conceptual FT reactor.

where:

F is the total feed molar flow rate

V is the vapour molar flow rate

L is the liquid molar flow rate

y_n is the mole fraction of hydrocarbon of chain length n in the vapour phase

x_n is the mole fraction of hydrocarbon of chain length n in the liquid phase

Z is the sum of the vapour and the liquid flow rates

z_n is the total mole fraction of hydrocarbon of chain length n.

4.5 MODEL DEVELOPMENT AND CALCULATIONS

We assumed three different scenarios (Cases 1–3) for the reaction, namely:

1. the *overall product* follow a single α distribution
2. the *vapour phase* follows a single α distribution
3. a single α distribution is set up in *the liquid phase*.

In all cases, except where specified otherwise, we specified that the conversion was 85%, and that an alpha of 0.85, temperature of 200 °C and a pressure of 20 bar were standard. The simulation was performed using a MatLab computer programme for the models described. For simplicity of simulation, we assumed that hydrocarbon products are linear paraffins from C1–30.

In the exposition below, we consider each of the three scenarios separately, and look at the predicted liquid, vapour and total distributions that each of these assumptions yields. The expected trends form the main focus of the Figures presented in these cases.

<u>For all cases</u>

The overall mass balance on hydrocarbon product after the FT reaction gives:

$$V + L = Z \tag{3}$$

the component balance on hydrocarbons of chain length n gives:

$$Vy_n + Lx_n = Zz_n \tag{4}$$

The vapour fraction is defined as:

$$f \equiv \frac{V}{Z} \tag{5}$$

hence the component balance can be written as

$$z_n = f y_n + (1 - f) x_n \quad (6)$$

Since the vapour fraction f ranges from 0–1, this means that x_n and y_n must lie on either side of z_n. It is worth noting that as the vapour fraction tends to 1, the vapour distribution and the total distribution become the same. Conversely, as the vapour fraction tends to 0, the total distribution and the liquid distribution become the same.

We assume that the vapour and liquid are in VLE, or

$$y_n = K_n x_n \quad (7)$$

Furthermore, we would expect that as the liquid phase is a mixture of homologous hydrocarbons, the liquid phase would tend to behave ideally. Also, because the partial pressures of individual product components in the gas phase are very small, one would expect that in many cases

$$K_n = \frac{P_{vap,n}}{P} \quad (8)$$

where:

$P_{vap,\,n}$ is the vapour pressure of hydrocarbon of chain length n and

P is the total pressure.

Case 1: The total product distribution follows a single α

The theory examined in this Case is that the reaction sets up a *single α for the total product distribution*, and this then distributes via VLE into a vapour and liquid phase. Almost all the researchers that have included VLE in their FT models have considered this single α for the total product distribution [16, 24, 30]. The residence time of the liquid in the reactor is much longer than that of the vapour (Chapter 5), and the initial product distribution observed would initially follow the vapour distribution. However, after a certain time that would be dependent on the

liquid residence time, the product distribution would be seen to correspond with the single α distribution of the total product more closely as the liquid flows reach steady state in the reactor. The proposed explanation is that the 2-α distribution is caused by the transience of the liquid phase inside the reactor.

Dictor and Bell [15] proposed an explanation for the deviations of FT products from a Schulz–Flory (SF) distribution. Their results showed that negative deviations from an SF distribution were attributable to a transient hold-up of higher molecular weight products in the oil phase surrounding the catalyst.

We assumed that the total (vapour and liquid) hydrocarbon products could be described by a single α ASF distribution at a reaction temperature T and pressure P.

Thus:

$$\frac{z_{n+1}}{z_n} = \alpha \tag{9}$$

therefore

$$\sum z_n = z_1 + \alpha z_1 + \alpha^2 z_1 + \cdots \tag{10}$$

$$\sum z_n = (1 + \alpha + \alpha^2 + \cdots) z_1 \tag{11}$$

$$\sum z_n = \frac{z_1}{1-\alpha} \tag{12}$$

If the total mole fraction of components in the product other than hydrocarbons is c, then

$$\sum z_n = 1 - c \tag{13}$$

hence

$$\frac{z_1}{1-\alpha} = 1 - c \tag{14}$$

thus

$$z_1 = (1-\alpha)(1-c) \tag{15}$$

The single α product distribution also gives

$$z_n = \alpha^{n-1} z_1 \tag{16}$$

therefore

$$z_n = \alpha^{n-1}(1-\alpha)(1-c) \tag{17}$$

From the component balance

$$Vy_n + Lx_n = Zz_n \tag{4}$$

and from vapour–liquid equilibrium

$$y_n = K_n x_n \tag{18}$$

substituting Equation (17) and (18) in Equation (4) gives

$$VK_n x_n + Lx_n = (L+V)[\alpha^{n-1}(1-\alpha)(1-c)] \tag{19}$$

Hence

$$x_n = \frac{(L+V)(1-\alpha)(1-c)\alpha^{n-1}}{VK_n+L} \tag{20}$$

therefore

$$\frac{x_{n+1}}{x_n} = \frac{(L+V)(1-\alpha)(1-c)\alpha^{n+1-1}(VK_n+L)}{(L+V)(1-\alpha)(1-c)\alpha^{n-1}(VK_{n+1}+L)} \tag{21}$$

This reduces to:

$$\frac{x_{n+1}}{x_n} = \frac{(VK_n+L)}{(VK_{n+1}+L)}\frac{\alpha^n}{\alpha^{n-1}} \tag{22}$$

which can be written as

$$\frac{x_{n+1}}{x_n} = \alpha\frac{(VK_n+L)}{(VK_{n+1}+L)} \tag{23}$$

Assuming that the VLE can be described by Raoult's law gives:

$$y_n = K_n x_n = \frac{P_{vap,n}}{P} x_n \tag{24}$$

According to Caldwell and van Vuuren [24]:

$$\frac{P_{vap,n+1}}{P_{vap,n}} = \beta \tag{25}$$

which is a function of T only and not of chain length.

For lighter hydrocarbons (that is, small n)

$$K_n = \frac{P_{vap,n}}{P} \gg 1 \tag{26}$$

therefore Equation (23) becomes:

$$\frac{x_{n+1}}{x_n} = \alpha \frac{K_n}{K_{n+1}} \tag{27}$$

This reduces to:

$$\frac{x_{n+1}}{x_n} = \alpha \frac{P_{vap,n}}{P_{vap,n+1}} \tag{28}$$

which is the same as

$$\frac{x_{n+1}}{x_n} = \frac{\alpha}{\beta} > 1 \tag{29}$$

since according to our postulated α

$$\alpha > \beta \tag{30}$$

Hence the plot of log x_n vs. n for the lighter hydrocarbons is a straight line. The slope is steeper than log(α), since β < 1, and indeed is above log(1). Further, β is a function of temperature and

not strongly of pressure. Therefore, even if α was fixed, temperature would affect the slope of the observed liquid distribution, while pressure would have minimal impact.

If we consider the vapour phase,

$$y_n = K_n x_n = \frac{P_{vap,n}}{P} x_n \tag{24}$$

we arrive at

$$\frac{y_{n+1}}{y_n} = \frac{\frac{P_{vap,n+1}}{P} x_{n+1}}{\frac{P_{vap,n}}{P} x_n} \tag{31}$$

which is equivalent to

$$\frac{y_{n+1}}{y_n} = \beta \frac{x_{n+1}}{x_n} \tag{32}$$

Therefore substituting Equation (29) into (32) gives

$$\frac{y_{n+1}}{y_n} = \alpha \tag{33}$$

Thus for lighter components, the gas phase mole fraction follows that of the total hydrocarbons, while the liquid phase slope rises beyond log(1), as shown in Figure 4.4.

<u>For heavier hydrocarbons (large n)</u>

$$K_n \ll 1 \tag{34}$$

Equation (23) becomes:

$$\frac{x_{n+1}}{x_n} = \alpha \tag{35}$$

The liquid phase mole fraction replicates the total mole fraction.

From Equation (32) the vapour phase mole fraction becomes

$$\frac{y_{n+1}}{y_n} = \alpha\beta \tag{36}$$

which means that the slope of the vapour phase for heavier hydrocarbons is lower than the liquid phase slope.

Since the overall product distribution was specified, we used a simple flash calculation to work out the mole fractions of the vapour and liquid phases. The expected product distribution results for α = 0.85 overall in this case are presented in Figure 4.4.

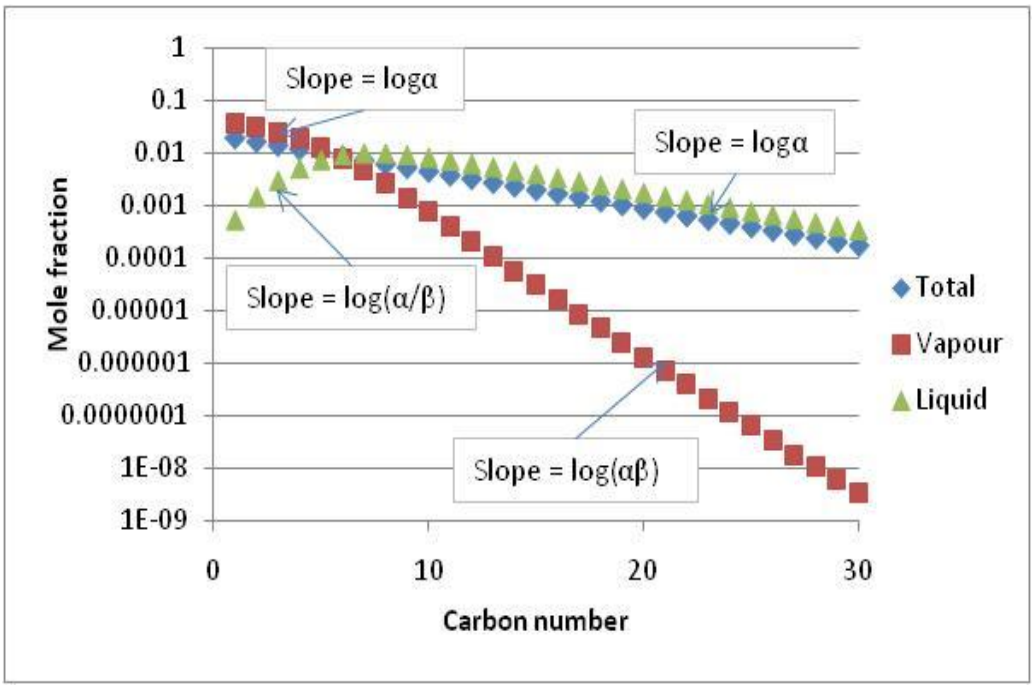


Figure 4.4: The expected product distribution if the overall product distribution is described by a single alpha (α=0.85). The vapour and liquid are assumed to be in VLE.

It is important to note that the values of the mole fractions on the y-axis are for demonstration/explanation only. The actual values of the mole fractions would depend on the

overall mass balance, which would take into account the unreacted and inert gases, CO_2 and water, which are all lumped into the constant c in the reasoning presented here. The mole fractions shown in Figure 4.4 are calculated for 85% CO conversion, given a feed-ratio of 1:2 for $CO:H_2$. Changing the conversion does not change the shape of the curves; it alters only the intercepts. The focus of discussion, therefore, remains the same.

We see that the total hydrocarbon distribution follows a single α pattern. Hence, over the long term (as the reactor reaches steady state), the overall product distribution would correspond with this. The vapour distribution, however, is no longer described by a single α, but instead by a 2-α distribution. The lighter hydrocarbons (C1–C5) occur mainly in the gas phases, and hence the vapour distribution in this range conforms with the α of the overall product. The heavier hydrocarbons follow a distribution with a slope of log(αβ), as described in Equation (36), and this slope is lower than that of the overall products.

Hence, if the total product distribution and VLE were set up quickly, and the liquid was given time to accumulate and then start flowing out of the reactor, one might expect that initially one would observe the gas phase distribution. This, although it would display the 2-α slope, would demonstrate the negative deviation from the classical ASF distribution. These results are consistent with those of Dictor and Bell [15], and might explain some of the two-alpha negative deviation reported in the published literature.

The liquid distribution for higher carbon numbers (C8 and above) resembles the total production distribution and hence has a slope log(α). The lighter hydrocarbons in the liquid phase follow a slope of log(α/β), as predicted by Equation (29).

We also looked at the effect of changing α on the vapour distribution. Intending to compare our results for Case 1 with those of Caldwell and van Vuuren [24], we made calculations based on

the equations described to determine the vapour phase product distribution as a function of the chain-propagation probability. We varied the assumed overall α, and the predicted vapour phase results we obtained are presented in Figure 4.5.

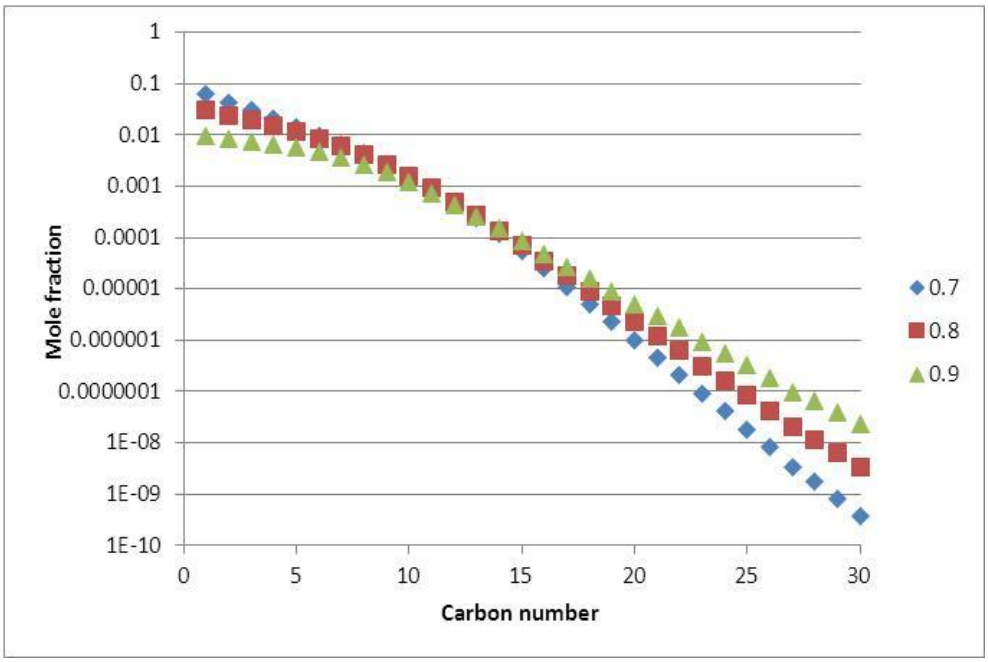


Figure 4.5: Predicted vapour phase product distribution for Case 1 at different overall chain-propagation probability.

At low values of α, that is α≅0.7, we see in Figure 4.5 that the gas phase distribution is approximately straight. Thus the product is all gas phase, and the distribution traces a single α pattern. This also shows that for an α of less than 0.7, all the products are in the gas phase. This is consistent with Caldwell and van Vuuren's [24] results, which showed that for all practical purposes the dew-point will not be reached for $\alpha < 0.653$ in an FT reactor.

As α increases, however, we see two effects. Firstly the gas phase distribution, which for light hydrocarbons follows the total production distribution α, continues to do so for fewer and fewer carbon numbers before it deviates. This indicates that more of the product is in the liquid phase.

Furthermore, as the α of the total product distribution increases, the slope of the vapour phase distribution for higher carbon numbers becomes progressively steeper, as expected.

However, the vapour phase modelling always shows a negative deviation from the ASF distribution. Thus the initial observed product distribution would track the vapour distribution more closely, and, as time went on and the liquid flow began to reach steady state, the observed product distribution would gradually approach a single α ASF distribution. Thus we can deduce that this effect does not explain the observed two-alpha plot with a positive deviation.

Case 2: A single α distribution is set up in the vapour phase.

In this case we test the theory that the reaction *sets up a single α ASF distribution in the vapour phase* and that the liquid is in VLE with the vapour.

Therefore we assume that:

$$\frac{y_{n+1}}{y_n} = \alpha \tag{37}$$

Applying the same derivation used in Case 1 from Equations (7–14) gives:

$$y_1 = (1-\alpha)(1-c) \tag{38}$$

and

$$y_n = \alpha^{n-1}(1-\alpha)(1-c) \tag{39}$$

Therefore, if there is VLE, according to Equation (18),

$$y_n = K_n x_n \tag{18}$$

this gives

$$x_1 = \frac{(1-\alpha)(1-c)}{K_1} \tag{40}$$

and hence

$$x_n = \frac{\alpha^{n-1}(1-\alpha)(1-c)}{K_n} \tag{41}$$

Thus

$$\frac{x_{n+1}}{x_n} = \frac{\alpha^n(1-\alpha)(1-c)K_n}{\alpha^{n-1}(1-\alpha)(1-c)K_{n+1}} \tag{42}$$

which simplifies to

$$\frac{x_{n+1}}{x_n} = \frac{\alpha}{\beta} \tag{43}$$

This implies that the liquid phase mole fraction slope is constant and is greater than log(1) for our assumed values of α.

The component balance can be written as

$$z_n = fy_n + (1-f)x_n \tag{5}$$

therefore

$$\frac{z_{n+1}}{z_n} = \frac{fy_{n+1}+(1-f)x_{n+1}}{fy_n+(1-f)x_n} \tag{44}$$

Substituting Equations (39) and (41) into (44) gives

$$\frac{z_{n+1}}{z_n} = \frac{f\alpha^n(1-\alpha)(1-c)+(1-f)\frac{\alpha^n(1-\alpha)(1-c)}{K_{n+1}}}{f\alpha^{n-1}(1-\alpha)(1-c)+(1-f)\frac{\alpha^{n-1}(1-\alpha)(1-c)}{K_n}} \tag{45}$$

which simplifies to

$$\frac{z_{n+1}}{z_n} = \alpha\frac{f+\frac{1-f}{K_{n+1}}}{f+\frac{1-f}{K_n}} \tag{46}$$

For lighter hydrocarbons (small n)

$$K_n \gg 1 \tag{26}$$

therefore

$$\frac{z_{n+1}}{z_n} = \alpha \tag{47}$$

In other words, the total mole fraction product distribution for lighter hydrocarbons follows the gas phase distribution.

For heavier hydrocarbons (large n)

$$K_n \ll 1 \tag{34}$$

then

$$\frac{z_{n+1}}{z_n} = \alpha \frac{K_n}{K_{n+1}} \tag{48}$$

hence

$$\frac{z_{n+1}}{z_n} = \frac{\alpha}{\beta} > 1 \tag{49}$$

It follows that the total mole fraction product distribution for heavier hydrocarbons corresponds with that of the liquid distribution, and it has a slope that is steeper than the vapour phase and higher than log(1).

Since the total mole fraction (z_n) for Case 1 was specified, no simplifying assumptions were required. We could easily calculate the vapour and the liquid product distribution. However, in this Case the vapour phase mole fraction (y_n) is specified, but the total (z_n), which is related to the conversion, is unknown.

For simplicity we assumed that H_2, CO and H_2O are present only in the vapour phase. Hence the liquid phase consists of hydrocarbons only. This gives the constraint that

$$\sum x_n = 1 \qquad (50)$$

thus the vapour fraction (f) in Equation (5) can be related to conversion. The value of f is related to conversion by the overall mass balance and therefore depends on the reactor conditions and the catalyst used. The value of f = 0.88 corresponds with a conversion close to 85%. Therefore the expected product distribution for f = 0.88 is as presented in Figure 4.6.

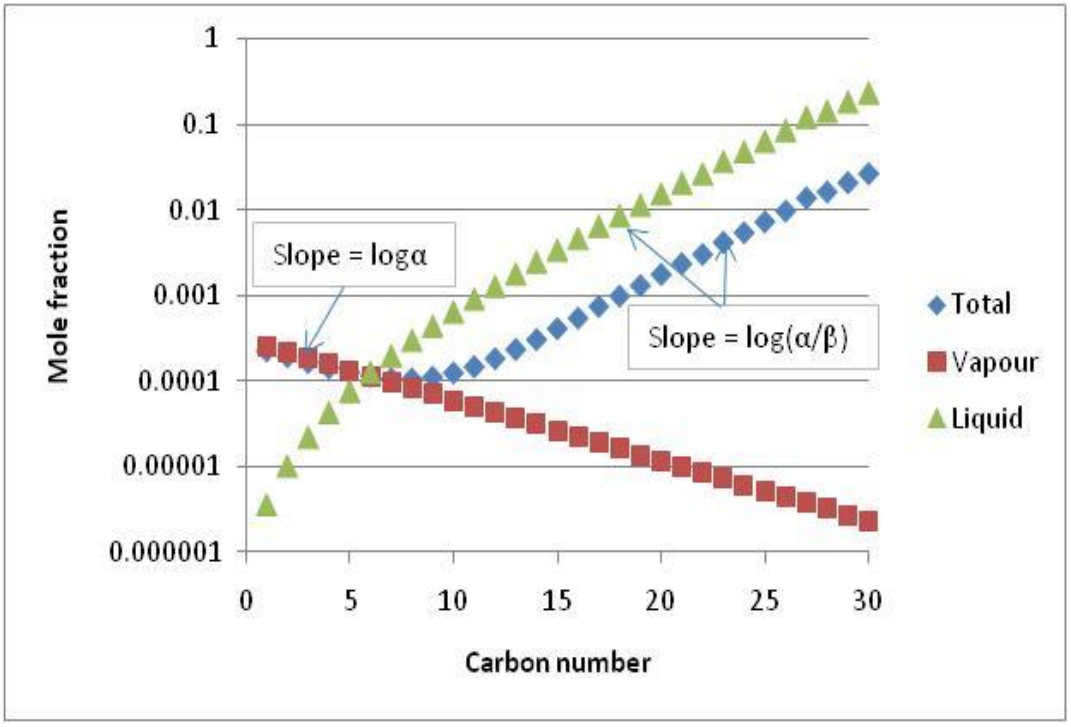


Figure 4.6: The expected liquid and total product distribution if the vapour phase has a single alpha (α=0.85) product distribution.

Changing the conversion/vapour fraction would affect the intercept of the vapour phase and the total product distribution, but not the shapes. Relaxing the assumption that the liquid phase consists of hydrocarbons only would not change the shape of the curves, which is the main point

under discussion. Since the focus is on the shape of the curves. The values of the mole fractions shown on the Figures have not been normalized and therefore depend on factors such as conversion.

We notice that the vapour and total distribution coincide for the lower carbon numbers (C1–5), while the total and the liquid distribution correspond for higher carbon numbers. The total product observed shows a positive deviation from the classical single-α ASF distribution; but the concentration of higher carbon numbers keeps increasing indefinitely, as the slope described by Equation (49) is log (α/β) where α/β>1, which leads to inconsistencies. This Case 2 theory also fails to explain the observed deviation.

It should be noted that other researchers [26] presents mole fractions of hydrocarbons only in their Figures and excludes the mole fractions of CO, H_2, N_2, CO_2 and H_2O. The Figures in this study presents overall mole fractions considering all the mole fractions in the system (hydrocarbons and non-hydrocarbons).

Most of the researchers who considered VLE in the FT reactor [15, 16, 24, 30] restricted their investigations to the theories explored in the above two Cases. However, we could reason that once the reaction begins, the catalyst would be filled with liquid, as would the reaction sites. So we might hypothesize that the reaction product distribution *is set up in the liquid phase*. This leads us to Case 3.

Case 3: A single α distribution is set up in the liquid phase, and the vapour is in equilibrium with the liquid.

We now propose that the reaction sets up a single-alpha ASF distribution in the liquid phase fairly quickly, and that it is accompanied by the forming of a vapour phase that is in equilibrium

with the liquid. The vapour phase distribution is described by VLE. As the vapour removes components from the liquid, the reaction occurs in the liquid phase so as to maintain the liquid distribution. The total product distribution can be calculated from the sum of the vapour and the liquid phase products, as described in Equation (3).

Assuming that the distribution in the liquid phase is set up very quickly and is described by a single α gives:

$$\frac{x_{n+1}}{x_n} = \alpha \tag{51}$$

As before, this implies that

$$x_1 = (1-\alpha)(1-c) \tag{52}$$

hence

$$x_n = \alpha^{n-1}(1-\alpha)(1-c) \tag{53}$$

Assuming further that the vapour phase distribution is set up so as to be in equilibrium with the liquid, then from Equation (7):

$$y_1 = K_1(1-\alpha)(1-c) \tag{54}$$

hence

$$y_n = K_n\alpha^{n-1}(1-\alpha)(1-c) \tag{55}$$

therefore

$$\frac{y_{n+1}}{y_n} = \frac{K_{n+1}\alpha^n}{K_n\alpha^{n-1}} \tag{56}$$

which simplifies to

$$\frac{y_{n+1}}{y_n} = \alpha\beta \tag{57}$$

This means that the vapour phase product distribution also has a constant slope, log(αβ). This slope is lower than that of the liquid phase, log(α).

The component balance is still given by

$$z_n = f y_n + (1 - f) x_n \tag{6}$$

therefore the total product distribution is described by

$$\frac{z_{n+1}}{z_n} = \frac{f K_{n+1} x_{n+1} + (1-f) x_{n+1}}{f K_n x_n + (1-f) x_n} \tag{58}$$

which is the same as

$$\frac{z_{n+1}}{z_n} = \frac{x_{n+1}}{x_n} \frac{f K_{n+1} + (1-f)}{f K_n + (1-f)} \tag{59}$$

and simplifies to

$$\frac{z_{n+1}}{z_n} = \alpha \frac{f K_{n+1} + (1-f)}{f K_n + (1-f)} \tag{60}$$

For lighter hydrocarbons (small n)

$$K_n \gg 1 \tag{26}$$

after which the total production distribution (Equation (60)) simplifies to

$$\frac{z_{n+1}}{z_n} = \alpha \frac{K_{n+1}}{K_n} \tag{61}$$

which can be written as

$$\frac{z_{n+1}}{z_n} = \alpha\beta \tag{62}$$

For heavier hydrocarbons (large n)

$$K_n \ll 1 \tag{34}$$

following which the total production distribution, as described by Equation (60), simplifies to

$$\frac{z_{n+1}}{z_n} = \alpha \tag{63}$$

Thus, as before, the total product distribution for lighter hydrocarbons follows the vapour phase distribution where the slope is given by log(αβ). On the other hand, the total product distribution for heavier hydrocarbons is consistent with the liquid phase product distribution where the slope is given by log(α). This Case 3 model gives a 2-α distribution. The product distribution expected is presented in Figure 4.7.

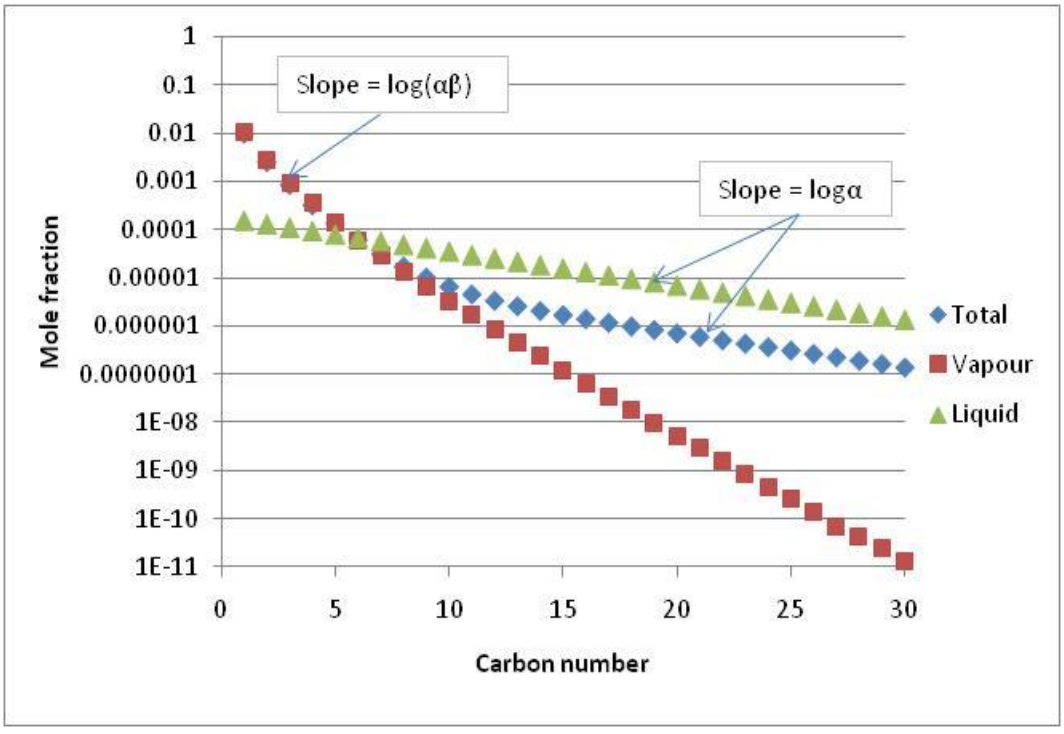


Figure 4.7: The expected product distribution for a single-alpha liquid product distribution. Alpha in liquid is 0.85 and beta is 0.63, corresponding to a temperature of 200 °C

This clearly shows the observed deviation from the single alpha ASF distribution. Hence, postulating a single alpha in the liquid phase does succeed in explaining the two-alpha product distribution. It is noticeable that the total distribution follows the vapour phase distribution up to a carbon number of around 10, and thereafter conforms to the liquid phase distribution. Even for a fixed alpha, this break depends on the temperature through the value of β, and would not be very pressure-sensitive. The values of the mole fractions in Figure 4.7 are for explanations only. The actual values would depend on the mass balance which is not fully specified in this Case due to the fact that the sum of the mole fractions of hydrocarbons in the liquid phase is less than one as discussed below. The values in Figure 4.7 are for $\sum x_n = 0.001$.

An interesting prediction we can make based on this Case is that if we consider the sum of hydrocarbons in the liquid phase, *we can show that the sum of mole fractions of hydrocarbons must be less than 1.*

Proof:

The sum of hydrocarbons in the liquid phase is given by

$$\sum x_n = x_1 + x_2 + x_3 + \cdots \tag{64}$$

A single alpha in the liquid phase gives

$$\sum x_n = x_1 + \alpha x_1 + \alpha^2 x_1 + \cdots \tag{65}$$

which is equivalent to

$$\sum x_n = (1 + \alpha + \alpha^2 + \cdots) x_1 \tag{66}$$

thus

$$\sum x_n = \frac{x_1}{(1-\alpha)} \tag{67}$$

Using Raoult's law gives

$$\sum x_n = \frac{y_1}{(1-\alpha)} \frac{P}{P_{vap1}} \tag{68}$$

but

$$P_{vap1} \gg P \tag{69}$$

hence, for $0 \leq y_1 \leq 1$ and $0 \leq \alpha \leq 1$,

$$\sum x_n < 1 \tag{70}$$

Two possible explanations are: that the liquid phase cannot consist purely of hydrocarbons; and/or that the assumption of an ideal VLE/Raoult's law is incorrect. Bremaud *et al.* [38] computed the liquid composition of CO, H_2 and H_2O in the reactor during their experiment. They found that H_2O is the most abundant species in the liquid phase, which would explain how the sum of mole fractions of hydrocarbons in the liquid phase is less than one. Even if a separate aqueous phase exists this does not affect the above argument.

The model predicts that; for $0 \leq \alpha \leq 1$, only hydrocarbons in the liquid phase, $\sum x_n < 1$, furthermore that the hydrocarbon with the highest concentration in the liquid phase is the lightest component. We will not take these results further in this paper, but the implications of these results are very interesting if they are indeed correct.

The focal point of discussion is the shapes of the curves. The actual values of mole fractions would be different depending on the catalyst and the conditions used. The relationship between the slopes predicted by Case 3 explains the observed product distribution.

4.6 DISCUSSION

The results in all three Cases carry some common implications. The total and vapour distributions correspond for the light hydrocarbons, while it is the total and liquid compositions that correspond in the instance of the heavier hydrocarbons.

We can deduce from these Cases that a single-alpha ASF distribution can be observed only for a vapour phase FT reactor (in other words low-alpha or high-temperature FT). Once the dew point of the reactor is reached and liquid is formed inside it, the two-alpha negative deviation can be observed only in the non-steady state condition, while liquid is still building up in the reactor. However, once VLE has been reached under steady state conditions, the expected product distribution would be as shown in Case 3. In this final Case, the lightest component is present in the highest concentration in the liquid, which is somewhat counterintuitive. Even if methane does not follow this model, then ethane or propane would, and in this case the highest concentration in the liquid would be ethane and/or propane.

In terms of testing whether Case 3 applies or not, various of the predictions can be checked. Firstly, by setting up an experiment we could compare both the predicted break in alpha and the predicted relationship between the two slopes to experimental data. We then do in the practical research described below.

However there are other tests that could be done, such as testing the composition of the liquid, particularly in the case of the lighter hydrocarbons. There may also be novel ways of running the reactor to try to determine if we do indeed have VLE in the reactor. None of these are addressed in this paper. The model results should describe the reactor at all relevant FT conditions. Therefore the experiment could be conducted at any relevant FT condition.

4.7 EXPERIMENTAL RESULTS

We conducted an experiment in a fixed bed micro-reactor at 270°C and 8 bar, using a 10% iron catalyst by mass on titania support. The catalyst was prepared by the incipient wetness impregnation method, and the catalyst support was Degussa Titania (TiO_2) P25, Surface Area = 50 m^2g^{-1}. The metal precursor selected was Aldrich $Fe(NO_3)_3 \cdot 9H_2O$.

A heating jacket was connected to a temperature controller and was mounted around the reactor's outer casing to supply heat, and we placed a thermocouple near the centre of the reactor to record the temperature in the chamber.

The reactor feed was a pre-mixed synthesis gas (10% N_2, 30% CO and 60% H_2). We used a by-pass line to allow a direct gas chromatograph (GC) analysis of the feed for calibration purposes. The synthesis gas was introduced through the reactor, allowed to flow through the catalyst bed, and then passed through a hot trap maintained at 150°C for wax collection. Thereafter it entered a cold trap maintained at room temperature (≈ 25°C) for collection of the liquid (oil and aqueous) fraction.

The operating pressure in the reactor was maintained at 8 bar by means of a pressure regulator on the gas cylinder and a needle valve at the reactor exit. The needle valve was also used to control the gas space velocity in the reactor and to de-pressurize the outlet gas stream before it reached the GCs. Two pressure indicators were used, one at the reactor feed and another one at the reactor exit, to check the total pressure in the reactor. Two solenoid valves, which automatically directed the reactor outlet gas to vent or to the GCs for analysis, were mounted behind the needle valve. The experimental setup is shown in Figure 4.8.

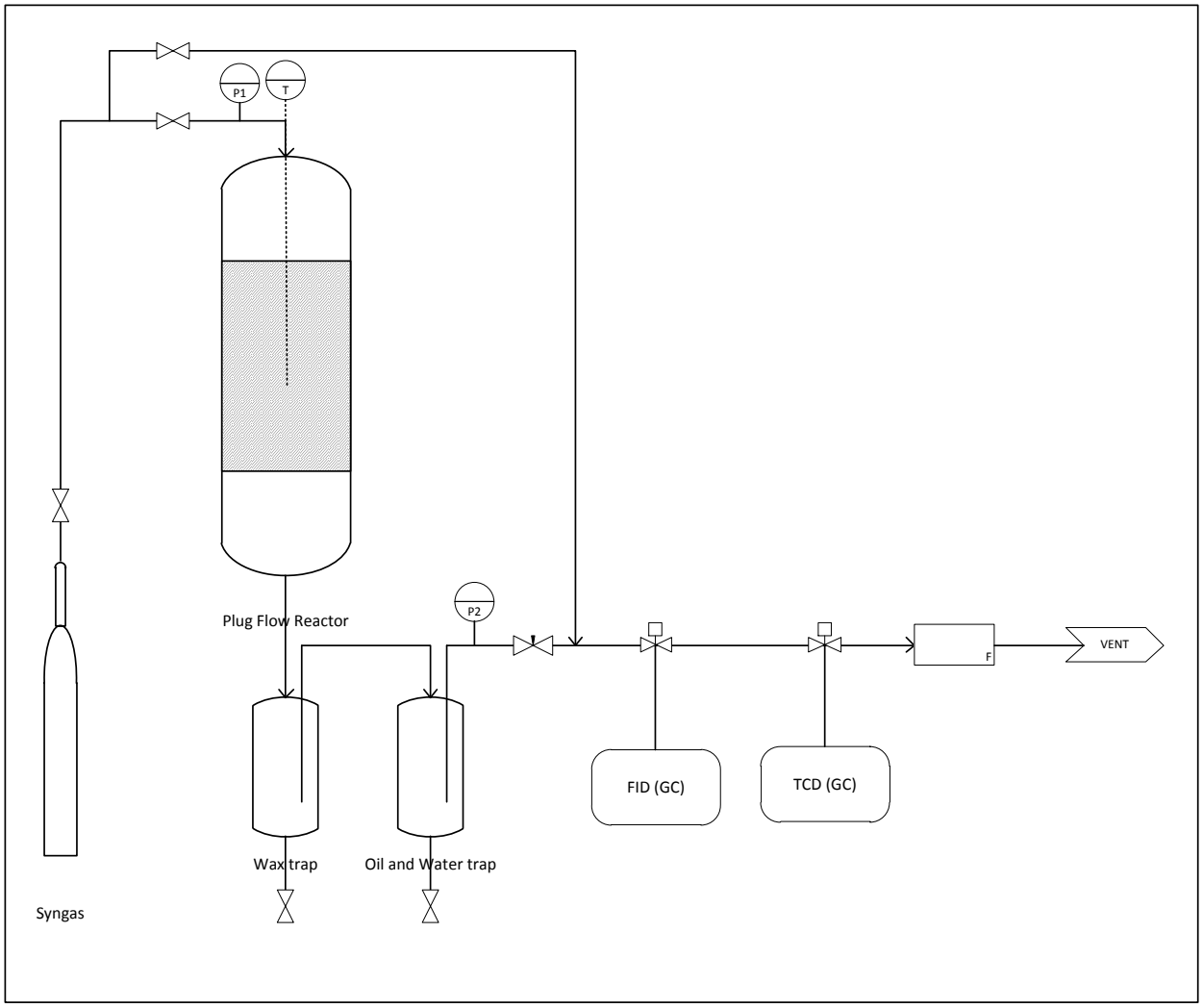


Figure 4.8: Setup of experimental Fischer-Tropsch system.

The gas was directed to the GCs for only the short period required to flush out the residual gas in the sampling loops, to allow for further sampling. For the remainder of the time the solenoid valves vented the outlet gas to the atmosphere to keep the sampling line clean. A new gas sample was analysed every two hours.

The gas analysis was carried out online using two GCs, one with a flame ionization detector (FID) and the other with a thermal conductivity detector (TCD). The GC equipped with FID had a Poropak-Q column that was used to separate hydrocarbons from C1–9. The GC fitted with the

TCD was employed in the analysis of the inorganic gases H_2, He, N_2, CO on a carbosieve S-II packed column. We determined the actual molar composition of the gas by means of calibration data and relative response factors.

Wax, oil and water were allowed to accumulate in the hot and cold traps respectively, and were collected at the end of the mass balance period. We carried out the oil and wax fractions analysis with an off-line GC with an FID on a BP-5 capillary column. For the analysis of these condensed phases we obtained a mass composition directly from the GC peak area percentages, as the mass response factors were around one. The product distribution obtained at the end of the mass balance period is shown in Figure 4.9.

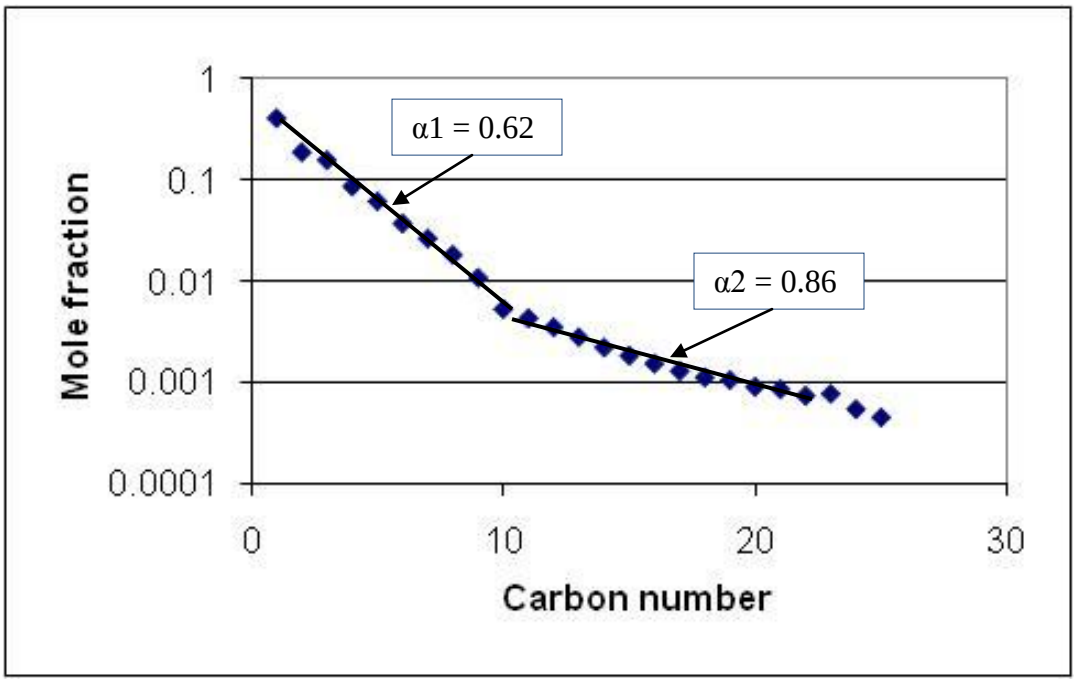


Figure 4.9: Total product distribution from the experimental results obtained using an iron catalyst at 270 °C and 8 bar.

The experimental results presented in Figure 4.9 clearly show a two-alpha positive deviation from the classical ASF product distribution. The break in alphas occurs at carbon number 10,

which is consistent with many of the experimental and industrial results reported in the scientific literature. The α_1 from C1–10 was found to be 0.62, and α_2 from C10–22 to be 0.86. We ignored the last three points to minimise experimental errors.

The Liquid-Phase ASF Product Distribution Model (Case 3) was applied to predict α_1 for the given experimental conditions, using the liquid phase alpha (α_2) of 0.86. According to Equation (62), α_1 is given by ($\alpha_2\beta$), in this case at 270 °C, $\beta \approx 0.71$. This anticipates that the value of α_1 is 0.61, which corresponds with the experimental value observed, and demonstrates that the model can predict the FT product distribution.

4.8 CONCLUSIONS

Pure vapour-phase FT can be carried out only at low alpha ($\alpha < 0.7$). In this case a single alpha would be expected. However, once the dew-point of the reactor content is reached, VLE should play a role.

If the total product distribution followed a single alpha (Case 1), the distribution and VLE were set up quickly, and the liquid had sufficient time to accumulate and start flowing out of the reactor, one might anticipate that initially one would observe the gas phase distribution. This, although it would display the two-alpha slope, would show the negative deviation from the classical ASF distribution. This might explain some of the two-alpha negative deviations reported in the literature. However, as the duration of the experiment increase and the liquid flow in the reactor begin to reach steady state, the observed product distribution would gradually approach a single-α ASF distribution. This effect does not explain the widely-reported two-alpha positive deviation.

If the reaction sets up a single alpha distribution in the vapour-phase (Case 2), and the liquid-phase is in VLE with that vapour, then the observed total product would show a positive deviation from the classical single-alpha ASF distribution. However, the concentration of higher carbon numbers would keep increasing indefinitely, as the slope described by Equation (49) is log (α/β) where $\alpha/\beta>1$, which is inconsistent.

Once the reaction begins, the catalyst and the reaction sites would become filled with liquid. This might lead us to assume that the single-alpha (α) reaction product distribution is set up in the liquid phase (Case 3). A vapour phase is formed in equilibrium with the liquid phase, therefore the total product distribution can be calculated from the sum of the vapour and the liquid phases. After that, the total product distribution for lighter hydrocarbons follows the vapour phase distribution where the slope is given by $\log(\alpha\beta)$. On the other hand, the total product distribution for heavier hydrocarbons follows the liquid phase product distribution where the slope is given by $\log(\alpha)$. Thus this model predicts a two-alpha distribution and also predicts the expected positive deviation product distribution. This model also predicts the relationship between the two slopes and we find that the break in between the two slopes is predicted to occur around carbon number ten.

In all models for the light hydrocarbons, the total and vapour distributions correspond, while for heavier hydrocarbons, the total and liquid compositions correspond.

Experimental results were compared to the predictions of Case 3 and they show that the liquid-phase ASF product distribution model can predict the FT product distribution, as we found that the experimentally measured α_1 was related to the experimentally measured α_2 by $\alpha_1 = \alpha_2\beta$.

An interesting prediction from this model is that the liquid phase cannot be only hydrocarbon as $\sum x_n < 1$. We would need to do further modelling as well as experimental work to investigate this prediction further.

NOMENCLATURE

m_n: mole fraction of hydrocarbon with chain length n.

α: chain-growth probability factor.

F: reactor feed molar flow rate.

V: vapour flow rate.

L: liquid flow rate.

Z: total flow rate (sum of the vapour and the liquid flow rates).

y_n: mole fraction of component n in the vapour phase.

x_n: mole fraction of component n in the liquid phase.

z_n: total mole fraction of component n.

f: vapour fraction (f = V/Z).

$P_{vap,n}(T)$: vapour-pressure of component n at temperature T.

K_n: $y_n/x_n = P_{vap,n}/P$

β: ratio of vapour pressure of component n+1 to the vapour pressure of component n.

c: total mole fraction of components other than hydrocarbons.

P: operating pressure.

REFERENCES

[1] D.F. Smith, C.O. Hawk, P.L. Golden, The Mechanism of the Formation of Higher Hydrocarbons from Water Gas, *J. Am. Chem. Soc. 52* (1930) 3221−3232.

[2] M.E. Dry, Catalytic aspects of industrial Fischer–Tropsch synthesis, *J. Mol. Catal. 17* (1982) 133−144.

[3] M.E. Dry, The Fischer–Tropsch process: 1950–2000. *Catal. Today 71* (2002) 227–241.

[4] P.J. Flory, Molecular size distribution in linear condensation polymers, *J. Am. Chem. Soc. 58* (1936) 1877−1885.

[5] E.F.G. Herington, The Fischer–Tropsch synthesis considered as a polymerization reaction, *Chem. Ind. 65* (1946) 346−347.

[6] R.B. Anderson, H. Friedel, H.H. Scorch, Fischer–Tropsch reaction mechanism involving stepwise growth of carbon chain, *J. Chem. Phys. 19* (1951) 313−319.

[7] R.B. Anderson, Catalysts for the Fischer–Tropsch Synthesis, Vol. IV. Reinhold, New York, 1956, pp. 337.

[8] C.N. Satterfield, G.A. Huff, Carbon number distribution of Fischer–Tropsch products formed on an iron catalyst in a slurry reactor, *J. Catal. 73* (1982) 187−197.

[9] C.N. Satterfield, G.A. Huff, J.P. Longwell, Product distribution from iron catalysts in Fischer–Tropsch slurry reactors, *Ind. Eng. Chem. Process Des. Dev. 21* (1982) 465−470.

[10] X. Zhan, B.H. Davis, Assessment of internal diffusion limitation on Fischer–Tropsch product distribution, *Appl. Catal. A: Gen. 236* (2002) 149–161.

[11] B.H. Davis, The two-alpha value for iron Fischer–Tropsch catalyst: fact or fiction?, *ACS Div. Fuel Chem. (Preprints) 37* (1992) 172−183.

[12] T.J. Donnelly, I.C. Yates, C.N. Satterfield, Analysis and Prediction of Product Distributions of the Fischer–Tropsch Synthesis, *Energy Fuels 2* (1988) 734−739.

[13] G.A. Huff, C.N. Satterfield, Evidence for two chain growth probabilities on iron catalysts in the Fischer–Tropsch synthesis, *J. Catal. 85* (1984) 370−379.

[14] B. Shi, B.H. Davis, Fischer–Tropsch synthesis: accounting for chain length related phenomena, *Appl. Catal. A: Gen. 277* (2004) 61−69.

[15] R.A. Dictor, A.T. Bell, An Explanation for Deviations of Fischer–Tropsch Products from a Schulz–Flory distribution, *Ind. Eng. Chem. Process Des. Dev. 22* (1983) 678–681.

[16] A.P. Raje, B.H. Davis, Effect of Vapor–Liquid Equilibrium on Fischer–Tropsch Hydrocarbon Selectivity for a Deactivating Catalyst in a Slurry Reactor, *Energy Fuels 10* (1996) 552−560.

[17] E. Iglesia, S.C. Reyes, R.J. Madon, S.L. Soled, Selectivity control and catalyst design in the Fischer-Tropsch synthesis: Sites, Pellets, and Reactors, *Adv. Catal. 39* (1993) 221−302.

[18] B.W. Wojciechowski, Mechanistic consideration of paraffin, olefins and alcohol distributions in FT synthesis, *Can. J. Chem. Eng. 64* (1986) 149−153.

[19] E.W. Kuipers, I.H. Vinkenburg, H. Oosterbeek, Chain length dependence of α-olefin readsorption in Fischer–Tropsch synthesis, *J. Catal. 152* (1995) 137–146.

[20] H. Schulz, M. Claeys, Kinetic modelling of Fischer–Tropsch product distributions, *Appl. Catal. A: Gen. 186* (1999) 91−107.

[21] H. Schulz, M. Claeys, Reactions of α-olefins of different chain length added during Fischer–Tropsch synthesis on a cobalt catalyst in a slurry reactor, *Appl. Catal. A: Gen. 186* (1999) 71−90.

[22] E. Iglesia, S.C. Reyes, R.J. Madon, Transport-enhanced α-olefin readsorption pathways in Ru-catalyzed hydrocarbon synthesis, *J. Catal. 129* (1991) 238–256.

[23] G.P. van der Laan, A.A.C.M. Beenackers, Kinetics and Selectivity of the Fischer–Tropsch synthesis: A literature review, *Catal. Rev. –Sci. Eng. 41* (1999) 255−318.

[24] L. Caldwell, D.S. van Vuuren, On the formation and composition of the liquid phase in Fischer–Tropsch reactor, *Chem. Eng. Sci. 41* (1986) 89−96.

[25] J.M. Fox, S.S Tam, Correlation of slurry reactor Fischer–Tropsch yield data, *Top. Catal. 2* (1995) 285−300.

[26] J.J. Marano, G.D. Holder, Characterization of Fischer–Tropsch liquids for vapor–liquid equilibria calculations, *Fluid Phase Equilib. 138* (1997) 1–21.

[27] I.V. Derevich, V.S. Ermolaev, V.Z. Mordkovich, Liquid–Vapor thermodynamic equilibrium in Fischer–Tropsch synthesis products, *Theor. Found. Chem. Eng. 42* (2008) 216−219.

[28] S. Srinivas, R.K. Malik, S.M. Mahajani, Feasibility of reactive distillation for Fischer–Tropsch synthesis, *Ind. Eng. Chem. Res. 47* (2008) 889−899.

[29] V.R. Ahon, E.F. Costa, J.E.P. Monteagudo, C.E. Fontes, E.C. Biscaia, P.L.C. Lage, A comprehensive mathematical model for the Fischer–Tropsch synthesis in well-mixed slurry reactors, *Chem. Eng. Sci. 60* (2005) 677−694.

[30] X. Zhan, B.H. Davis, Two alpha Fischer–Tropsch product distribution. A role for vapor–liquid equilibrium?, *Pet. Sci. Technol. 18(9/10)* (2000) 1037−1053.

[31] C.M. Masuku, W. Ma, D. Hildebrandt, D. Glasser, B.H. Davis, A vapor–liquid equilibrium thermodynamic model for a Fischer–Tropsch reactor, *Fluid Phase Equilib. 314* (2012) 38–45.

[32] R.J. Madon, E. Iglesia, Catalytic reaction rates in thermodynamically non-ideal systems, *J. Mol. Catal. A: Chem. 163* (2000) 189–204.

[33] A. Behkish, R. Lemoine, L. Sehabiague, R. Oukaci, B.I. Morsi, Prediction of the gas holdup in industrial-scale bubble columns and slurry bubble column reactors using back-propagation neural networks, *Int. J. Chem. React. Eng. 3* (2005) A53.

[34] A. Behkish, R. Lemoine, R. Oukaci, B.I. Morsi, Novel correlations for gas holdup in large-scale slurry bubble column reactors operating under elevated pressures and temperatures, *Chem. Eng. J. 115* (2006) 157–171.

[35] A. Behkish, R. Lemoine, L. Sehabiague, R. Oukaci, B.I. Morsi, Gas holdup and bubble size behavior in large-scale slurry bubble column reactor operating with an organic liquid under elevated pressures and temperatures. *Chem. Eng. J. 128* (2007) 69–84.

[36] A. Behkish, Z. Men, J.R. Inga, B.I. Morsi, Mass transfer characteristics in a large-scale slurry bubble column reactor with organic liquid mixtures. *Chem. Eng. Sci. 57* (2002) 3307–3324.

[37] L. Sehabiague, R. Lemoine, A. Behkish, Y.J. Heintz, M. Sanoja, R. Oukaci, B.I. Morsi, Modeling and optimization of a large-scale slurry bubble column reactor for producing 10,000 bbl/day of Fischer–Tropsch liquid hydrocarbons, *J. Chin. Inst. Chem. Eng. 39* (2008) 169–179.

[38] M. Bremaud, P. Fongarland, J. Anfray, S. Jallais, D. Schweich, A.Y. Khodakov, Influence of syngas composition on the transient behavior of a Fischer–Tropsch continuous slurry reactor, *Catal. Today 106* (2005) 137−142.

Chapter 5 : VARIATION OF RESIDENCE TIME WITH CHAIN LENGTH FOR PRODUCTS IN A SLURRY PHASE FISCHER–TROPSCH REACTOR

ABSTRACT

The phrases “product accumulation” or “accumulated products” or “product holdup” have appeared in literature during the past several decades to qualitatively explain the experimental results for Fischer–Tropsch synthesis (FTS). This study develops an experimental method for a slurry reactor to evaluate the product accumulation inside the FT reactor by measuring the average residence time of products as a function of carbon number. The effect of accumulation of products on vapour–liquid equilibrium (VLE) in the reactor is also investigated. The results show that VLE is reached inside the FT reactor for components up to C_{17}. Furthermore, the relationship between the mole fractions of components in the vapour and the liquid phase for lighter hydrocarbons, up to around C_{17} are adequately described by Raoult’s law. These results suggests that chain length-dependent solubility in the liquid phase is the predominant cause for chain length-dependencies of secondary olefin reactions in FTS and diffusion limited removal of products is only significant for products with carbon number greater than 17.

Keywords: *Hydrocarbons Residence Time; Deuterium Tracer; Vapour–Liquid Equilibrium; Fischer–Tropsch Product Accumulation; Chain Length Related Phenomena.*

5.1 INTRODUCTION

The chemical industry faces unparalleled challenges, in terms of providing for growing energy markets and meeting the needs of an increasing world population that aspires to a more advanced material quality of life, while simultaneously minimizing the environmental impacts of pollution from the process industry. The world's resources are limited, particularly crude oil and the other fossil fuels, and hence an improvement in the efficiency of chemical manufacture is required to increase product yields, improve selectivities and reduce energy costs. The Fischer–Tropsch synthesis (FTS) reaction is an area that is receiving revived interest worldwide as a technology alternative to produce both transportation fuels and chemicals from synthesis gas (syngas). FTS has been studied for over 80 years [1]. FTS produces a range of hydrocarbons of different chain lengths and based on the product analysis, Friedel and Anderson [2] in the 1950s found that the products obtained during synthesis followed an Anderson–Schulz–Flory (ASF) distribution as shown in Equation (1):

$$m_n = (1-\alpha)\alpha^{n-1} \quad (1)$$

where:

n is the number of carbon atoms in the hydrocarbon,

m_n is the mole fraction of products containing n carbon atoms, and

α is the probability of chain growth.

Around the same period, Emmett and co-workers [3–5] found that the C_2 species derived from ethanol or ethylene acted as an initiator for the FTS reaction. This conclusion was based on the observation that the molar radioactivity of hydrocarbons from C_3 to about C_8 are the same when ^{14}C labeled ethanol or ethylene were used as tracers. The ASF distribution equation and the conclusions obtained from ^{14}C tracer studies provided the bases for understanding the mechanism of the FTS reaction.

However, subsequent studies showed that the measured product distribution from the FTS reactions seldom obeyed the ASF kinetics, especially when the carbon number of the

hydrocarbons was greater than around 8, leading to either negative [6–9] or positive deviations [10–15] from the ASF distribution; the measured α values increases with decreasing syngas flow rate [14, 16]; the paraffin to olefin ratio increases exponentially with increasing the molecular size [17]; and the molar radioactivity or stable isotope content of hydrocarbons decrease with increasing molecular size for an initiator [18–21].

To explain these chain length related phenomena, theories proposed include: models based on the assumption of two-active-sites [12, 13], models based on diffusion-enhanced olefin readsorption effects [14, 22, 23], olefin readsorption product distribution models [24], models based on the different physisorption strength of the olefins [15–17], or the greater solubility of larger olefins [16, 17], and VLE phenomena based models [9, 25, 26]. Some of the theories proposed over the past several decades can address some of the observed chain length related anomalies, but none of them can describe all the observations.

Based on the studies of accumulated products in FTS reactions conducted in a continuously stirred autoclave slurry reactor, Shi and Davis [27] proposed that the apparent products of the FTS reaction is a mixture of freshly produced FTS products and the products left in the reactor. Using this concept, most of the chain length related anomalies were accounted for. According to their model, they concluded that in order to obtain the correct product distribution and the paraffin to olefin ratio of an FTS reaction, it is necessary to find a way to eliminate or evaluate products left in the reactor, which requires conducting FTS research in a different way. However, they did not quantitatively determine the residence times of various hydrocarbons in the FT reactor. In this study we experimentally measure the residence times of heavier hydrocarbons in the FT slurry reactor and discusses the implications of the results on the modeling of the product distribution. We believe that these observations contribute fundamentally to the understanding of the complex Fischer–Tropsch kinetic regime.

5.2 DEUTERIUM TRACER EXPERIMENTS

In studying the mechanism of FTS, isotopic tracer techniques have been widely used and, based on the results several very important conclusions have been reported [4, 5, 28–33]. The most frequently used isotopes in FT reactions are carbon-14- and carbon-13-labeled compounds. Almost all of the possible carbon-14- and carbon-13-labeled compounds suitable for studying the mechanism of FT reactions, such as alcohols, alkenes, CO, CO_2, aldehyde, and many others, have been used as probes [34]. Compared to the number of carbon-14 and carbon-13 tracer experiments, few deuterium tracer experiments have been conducted to study the mechanism of the FT reaction [35].

Recently, Shi and Davis [36] reported that product hold-up has a very important impact on the data interpretation in isotopic tracer studies of FT reactions. They reported that due to the nature of isotope tracer experiments in FTS, this product accumulation factor could be minimized, but could not be removed completely in ^{14}C tracer studies.

The belief that H/D exchange might occur under FT reaction conditions is the main reason why just a few deuterium tracer experiments have been conducted even though the deuterium tracer technique is one of the most frequently used methods in homogeneous organic reactions [35]. However until recently, no experiment had been performed to show whether there is an H/D exchange reaction among the major products under FT reaction conditions. The importance of this is that if there is no H/D exchange in alkanes, it would be possible to study the chemical behavior of alkanes under FT reaction conditions using the deuterated alkane as the probe.

Shi *et al.* [35] addressed the questions of whether there is H/D exchange in alkanes under the iron-catalyzed FT reaction conditions and the extent of isomerization of 1-alkene products. They found that deuterium/hydrogen exchange does not occur in alkanes under reaction conditions. Since there was no H/D exchange in the alkane, the opportunity to use deuterium tracer techniques to study the mechanism for FT reaction is appropriate.

Deuterium has been used to study the Fischer–Tropsch reaction for over 60 years [37–40]. Olefin readsorption has also been confirmed using deuterium tracing [35]. Some researchers [14, 17, 41–43] stated that long chains hydrocarbons have longer residence time in the reactor. Schulz and Claeys [43] estimated the residence times of lighter hydrocarbons (C_2–C_{11}). However, the residence times of long chain hydrocarbons have not been experimentally quantified. We devised a novel combination of experiment and modeling to quantify the residence times of long chain hydrocarbons using deuterium tracing.

5.3 EXPERIMENTAL SECTION

5.3.1 FT Reactor and Analysis of Products

The FT reaction is carried out in a slurry phase 1 L CSTR autoclave reactor as shown in Figure 5.1. CO and H_2 are metered separately and premixed in a 0.5 L vessel before being fed to the reactor. The vapour phase products exit the reactor out the top of the reactor and pass through a fritted filter and then through two traps in series. The warm trap is maintained at 373 K, while the cold trap is maintained at 273 K. The uncondensed gases from these two traps pass through a back-pressure regulator to a flow meter to measure the exit gas flow rate. The uncondensed gases are periodically sampled and analysed by on-line gas chromatographs (GCs). The condensed products from the warm and cold traps are collected as required and analysed through off-line GCs. The liquid phase product is collected as required through the internal filter into the hot trap maintained at 473 K.

A cobalt catalyst on alumina (25% Co/Al_2O_3) with 0.5% Pt was used. 8.3 grams of calcined catalyst were reduced ex situ in a plug flow reactor using 25% H_2/He mixture at 623 K for 10 h. The reduced catalyst was transferred to the 1 L CSTR which already contained 310 g of melted Polywax 3000 (polyethylene with average MW of 200) as a start-up solvent under flowing nitrogen. The catalyst was further reduced in situ using pure H_2 (4.2×10^{-6} m^3/s (STP)) for 24 h at

503 K. The FT synthesis reaction was conducted at 493 K, 2.0 MPa with a space velocity of 0.0011 $m^3(kg_{cat})^{-1}s^{-1}$ (STP) and at a constant H_2/CO ratio of 2.0.

The composition of the uncondensed product gases is obtained from a Hewlett–Packard Quad Series Micro GC, specifically used as a refinery gas analyser (RGA). The micro GC has four columns that run in parallel. This is used to quickly obtain the mole fractions of CO, H_2, N_2, CO_2, and C_1 to C_6 hydrocarbons in the uncondensed product gases.

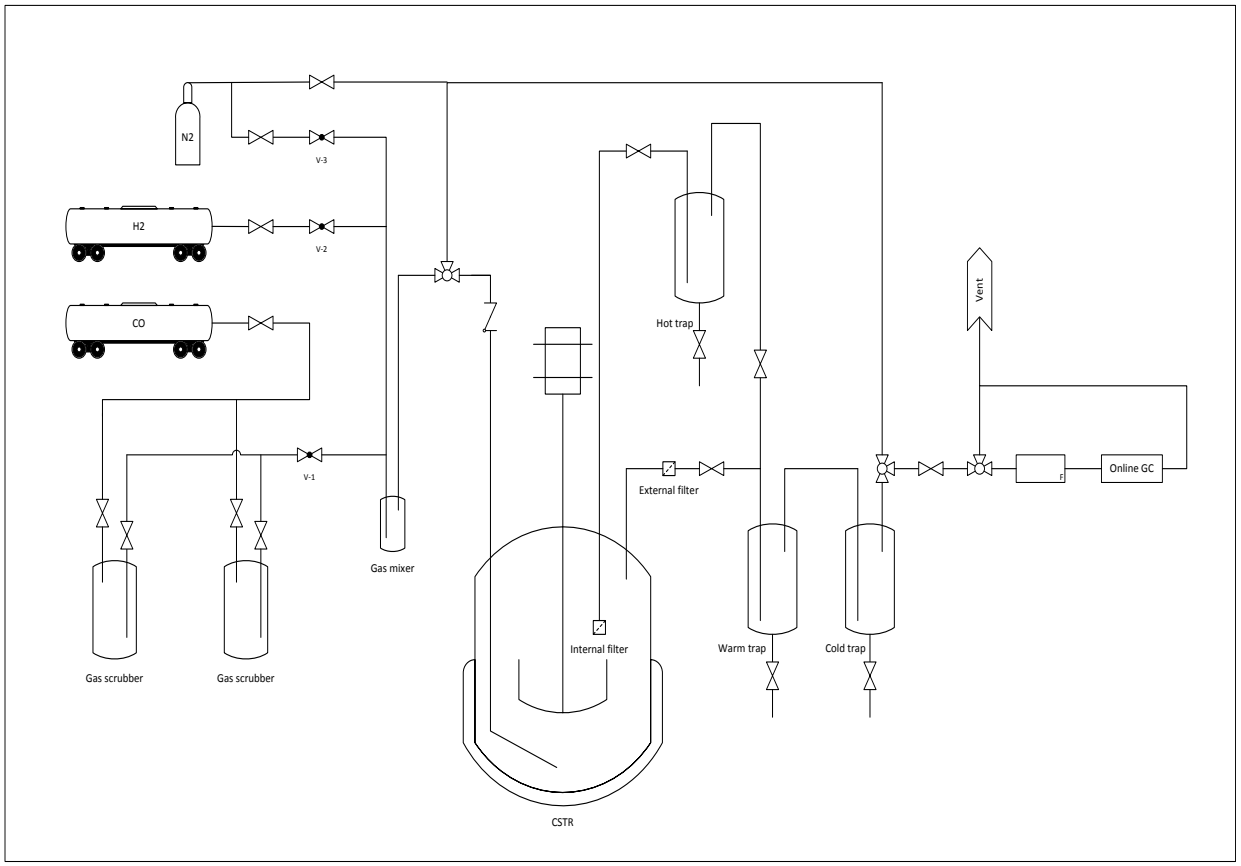


Figure 5.1: A schematic diagram of the Fischer–Tropsch reactor system.

The condensed liquid products are separated into an aqueous and a hydrocarbon (oil + wax) phase. The aqueous phase is analysed in a Hewlett–Packard 5790A gas chromatograph with a

Porapak Q packed column using a thermal conductivity detector (TCD). The oil phase is analysed using a 6890 Agilent GC with a DB-5 capillary column and a flame ionization detector (FID). The wax phase is analysed using 6890 Agilent GC FID with a high temperature DB-1 capillary column.

5.3.2 Analysis of Accumulated Products

Applications of isotopic tracer techniques have played important roles in developing and understanding of the mechanism for FTS [28]. The general procedure for determining the accumulated products in FTS is as follows: (1) the FTS is started in the 1 L CSTR using H_2/CO as the synthesis gas as described above; (2) after several days (15 days in this case), when the reaction has reached a stable CO conversion and/or at the point where the accumulation is to be evaluated, all the collection vessels are emptied and the feed is switched from CO/H_2 to CO/D_2 for 24 hours and then switched back to CO/H_2; and (3) a sample is collected every 24 h until deuterium-containing compounds cannot be detected. Likewise, the reaction can also be started by using CO/D_2 as the reagents and then switch to CO/H_2. The deuterium content of the tracer compounds and its products was determined using GC–MS. The quantitative analysis of the isotopomers of products by GC–MS method has been described previously [35].

5.3.3 CO Conversion

The pseudo-steady state CO conversion attained before the isotope switch was around 32% as shown in Figure 5.2. The results in Figure 5.2 show an increase in the CO conversion after switching from H2 to D2. Shi and Jin [44] and Yang et al. [45] also observed an increase in the CO conversion when the synthesis gas was switched from H_2 to D_2. They attributed this change in conversion to the inverse kinetic isotope effect which is a possible explanation.

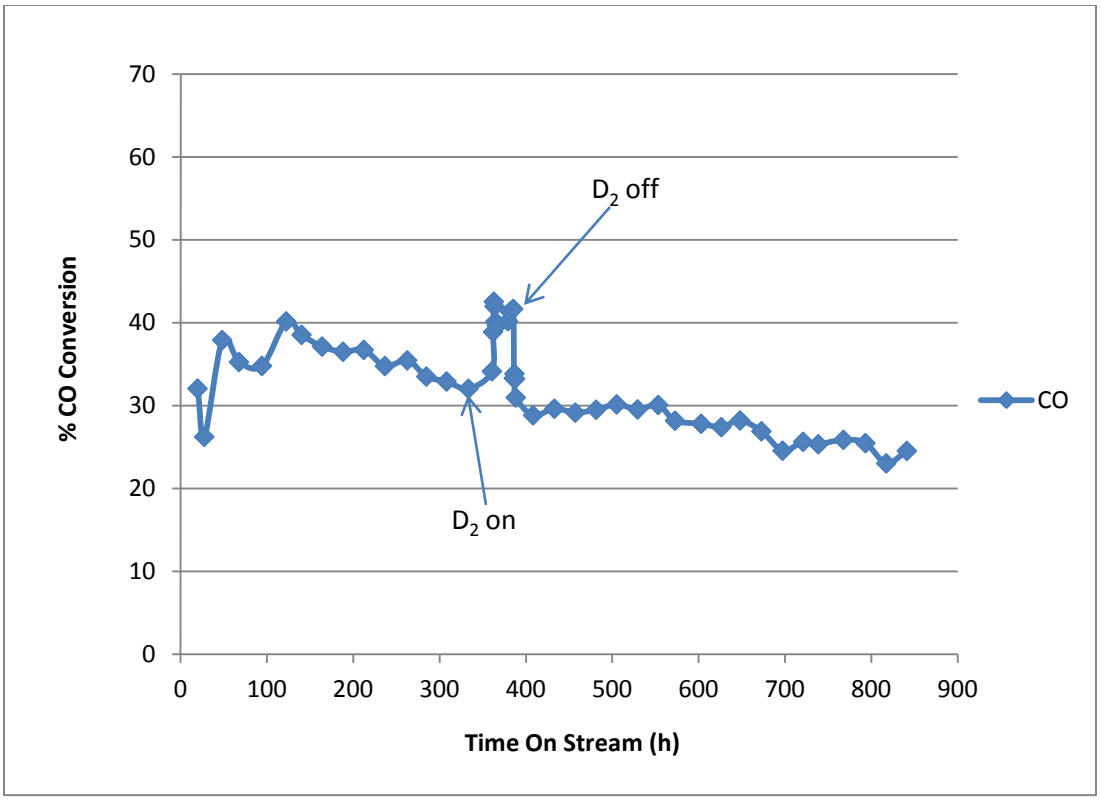


Figure 5.2: Percentage CO conversion for the duration of the experiment. Time = 0 corresponds to the reactor start up. (T = 493 K, P = 2.0 MPa, H_2/CO = 2)

However, the vapour pressure of hydrogen is greater than the vapour pressure of deuterium [46–48]. Therefore, more deuterium should be in the liquid phase compared to hydrogen. This may also explain the increase in the CO conversion shown in Figure 5.2 when hydrogen is switched to deuterium. However, this should have negligible effect on the residence time determination.

5.4 ESTIMATION OF THE RESIDENCE TIME OF THE GAS PHASE

Hydrogen and deuterium have different thermal conductivities. Hence the TCD response was used as a quick measure to determine how long it takes to replace H_2 with D_2 in the gas phase as a measure of the residence time in the gas phase. The TCD response shows that in the gas phase hydrogen is replaced by deuterium within six hours as shown in Figure 5.3.

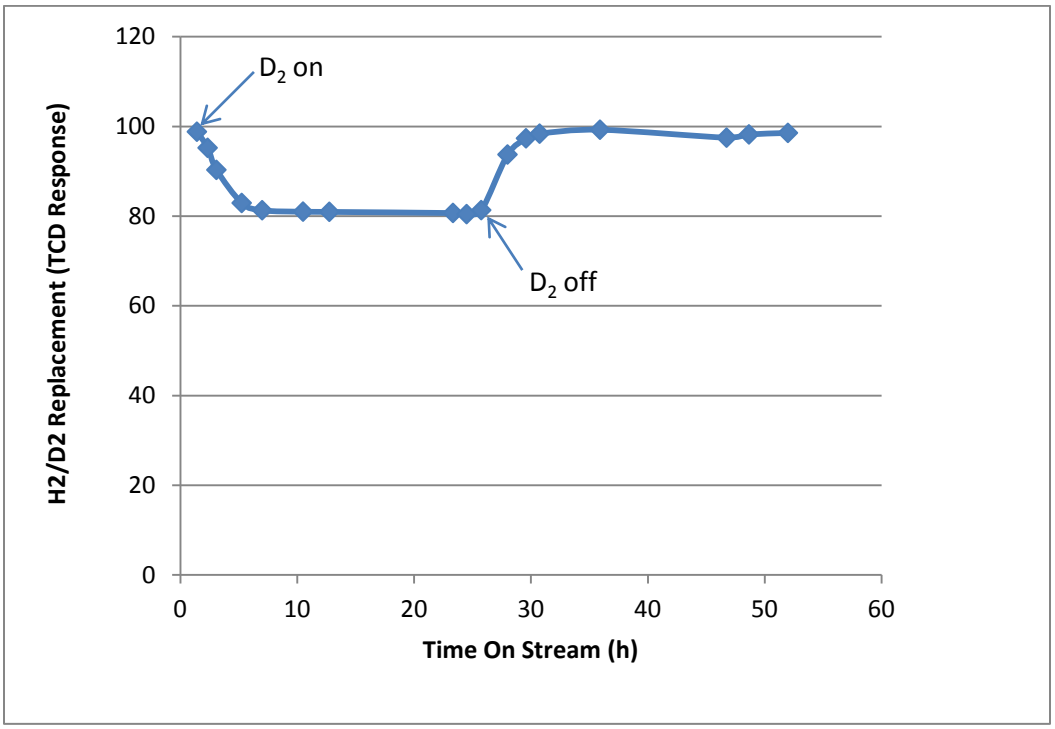


Figure 5.3: Measurement of hydrogen–deuterium replacement in the gas phase as indicated by the TCD response as a function of time. (T = 493 K, P = 2.0 MPa, H_2/CO = 2)

After the feed gas has been changed from CO/H_2 to CO/D_2 part of the hydrogen inside the reactor continues reacting while some of it is removed with the gas flowing out of the reactor. The results in Figure 5.3 show that it takes around six hours to completely replace hydrogen with deuterium inside the reactor. The residence time of hydrogen would give a good indication of the gas phase residence time even though hydrogen is reacting.

If we neglect the effects of reaction and the amount of hydrogen dissolved in the liquid phase then the unsteady state mass balance becomes:

$$y_{H2} V_G C_G|_t = y_{H2} V_G C_G|_{t+\Delta t} + y_{H2} Q_G C_G \Delta t \qquad (2)$$

where:

V_G is the volume of gas/vapour inside the reactor,

C_G is the molar concentration of the vapour inside the reactor,

Q_G is the molar flow rate of vapour out of the reactor, and

y_{H2} is the mole fraction of hydrogen in the vapour phase.

Therefore the unsteady state mass balance can be reduced to

$$V_G C_G \frac{dy_{H2}}{dt} = -Q_G C_G y_{H2} \quad (3)$$

The average gas residence time is defined as:

$$\tau_G \equiv \frac{V_G}{Q_G} \quad (4)$$

Substituting the residence time into Equation (3) gives

$$\frac{dy_{H2}}{dt} = -\frac{1}{\tau_G} y_{H2} \quad (5)$$

which simplifies to:

$$ln\left(\frac{y_{H2}}{y_{H2,0}}\right) = -\frac{1}{\tau_G}(t - t_0) \quad (6)$$

Therefore Equation (6) shows that plotting the log of the mole fractions of hydrogen in the reactor versus time on stream should result in a straight line in which the slope is given by $-1/\tau_G$. Using the data in Figure 5.3 the mole fraction of hydrogen was calculated and the results for a short period after switching from CO/H_2 to CO/D_2 are presented in Figure 5.4.

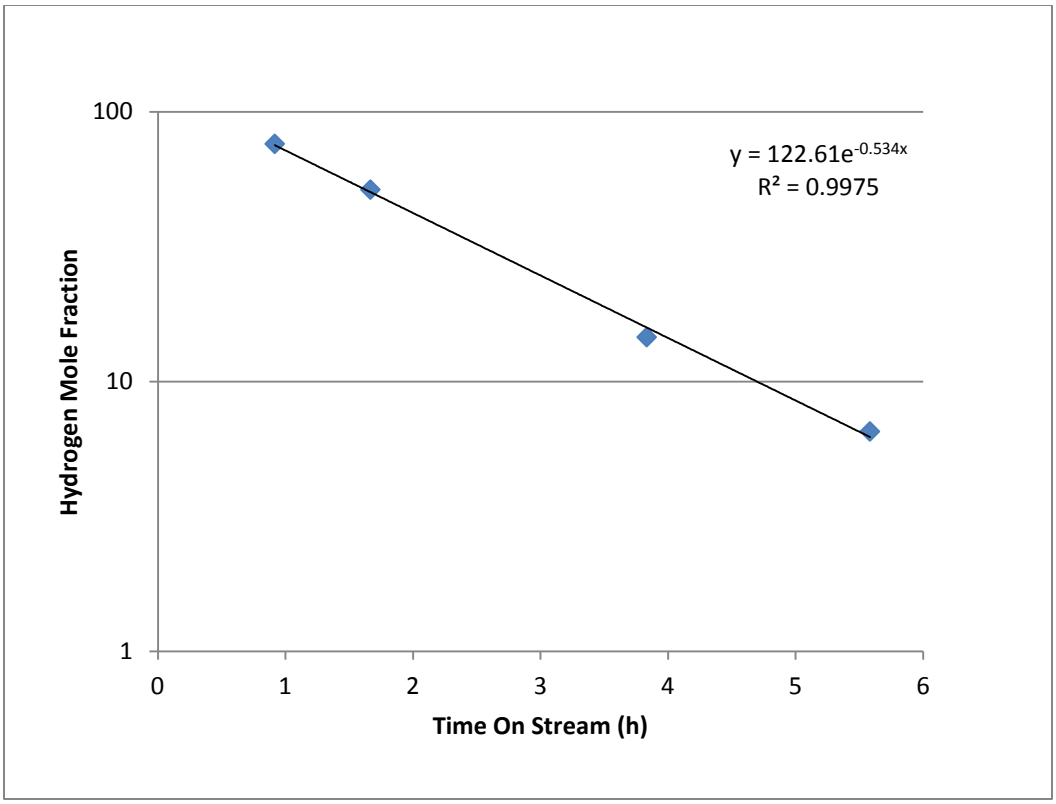


Figure 5.4: Logarithm of the mole fraction of hydrogen after switching from CO/H_2 to CO/D_2. Time = 0 is when H_2 is replaced by D_2 in the feed.

As expected the log of the mole fractions of hydrogen in the reactor versus time on stream is a straight line. The slope of the trend line is -0.534 which results in the average gas phase residence time of 1.87 hours. This estimates the residence time of highly-volatile/insoluble components.

5.5 MEASUREMENT OF RESIDENCE TIME OF POLYWAX IN THE REACTOR

The CSTR was loaded with polywax 3000 as a start-up solvent. To be able to determine the amount of product accumulating in the reactor, the amount of solvent in the reactor has to be quantified. The liquid phase product is collected intermittently, and this product contains both FT products and the polywax solvent. We can use the data about the amount of polywax remaining in the reactor as a function of time to estimate the residence time of the polywax (and thus any

non volatile liquid) in the reactor. The details of the determination of the mass fraction inside an FT reactor are discussed in Chapter 3 and [49].

Based on the experimentally measured mass and composition of the liquid sample collected for the experimental run, the mass fraction of polywax inside the reactor was calculated and is shown in Figure 5.5.

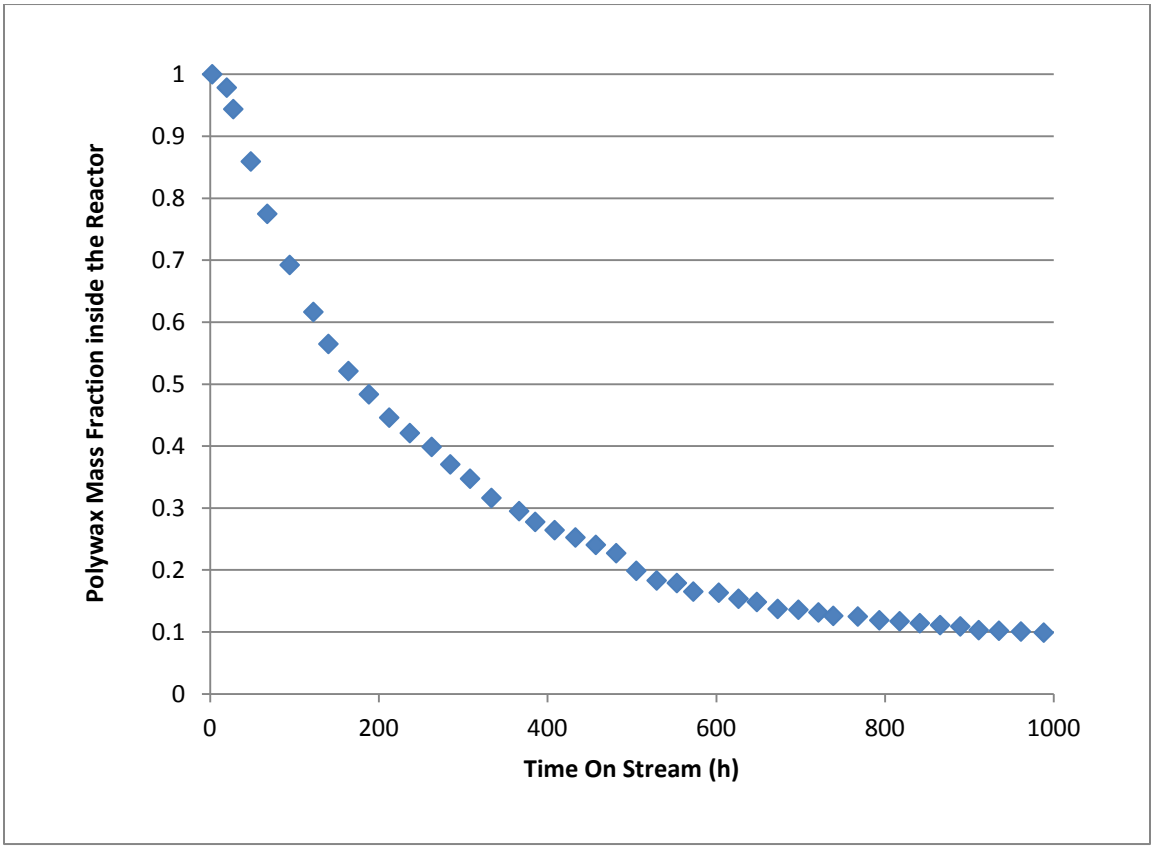


Figure 5.5: Calculated Polywax mass fraction inside the reactor as a function of time. Time = 0 corresponds to start up of the reactor. (T = 493 K, P = 2.0 MPa, $H_2/CO = 2$)

Comparing with the hydrogen replacement rate in the gas phase which was around six hours, Figure 5.5 shows that it took roughly 900 hours for the polywax fraction to get to 10 percent of

the liquid inside the reactor. This signifies that the gas phase and the liquid phase have very different residence times.

If we assume that the vapour pressure of the polywax is very low then it follows that there is no or very little polywax in the vapour phase. The unsteady state mass balance on the polywax in the reactor is given by:

$$V_L \frac{dm_p}{dt} = -Q_L m_p \tag{7}$$

where:

V_L is the volume of liquid inside the reactor,

Q_L is the liquid flow out of the reactor, and

m_p is the mass fraction of polywax in the liquid phase.

The average liquid residence time is defined as:

$$\tau_L \equiv \frac{V_L}{Q_L} \tag{8}$$

Substituting the residence time into Equation (7) and integrating results in:

$$ln\left(\frac{m_p}{m_{p,0}}\right) = -\frac{1}{\tau_L}(t - t_0) \tag{9}$$

According to Equation (9) the plot of the logarithm of the polywax mass fractions in the reactor versus time on stream should result in a straight line in which the slope is given by $-1/\tau_L$. To get a good estimate of the average residence time of the liquid the data between 100 and 700 hours was used and the results are presented in Figure 5.6.

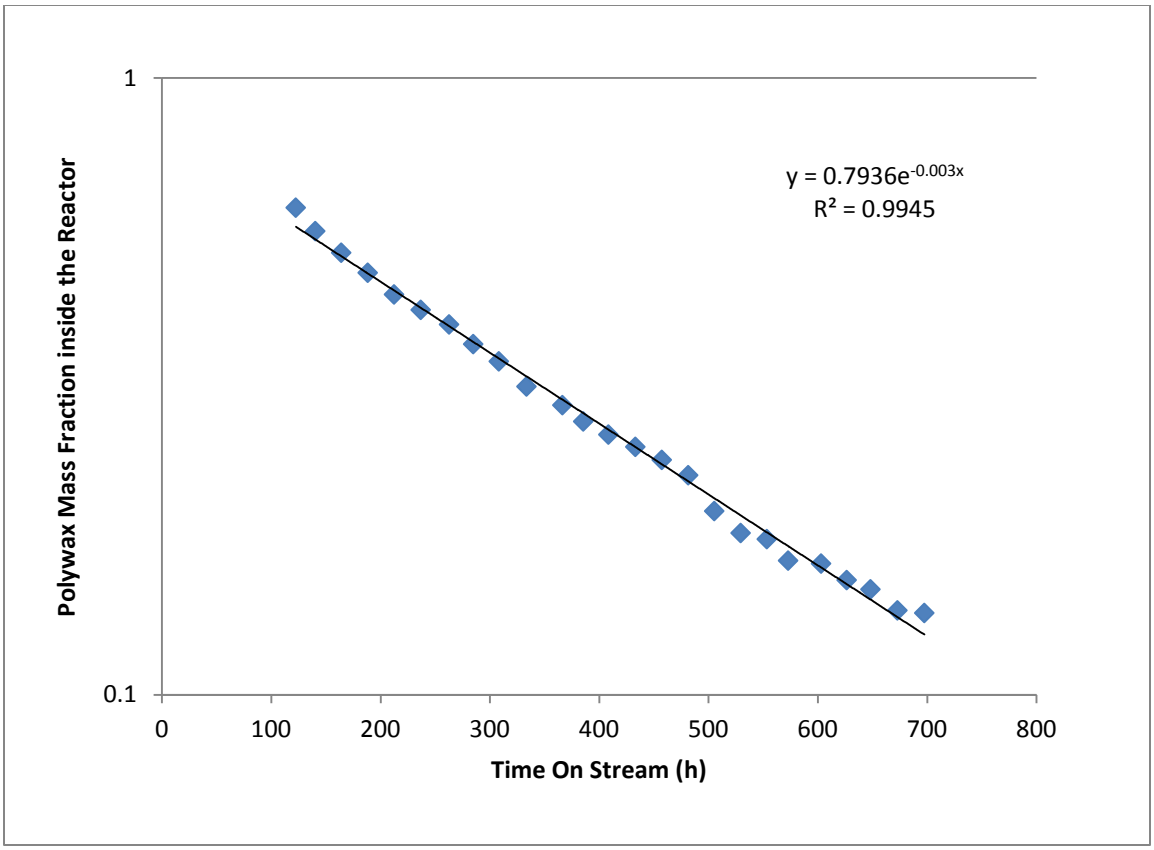


Figure 5.6: Logarithm of the polywax mass fraction inside the reactor as a function of time on stream.

It can be seen from Figure 5.6 that the log of the polywax mass fractions in the reactor versus time on stream is a straight line. The slope of the trend line is -0.003 which results in the average liquid phase residence time of 333 hours (≈ 13.9 days). This estimates the residence time of non-volatile liquid in the reactor. The residence time distribution presented in Figure 5.5 also indicate that the reactor is well mixed and can be considered as an ideal slurry phase CSTR.

These results show that as expected there is a large difference between the residence time of the gas phase (1.87 hours) and the non volatile liquids in the reactor (333 hours). This implies that it takes a long time for the liquid phase to reach steady state.

5.6 ANALYSIS OF THE LIQUID PHASE PRODUCT DISTRIBUTION

Based on the mass balance and the samples of the reactor wax collected daily, the composition of the slurry inside the reactor was determined and the liquid phase product distribution is presented in Figure 5.7.

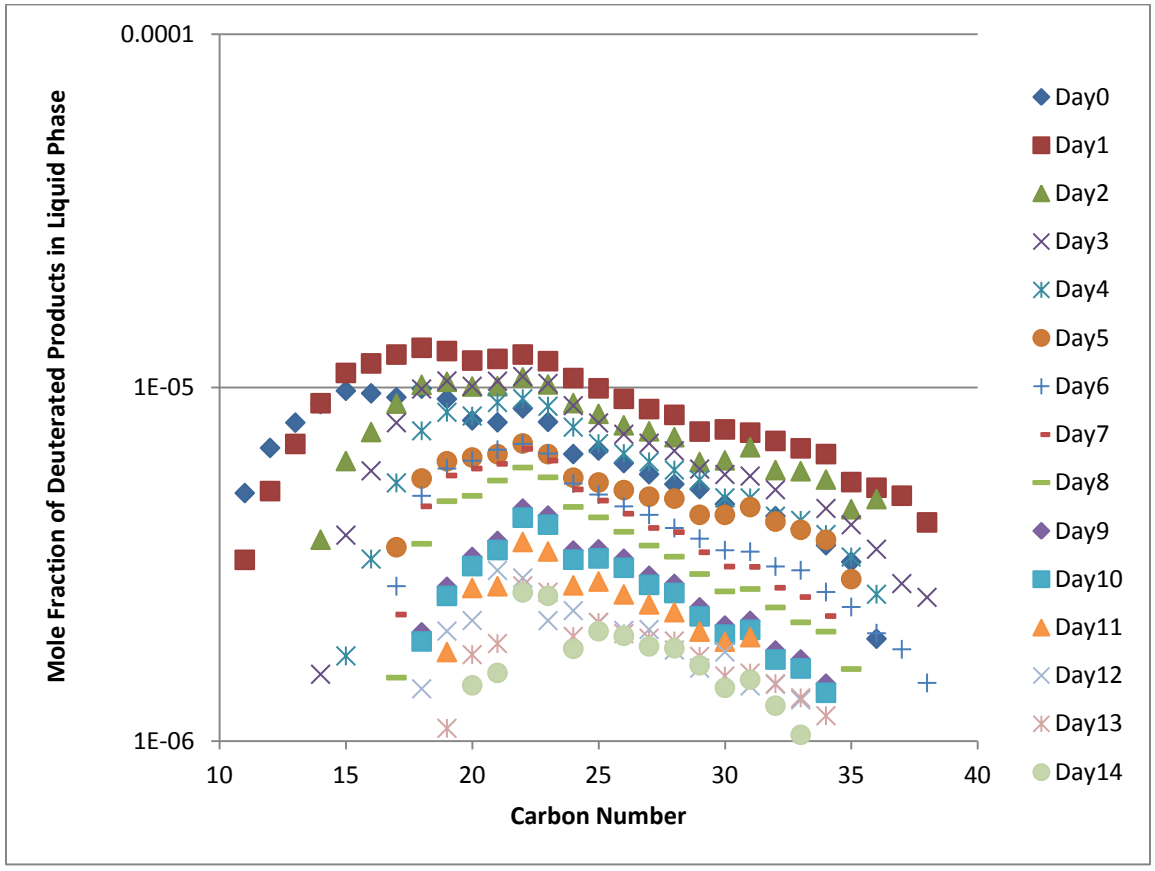


Figure 5.7: Liquid phase product distribution of deuterated products as a function of carbon number on different days on stream. Day 0 represents the end of D_2 tracing. (T = 493 K, P = 2.0 MPa, $H_2/CO = 2$)

The results in Figure 5.7 show that the mole fraction of heavy products in the liquid phase is steadily decreasing while the mole fraction of lighter products drops quicker than the heavier products.

5.7 ANALYSIS OF THE VAPOUR PHASE PRODUCT DISTRIBUTION

The experimental setup is designed such that the vapour phase products from the reactor can be collected and analysed separately from the liquid phase products. The log of the mole fraction of deuterated products in the vapour phase is plotted versus hydrocarbon length n for different days after the CO/D_2 feed was switched back to CO/H_2 in Figure 5.8.

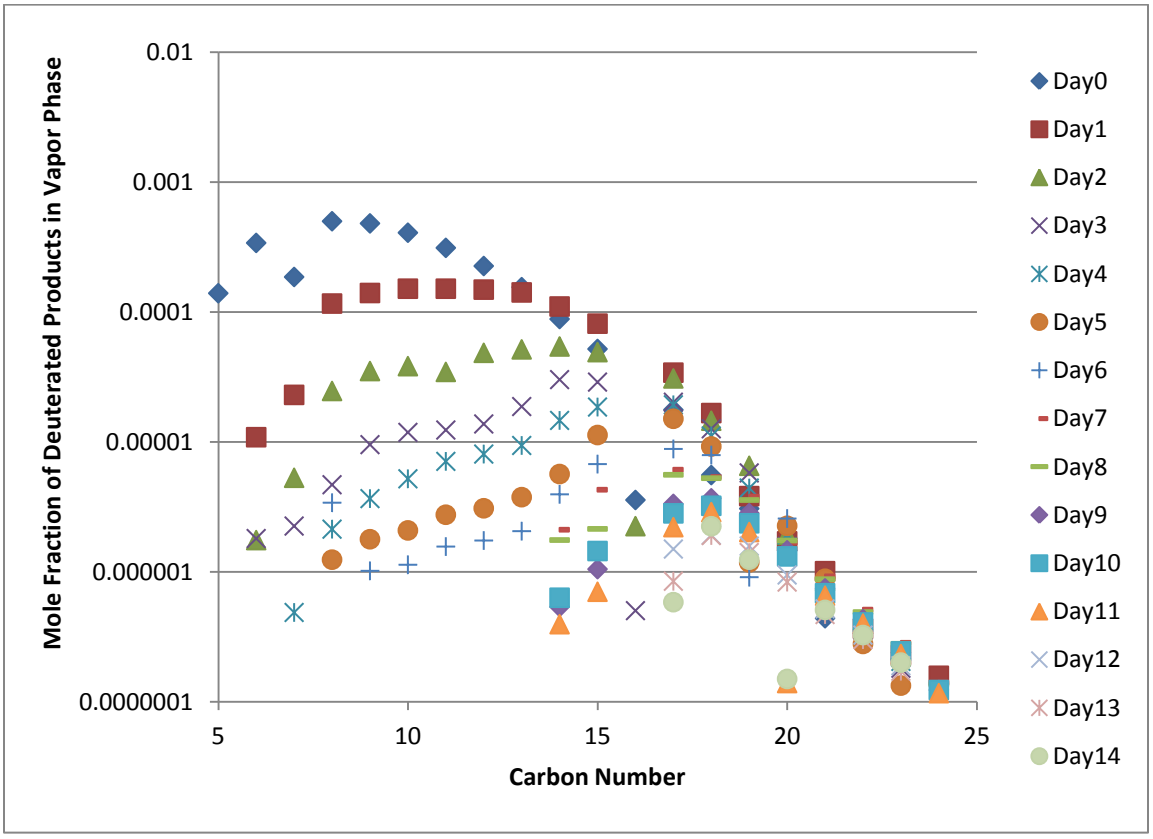


Figure 5.8: The log of the mole fraction of deuterated products in the vapour phase plotted against length of hydrocarbon n distribution for different days. Day 0 represents the end of D_2 tracing. (T = 493 K, P = 2.0 MPa, H_2/CO = 2)

The results in Figure 5.8 show that the mole fractions of lighter products decrease faster than the mole fractions of heavier products. This suggests that the lighter products have a lower residence time hence are being stripped out quicker than the heavier products.

5.8 THE INTERACTION OF PRODUCT ACCUMULATION WITH VAPOUR–LIQUID EQUILIBRIUM

The Fischer–Tropsch reaction has been known and used since the 1930's [1]. Despite being studied for over 80 years the reaction is still not that well understood. We find different results from different researchers; different results for different catalysts. The results are complex and confusing. Perhaps the complexity is not just due to the reaction mechanism. What if some of the complexity is caused by a combination of simple phenomena like vapour–liquid equilibrium (VLE) and product accumulation inside the reactor? The individual phenomena are quite simple. However the interactions of these phenomena cause quite complex behavior. The question remains if this could occur in the FT reaction.

At vapour–liquid equilibrium: the partition coefficient or K-value is defined as:

$$K_n \equiv \frac{y_n}{x_n} \tag{10}$$

where:

y_n is the mole fraction of species n in the vapour phase, and

x_n is the mole fraction of species n in the liquid phase.

According to Raoult's law:

$$y_n P = x_n P_{vap,n} \tag{11}$$

where:

$P_{vap,\,n}$ is the vapour pressure of component n, and

P is the operating pressure.

This results in:

$$K_n = \frac{P_{vap,n}}{P} \tag{12}$$

Subsequently, the K-values calculated from the vapour pressure can be plotted and compared with the experimental results as shown in Figure 5.9 to determine if VLE is reached inside an FT reactor and to assess the impact of product accumulation on VLE. The vapour pressure of hydrogen is greater than the vapour pressure of deuterium [46–48]. Zhao *et al.* [50] measured vapour pressures of some deuterated hydrocarbons as a function of temperature. Using the reported equation with corresponding constants results in the vapour pressures at 493 K of hexane-d_{14} and heptane-$d_{16}$of 24.5331 and 13.6954 bar respectively. *Yaws' handbook of Antoine coefficients for vapor pressure (2nd Electronic Edition)* [51] gives the vapour pressures of normal hexane and heptane at 493 K of 24.4914 and 13.8402 bar respectively which are similar to the deuterated product vapour pressures. Thus, the vapour pressure data were obtained from *Yaws' handbook of Antoine coefficients for vapor pressure* [51].

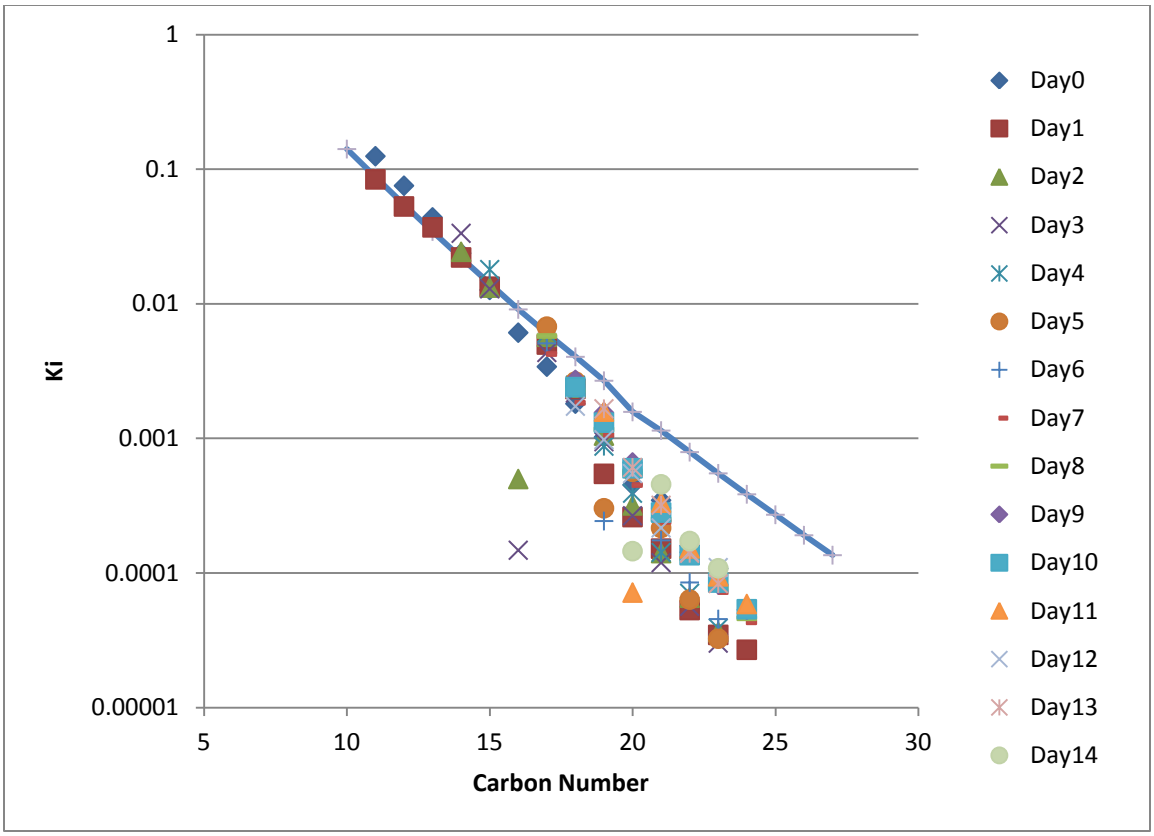


Figure 5.9: The ratio of the mole fraction in the vapour phase to the mole fraction in the liquid phase ($K_n \equiv y_n/x_n$) with carbon number. Solid line is calculated from Raoult's law and is given by $P_{vap,n}/P$. (T = 493 K, P = 2.0 MPa, $H_2/CO = 2$)

The results in Figure 5.9 show that vapour–liquid equilibrium is reached inside the FT reactor since the lighter hydrocarbons, up to around C_{17} are accurately described by Raoult's law. The heavier hydrocarbons deviate from Raoult's law. Their vapour phase mole fraction is lower than Raoult's law's predictions; alternatively, their liquid phase mole fraction is higher than Raoult's law's predictions. This is because heavier hydrocarbons are preferentially retained inside the reactor because they have low diffusion coefficients and therefore do not have enough time to reach VLE. This would cause the measured K-values of heavier hydrocarbons to be less than predicted from Raoult's law. Thus product accumulation affects VLE modelling. This suggests that some of the complexities in the FTS are caused by a combination of simple phenomena like Product hold-up and VLE.

5.9 OVERALL PRODUCT DISTRIBUTION OF DEUTERATED PRODUCTS

It is generally assumed, that the olefin readsorption probability increases with increasing carbon number due to increased residence times of longer chains in the liquid-filled pores of the catalyst. Chain length-dependent solubility [52–54] and chain length-dependent diffusivity [14, 41, 42] have been proposed as possible reasons.

Iglesia *et al.* [41] proposed that diffusion limited removal of products from catalyst pellets can lead to enhanced readsorption and chain initiation by α-olefins, which reverses the chain termination steps that form these olefins and leads to heavier, more paraffinic products. Furthermore they assert that exclusively diffusion enhanced readsorption of olefins accounts for non-Schulz–Flory carbon number product distributions and decreasing olefin contents with increasing carbon number observed during FT synthesis on cobalt and ruthenium catalysts.

In contrast to this, chain length-dependent contact time due to chain length-dependent solubility in the liquid product has been earlier proposed to cause the generally observed chain length dependences of olefin selectivities [52–54]. Kuipers *et al.* [17] showed that dissolution and physisorption can cause a much stronger chain length-dependence than diffusion and would usually dominate.

To obtain more insight into the cause for chain length-dependencies of secondary olefin reactions in FTS the overall weight percent of deuterated hydrocarbon obtained after introducing D_2 into the reactor for 24 hours is presented in Figure 5.10.

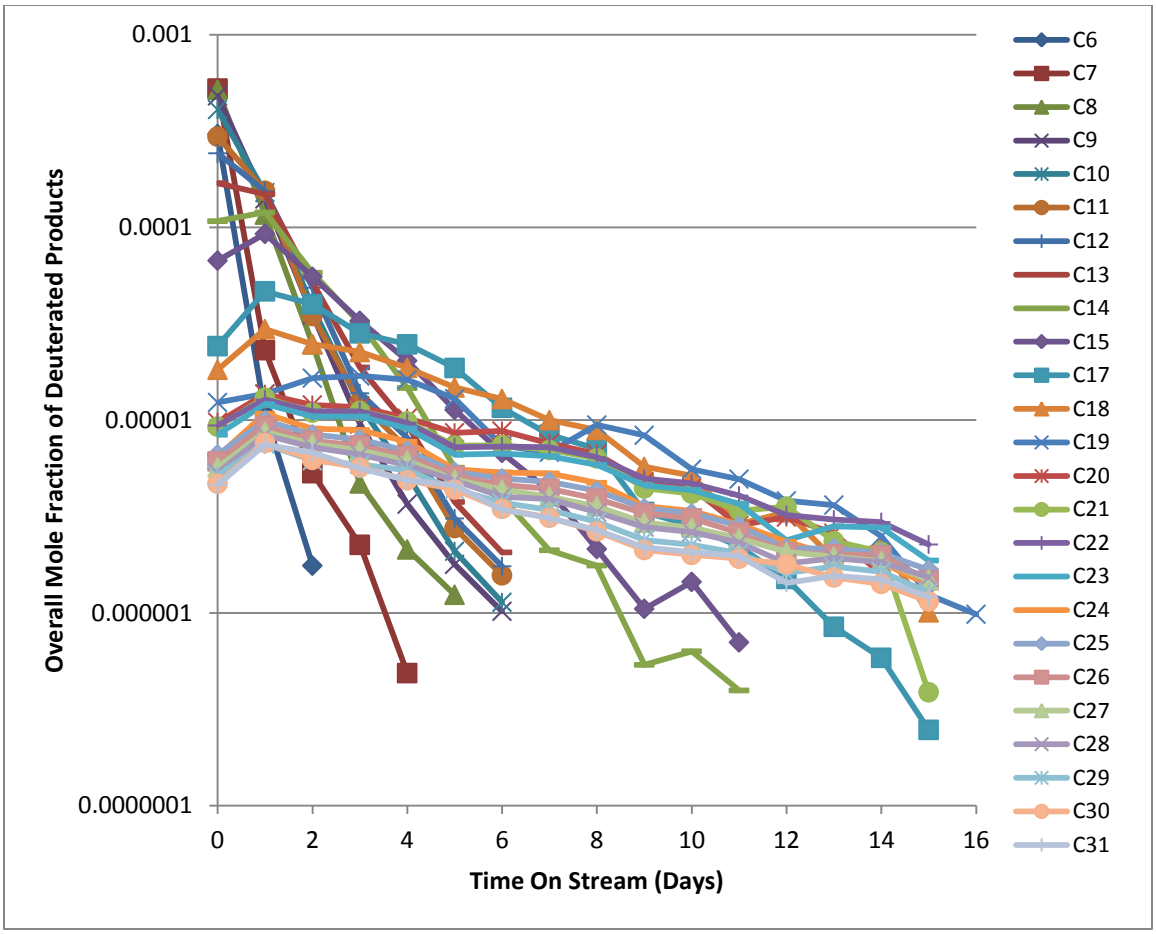


Figure 5.10: Calculated mole fractions of total (vapour + liquid) deuterated products after introducing D_2 into the reactor. The D_2 is switched off and replace with H_2 at the end of Day 0. (T = 493 K, P = 2.0 MPa, H_2/CO = 2)

The experimental results presented in Figure 5.10 show that initially after the introduction of D_2/CO syngas, more lower-boiling deuterated products are formed when compared to the higher-boiling deuterated products. This is consistent with typical FT products which usually follow an ASF product distribution or a slight variation of it. It is worth noting that after the syngas has been switched back to H_2/CO at TOS = 24 hours, the percentage of lower-boiling deuterated products drops more quickly than the higher-boiling deuterated products. Some of the higher-boiling deuterated compounds appear to be increasing in concentration for up to 50 hours after the deuterium has been switched off. Although the amount of the heavier product in the reactor is changing slowly, the lighter ones are changing very fast and thus the observed increase in mole fraction of the heavier ones is due to stripping of the lighter components and not making heavier

ones. This means that the lower molecular weight products exit the reactor very quickly and the labeled fraction of these lower molecular weight products will be little affected by accumulation. On the other hand, the average residence time will increase with carbon number and the higher carbon number products may be affected by accumulation of unlabeled products.

Schulz and Claeys [43] estimated average residence times of certain product molecules C_2–C_{11} in CSTR system by the ratio of the actual number of moles of a compound to the total molar exit flow rate of this compound. Their results showed strongly increasing residence times of product compounds with carbon number which signified that chain length-dependent solubility can affect residence times of products and thereby the extent of secondary olefin reactions. They never measured the residence time of heavier products. To calculate the residence time of heavier products we compute an unsteady state mass balance on the deuterated products inside the reactor.

5.10 UNSTEADY STATE MASS BALANCE ON THE DEUTERATED PRODUCTS INSIDE THE REACTOR

After the feed gas has been changed from CO/D_2 back to CO/H_2 the reactor can be considered as a vessel in which deuterated products are being stripped out and removed in the vapour phase by the gas stream and removed in the liquid phase by flow as illustrated in Figure 5.11. We assume that the reactor is well mixed such that the mole fraction of component n in the vapour/liquid removed from the reactor at some time t is the same as the mole fraction of that component in the vapour/liquid phase in the reactor.

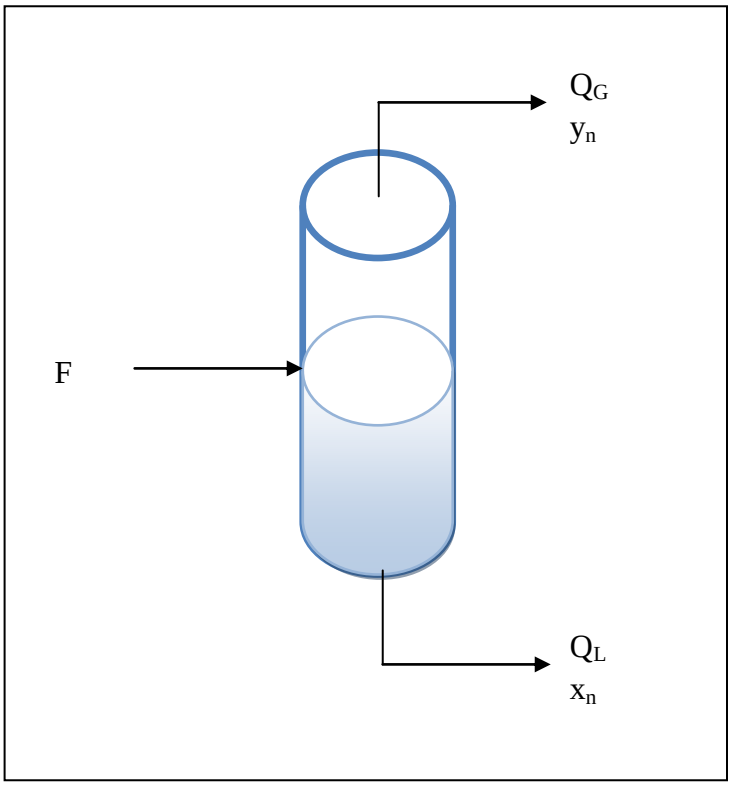


Figure 5.11: Schematic diagram of the reactor as a stripping vessel for deuterated products. (F is the total molar feed flow rate, Q_G is the vapour molar flow, Q_L is the liquid molar flow, y_n is the mole fraction of component n in the vapour phase, and x_n is the mole fraction of component n in the liquid phase.)

If we ignore the effects of reacting products (olefin reactivity) on the products modeling then the unsteady state mass balance on component n can be written as:

$$V_G C_G \frac{dy_n}{dt} + V_L C_L \frac{dx_n}{dt} = -Q_L C_L x_n - Q_G C_G y_n \qquad (13)$$

where:

C_L is the molar concentration of both the liquid inside the reactor as well as the liquid stream product stream, and other symbols are as defined before.

Assuming that the vapour and the liquid are in equilibrium then

$$y_n = K_n x_n \tag{14}$$

Thus Equation (13) becomes:

$$\frac{dx_n}{dt} = -\frac{(Q_G C_G K_n + Q_L C_L)}{(V_G C_G K_n + V_L C_L)} x_n \tag{15}$$

Alternatively

$$\frac{dy_n}{dt} = -\frac{\left(Q_G C_G + \frac{Q_L C_L}{K_n}\right)}{\left(V_G C_G + \frac{V_L C_L}{K_n}\right)} y_n \tag{16}$$

Hence we defined the mean residence time of each product to be the inverse of the slopes of Equation (15) or (16).

For heavier hydrocarbons, with a low vapour pressure $K_n << 1$

For hydrocarbons which are relatively involatile Equation (15) reduces to:

$$\frac{dx_n}{dt} = -\frac{Q_L}{V_L} x_n = -\frac{1}{\tau_L} x_n \tag{17}$$

Integrating both sides results in:

$$ln\left(\frac{x_n}{x_{n,0}}\right) = -\frac{1}{\tau_L}(t - t_0) \tag{18}$$

Thus for the heavier hydrocarbons, the main mode of removal from the reactor is through the liquid flow and these hydrocarbons will have the same residence time as the liquid. We can plot the logarithm of the mole fraction of the deuterated hydrocarbon n in the liquid phase, x_n, versus time, where the slope of the line is the inverse of the average residence time in the liquid for that hydrocarbon. The measured change of liquid phase mole fraction with time is presented in Figure 5.12.

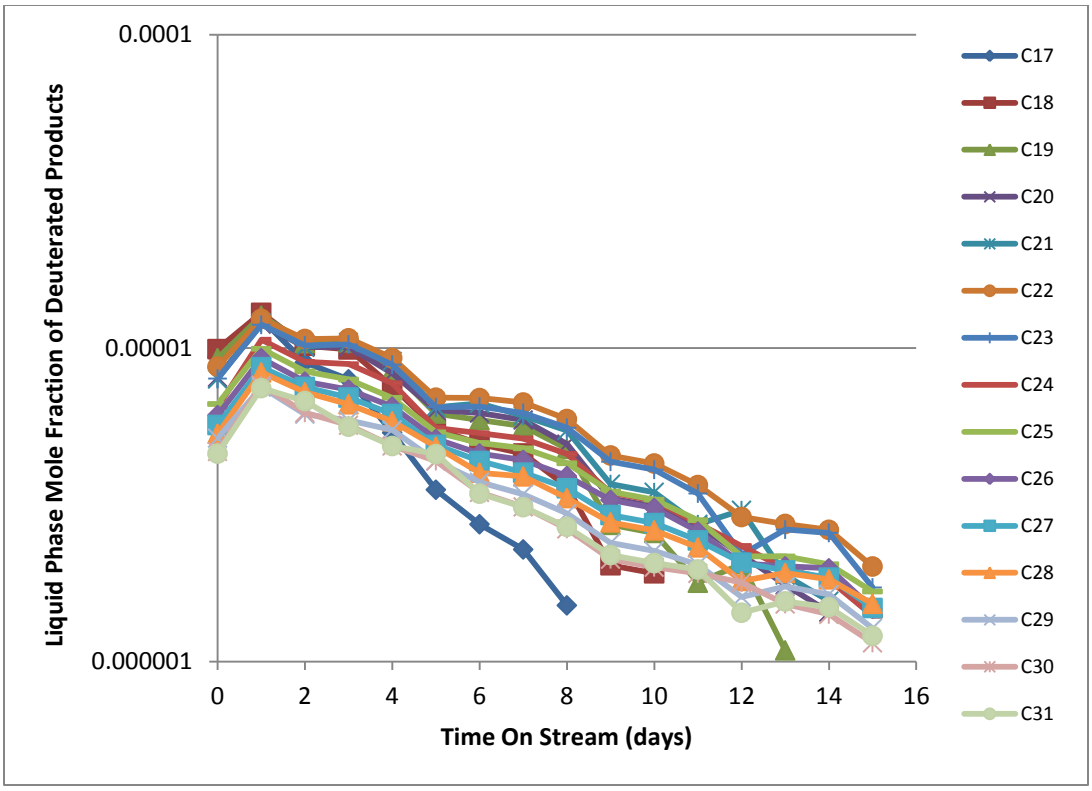


Figure 5.12: The log of mole fraction of deuterated products in the liquid phase with time on stream. The slope of each line represents the inverse of the residence time of that product in the reactor. (T = 493 K, P = 2.0 MPa, H_2/CO = 2)

The slopes of the mole fractions with time for the carbon numbers shown in Figure 5.12 were calculated. Assuming that each slope is given by $-1/\tau_{n,L}$ provides a method for calculating the residence time of each carbon number.

<u>For lighter hydrocarbons, with a high vapour pressure K_n >> 1</u>

For hydrocarbons which are relatively insoluble Equation (16) reduces to:

$$\frac{dy_n}{dt} = -\frac{Q_G}{V_G} y_n = -\frac{1}{\tau_G} y_n \qquad (19)$$

Integrating both sides results in:

$$ln\left(\frac{y_n}{y_{n,0}}\right) = -\frac{1}{\tau_G}(t - t_0) \qquad (20)$$

Thus for the lighter hydrocarbons, the main mode of removal from the reactor is through the gas flow or stripping and these hydrocarbons will have the same residence time as the gas/vapour. We can plot the logarithm of the mole fraction of the deuterated hydrocarbon n in the vapour phase, y_n, versus time, where the slope of the line is the inverse of the average residence time in the vapour for that hydrocarbon. The measured change of vapour phase mole fraction with time is presented in Figure 5.13.

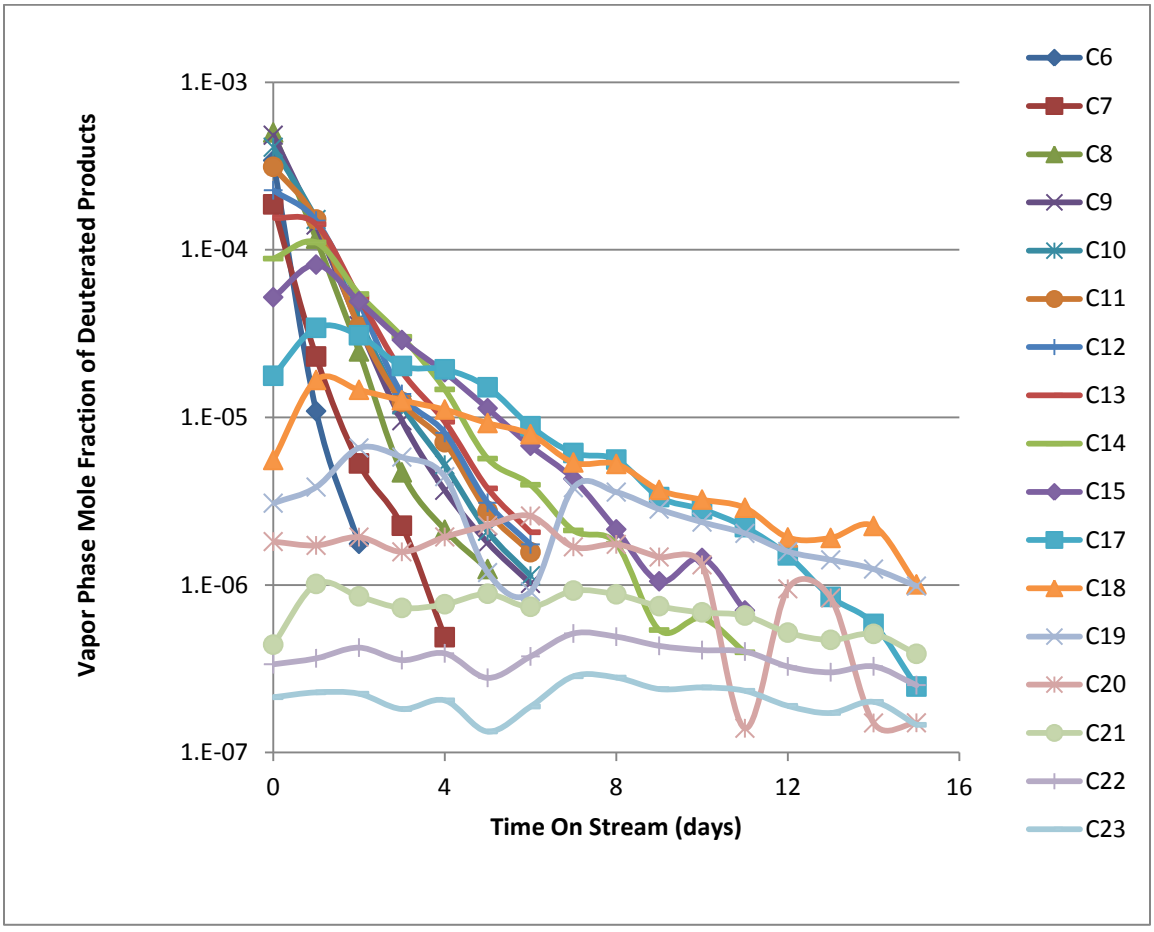


Figure 5.13: The log of mole fraction of deuterated products in the vapour phase with time on stream. The slope of each line represents the inverse of the residence time of that product in the reactor. (T = 493 K, P = 2.0 MPa, H_2/CO = 2)

The average residence times of products with carbon number 16 and higher were calculated from the liquid phase slopes. The residence time of products lighter than C_{16} were calculated from the vapour phase slopes. The overall results of the residence time of the hydrocarbons versus chain length are presented in Figure 5.14.

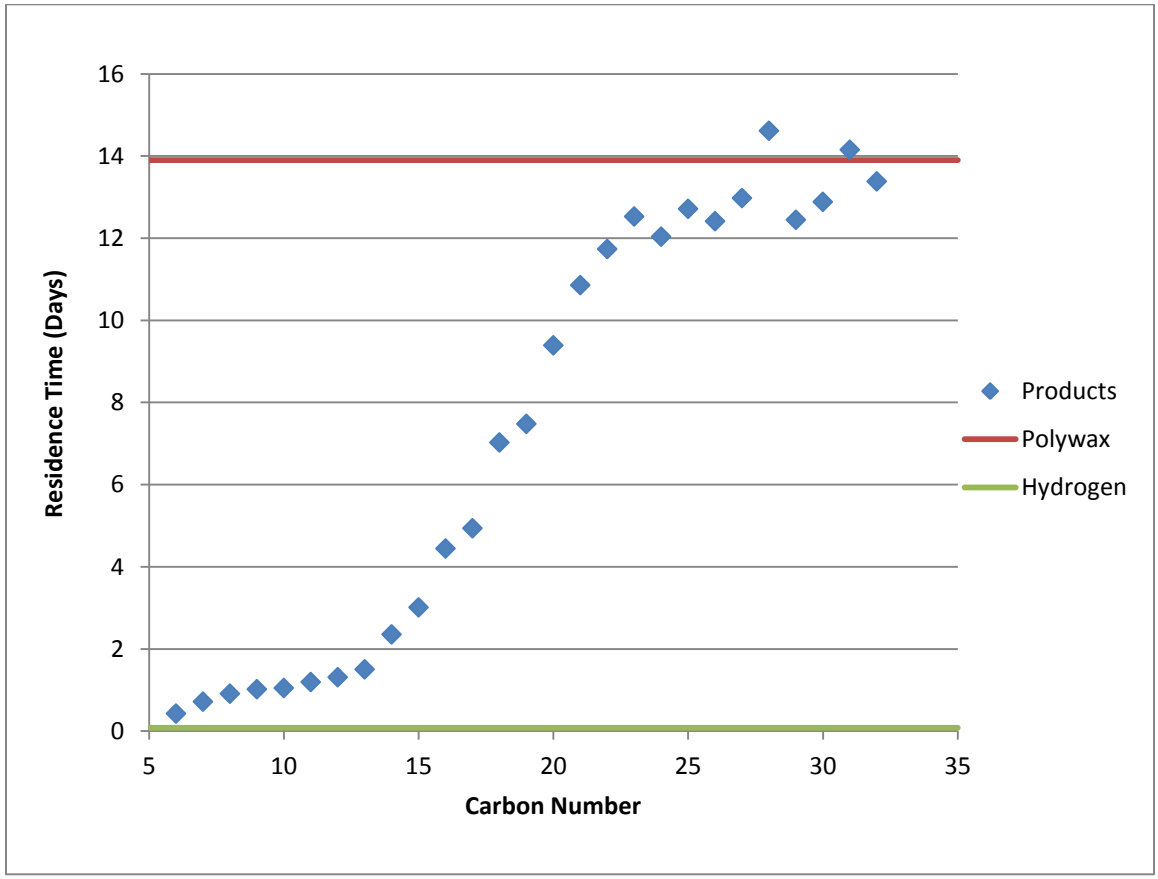


Figure 5.14: The average residence time with carbon number for products inside a reactor calculated from the slopes of the curves in Figures 12 and 13. (T = 493 K, P = 2.0 MPa, H_2/CO = 2)

The results presented in Figure 5.14 shows that the residence time increases with carbon number up to C_{22} and products with chain length 22 and higher have the same residence time as the non volatile polywax. This implies that the major removal method for products C_{22} and heavier is the liquid phase flow because these products have low vapour pressures. Therefore the stripping by the vapour flow is not a major method of removal for these products. The major removal method

for products lighter than C_{10} is the gas phase. These products will have a similar residence time as the highly-volatile/insoluble component. The products with chain length between 10 and 22 are removed by both the vapour flow and the liquid flow as can be seen by their average residence time being higher than the gas phase residence time but less than the average residence time of the non-volatile liquid. The lighter products would be expected to be in vapour–liquid equilibrium more quickly than the higher molecular weight products.

These results confirm that the lower molecular weight products have a lower residence time than the longer chain products (i.e. tend to the residence time of the insoluble gas) and the fraction of these lower molecular weight products will be little affected by accumulation in the liquid phase/reactor. The results also imply that the lighter products will reach steady state quicker than the heavier products.

Olefin/paraffin ratio is one of the important parameters used to characterize the behavior of the FT reactor. Thus α-olefin/paraffin ratio was measured in this experiment and is presented in Figure 5.15.

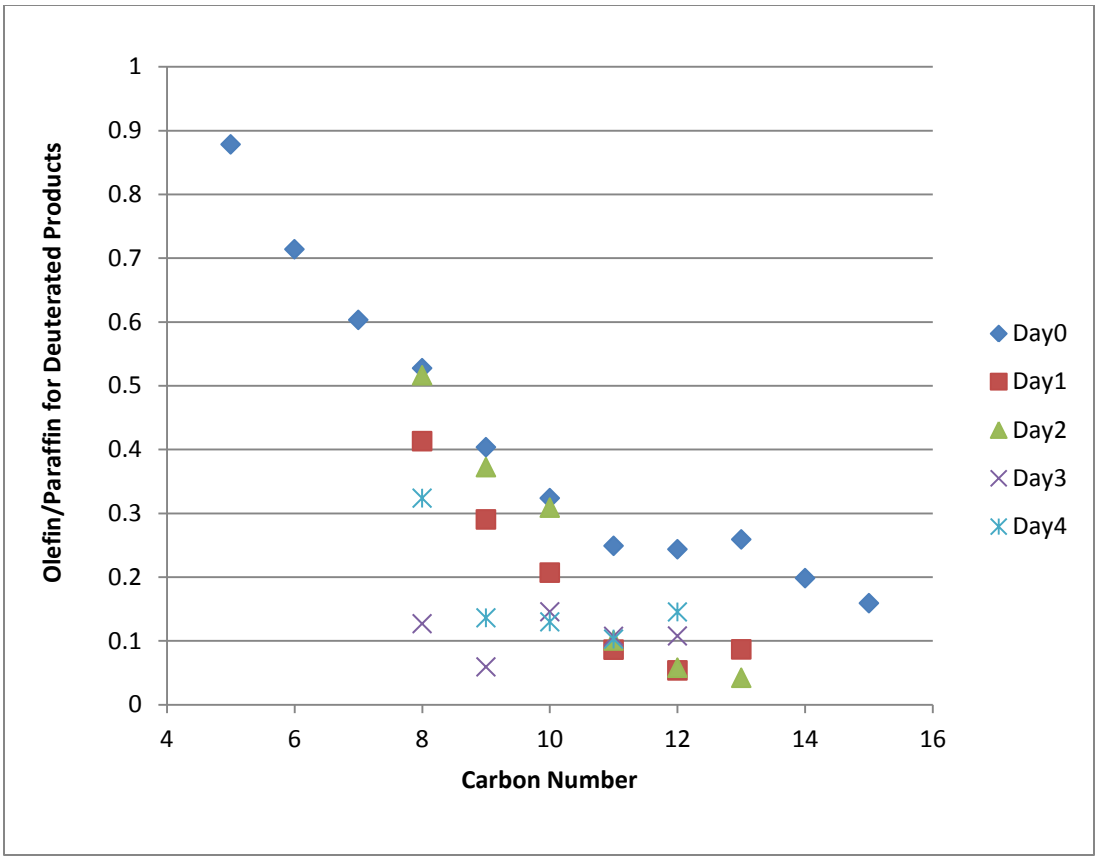


Figure 5.15: Olefin to paraffin ratio of deuterated products with carbon number. Day 0 represents the end of D_2 tracing. (T = 493 K, P = 2.0 MPa, H_2/CO = 2)

The results presented in Figure 5.15 shows that olefin to paraffin ratio decreases with increasing carbon number. This is consistent with olefin readsorption but not necessarily diffusion enhanced olefin readsorption. We therefore rely on VLE measurements to infer product diffusion limitations. Furthermore, Tau *et al.* [54] reported results using ^{14}C-labeled ethane, propene, 1-pentene, 2-pentene, decene and nonene to define the secondary hydrogenation reactions of alkenes.

Secondary reactions of alpha olefins such as re-incorporation into chain growth processes as well as double-bond migration and hydrogenation are well established [14–17, 22–26, 35, 41–43]. However, transport restrictions of primary olefins inside an FT reactor have not been compellingly proven. The experimental setup is designed such that the intra-pore liquid phase

cannot be analysed; only the bulk liquid and the vapour phases are analysed. Nonetheless, because lighter products up to C_{17} attains VLE signifies no transport constraints. We have shown in Chapter 4 and [55] that the two-alpha product distribution can be explained by simple VLE considerations which requires no transport limitations. In fact, it has been shown that if ethane does not have internal diffusion limitations then alkenes up to about carbon number twenty do not have internal pore diffusion limitations [56].

5.11 TIME REQUIRED FOR PRODUCTS TO REACH STEADY STATE

If we consider that in the reactor shown in Figure 5.11 the vapour phase products and the liquid phase products are added together to get an overall product distribution, z, then the overall unsteady state mass balance can be written as

$$F\Delta t + N|_t + N_r\Delta t = Q_T\Delta t + N|_{t+\Delta t} \quad (21)$$

where:

N_r is the change of moles due to reaction,

N is the total moles inside the reactor, and

Q_T is the sum of the vapour and liquid flow rates out of the reactor.

Therefore, Equation (21) in the limit becomes

$$\frac{dN}{dt} = F + N_r - Q_T \quad (22)$$

It is well known that the number of moles decrease in an FT reactor. However, this change in moles can be neglected for simplicity of modeling. Thus, Equation (22) simplifies to

$$\frac{dN}{dt} = F - Q_T \quad (23)$$

The component balance for a product with chain length n is given by

$$z_n N|_t + r_n\Delta t = z_n N|_{t+\Delta t} + z_n Q_T\Delta t \quad (24)$$

where:

r_n is the rate of production of component n, and

z_n is the overall mole fraction of component n.

Therefore, Equation (24) in the limit becomes

$$\frac{d(z_n N)}{dt} = r_n - z_n Q_T \tag{25}$$

This is the same as

$$z_n \frac{dN}{dt} + N \frac{dz_n}{dt} = r_n - z_n Q_T \tag{26}$$

Substituting Equation (23) into (26) gives

$$z_n (F - Q_T) + N \frac{dz_n}{dt} = r_n - z_n Q_T \tag{27}$$

which simplifies to

$$\frac{dz_n}{dt} + \frac{F}{N} z_n = \frac{r_n}{N} \tag{28}$$

Neglecting the change of moles upon reaction implies that N does not change with time. So, if we assume that the rate of production of component n is constant with time then Equation (28) is a linear first-order ordinary differential equation. Therefore, the integrating factor is

$$IF = e^{\int \frac{F}{N} dt} = e^{\frac{F}{N} t} \tag{29}$$

Hence, the solution to Equation (28) is given by

$$z_n = \frac{1}{e^{\frac{F}{N} t}} \int \frac{r_n}{N} e^{\frac{F}{N} t} dt \tag{30}$$

This is the same as

$$z_n = \frac{\frac{r_n}{N}}{e^{\frac{F}{N} t}} \left(\frac{e^{\frac{F}{N} t}}{\frac{F}{N}} + C \right) \tag{31}$$

where:

C is a constant of integration.

At time t = 0, $z_n = 0$, therefore, Equation (31) gives

$$C = -\frac{N}{F} \tag{32}$$

Thus, the overall mole fraction of component n is given by

$$z_n = \frac{r_n}{F}\left(1 - e^{-\frac{F}{N}t}\right) \tag{33}$$

From the experimental data, the average values of r_n, F, and N are used to calculate the change of the overall mole fraction with time on stream and the results obtained are presented in Figure 5.16.

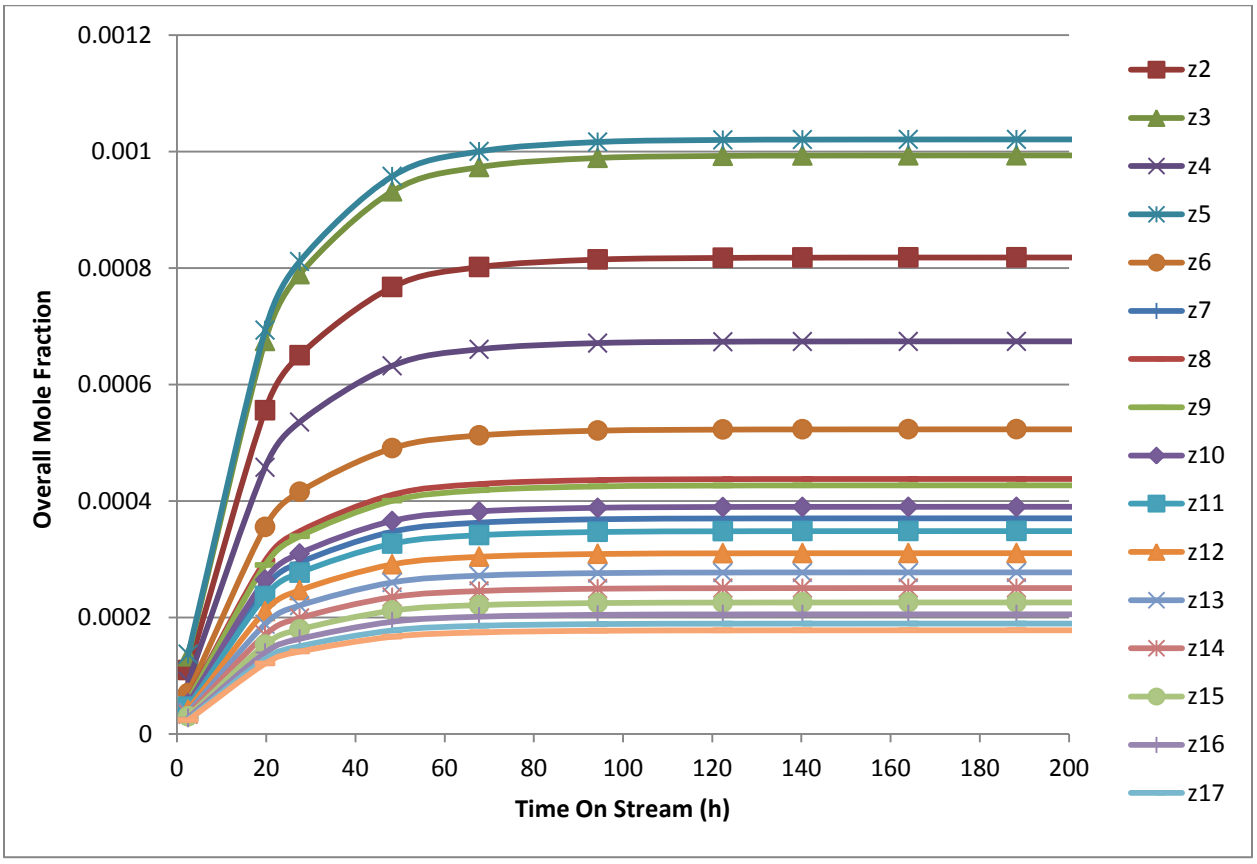


Figure 5.16: Overall mole fractions of products with different carbon numbers with time on stream as an indication for time required for each carbon number to reach steady state. (Only a

few carbon numbers are show in this Figure for ease of visualization. Time = 0 corresponds to reactor start up.) (T = 493 K, P = 2.0 MPa, $H_2/CO = 2$)

The results in Figure 5.16 show that around 120 h the overall mole fractions would have reached steady state. Thus, for overall mass balance purposes the overall mole fraction can be used as a guide to establish steady state.

CONCLUSIONS

The average residence time of the highly-volatile/insoluble gas is around 1.87 hours while the non-volatile liquid has an average residence time of around 13.9 days. The lower molecular weight products exit the reactor very quickly and the fraction of these lower molecular weight products will be little affected by accumulation as their residence time approaches that of the gas phase. The average residence time increase with carbon number and the higher carbon number products have a longer residence time in the reactor as their residence time approaches that of the non-volatile polywax. These products will be more affected by accumulation in the liquid phase and hence will take longer to reach equilibrium. The results show that products with a chain length of 22 and higher have the same residence time as the liquid.

Vapour–liquid equilibrium plays an important role in modeling the behavior of an FT reactor. The results show that VLE is reached inside an FT reactor for components up to around C_{17}. This suggests that chain length-dependent solubility in the liquid phase is the predominant cause for chain length dependencies of secondary olefin reactions in Fischer–Tropsch synthesis and diffusion limited removal of products is only significant for products with carbon number greater than 17.

The results obtained suggest that Raoult's law sufficiently describe VLE in a Fischer–Tropsch reactor. The preferential holdup of heavier products in the reactor affects the VLE modeling.

Thus, some of the complexities in the FTS is caused by a combination of simple phenomena (e.g. Product hold-up and VLE). The interactions of these phenomena cause quite complex behavior.

NOMENCLATURE

n number of carbon atoms in the hydrocarbon

m_n mole fraction of products containing n carbon atoms

α probability of chain growth

V_G volume of gas/vapour inside the reactor

C_G molar concentration of both the vapour product stream as well as the vapour inside the reactor

Q_G molar flow rate of vapour out of the reactor

y_{H2} mole fraction of hydrogen in the vapour phase

τ_G average gas/vapour residence time

V_L volume of liquid inside the reactor

Q_L molar flow of liquid out of the reactor

C_L molar concentration of both the liquid product stream as well as the liquid inside the reactor

m_p mass fraction of polywax in the liquid phase

τ_L average liquid residence time

K_n partition coefficient or K-value of component n

y_n mole fraction of component n in the vapour phase in both the reactor as well as the vapour product leaving the reactor

x_n mole fraction of component n in the liquid phase in both the reactor as well as the liquid product removed from the reactor

$P_{vap, n}$ vapour pressure of component n

P operating pressure

F total molar feed flow rate

N total moles inside the reactor

N_r change of moles due to reaction

Q_T sum of the vapour and liquid flow rates out of the reactor

r_n rate of production of component n

z_n overall mole fraction of component n

C constant of integration

REFERENCES

[1] D.F. Smith, C.O. Hawk, P.L. Golden, The mechanism of the formation of higher hydrocarbons from water gas, *J. Am. Chem. Soc. 52* (1930) 3221–3232.

[2] R.A. Friedel, R.B. Anderson, Composition of synthetic liquid fuels. I. Product distribution and analysis of C_5–C_8 paraffin isomers from cobalt catalyst, *J. Am. Chem. Soc. 72* (1950) 1212–1215.

[3] J.T. Kummer, H.H. Podgurski, W.B. Spencer, P.H. Emmett, Mechanism studies of the Fischer–Tropsch synthesis. The addition of radioactive alcohol, *J. Am. Chem. Soc. 73* (1951) 564–569.

[4] W. Keith Hall, R.J. Kokes, P.H. Emmett, Mechanism studies of the Fischer–Tropsch Synthesis. The addition of radioactive methanol, carbon dioxide and gaseous formaldehyde, *J. Am. Chem. Soc. 79* (1957) 2983–2989.

[5] W. Keith Hall, R.J. Kokes, P.H. Emmett, Mechanism studies of the Fischer–Tropsch Synthesis: The incorporation of radioactive ethylene, propionaldehyde and propanol, *J. Am. Chem. Soc. 82* (1960) 1027–1037.

[6] G. Henrici–Olive, S. Olive, The Fischer–Tropsch synthesis: molecular weight distribution of primary products and reaction mechanism, *Angew. Chem. Int. Ed. Engl. 15* (1976) 136–141.

[7] C.N. Satterfield, G.A. Huff, Carbon number distribution of Fischer–Tropsch products formed on an iron catalyst in a slurry reactor, *J. Catal. 73* (1982) 187–197.

[8] C.N. Satterfield, G.A. Huff, J.P. Longwell, Product distribution from iron catalysts in Fischer–Tropsch slurry reactors, *Ind. Eng. Chem. Process. Des. Dev. 21* (1982) 465–470.

[9] R.A. Dictor, A.T. Bell, An explanation for deviations of Fischer–Tropsch products from a Schulz–Flory distribution, *Ind. Eng. Chem. Process. Des. Dev. 22* (1983) 678–681.

[10] R.B. Anderson, in: P.H. Emmett (Ed.), Catalysis, Vol. IV, Reinhold, New York, 1956, pp. 123–163.

[11] H.E. Atwood, C.O. Bennett, Kinetics of the Fischer–Tropsch reaction over iron, *Ind. Eng. Chem. Process. Des. Dev. 18* (1979) 163–170.

[12] R.J. Madon, W.F. Taylor, Fischer–Tropsch synthesis on a precipitated iron catalyst, *J. Catal. 69* (1981) 32–43.

[13] G.A. Huff, C.N. Satterfield, Evidence for two chain growth probabilities on iron catalysts in the Fischer–Tropsch synthesis, *J. Catal. 85* (1984) 370–379.

[14] E. Iglesia, S.C. Reyes, R.J. Madon, Transport-enhanced α-olefin readsorption pathways in Ru-catalyzed hydrocarbon synthesis, *J. Catal. 129* (1991) 238–256.

[15] E.W. Kuipers, C. Scheper, J.H. Wilson, I.H. Vinkenburg, H. Oosterbeek, Non-ASF product distributions due to secondary reactions during Fischer–Tropsch synthesis, *J. Catal. 158* (1996) 288–300.

[16] T. Komaya, A.T. Bell, Estimates of rate coefficients for elementary processes occurring during Fischer–Tropsch synthesis over Ru/TiO_2, *J. Catal. 146* (1994) 237–248.

[17] E.W. Kuipers, I.H. Vinkenburg, H. Oosterbeek, Chain length dependence of α-olefin readsorption in Fischer–Tropsch synthesis, *J. Catal. 152* (1995) 137–146.

[18] L.–M. Tau, H.A. Dabbagh, B.H. Davis, Fischer–Tropsch synthesis: comparison of carbon-14 distributions when labeled alcohol is added to the synthesis gas, *Energy Fuels 5* (1991) 174–179.

[19] L.–M. Tau, H.A. Dabbagh, B. Chawla, B.H. Davis, Fischer–Tropsch synthesis with an iron catalyst: incorporation of ethene into higher carbon number alkanes, *Catal. Lett. 7* (1990) 141–149.

[20] L.–M. Tau, H.A. Dabbagh, S. Bao, B.H. Davis, Fischer–Tropsch synthesis. Evidence for two chain growth mechanisms, *Catal. Lett. 7* (1990) 127–140.

[21] K.R. Krishna, A.T. Bell, The role of C_2 intermediates in Fischer–Tropsch synthesis over ruthenium, *Catal. Lett. 14* (1992) 305–313.

[22] R.J. Madon, E. Iglesia, The importance of olefin readsorption and H_2/CO reactant ratio for hydrocarbon chain growth on ruthenium catalysts, *J. Catal. 139* (1993) 576–590.

[23] R.J. Madon, S.C. Reyes, E. Iglesia, Primary and secondary reaction pathways in ruthenium-catalyzed hydrocarbon synthesis, *J. Phys. Chem. 95* (1991) 7795–7804.

[24] G.P. van der Laan, A.A.C.M. Beenackers, Hydrocarbon selectivity model for the gas–solid Fischer–Tropsch synthesis on precipitated iron catalysts, *Ind. Eng. Chem. Res. 38* (1999) 1277–1290.

[25] X. Zhan, B.H. Davis, Two alpha Fischer–Tropsch product distribution. A role for vapor–liquid equilibrium?, *Petrol. Sci. Techn. 18* (2000) 1037–1053.

[26] A.P. Raje, B.H. Davis, Effect of Vapor–Liquid equilibrium on Fischer–Tropsch hydrocarbon selectivity for a deactivating catalyst in a slurry reactor, *Energy Fuels 10* (1996) 552–560.

[27] B. Shi, B.H. Davis, Fischer–Tropsch synthesis: accounting for chain length related phenomena, *Appl. Catal. A: Gen. 277* (2004) 61–69.

[28] J.T. Kummer, T.W. Dewitt, P. H. Emmett, Some mechanism studies on the Fischer–Tropsch synthesis using C14, *J. Am. Chem. Soc. 70* (1948) 3632–2643.

[29] J.T. Kummer, P.H. Emmett, Fischer–Tropsch synthesis mechanism studies. The addition of radioactive alcohols to the synthesis gas, *J. Am. Chem. Soc. 75* (1953) 5177–5183.

[30] G. Blyholder, P.H. Emmett, Fischer–Tropsch synthesis mechanism studies. The addition of radioactive ketene to the synthesis gas, *J. Phys. Chem. 63* (1959) 962–965.

[31] G. Blyholder, P.H. Emmett, Fischer–Tropsch synthesis mechanism studies. II. The addition of radioactive ketene to the synthesis gas, *J. Phys. Chem. 64* (1960) 470–472.

[32] P.M. Maitlis, H.C. Long, R. Quyoum, M.L. Turner, Z.–Q. Wang, Heterogeneous catalysis of C–C bond formation: black art or organometallic science?, *Chem. Commun.* (1996) 1–8.

[33] M.L. Turner, H.C. Long, A. Shenton, P.K. Byers, P.M. Maitlis, The alkenyl mechanism for Fischer–Tropsch surface methylene polymerisation; the reactions of vinylic probes with CO/H_2, over rhodium catalysts, *Chem. Eur. J. 1* (1995) 549–556.

[34] A. Raje, B.H. Davis, in: J. J. Spring (Ed.), "Fischer–Tropsch synthesis. Mechanism studies using isotope, catalysis", The Royal Chem. Soc. 12, Cambridge, 1996, pp. 52.

[35] B. Shi, R.J. O'Brien, S. Bao, B.H. Davis, Mechanism of the isomerization of 1-alkene during iron-catalyzed Fischer–Tropsch synthesis, *J. Catal. 199* (2001) 202–208.

[36] B. Shi, B.H. Davis, ^{13}C-tracer study of the Fischer–Tropsch synthesis: another interpretation, *Catal. Today 58* (2000) 255–261.

[37] S.O. Thompson, J. Turkevich, A.P. Irsa, Reaction of deuterium with hydrocarbons over a cobalt–thoria Fischer–Tropsch catalyst, *J. Am. Chem. Soc. 73* (1951) 5213–5215.

[38] S.O. Thompson, J. Turkevich, A.P. Irsa, Study of the Fischer–Tropsch reaction using deuterium gas, *J. Phys. Chem. 56* (1952) 243–250.

[39] J.R. Anderson, C. Kemball, The catalytic reaction between aliphatic alcohols and deuterium, *Trans. Faraday Soc. 51* (1955) 966–973.

[40] C.S. Kellner, A.T. Bell, Evidence for H_2/D_2 isotope effects on Fischer–Tropsch synthesis over supported ruthenium catalysts, *J. Catal. 67* (1981) 175–185.

[41] E. Iglesia, S.C. Reyes, R.J. Madon, S.L. Soled, Selectivity control and catalyst design in the Fischer–Tropsch synthesis: sites, pellets, and reactors. *Adv. Catal. 39* (1993) 221–302.

[42] R.J. Madon, E. Iglesia, Hydrogen and CO intrapellet diffusion effects in ruthenium-catalyzed hydrocarbon synthesis, *J. Catal. 149* (1994) 428–437.

[43] H. Schulz, M. Claeys, Reactions of α-olefins of different chain length added during Fischer–Tropsch synthesis on a cobalt catalyst in a slurry reactor, *Appl. Catal. A: Gen. 186* (1999) 71–90.

[44] B. Shi, C. Jin, Inverse kinetic isotope effects and deuterium enrichment as a function of carbon number during formation of C–C bonds in cobalt catalyzed Fischer–Tropsch synthesis, *Appl. Catal. A: Gen. 393* (2011) 178–183.

[45] J. Yang, E.Z. Tveten, D. Chen, A. Holmen, Understanding the effect of cobalt particle size on Fischer–Tropsch synthesis: surface species and mechanistic studies by SSITKA and kinetic isotope effect, *Langmuir 26(21)* (2010) 16558–16567.

[46] G.N. Lewis, W.T. Hanson, The vapor pressure of solid and liquid deuterium and the heats of sublimation, of fusion and of vaporization, *J. Am. Chem. Soc. 56* (1934) 1687–1690.

[47] R.B. Scott, F.G. Brickwedde, H.C. Urey, M.H. Wahl, The vapor pressures and derived thermal properties of hydrogen and deuterium, *J. Chem. Phys. 2* (1934) 454–464.

[48] E.R. Grilly, The vapor pressures of hydrogen, deuterium and tritium up to three atmospheres, *J. Am. Chem. Soc. 73* (1951) 843–846.

[49] C.M. Masuku, W. Ma, D. Hildebrandt, D. Glasser, B.H. Davis, A vapor–liquid equilibrium thermodynamic model for a Fischer–Tropsch reactor, *Fluid Phase Equilib. 314* (2012) 38–45.

[50] H. Zhao, P. Unhannanant, W. Hanshaw, J.S. Chickos, *J. Chem. Eng. Data 53* (2008) 1545.

[51] C.L. Yaws, P.K. Narasimhan, C. Gabbula, Yaws' handbook of Antoine coefficients for vapor pressure, *2nd Electronic Ed.*, Knovel, 2009 (Accessed 08/30/2010).

[52] R. Dictor, A.T. Bell, Fischer–Tropsch synthesis over reduced and unreduced iron oxide catalysts, *J. Catal. 97* (1986) 121–136.

[53] R. Dictor, A.T. Bell, Studies of Fischer–Tropsch synthesis over a fused iron catalyst, *Appl. Catal. 20* (1986) 145–162.

[54] L.–M. Tau, H.A. Dabbagh, B.H. Davis, Fischer–Tropsch synthesis: ^{14}C tracer study of alkene incorporation, *Energy Fuels 4* (1990) 94–99.

[55] C.M. Masuku, D. Hildebrandt, D. Glasser, *Chem. Eng. Sci. 66* (2011) 6254.

[56] X. Zhan, B.H. Davis, Assessment of internal diffusion limitation on Fischer–Tropsch product distribution, *Appl. Catal. A: 236* (2002) 149–161.

Chapter 6 : REACTIVE DISTILLATION IN CONVENTIONAL FISCHER–TROPSCH REACTORS

ABSTRACT

The Flory distribution that is often observed in Fischer–Tropsch (FT) reactors could be described by reaction equilibrium between species. Furthermore, it has been suggested that vapour–liquid equilibrium (VLE) exists in the reactor and this could cause the two-alpha product distribution that is often observed experimentally. Simultaneous reaction and VLE lead us to ask the question: can we not describe the FT reaction as a reactive distillation system? In this paper we develop a mathematical model to describe the behaviour and performance of an FT reactor by considering the dynamic interaction between reaction and VLE. The model results show that the rate of formation of component hydrocarbons is dependent on either the reaction rate or stripping rate, depending on which one is rate-limiting. Furthermore we show that at steady state, the rate of formation of hydrocarbons is given by the stripping rate. We conducted an experiment which showed a reaction rate increment when the reactor was switched from CSTR to Batch mode, with all other operation conditions remaining the same. In the Batch mode the stripping vector is eliminated and the CO rate increases because reactant stripping was limiting the reaction rate. Modelling an FT reactor as a reactive distillation column is also consistent with the observed two-alpha positive deviation product distribution observed experimentally and industrially.

Keywords: *Reactive Distillation; Vapour–Liquid Equilibrium; Product Distribution; Fischer–Tropsch Batch Reactor.*

6.1 INTRODUCTION

The Fischer–Tropsch (FT) reaction may be viewed as a simple polymerization reaction [1, 2]. Thus, the products can be described by a Flory-type [1] carbon number distribution when chain growth and termination rates are independent of chain size such that:

$$m_n = (1-\alpha)\alpha^{n-1} \quad (1)$$

where m_n is the mole fraction of a hydrocarbon with chain length n and the growth probability factor α is independent of n. Hence, a plot of the logarithm of the molar concentration versus the carbon number would produce a straight line plot whose slope is related to alpha (α), the chain propagation probability. Most studies assume the Flory distribution to model the product selectivity [3]. This describes the entire product range by a single parameter α. However, significant deviations are reported in literature [4, 5]. The prevalent deviation is the two-alpha positive deviation product distribution model [6, 7].

The classical single α Flory-type distribution has also been derived from chemical reaction equilibrium modelling (Chapter 2, [8]). The two-alpha product distribution in the FT reactor has been explained using vapour–liquid equilibrium (VLE) calculations (Chapter 4, [9]). This suggests a dynamic interaction between chemical reaction equilibrium and VLE in an FT reactor. These are the fundamental phenomena occurring in reactive distillation and we thus pose the question: could we model the FT process using a reactive distillation approach and what insights might this give us?

6.2 REACTIVE DISTILLATION CONSIDERATIONS

Reactive distillation, also called catalytic distillation, can be considered as reaction and distillation combined into one unit operation [10]. In reactive distillation, as in conventional distillation, knowledge of VLE is vital [11–15]. When this equilibrium is superimposed on a chemical reaction, however, the concentration curve in a distillation column is appreciably influenced [16].

The design and operation issues for reactive distillation systems are considerably more complex than those involved for either conventional reactors or conventional distillation columns. The introduction of an in situ separation function within the reaction zone leads to complex interactions between VLE, vapour–liquid mass transfer, intra-catalyst diffusion (for heterogeneously catalysed processes) and chemical kinetics. Such interactions have been shown to lead to the phenomenon of multiple steady-states and complex dynamics [17].

Reactive distillation has received increasing attention in recent years as an alternative to conventional processes; in particular, to processes in which the conversion is limited by unfavourable chemical reaction equilibrium. The two main advantages of this process relative to the conventional alternatives are the possibility of carrying equilibrium-limited chemical reactions to completion, and the simultaneous separation of the reaction products in only one unit. This reduces or eliminates reactor and recycle costs [18]. Due to an increased demand for processes that produce no waste, require little energy, are low in cost and produce products of excellent quality, it is expected that more multi-functional reactors will be developed and operated in future [19].

Most of the work published on reactive distillation is restricted to either experimental studies to assess the feasibility of the process for specific types of reactions or the extension to reactive distillation of the algorithms developed for the solution of the equations for conventional distillation. However, very little work has been published to explain how the presence of chemical reaction affects the VLE, even though an understanding of this topic is fundamental for the correct design and synthesis of reactive distillation columns [18].

Srinivas et al. [20–22] investigated the feasibility of using a reactive distillation column for the FT synthesis. However, the conventional FT reactor has properties of a reactive separator. Therefore, to adequately understand the behaviour and performance of an FT reactor we develop

a mathematical model that takes into account the dynamic interaction between reaction and separation.

6.3 REACTOR MODELLING

To develop a model for the product distribution we considered a simple FT reactor in which we have a gaseous feed stream flowing into the reactor and a vapour and liquid stream flowing out of the reactor as shown in Figure 6.1.

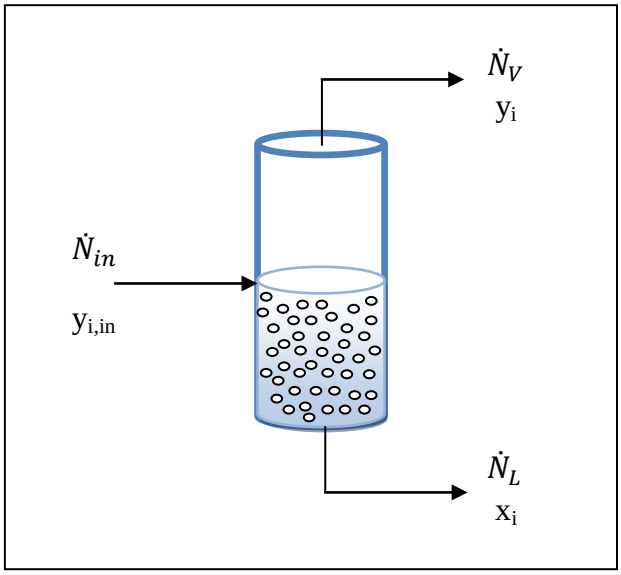


Figure 6.1: Schematic diagram of a Fischer–Tropsch reactor with vapour and liquid removal.

We assume that there is liquid held up in the reactor and this liquid may cover the catalyst or fill the catalyst pores. In this simplified model we assume that both the liquid and vapour in the reactor is well mixed and that the composition of the liquid in the reactor and that leaving the reactor is the same and similarly that the composition of the vapour in the reactor and that of the vapour stream leaving the reactor are the same. Furthermore we assume that that the vapour in the reactor is in equilibrium with the liquid in the reactor. These assumptions would more closely

approximate the behaviour of a stirred basket or slurry reactor and more complex models of the vapour–liquid contacting for reactors such as plug flow reactor might be needed.

The stream flowing into the reactor (with molar flow rate $\dot{N}_{in}$) consists of CO, H_2, perhaps inert gases (e.g. N_2) and products in the feed if required (i.e. product co-feeding). The vapour stream flowing out of the reactor (with molar flow rate $\dot{N}_V$) consists of the inert gases and unreacted CO and H_2, H_2O in the vapour phase and hydrocarbon products in the vapour phase. The liquid stream flowing out of the reactor (with molar flow rate $\dot{N}_L$) consists of hydrocarbon products in the liquid phase and any H_2O which may be in the liquid phase. We denote that $y_{i,in}$ is the mole fraction of component I in the feed, y_i is the mole fraction of component I in the vapour phase, and x_i is the mole fraction of component I in the liquid phase. The reactor has catalyst in it and N_L moles of liquid are held up inside the reactor. This is probably the simplest reactor model with VLE and we wish to use this to see what effects, if any, the interaction of reaction and VLE has on the reactor behaviour.

We will start with a general mass balance that considers addition of products/water in the feed. Special cases without product addition can be easily deduced from this general case. Thus, the overall mass balance across the liquid inside the reactor is given by

$$\dot{N}_{in}\Delta t + N_L|_t + N_r\Delta t = \dot{N}_V\Delta t + \dot{N}_L\Delta t + N_L|_{t+\Delta t} \quad (2)$$

where N_r is the change of moles upon reaction. It is well known that the number of moles decrease in an FT reactor. However, this change in moles can be neglected for simplicity of modelling [23]. Therefore, Equation (2) simplifies to

$$-\frac{dN_L}{dt} = \dot{N}_V + \dot{N}_L - \dot{N}_{in} \quad (3)$$

The component balance on water or any product I present in the feed is given by

$$\dot{N}_{in}y_{i,in}\Delta t + (N_L x_i)\big|_t + r_i N_L\Delta t = (N_L x_i)|_{t+\Delta t} + \dot{N}_V y_i\Delta t + \dot{N}_L x_i\Delta t \quad (4)$$

where r_i is the rate of formation of component i. The rate is usually defined per gram of catalyst or per volume of reactor. In this case the rate is defined per mole of reactor liquid for convenience. Equation (4) in the limit becomes

$$\frac{d}{dt}(N_L x_i) = r_i N_L + \dot{N}_{in} y_{i,in} - \dot{N}_V y_i - \dot{N}_L x_i \tag{5}$$

which is the same as

$$N_L \frac{dx_i}{dt} + x_i \frac{dN_L}{dt} = r_i N_L + \dot{N}_{in} y_{i,in} - \dot{N}_V y_i - \dot{N}_L x_i \tag{6}$$

Substituting Equation (3) into Equation (6) gives

$$N_L \frac{dx_i}{dt} = r_i N_L + x_i\left(\dot{N}_V + \dot{N}_L - \dot{N}_{in}\right) + \dot{N}_{in} y_{i,in} - \dot{N}_V y_i - \dot{N}_L x_i \tag{7}$$

This simplifies to

$$\frac{dx_i}{dt} = r_i - \frac{\dot{N}_V}{N_L}(y_i - x_i) + \frac{\dot{N}_{in}}{N_L}\left(y_{i,in} - x_i\right) \tag{8}$$

Note: Equation (8) is independent of the amount of liquid removed from the reactor ($\dot{N}_L$). This implies that the rate of liquid removal has no influence on the modelling of the liquid composition in the reactor. If this reactor was a single stage in a distillation column then, y_i and x_i would be in equilibrium and related by VLE, $y_{i,in}$ and x_i would be compositions of passing streams and would be related by mass balance and would lie on the distillation column operating line.

Equation (8) portrays that the rate of change of component I in the liquid phase is related to the reaction rate (r_i), the stripping rate ($\frac{\dot{N}_V}{N_L}(y_i - x_i)$), and the relationship between passing streams of a distillation column ($\frac{\dot{N}_{in}}{N_L}\left(y_{i,in} - x_i\right)$). This is typical of reactive distillation columns [11]. The combination of simple phenomena such as VLE and reaction can result in complex behaviour as we will explain below.

When the liquid composition reaches steady state then

$$\frac{dx_i}{dt} = 0 \tag{9}$$

Therefore, Equation (8) simplifies to

$$r_i = \frac{\dot{N}_V}{N_L}(y_i - x_i) - \frac{\dot{N}_{in}}{N_L}\left(y_{i,in} - x_i\right) \tag{10}$$

Equation (10) states that the rate of formation of component I is proportional to the stripping rate. Therefore the composition in the reactor must set itself up such that the rate of formation of component I matches the stripping rate of that component.

6.4 STRIPPING AS A RATE LIMITING PHENOMENA

As we said previously, the composition in the FT reactor at steady state must set itself up so that the reaction rate matches the stripping rate for all components. Typically one of the phenomena is rate controlling as we could postulate that under some reaction conditions the reaction rate would be rate limiting, and when we change the conditions separation may become controlling. We demonstrate this schematically in Figure 6.2.

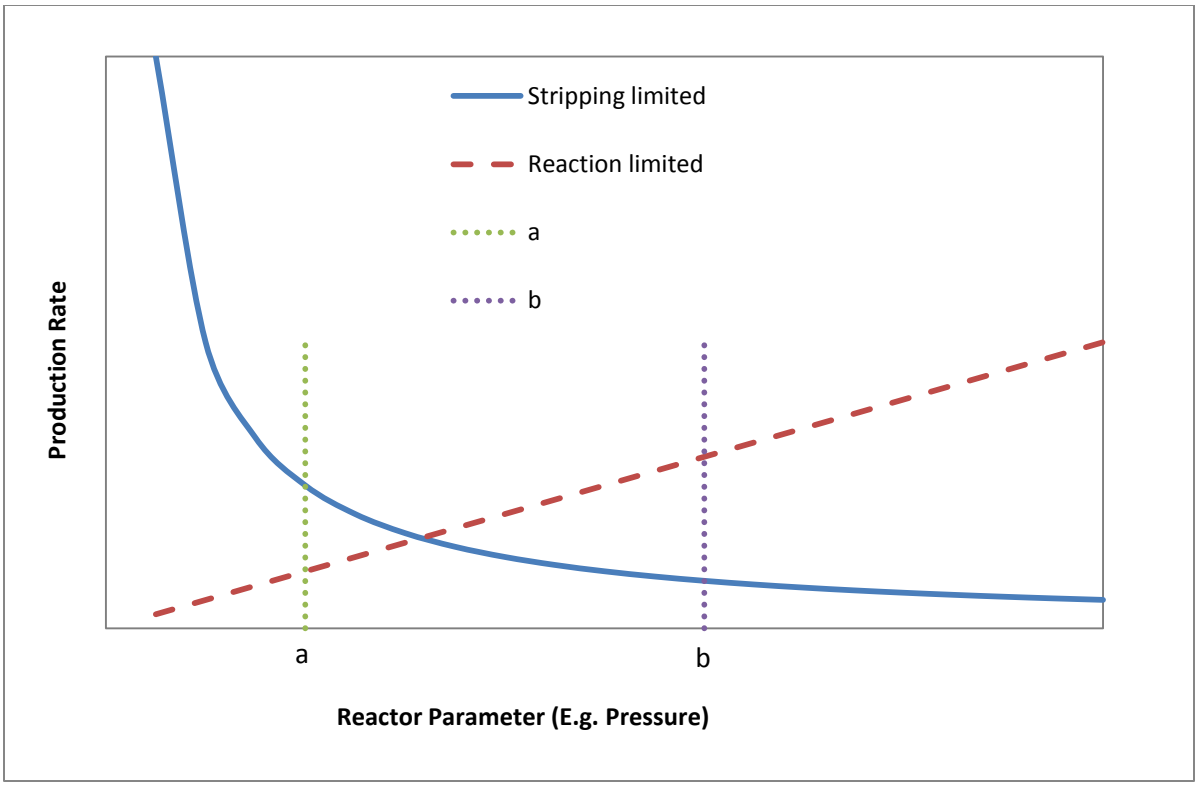


Figure 6.2: Schematic illustration of reaction rate limitation and stripping rate limitation for a particular reactor parameter, e.g. pressure in this case. The temperature dependence of the stripping rate limitation might have a different form but the discussion still holds.

Thus for example at low temperatures/pressures (e.g. point a in Figure 6.2) the reaction rate may be limiting, and thus the measured reaction rate may behave as a typical reaction. If we change conditions, for example increase temperature or change pressure (e.g. to point b in Figure 6.2), the inherent reaction may increase more quickly than the separation rate, so that the stripping rate becomes rate limiting. In this case the apparent or observed reaction would depend on the VLE and the temperature and pressure dependence of the observed rate would be different to that when the reaction was rate controlling.

Is it possible that stripping could be rate limiting in the FT reaction? We explored this experimentally.

6.5 CSTR TO BATCH REACTOR EXPERIMENT

Laboratory-scale research is normally carried out in continuous mode fixed bed or slurry bed reactor operated at steady state and seldom in a batch reactor which operates at unsteady state where the pressure of the reactor and partial pressure of the reactants and products change with the extent of the reaction. The batch reactor provides extra information that could be of value in understanding the behaviour of the FT reaction. Thus to further evaluate the behaviour and performance of FT we conducted an experiment in a batch reactor on cobalt catalyst.

The experiment was carried out in a 100 ml CSTR (*Autoclave Engineers*) in a gas-solid system without adding any solvent. Residence time distribution experiments [24] showed that the reactor could be regarded as an ideal CSTR when the stirring speed is higher than around 65 rpm. The reactor was operated at continuous operating mode (CSTR mode) and batch mode according to the requirement of the experiments. Premixed syngas (10% N_2, 30% CO and 60% H_2) was fed to the reactor at 2.0 MPa, with the flow rate controlled by a Brooks 5850 Mass Flow Controller. The product was drained from the bottom of the tank to ensure that the entire contents, including liquid phase products, could be fully taken out of the reactor. To prevent product condensation in the outlet lines, these lines were heated at 453 K down to the two product traps, which were kept at reactor pressure and at 423 K and 303 K, to collect wax and liquid products respectively. The gaseous stream was then reduced to atmospheric pressure and connected to an on-line GC (Agilent 6890A with a TCD and an FID). The details of the experimental setup are discussed elsewhere [25].

A supported cobalt catalyst (BET area 28.6 m^2/g, average pore diameter 35.8 nm) with 10% Co (by mass) on TiO_2 was used in the experiments. Approximately 3g of prepared cobalt catalyst was loaded into a catalyst basket (provided within the reactor). The frame of the basket was fixed to the inner wall of the tank but the basket itself did not extend over the whole diameter. A stirrer in the inner radius was used to stir the gas and force it through the catalyst held in the basket. The catalyst basket together with the catalyst inside was suspended in the tank, without shaking during the experiment.

The catalyst was prepared by the incipient wetness impregnation method and metal precursor selected was Sigma Aldrich $Co(NO_3)_2 \cdot 6H_2O$. TiO_2 (Degussa P-25) was mixed with distilled water in a 1:1 ratio to prepare a paste, which was dried at 393 K for two hours, calcined at 673 K for six hours and then cooled overnight. The calcined paste was crushed and sieved to a particle size between 0.5 and 1 mm to serve as the support for the catalyst. The required amount of $Co(NO_3)_2 \cdot 6H_2O$ was dissolved in distilled water to form a solution, which was then mixed with the support and allowed to absorb uniformly into it by impregnation. The wet catalyst pellets were dried at 393 K for two hours and then calcined at 673 K for six hours.

The catalyst was reduced with H_2 at 5.0×10^{-4} $Nm^3(kg_{cat})^{-1}s^{-1}$ and ambient pressure. The gas space velocity was based on the total mass of the unreduced catalyst. The temperature was increased from room temperature to 393 K, first at a ramping rate of 60 K/h, and held for two hours before being increased to 553 K at the same ramping rate, and maintained at this temperature for 24 hours. After reduction the reactor was cooled to 373 K.

The feed gas was switched from H_2, which had been used for the reduction, to the premixed syngas. The pressure of the reactor was stabilized at 2.0 Mpa by a back pressure regulator (Swagelok), and the flow rate of the feed was controlled at 3.3×10^{-4} $Nm^3(kg_{cat})^{-1}s^{-1}$ by a mass flow controller. The temperature used in the experiment was 483 K. The stirring speed inside the reactor was set at 100 rpm.

We operated the reactor at CSTR mode until steady state was reached before beginning each batch operation. The procedure was carried out as a cyclical sequence: using CSTR operation mode until steady state, followed by a batch operation for a certain period of reaction and sampling, and then the resumption of CSTR operation until the achievement of steady state marked the start of the next batch operation timed for a different duration.

We started the batch operation by isolating the reactor by closing the inlet and outlet valves, and starting the time record simultaneously. Once the designated duration (20 min, 40 min, 1 h and so on) of the batch operation had been completed, a sample was taken and analysed. During sampling, we flushed the sampling loop of the GC completely with the sample from the reactor to ensure the accuracy of the experiment. All the material in the reactor, including the light and heavy hydrocarbons, could be collected and injected into the GC.

Once the sample had been injected into the GC, we set the reactor into the original CSTR mode under the same operational conditions as previously. After around 24 hours the steady state had been achieved again and we started the next batch mode operation. In each CSTR operation after batch operation, the conversion of reactants and reaction rate could reach the same values before.

6.6 CSTR TO BATCH REACTOR RESULTS

The reaction rate for CSTR mode and batch mode are presented in Figure 6.3. The reaction rate in batch operation mode is an average reaction rate for the time interval. The operational conditions for CSTR and batch experiments were identical in all but one respect: no feed and products were taken out during the batch operation.

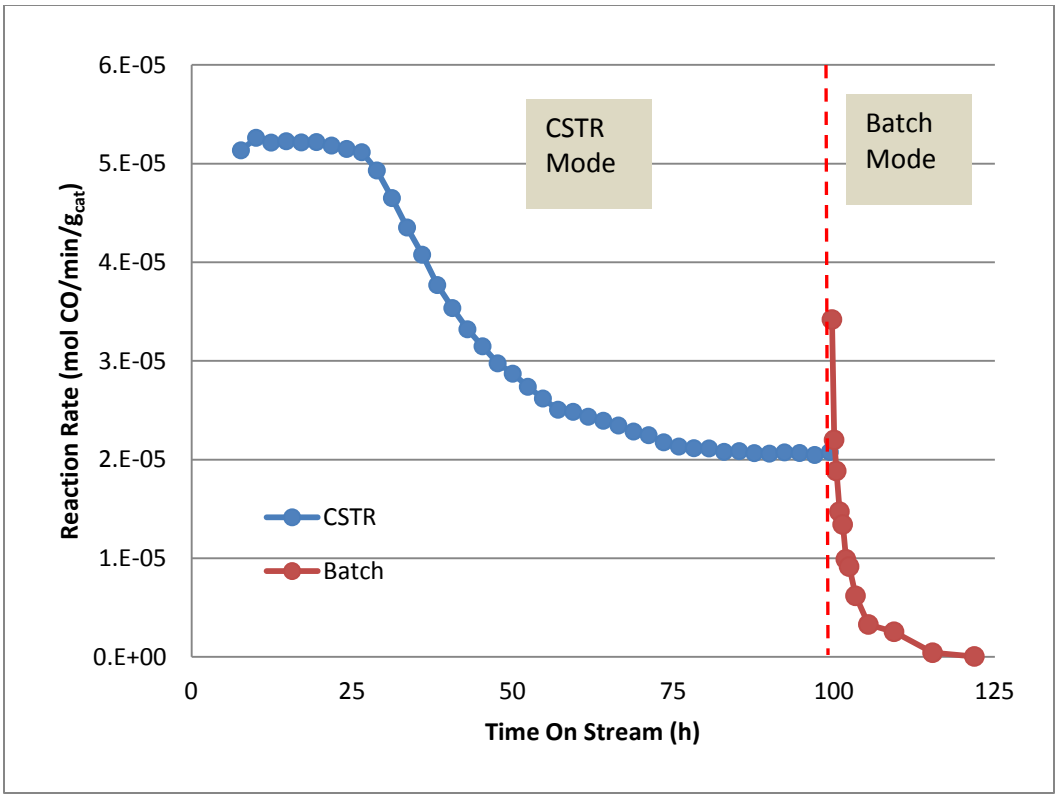


Figure 6.3: Reaction rates in the CSTR and Batch operation modes as a function of time on stream. (T = 483 K, P = 2.0 MPa, $H_2/CO = 2$)

From Figure 6.3, the reaction rate was around 2.0×10^{-5} mol CO/(g_{cat}·min) at the point when we switched the reactor from CSTR to batch, while the average CO reaction rate in the first 20 minutes of the batch operation jumped to around 3.4×10^{-5} mol CO/(g_{cat}·min). Then the reaction rate decreased with time on stream as the reactants in the reactor diminished.

A decrease in the reaction rate corresponding with the reduced concentration of the reactants in the reactor is understandable from a kinetic point of view, as the reaction rate is likely to be a function of the concentrations of the reactants in the reactor. However, the jump in the reaction rate by around 70% when we switched the operational mode from CSTR to batch was unexpected as the average concentration of the reactants in the first 20 minutes of the reaction is only slightly lower than that of the CSTR mode. Remember that the catalyst had been conditioned, as the reactor had been operated at CSTR mode for more than a week before being

switched to batch operations, and was at steady state. Thus no sudden change in the catalyst properties would be expected when the batch operation was started, so that the jump of the reaction rate was unlikely to be caused by property changes in the catalyst.

When the reactor is in CSTR mode, there are two processes occurring, namely reaction and stripping. When we stop the flow we remove the stripping vector and we are left with reaction occurring. Note that the effect is not caused by a change in mass transfer as we are still stirring vigorously and the catalyst has been deposited well with liquid phase products during the CSTR operating mode, thus it must be because we have stopped the flow and the removal of products or reactants.

We have shown earlier that, for product/water addition the mass balance simplifies to:

$$\frac{dx_i}{dt} = r_i - \frac{\dot{N}_V}{N_L}(y_i - x_i) + \frac{\dot{N}_{in}}{N_L}\left(y_{i,in} - x_i\right) \quad (8)$$

which can be rearranged to

$$r_i = \frac{dx_i}{dt} + \frac{\dot{N}_V}{N_L}(y_i - x_i) - \frac{\dot{N}_{in}}{N_L}\left(y_{i,in} - x_i\right) \quad (11)$$

Equation (11) illustrates that the rate of formation of component I (r_i), is related to the change of component I in the liquid phase ($\frac{dx_i}{dt}$), the stripping rate ($\frac{\dot{N}_V}{N_L}(y_i - x_i)$), and the relationship between passing streams of a distillation column ($\frac{\dot{N}_{in}}{N_L}\left(y_{i,in} - x_i\right)$) where ($y_{i,in}$) and ($x_i$) lie on the operating line of a distillation column.

The rate of consumption of a reactant I is given by a negative of the rate of formation of component i. Therefore, the mass balance for CO would result in:

$$r_{CO} = \frac{\dot{N}_{in}}{N_L}\left(y_{CO,in} - x_{CO}\right) - \frac{dx_{CO}}{dt} - \frac{\dot{N}_V}{N_L}(y_{CO} - x_{CO}) \quad (12)$$

When the liquid composition reaches steady state, then Equation (12) simplifies to

$$r_{CO} = \frac{\dot{N}_{in}}{N_L}\left(y_{CO,in} - x_{CO}\right) - \frac{\dot{N}_V}{N_L}\left(y_{CO} - x_{CO}\right) \quad (13)$$

Equation (13) reveals that the rate of consumption of CO dependents on the molar flow in multiplied by the difference between the mole fraction into the reactor and the mole fraction in the liquid phase minus the stripping rate of CO (i.e. $\frac{\dot{N}_V}{N_L}(y_{CO} - x_{CO})$). This shows that the stripping rate is negative which implies that the reactant stripping limits the reaction rate.

This illustrates the reason for an increase in the reaction rate from switching from CSTR to Batch mode. When the change took place we had moved from a situation where reaction and stripping of the liquid were occurring simultaneously to one in which only reaction was occurring. When switching to Batch mode the stripping vector is eliminated and the CO rate increases because the stripping rate was limiting it. As time goes on the CO rate in the Batch reactor decreases as expected because the mole fraction of CO decreases inside the reactor. Hence, stripping of reactants resulted in a lower reaction rate in the steady state CSTR mode.

The Batch reactor unveils that the behaviour and performance of the FT reactor can be described by considering FT reactors as reactive distillation systems. To gain further insight into the FT reaction we consider the product distribution expected from modelling an FT reactor as a reactive distillation system.

6.7 PRODUCT DISTRIBUTION

The rate of formation is normally reported in terms of total production after the vapour and the liquid products have been added together. Therefore, assuming that the rate of formation of component i is proportional to the total mole fraction of that component i.e.

$$r_i \propto z_i \quad (14)$$

where z_i is the overall mole fraction from the combined vapour and liquid phase streams, then

$$\frac{r_{i+1}}{r_i} = \frac{z_{i+1}}{z_i} \tag{15}$$

If there is no product in the feed then Equation (10) becomes

$$r_i = \frac{\dot{N}_V}{N_L}(y_i - x_i) + \frac{\dot{N}_{in}}{N_L}x_i \tag{16}$$

Substituting the rate into Equation (15) gives

$$\frac{r_{i+1}}{r_i} = \frac{\dot{N}_V(y_{i+1} - x_{i+1}) + x_{i+1}\dot{N}_{in}}{\dot{N}_V(y_i - x_i) + x_i\dot{N}_{in}} = \frac{z_{i+1}}{z_{i+1}} \tag{17}$$

If we assume VLE then we can relate the vapour composition y_i to the liquid composition x_i by

$$y_i = K_i x_i \tag{18}$$

where K_i is the partition coefficient (K-value) for component i, thus, Equation (17) becomes

$$\frac{z_{i+1}}{z_i} = \frac{x_{i+1}}{x_i}\left(\frac{\dot{N}_{in} + \dot{N}_V(K_{i+1} - 1)}{\dot{N}_{in} + \dot{N}_V(K_i - 1)}\right) \tag{19}$$

We have shown in Chapter 3 that Raoult's law can sufficiently describe VLE in an FT reactor [26]. Consequently, if we use Raoult's law then

$$K_i = \frac{P_{vap\ i}}{P} \tag{20}$$

According to Caldwell and van Vuuren [27]

$$P_{vap\ i+1} = \beta P_{vap\ i} \tag{21}$$

where $P_{vap\ i}$ is the vapour pressure of component i, thus

$$K_{i+1} = \beta K_i \tag{22}$$

Therefore substituting into Equation (19) gives

$$\frac{z_{i+1}}{z_i} = \frac{x_{i+1}}{x_i}\left(\frac{\dot{N}_{in} + \dot{N}_V(\beta K_i - 1)}{\dot{N}_{in} + \dot{N}_V(K_i - 1)}\right) \tag{23}$$

The rate expression was used to derive Equation (23) which expresses the overall mole fraction in terms of the liquid phase product distribution. This expression should correspond to the expression derived in Chapter 4 by simple VLE modelling on the FT products [9]. To confirm this we use the constant alpha in the liquid phase hypothesis.

6.8 CONSTANT ALPHA PRODUCT DISTRIBUTION IN THE LIQUID PHASE

We postulate that the reaction happens as described by the simple polymerization reaction [1, 2]. Therefore at high reactor liquid content or in a reactor where the catalyst pores are filled with liquid we postulate that a classical single α Flory distribution is set up in the liquid phase (Case 3, Chapter 4) [9]. This liquid phase is in equilibrium with a vapour phase. Thus

$$\frac{x_{i+1}}{x_i} = \alpha \tag{24}$$

Therefore Equation (23) becomes

$$\frac{z_{i+1}}{z_i} = \alpha \left(\frac{\dot{N}_{in} + \dot{N}_V(\beta K_i - 1)}{\dot{N}_{in} + \dot{N}_V(K_i - 1)} \right) \tag{25}$$

We now consider special cases: for low carbon numbers

$$P_{vap\ i} \gg P \tag{26}$$

Therefore Equation (20) results in

$$K_i \gg 1 \tag{27}$$

As a result Equation (25) simplifies to

$$\frac{z_{i+1}}{z_i} = \alpha\beta \tag{28}$$

But

$$\frac{y_{i+1}}{y_i} = \frac{P_{vap\ i+1} x_{i+1}}{P_{vap\ i} x_i} = \alpha\beta \tag{29}$$

This means that the overall product distribution follows the gas phase distribution.

For high carbon numbers

$$P_{vap\ i} \ll 1 \tag{30}$$

Therefore Equation (20) results in

$$K_i \ll 1 \tag{31}$$

Consequently, Equation (25) simplifies to

$$\frac{z_{i+1}}{z_i} = \alpha \tag{32}$$

This means that the overall product distribution follows the liquid phase distribution. This result in a product distribution in which the lighter components corresponds with the vapour phase distribution and the heavier components follows the liquid phase distribution. This is consistent with the distribution obtained by modelling VLE in an FT reactor [9]. Hence the overall product distribution would be as shown in Figure 6.4.

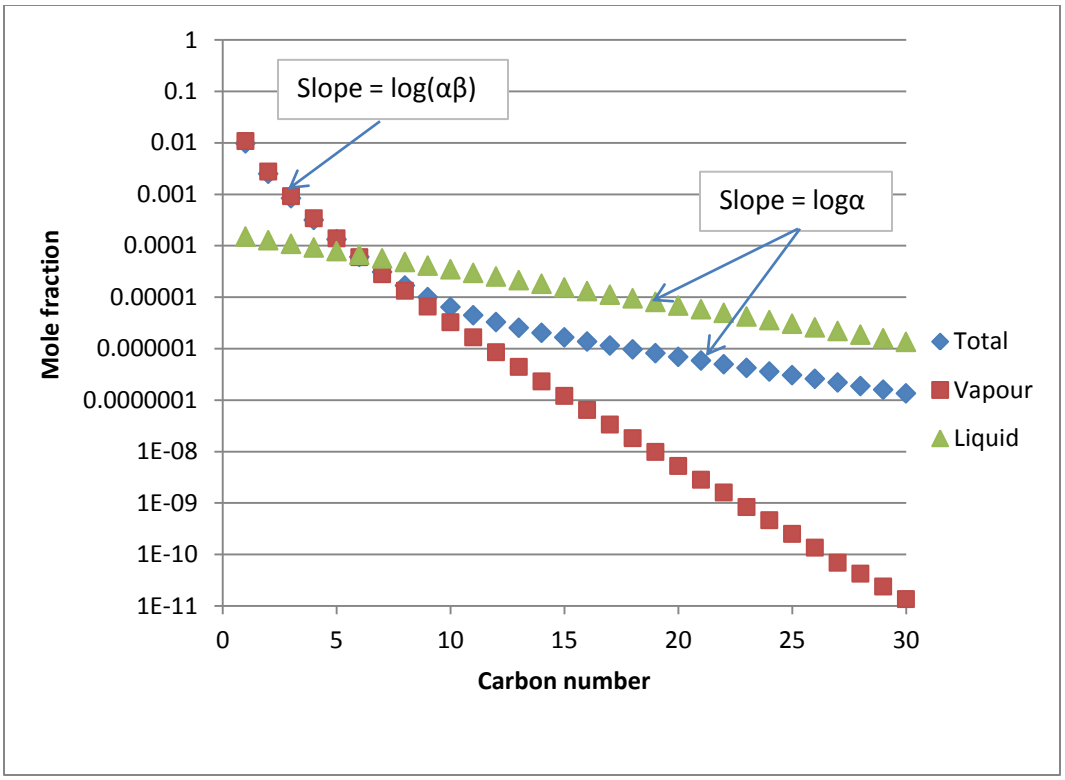


Figure 6.4: Observed product distribution for modelling reaction and stripping in an FT reactor reproduced from Ref. [9].

The overall product distribution presented in Figure 6.4 is consistent with the observed literature and industrial product distribution as it predicts a two-alpha positive deviation product distribution. Therefore, VLE is a possible reason for the observation of a two-alpha product distribution. This model relates the second slope (log(α)) to the first slope (log(αβ)) of a two-alpha product distribution.

The model predicts that the component with the highest mole fraction in the liquid phase is methane ($x_{i+1}/x_i = \alpha$). This is counter intuitive because most researchers refer to the liquid phase as the oily/waxy liquid phase [28]. This occurs because of reactive distillation. The species with the highest reaction rate is methane ($r_i \propto z_i$). Species with the highest stripping rate is also methane ($y_{i+1}/y_i = \alpha\beta$). Therefore methane reaction replaces methane removed by stripping. If no

reaction takes place and only stripping occurs then lighter components (e.g. methane) would be removed the fastest [25] which would then lead to an oily/waxy liquid phase.

To further explore the behaviour of the reactor it is important to evaluate the effect of the vapour/liquid fraction inside the reactor on the product distribution.

6.9 VAPOUR FRACTION INSIDE THE REACTOR

To determine the effect of vapour/liquid fraction inside the reactor we have to consider the latter part of the FT reactor in which $\dot{N}_V$ and $\dot{N}_L$ moles flowing out per second are combined for an overall mass balance to give $\dot{N}_Z$ moles per second as shown in Figure 6.5.

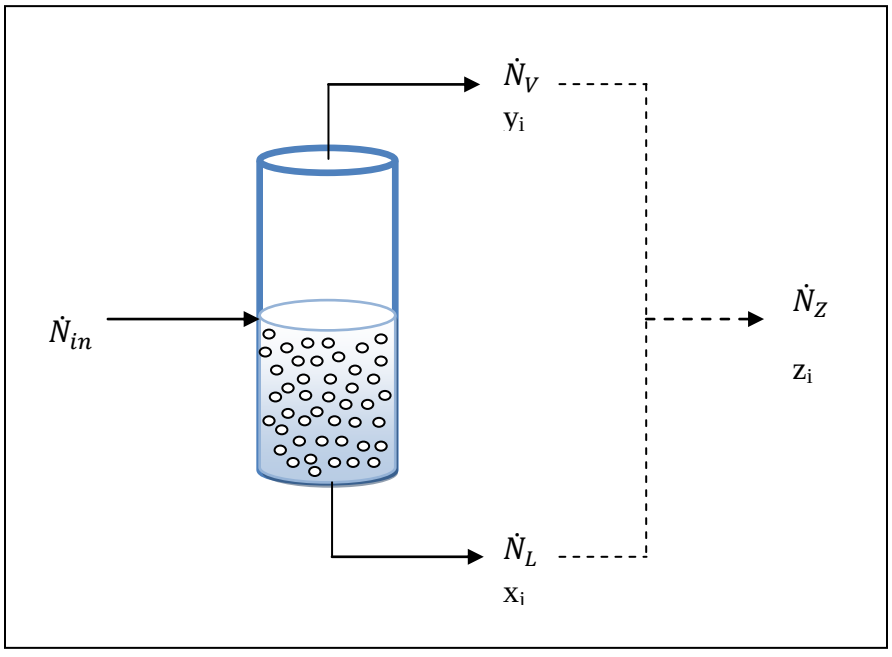


Figure 6.5: Schematic diagram for a reactive flash drum

The overall mass balance for the VLE gives:

$$\dot{N}_V + \dot{N}_L = \dot{N}_Z \tag{33}$$

The component balance gives:

$$\dot{N}_V y_i + \dot{N}_L x_i = \dot{N}_Z z_i \tag{34}$$

The vapour fraction is defined as:

$$f \equiv \frac{\dot{N}_V}{\dot{N}_Z} \tag{35}$$

Therefore:

$$f y_i + (1 - f) x_i = z_i \tag{36}$$

Since f ranges from zero to one, this means that x_i and y_i must lie on either side of z_i. For a given alpha in the liquid phase

$$x_i = \alpha^{i-1} x_1 \tag{37}$$

From Equation (29)

$$y_i = (\alpha\beta)^{i-1} y_1 \tag{38}$$

At a given temperature the value of β is fixed. If we select a value of α then we can vary the vapour fraction and calculate the overall compositions to determine the effects of vapour fractions on the product distribution. At 493 K, β ≈ 0.65, we selected α = 0.85 and varied the vapour fraction to generate a plot of the hydrocarbon product distributions and the results are shown in Figure 6.6.

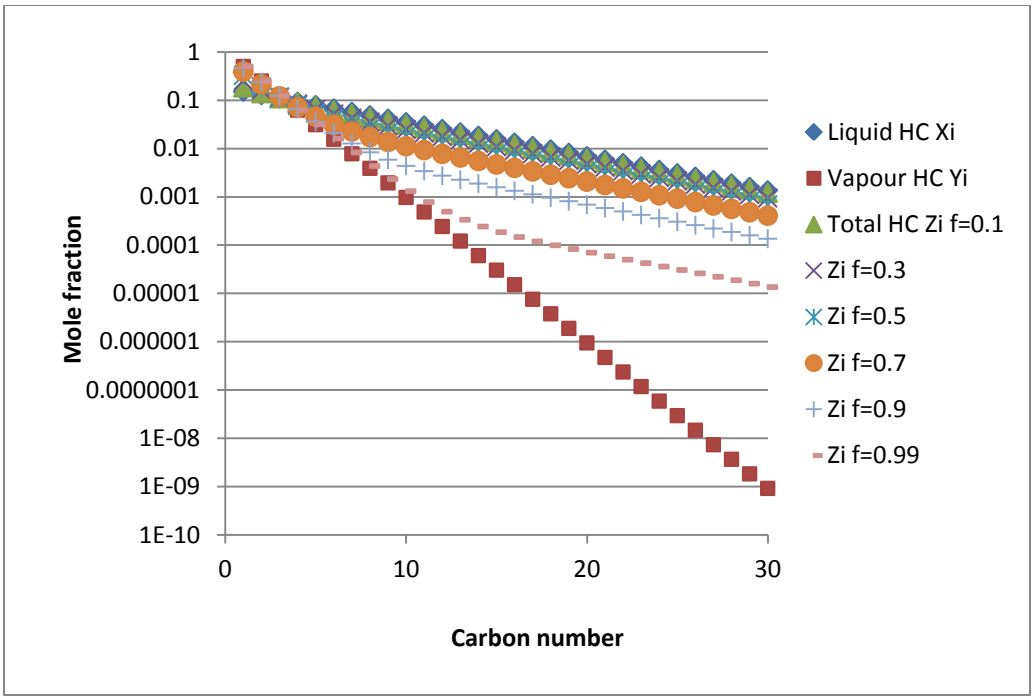


Figure 6.6: Mole fractions of hydrocarbons at different vapour fractions.

The results in Figure 6.6 show that the observed two-alpha product distribution is obtained at high vapour fractions (0.99). This means that only a small fraction of liquid (0.01) is required in the reactor to produce a two-alpha plot.

VLE modelling of the two-alpha product distribution was previously demonstrated on an iron catalyst. However, VLE results are catalyst insensitive. Therefore, we conducted an experiment using a cobalt catalyst to test the product distribution model.

6.10 PRODUCT DISTRIBUTION EXPERIMENTAL RESULTS

An experiment was conducted in a fixed bed micro-reactor at 493 K and 0.8 MPa using a 10% cobalt catalyst by mass on titania support. The catalyst preparation is as described in Section 5. The reactor feed was a pre-mixed synthesis gas (10% N_2, 30% CO and 60% H_2). The synthesis

gas was introduced through the reactor, allowed to flow through the catalyst bed, and then passed through a hot trap maintained at 423 K for wax collection. Thereafter it entered a cold trap maintained at room temperature (≈ 298 K) for collection of the liquid (oil and aqueous) fraction. The operating pressure in the reactor was maintained at 0.8 MPa by means of a pressure regulator on the gas cylinder and a needle valve at the reactor exit. The needle valve was also used to control the gas space velocity in the reactor and to de-pressurize the outlet gas stream before it reached the GCs. Two solenoid valves, which automatically directed the reactor outlet gas to vent or to the GCs for analysis, were mounted behind the needle valve. The gas was directed to the GCs for only the short period required to flush out the residual gas in the sampling loops, to allow for further sampling. For the remainder of the time the solenoid valves vented the outlet gas to the atmosphere to keep the sampling line clean. A new gas sample was analysed every two hours.

The gas analysis was carried out online using two GCs, one with a flame ionization detector (FID) and the other with a thermal conductivity detector (TCD). The GC equipped with FID had a Poropak-Q column that was used to separate hydrocarbons from C_1 to C_9. The GC fitted with the TCD was employed in the analysis of the inorganic gases H_2, He, N_2, CO on a carbosieve S-II packed column. We determined the actual molar composition of the gas by means of calibration data and relative response factors.

Wax, oil and water were allowed to accumulate in the hot and cold traps respectively, and were collected at the end of the mass balance period. We carried out the oil and wax fractions analysis with an off-line GC with an FID on a BP-5 capillary column. For the analysis of these condensed phases we obtained a mass composition directly from the GC peak area percentages, as the mass response factors were around one. Further details of the experimental setup are discussed in Section 4.7. The overall product distribution obtained at the end of the mass balance period is shown in Figure 6.7.

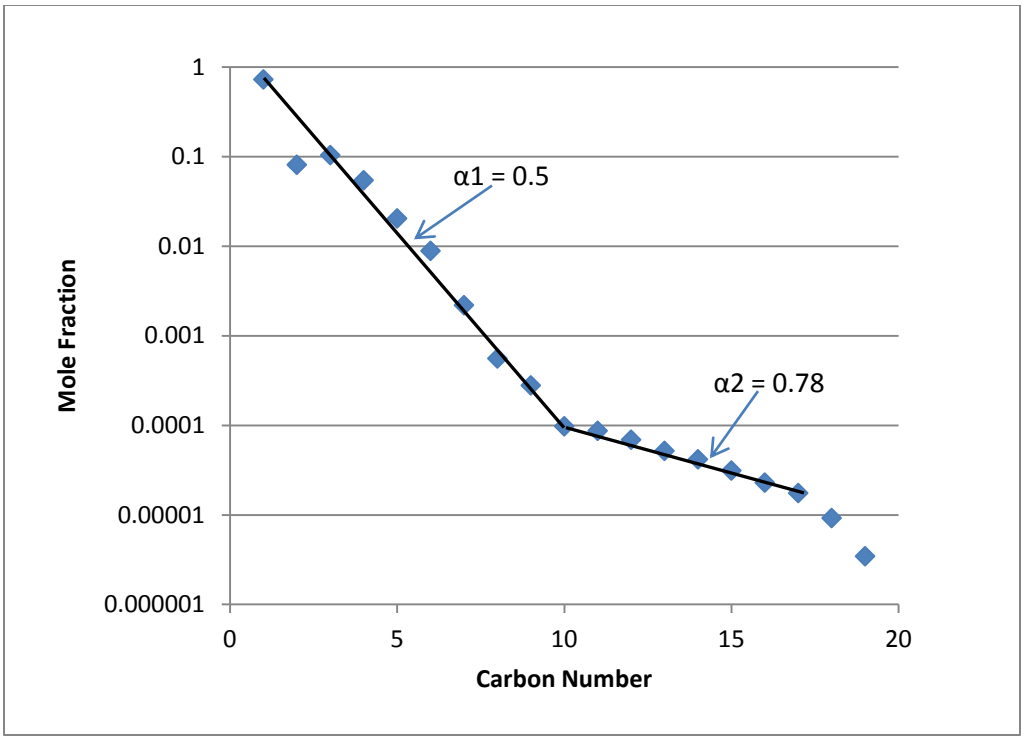


Figure 6.7: Total product distribution from the experimental results obtained using a cobalt catalyst at 493 K and 0.8 MPa.

The experimental results presented in Figure 6.7 show a two-alpha positive deviation from the classical Flory product distribution. The break in alphas occurs at carbon number 10 which is consistent with many reported experimental and industrial results [6]. On average α_1 from C_1 to C_{10} was found to be 0.5 and α_2 from C_{10} to C_{17} was found to be 0.78, the last two points were ignored to minimise experimental errors.

The liquid phase Flory product distribution model was used to predict α_1 for the given experimental conditions and using the liquid phase alpha (α_2) of 0.78. According to Caldwell and van Vuuren [27] the ratio of the vapour pressures at a given temperature T (K) can be estimated from

$$\beta = exp\left[-427.218\left(\frac{1}{T} - 1.029807 \times 10^{-3}\right)\right] \quad (39)$$

Therefore, at 493 K, $\beta \approx 0.65$ thus given $\alpha_2 = 0.78$, the model predicts $\alpha_1 = \alpha_2\beta = 0.5$. This shows that the model can predict the FT product distribution regardless of the type of catalyst used.

Some researchers have reported the values of the two-alpha product distribution. We therefore tested the model on a few reported literature results.

6.11 TWO-ALPHA LITERATURE RESULTS

Bukur et al. [29] tested a commercial Ruhrchemie catalyst in a fixed bed and in a slurry reactor. Their results show a two-alpha product distribution for both reactors. The fixed bed reactor at a time on stream of 427 hours had $\alpha_1 = 0.60$ and $\alpha_2 = 0.88$. The experiment was carried out at 523 K, therefore from Equation (39), $\beta \approx 0.69$. The model predicts $\alpha_1 = \alpha_2\beta = 0.60$ which is the same as the measured α_1.

Their results for the slurry reactor at 619 hours at the same temperature show $\alpha_1 = 0.60$ and $\alpha_2 = 0.85$. The model predicts $\alpha_1 = \alpha_2\beta = 0.58$ which is slightly different from the measured value. It should be noted that their results at 619 hours come after their results at 571 hours which was at 538 K. We have calculated the average residence time of different hydrocarbons in a slurry reactor in Chapter 5. The heavier hydrocarbons had an average residence time of around 13 days. Therefore, their heavier products might not have reached steady state yet which might explain the slight deviation.

Bukur et al. [30] at another point tested a doubly promoted precipitated iron catalyst in a fixed bed reactor. The experiments were carried out at 523 K. Their results that show a clear two-alpha product distribution had $\alpha_1 = 0.63$ and $\alpha_2 = 0.92$. The model predicts $\alpha_1 = \alpha_2\beta = 0.63$ which is the same as the measured α_1. Accordingly, the model fits literature data.

Therefore modelling an FT reactor as a reactive separator is also consistent with the observed two-alpha positive deviation product distribution observed experimentally and industrially.

6.12 CONCLUSIONS

The mathematical model developed for the reactor show that the rate of formation of component hydrocarbons is independent of the amount of liquid removed from the reactor, but depends on the reaction rate and stripping rate. At steady state, the rate of formation of hydrocarbons is given by the stripping rate.

The FTS reaction was performed in a batch reactor. A reaction rate increment of around 70% was observed when the reactor was switched from CSTR mode to Batch mode, with all other operation conditions remaining the same. When the change took place we had moved from a situation where reaction and stripping of the liquid were occurring simultaneously to one in which only reaction was occurring. When switching to Batch mode the stripping vector is eliminated and the CO rate increases because the stripping of reactants was limiting the reaction rate. Thus, modelling an FT reactor as a reactive distillation system explains a number of phenomena observed experimentally.

Conventional FT reactors behave like reactive distillation systems. The production rate in the reactor may be limited by the reaction rate and thus the measured reaction rate may behave as a typical reaction or the stripping rate and thus the apparent/observed rate would depend on VLE, depending on which phenomena is rate limiting.

Modelling an FT reactor as a reactive separator is consistent with the constant alpha in the liquid phase hypothesis. This explains the experimentally and industrially observed two-alpha positive deviation product distribution. The vapour fraction results show that only a small fraction of

liquid (0.01) is required in the reactor to produce a two-alpha plot. Experimental results confirm that this model is catalyst insensitive. This model also fits some reported literature product distributions.

NOMENCLATURE

m_n mole fraction of hydrocarbon with chain length n

α chain growth probability factor

$\dot{N}_{in}$ total molar flow into the reactor

$\dot{N}_V$ vapour phase molar flow out of the reactor

$\dot{N}_L$ total liquid molar flow out of the reactor

N_L total moles of liquid inside the reactor

$\dot{N}_r$ is the change of moles upon reaction

r_i rate of formation of component i

x_i mole fraction of component i in the liquid phase

y_i mole fraction of component i in the vapour phase

z_i overall mole fraction of component i

$y_{i,in}$ mole fraction of added product in the feed to the reactor

$P_{vap\ i}$ vapour pressure of component i

β ratio of vapour pressures of hydrocarbons

$\dot{N}_Z$ sum of the vapour and the liquid molar flows

f vapour fraction

$\bar{n}$ average carbon number

K_i Partition coefficient (K-value = y_i/x_i) of component i

ACKNOWLEDGEMENTS

We would like to acknowledge financial support from the National Research Foundation (NRF), South African Research Chairs Initiative (SARChI), Technology and Human Resources for Industry Programme (THRIP), South African National Energy Research Institute (SANERI), and the University of the Witwatersrand, Johannesburg.

REFERENCES

[1] P.J. Flory, Molecular size distribution in linear condensation polymers, *J. Am. Chem. Soc. 58* (1936) 1877–1885.

[2] E.F.G. Herington, The Fischer–Tropsch synthesis considered as a polymerization reaction, *Chem. Ind. 65* (1946) 346–347.

[3] M.E. Dry, Practical and theoretical aspects of the catalytic Fischer–Tropsch process, *Appl. Catal. A: Gen. 138* (1996) 319–344.

[4] B. Shi, B.H. Davis, Fischer–Tropsch synthesis: accounting for chain length related phenomena, *Appl. Catal. A: Gen 277* (2004) 61–69.

[5] E. Iglesia, Design, synthesis, and use of cobalt-based Fischer–Tropsch synthesis catalysts, *Appl. Catal. A: Gen. 161* (1997) 59–78.

[6] B.H. Davis, The two-alpha value for iron Fischer–Tropsch catalyst: fact or fiction?, *ACS Div. Fuel Chem. Preprints 37* (1992) 172–183.

[7] H. Schulz, M. Claeys, Kinetic modelling of Fischer–Tropsch product distributions, *Appl. Catal. A: Gen. 186* (1999) 91–107.

[8] C.M. Masuku, D. Hildebrandt, D. Glasser, Olefin pseudo-equilibrium in the Fischer–Tropsch reaction, *Chem. Eng. J. 181–182* (2012) 667–676.

[9] C.M. Masuku, D. Hildebrandt, D. Glasser, The role of vapour–liquid equilibrium in Fischer–Tropsch product distribution, *Chem. Eng. Sci. 66* (2011) 6254–6263.

[10] G.J. Harmsen, Reactive distillation: The front-runner of industrial process intensification: A full review of commercial applications, research, scale-up, design and operation, *Chem. Eng. Process. 46* (2007) 774–780.

[11] S. Hauan, K.M. Lien, Geometric visualisation of reactive fixed points, *Comput. Chem. Eng. 20* (1996) S133–S138.

[12] S. Kauchali, C. McGregor, D. Hildebrandt, Binary distillation re-visited using the attainable region theory, *Comput. Chem. Eng. 24* (2000) 231–237.

[13] S. Huaun, A.R. Ciric, A.W. Westerberg, K.M. Lien, Difference points in extractive and reactive cascades. I – Basic properties and analysis, *Chem. Eng. Sci. 55* (2000) 3145–3159.

[14] S.T. Holland, M. Tapp, D. Hildebrandt, D. Glasser, B. Hausberger, Novel separation system design using "moving triangles", *Comput. Chem. Eng. 29* (2004) 181–189.

[15] S.T. Holland, M. Tapp, D. Hildebrandt, D. Glasser, Column profile maps. 2. Singular points and phase diagram behaviour in ideal and nonideal systems, *Ind. Eng. Chem. Res. 43* (2004) 3590–3603.

[16] A. Tuchlenski, A. Beckmann, D. Reusch, R. Düssel, U. Weidlich, R. Janowsky, Reactive distillation – industrial applications, process design & scale-up, *Chem. Eng. Sci. 56* (2001) 387–394.

[17] R. Taylor, R. Krishna, Review: Modelling reactive distillation, *Chem. Eng. Sci. 55* (2000) 5183–5229.

[18] D. Barbosa, M.F. Doherty, The influence of equilibrium chemical reactions on vapor–liquid phase diagrams, *Chem. Eng. Sci. 43* (1988) 529–540.

[19] G.J. Harmsen, L.A. Chewter, Industrial applications of multi-functional, multi-phase reactors, *Chem. Eng. Sci. 54* (1999) 1541–1545.

[20] S. Srinivas, R.K. Malik, S.M. Mahajani, Feasibililty of reactive distillation for Fischer–Tropsch synthesis, *Ind. Eng. Chem. Res. 47* (2008) 889–899.

[21] S. Srinivas, R.K. Malik, S.M. Mahajani, Reactive distillation for Fischer–Tropsch synthesis: Simulation based design methodology using Aspen Plus, *Ind. Eng. Chem. Res. 49* (2010) 9673–9692.

[22] S. Srinivas, R.K. Malik, S.M. Mahajani, Reactive distillation for Fischer–Tropsch synthesis: Feasible solution space, *Ind. Eng. Chem. Res. 49* (2010) 6350–6361.

[23] C.M. Masuku, W.D. Shafer, W. Ma, M.K. Gnanamani, G. Jacobs, D. Hildebrandt, D. Glasser, B.H. Davis, Variation of residence time with chain length for products in a slurry phase Fischer–Tropsch reactor, *J. Catal. 287* (2012) 93–101.

[24] X. Lu, D. Hildebrandt, X. Liu, D. Glasser, Making sense of the Fischer–Tropsch synthesis reaction: Start-up, *Ind. Eng. Chem. Res. 49* (2010) 9753–9758.

[25] X. Lu, X. Zhu, D. Hildebrandt, X. Liu, D. Glasser, A new way to look at Fischer–Tropsch synthesis using flushing experiments, *Ind. Eng. Chem. Res. 50* (2011) 4359–4365.

[26] C.M. Masuku, W. Ma, D. Hildebrandt, D. Glasser, A vapor–liquid equilibrium thermodynamic model for a Fischer–Tropsch reactor, *Fluid Phase Equilib. 314* (2012) 38–45.

[27] L. Caldwell, D.S. van Vuuren, On the formation and composition of the liquid phase in Fischer–Tropsch reactor, *Chem. Eng. Sci. 41* (1986) 89–96.

[28] R.A. Dictor, A.T. Bell, An explanation for deviations of Fischer–Tropsch products from a Schulz–Flory distribution, *Ind. Eng. Chem. Process Des. Dev. 22* (1983) 678–681.

[29] D.B. Bukur, S.A. Patel, X. Lang, Fixed bed and slurry reactor studies of Fischer–Tropsch synthesis on precipitated iron catalyst, *Appl. Catal. 61* (1990) 329–349.

[30] D.B. Bukur, M. Koranne, X. Lang, K.R.P. Rao, G.P. Huffman, Pretreatment effect studies with a precipitated iron Fischer–Tropsch catalyst, *Appl. Catal. A: Gen. 126* (1995) 85–113.

Chapter 7 : CONCLUDING REMARKS

7.1 INTRODUCTION

Thermodynamic equilibrium analysis is an important tool in the study of reacting systems. It is an aid in reactor modelling, in examining kinetic schemes or reaction mechanisms, and in identifying rate-controlling processes. Therefore, the aim of the thesis was to describe the behaviour and performance of the Fischer–Tropsch (FT) reactor by considering the dynamic interaction between reaction equilibrium and vapour–liquid equilibrium (VLE).

7.2 REACTION EQUILIBRIUM

Overall or global thermodynamic equilibrium predicts a predominately methane product for the FT reaction. Even though the FT product distribution may not be described by overall thermodynamic equilibrium, there may be aspects of it that can be described by equilibrium. A stepwise chain-growth thermodynamic model supports a single alpha Flory product distribution. The reaction model described in this work provides a method for calculating alpha from thermodynamic formulation.

The calculated results predict that equilibrium between the species of any homologous series would results in a Flory-type distribution, where the ratio of the moles of species n to that of the moles of species n+1 would be constant. When the value of this ratio α is calculated for olefins, it is found that the experimentally measured values match those calculated and thus the measured and predicted distribution of the olefins agree. However, assuming that the alcohols or paraffin distribution approaches equilibrium, leads to calculated values of α that are not consistent with the experimental results.

Therefore, there may be an equilibrium set up between species of either an olefin precursor or the olefins themselves which leads to the Flory-type distribution found in the FT reaction. This substantiates the fact that olefins are primary FT products and paraffins are formed from them since the whole product distribution is determined by the olefins. This implies that paraffins are formed by secondary reactions which are kinetically determined. Some paraffins might be primary products which would explain the abnormally high methane yields in the FT reactor. Therefore, reaction equilibrium is of much greater importance to the FT system than previously thought.

7.3 VAPOUR–LIQUID EQUILIBRIUM THERMODYNAMIC MODEL

VLE plays an important role in modelling an FT reactor. Recently, a variety of VLE thermodynamic models have been used to model FT products. Therefore, we conducted an experiment to measure actual vapour and liquid compositions of long chains hydrocarbons under FT reaction conditions to ascertain whether Raoult's law is sufficient or other elaborate VLE models are required.

The results obtained show that VLE is attained inside an FT reactor. The measured vapour and liquid compositions (K-values) can be sufficiently described by Raoult's law. Hydrocarbons with carbon number greater than 18 deviates from Raoult's law. The deviations from Raoult's law are due to diffusion limitations. Elaborate thermodynamic models could be used given the pure component parameters with relevant mixing rules for a higher degree of accuracy.

7.4 VAPOUR–LIQUID EQUILIBRIUM IN FISCHER–TROPSCH PRODUCT DISTRIBUTION

Deviations from the classical Flory-type product distribution have been reported. The most widely-reported of these is the two-alpha positive deviation. A number of postulates have been suggested to account for the observed two-alpha phenomenon, but most of them neglect the effect of VLE. The few scientists who have considered VLE have not provided satisfactory explanations for the deviation.

We use VLE to explain the observed two-alpha product distribution in FT reactors. We discuss three possible scenarios or cases of the Flory product distribution and VLE. The three cases assume that: (1) the reaction sets up a single alpha Flory distribution in the total (vapour + liquid) products, (2) the vapour phase follows a single alpha distribution, and (3) a single alpha distribution is set up in the liquid phase. We then look at the consequences of these assumptions in conjunction with a simple Raoult's law VLE model on the exit product distributions. We find that only Case 3 gives rise to a two-alpha model in accordance with experimental results that is frequently observed in FT reactors. This model further predicts a relationship between the two values of alpha that is consistent with the measured experimental results.

7.5 PRODUCT RESIDENCE TIME

It is generally assumed, that the olefin readsorption probability increases with increasing carbon number due to increased residence times of longer chains in the liquid-filled pores of the catalyst. VLE and diffusion limitations have been proposed as possible reasons. To obtain more insight into the cause for chain-length dependencies of secondary olefin reactions in an FT reactor we conducted an experiment to measure the variation of residence time of hydrocarbons with chain length.

The results confirm that the average residence time increase with carbon number and the higher carbon number products have a longer residence time in the reactor as their residence time approaches that of the non-volatile polywax. Products with a chain length of 22 and higher have the same residence time as the liquid. This suggests that VLE is the predominant cause for chain length dependencies of secondary olefin reactions in FT synthesis and diffusion limited removal of products is only significant for products with carbon number greater than 17.

7.6 REACTIVE DISTILLATION

The Flory distribution that is often observed in FT reactors could be described by reaction equilibrium between species. Furthermore, it has been suggested that VLE exists in the reactor and this could cause the two-alpha product distribution that is often observed experimentally. Simultaneous reaction and VLE is characteristic of reactive distillation system. We therefore developed a mathematical model to describe the behaviour and performance of an FT reactor by considering the dynamic interaction between reaction and VLE.

The model results show that the rate of formation of component hydrocarbons is dependent on either the reaction rate or stripping rate, depending on which one is rate-limiting. Furthermore, that at steady state, the rate of formation of hydrocarbons is given by the stripping rate. We conducted an experiment which showed a reaction rate increment when the reactor was switched from CSTR to Batch mode, with all other operation conditions remaining the same. In the Batch mode the stripping vector is eliminated and the CO rate increases because reactant stripping was limiting the reaction rate. Modelling an FT reactor as a reactive distillation column is also consistent with the observed two-alpha positive deviation product distribution observed experimentally and industrially.

7.7 FUTURE WORK AND RECOMMENDATIONS

It is well known that liquid is formed to a lesser or greater extent in the FT reaction, however when modelling the reaction and its kinetics, very little account is taken of the phenomenon. Also, even though water is the main product of the reaction, because it is not valuable, very little attention has been given to its role in the reaction. The effect of water solubility in an organic phase or the likelihood of even forming a two-phase mixture has not been adequately explored.

The hydrocarbon removal rate of some species and possibly the water could be controlled by the rate at which they are stripped from the liquid rather than the actual kinetics. Thus the presence of a volatile liquid-phase may have a profound effect on the apparent kinetics of the reaction. The presence of water in the liquid phase and its affect on kinetics and selectivity is a factor that deserves more attention. Maybe the system can best be modelled as a reactive distillation system rather than as pure chemical kinetics.

The interaction between such simple phenomena such as vapour liquid equilibrium, partial reaction equilibrium and kinetics can lead to quite complex behaviour and may help to explain the apparently conflicting behaviour found by many researchers in trying to model the system.